



**UNIVERSIDAD  
DE ANTIOQUIA**

**Nutrients (N and P) recovery from thickening and dewatering sludge  
concentrates of a wastewater treatment plant**

**Carolina González Morales**

Universidad de Antioquia

Facultad de Ingeniería

Medellín, Colombia

2021



---

**Nutrients (N and P) recovery from thickening and dewatering sludge centrates of a wastewater treatment plant**

**Carolina González Morales**

Thesis presented as a partial requirement to qualify for the title of:  
**Ph. D., Environmental Engineering**

Adviser:

Ph. D., Francisco José Molina Pérez

External Advisors:

Ph. D., Belén Fernández García

Ph. D., Miller Alonso Camargo-Valero

Ph. D., Carlos Alberto Peláez Jaramillo

Area: Water Resources

Research Line: Water quality and treatment.

GAIA research group

Universidad de Antioquia  
Facultad de Ingeniería, Escuela Ambiental  
Medellín, Colombia

2021

---

*“El hombre nunca sabe de lo que es capaz  
hasta que lo intenta.”*

*Charles Dickens*

*A mis padres.*

---

## Agradecimientos/ Acknowledgment

*This section is writing in Spanish, my mother tongue*

La escritura de este manuscrito representa la culminación de una etapa muy importante en mi vida. El camino no ha sido fácil y para lograrlo han sido muchas las personas que han participado del proceso y a las que agradezco mucho por su compañía y apoyo.

Inicialmente quiero agradecer a mi tutor el profesor Francisco Molina que en medio de todas sus ocupaciones siempre estuvo para apoyarme y guiarme en este largo proceso de realizar una tesis doctoral. A mis asesores los profesores Belén Fernández, Miller Camargo y Carlos Peláez. A la profesora Belén con su ternura y paciencia, le agradezco inmensamente por haberme recibido durante mi pasantía en el instituto de investigación IRTA, gracias por acompañarme, escucharme y guiarme tanto en mi estancia en Barcelona como durante todo el proceso del doctorado. Al profesor Miller por recibirme en Leeds, guiarme y estar presente cuando lo necesité. Al profesor Carlos por abrir las puertas de su laboratorio para este proyecto y estar dispuesto a asesorarme en temas que en ese entonces estaban alejados de mi conocimiento.

Le agradezco a mis compañeros del grupo GAIA, especialmente al área de fisicoquímicos inicialmente conformada por Marcela, Camilo, Sara, Luis y luego por Pedro, Diana, Gabriel, Silvana y Carlos. A las chicas de micro que fueron una compañía en aquellas jornadas largas en el laboratorio, a Astrid, Irina, Fátima, Paola y especialmente a Michael y Luis que estuvieron presentes en la mayor parte de las largas campañas de muestreo.

Agradezco muy especialmente a Christian Camilo Acevedo y a Carolina Giraldo, estudiantes de pregrado que ofrecieron su apoyo técnico y demostraron tener un gran amor por el conocimiento, aportando mucho en esta investigación. Así como también a Daniela y Ana Maria por el apoyo en la elaboración de pruebas.

Adicionalmente fueron varias las personas que durante los momentos difíciles tuvieron la disposición de apoyarme, especialmente en conseguir un espacio para hacer las pruebas de laboratorio cuando pensaba que no iba a poder, entre ellos, la profesora Diana Catalina y los profesores Camilo Castro y Darío Naranjo de la escuela ambiental que abrieron las puertas del laboratorio de docencia para hacer investigación. Mary Luz Gallego y Maria Cecilia por su buena disposición cuando necesitaba algo, al profesor Julio Saldarriaga por estar dispuesto a brindarme un espacio de trabajo. A los profesores Juan Carlos Muñoz y Diana López por brindarme parte de su conocimiento en el campo de la cristalización y a Sandra Zapata del grupo catalizadores y absorbentes.

Quiero agradecer al grupo de investigación GIEM por permitirme trabajar en su laboratorio, muy especialmente a Miguel por su asesoría técnica en el campo de los fertilizantes, a Alejandro por su coordinación en la entrega de resultados y a todo el equipo técnico: Mónica, Diego, Nelson, Alejandro y Rodrigo. A las personas que tuve el placer de conocer durante mi pasantía en el IRTA; Edu, Lluís, Joseph, Nancy, Martina, Erica, Laura, Ana, Marco y Jordi. Al personal de las estaciones depuradoras Manresa y La Llagosta, especialmente al Ingeniero José Miguel y al personal de la Universidad autónoma de Barcelona por su asesoría y paciencia en las pruebas DRX y SEM realizadas allí.

A la facultad de ingeniería civil de la Universidad de Leeds y todo su personal y a los amigos y compañeros que tuve la oportunidad de conocer, entre ellos Christian, Cynthia, Mariana, Daymaru,

---

Raúl y Claudia, sin ustedes la estadía allí no hubiera sido lo mismo. Gracias al personal técnico de la PTAR Esholt en Bradford (UK) y a la PTAR San Fernando en Itagüí (Colombia) por permitirme entrar a las plantas y realizar los muestreos. Especialmente agradezco a la ingeniera Andrea González que siempre estuvo dispuesta a darnos toda la información necesaria.

A los amigos y compañeros que estuvieron en el transcurso de este proyecto. A Isabel que a pesar de ser bio-ingeniera me brindó su apoyo incondicional, incluso haciendo muestreos de agua residual, a Maria Bernarda, Juan Pablo, Henry, Tatiana, Priscilla, Danny, que con nuestras charlas en las mesitas lográbamos desestresarnos un poco y salvar el mundo con un tinto. Al profesor Julio Cañón que dispuso de su tiempo para apoyarme en la revisión del documento final, a Liliana Betancurth que apareció en el momento más oportuno cuando no encontraba los recursos económicos para continuar y a todos los compañeros de la sala de posgrados.

Finalmente, y no menos importante quiero agradecer a mi familia, a mi hermana Andrea que más que una hermana es una gran amiga, a mi hermano Luis que siempre se sintió orgulloso de su hermanita menor, a mis papás que estuvieron siempre presentes en este largo camino. Mi padre que siempre lo he considerado un ejemplo a seguir y mi madre que con su ternura ha estado ahí para apoyarme. A mi novio Gabriel que estuvo presente en los momentos más difíciles y con la disposición para ayudarme cuando lo necesité y a Dios que me brindó la fortaleza para continuar con este proyecto de vida.

¡Mil gracias a todos!

---

## Abstract

Wastewater treatment plants (WWTPs) have been conceived as a method to remove polluting compounds from water, especially organic matter. However, a recent change of paradigm conceives wastewater as a valuable resource to recover energy and nutrients, mainly nitrogen (N) and phosphorus (P), which is a finite natural substance from phosphate rock that is predicted to be in short supply within the next 100 to 150 years. Both N and P are critical nutrients for crop growth and agronomic productivity. Still, their uncontrolled discharge into water bodies causes environmental deterioration due to eutrophication, so their recovery from wastewater will reduce the level of eutrophication and the risk of a food security emergency in the future.

Although there are different physical, chemical and biological techniques for the removal and recovery of nutrients from wastewater, struvite crystallisation is one of the most investigated worldwide, because it allows the joint recovery of N and P as effective fertilisers with low accumulation of heavy metals. However, research in this field has been scarce in Latin America, possibly due to the low number of existing WWTP. Therefore, it is necessary to conduct further research in nutrient recovery strategies as an opportunity to increase the level of sanitation in the region.

In this regard, this doctoral research evaluated the possibility of recovering nutrients in the form of struvite from the sludge dewatering and thickening supernatants (centrates) of a WWTP located in the south of the Aburrá valley, close to Medellín (Colombia) that treats domestic and industrial wastewater. The thesis is divided into seven chapters, which are described below:

**Chapter 1** provides an overview of the context in which the thesis was developed. The chapter discusses the importance of recovering nutrients within a circular economy, the associated legislation, presents the main techniques used for the removal and recovery of nutrients from wastewater and explains the main characteristics of the mineral struvite. The research question, hypotheses and objectives are also posed.

**Chapters 2 to 6**, presented in the form of articles, address the following aspects:

**Chapter 2** presents the mass balance of N and P developed in the San Fernando WWTP. The mass balance was conducted over seven composite samplings (lasting 7 hours with a frequency of 1.5 h) to address different climatic conditions. The objective of this chapter was to evaluate the behaviour of the nutrients in the different 15 identified flows of the WWTP to establish their possible recovery. In addition, the characteristics of the centrate from the San Fernando WWTP were compared with those of other two WWTPs that use chemical precipitation for the removal of P.

**Chapter 3** evaluates the effect of stirring speed on the quantity, size and quality of the struvite precipitates obtained. For this, 6 agitation speeds were evaluated using the sludge dewatering centrate of the La Llagosta WWTP (Catalonia-Spain).

**Chapter 4** examines the effect of pH and temperature on struvite formation; for these experiments, the optimal velocity gradient obtained in chapter 3 and the centrate of the Esholt WWTP (Bradford-England) was used.

---

**Chapter 5** assesses the effect of 3 variables (initial concentration of phosphorus, aeration and seed material) on reactor efficiency and the quantity and quality of the precipitated product, based on experiments developed in two types of designed reactors: the 5L full-mix reactor (CSTR) and the 6.5L fluidised bed reactor (FBR). For this evaluation, the actual sludge dewatering centrate of the San Fernando WWTP (Colombia) was used with a  $3 \times 2^2$  factorial design.

**Chapter 6** evaluates the quality of the struvite obtained in chapter 5 as a fertiliser, considering the Colombian and European regulations. The evaluation considered two struvite samples (one for each reactor), and a one-factor design, using the biomass produced and the amounts of N and P in this biomass as the response variables. The fertilisers evaluated in the selected crop (Pasto *Brachiaria Brizantha Marandú*) were the struvite obtained from the two reactors, biosolids from the same San Fernando WWTP and two fertilisers used commercially (Urea and Triple 15). A leaching test was also included in this chapter.

**Chapter 7** presents the general conclusions and recommendations of this research.

Finally, the **ANNEXES** section introduces the general materials and methods used in the research, starting with the analytical methods at the laboratory level, the main calculations used in the different chapters of this thesis, following with the design of the reactors, the preliminary design tests, the equations used for the design of continuous stirred tank reactor (CSTR) and a fluidised bed reactor (FBR) and the residence times distribution tests (RTD) for the hydraulic evaluation of the reactors designed. Finally, annex 4 presents additional information of chapter 5.

---

## Resumen

Las plantas de tratamiento de aguas residuales (PTARs) han sido concebidas como un método para eliminar los compuestos contaminantes del agua, especialmente la materia orgánica. Sin embargo, un cambio reciente de paradigma concibe las aguas residuales como un recurso valioso para recuperar energía y nutrientes, principalmente nitrógeno (N) y fósforo (P). Aunque el nitrógeno (N) está ampliamente disponible en la atmósfera, el P es considerado una sustancia natural finita de la roca fosfórica que se prevé escaseará en los próximos 100 a 150 años. Tanto el N como el P son nutrientes fundamentales para el crecimiento de los cultivos y la productividad agronómica. Aun así, su vertido incontrolado en cuerpos de agua provoca un deterioro ambiental debido a la eutrofización, por lo que su recuperación de las aguas residuales reducirá el nivel de eutrofización y el riesgo de una futura emergencia de seguridad alimentaria.

Aunque existen diferentes técnicas físicas, químicas y biológicas para la remoción y recuperación de nutrientes de las aguas residuales, la cristalización de estruvita es una de las más ampliamente investigadas a nivel mundial, ya que permite la recuperación conjunta de N y P, presenta baja acumulación de metales pesados y ha demostrado ser efectiva como fertilizante. Sin embargo, la investigación en este campo ha sido escasa en América Latina, posiblemente debido al bajo número de PTARs existentes. Por lo tanto, es necesario realizar más investigaciones en estrategias de recuperación de nutrientes como una oportunidad para aumentar el nivel de saneamiento en la región.

En este sentido, esta investigación doctoral evaluó la posibilidad de recuperar nutrientes en forma de estruvita de los sobrenadantes de deshidratación y espesamiento de lodos (centrados) de una PTAR ubicada en el sur del valle de Aburrá, cerca de Medellín (Colombia) que trata aguas residuales domésticas e industriales. La tesis se divide en siete capítulos, que se describen a continuación:

El **Capítulo 1** aporta una descripción general del contexto en el que se desarrolló la tesis. El capítulo analiza la importancia de la recuperación de nutrientes dentro de una economía circular, la legislación asociada, presenta las principales técnicas utilizadas para la eliminación y recuperación de nutrientes de las aguas residuales y explica las principales características del mineral estruvita. También se plantea la pregunta de investigación, hipótesis y objetivos.

Los capítulos 2 a 6, presentados en forma de artículos, abordan los siguientes aspectos:

El **Capítulo 2** presenta el balance de masa de N y P desarrollado en la PTAR San Fernando. El balance de masa se realizó en siete muestreos compuestos (que duraron 7 horas con una frecuencia de 1,5 h) para abordar diferentes condiciones climáticas. El objetivo de este capítulo fue evaluar el comportamiento de los nutrientes en los diferentes 15 caudales identificados de la PTAR para establecer su posible recuperación. Adicionalmente se compararon las características de los centrados de la PTAR San Fernando con los centrados de otras dos PTAR que usan precipitación química para la remoción de P.

El **Capítulo 3** evalúa el efecto de la velocidad de agitación sobre la cantidad, tamaño y calidad de los precipitados de estruvita obtenidos. Para ello, se evaluaron 6 velocidades de agitación utilizando el centrado de deshidratación de lodos de la EDAR de La Llagosta (Cataluña-España).



---

El **Capítulo 4** examina el efecto del pH y la temperatura sobre la formación de estruvita; para estos experimentos se utilizó el gradiente de velocidad óptimo obtenido en el capítulo 3 y el centrado de la PTAR de Esholt (Bradford-Inglaterra).

El **Capítulo 5** evalúa el efecto de 3 variables (concentración inicial de fósforo, aireación y material de siembra) sobre la eficiencia del proceso y la cantidad y calidad del producto precipitado, basándose en experimentos desarrollados en dos tipos de reactores diseñados: el reactor de mezcla completa de 5L (CSTR) y el reactor de lecho fluidizado de 6,5 L (FBR). Para esta evaluación se utilizó el centrado de deshidratación de lodos real de la EDAR San Fernando (Colombia) con un diseño factorial  $3 \times 2^2$ .

El **Capítulo 6** evalúa la calidad como fertilizante de la estruvita obtenida en el capítulo 5, teniendo en cuenta la normativa colombiana y europea. La evaluación consideró dos muestras de estruvita (una para cada reactor), se realizó un diseño unifactorial, utilizando la biomasa producida y las cantidades de N y P en esta biomasa como variables de respuesta. Los fertilizantes evaluados en el cultivo seleccionado (Pasto *Brachiaria Brizantha Marandú*) fueron la estruvita obtenida de los dos reactores, biosólidos de la misma PTAR San Fernando y dos fertilizantes utilizados comercialmente (Urea y Triple 15). También se incluyó en este capítulo una prueba de lixiviación.

El **capítulo 7** presenta las conclusiones y recomendaciones generales de esta investigación.

Finalmente, en el apartado **ANEXOS** se presentan los materiales y métodos generales utilizados en la investigación, comenzando por los métodos analíticos a nivel de laboratorio, los principales cálculos utilizados en los diferentes capítulos de esta tesis, siguiendo con el diseño de los reactores, las pruebas preliminares de diseño, las ecuaciones utilizadas para el diseño de un reactor de tanque agitado continuo (CSTR) y un reactor de lecho fluidizado (FBR) y los ensayos de distribución de tiempos de residencia (RTD) para la evaluación hidráulica de los reactores diseñados. Finalmente, el anexo 4 presenta información complementaria del capítulo 5.

---

# Table of contents

<i>Agradecimientos/ Acknowledgment</i>	<i>i</i>
<i>Certificate of Thesis Direction</i>	<i>¡Error! Marcador no definido.</i>
<i>Abstract</i>	<i>iii</i>
<i>Resumen</i>	<i>v</i>
<i>Table of contents</i>	<i>vii</i>
<b>Chapter 1. Introduction and objectives</b>	<b>10</b>
1.1 Importance of nutrients recovery in WWTP	10
1.2 Principal techniques used for nutrients removal/ recovery in WWTP.	12
1.2.1 Technologies used for nutrient accumulation	14
1.2.2 Technologies used for nutrient release	14
1.2.3 Technologies used for nutrient extraction	15
1.3 Struvite crystallisation	16
1.3.1 Phases of struvite crystallisation	17
1.3.2 Main factors influencing crystallisation	18
1.3.3 Reactors used in the struvite crystallisation	19
1.3.4 Main uses of struvite	20
1.3.5 Economic viability	20
1.4 Nutrient recovery within a circular economy	21
1.5 Problem statement and research objectives	23
1.5.1 Research question and hypothesis	24
1.5.2 Objectives	24
1.6 Thesis Context	25
1.6.1 Congresses	25
1.6.2 Publications	26
<b>Chapter 2. Nutrient mass balance (N, P) and recovery potential in San Fernando WWTP</b>	<b>27</b>
2.1 Introduction	27
2.2 Materials and Methods	29
2.2.1 Description of the full-scale wastewater plant	29
2.2.2 Analytical methods	30
2.2.3 Mass balance calculation	31
2.3 Results and discussion	32
2.3.1 Flows characterisation	32
2.3.2 Mass balance calculations	34
2.3.3 Comparison with other WWTP	38
2.4 Conclusions	39
2.5 Acknowledgements	40

---

**Chapter 3. Effect of the stirring speed on the struvite formation using the centrate from a WWTP. 41**

3.1	Introduction	42
3.2	Materials and methods	43
3.2.1	WWTP	43
3.2.2	Analytical methods	44
3.2.3	Methods	44
3.2.4	Experimental setup	45
3.3	Results and discussion	46
3.4	Conclusions	49
3.5	Acknowledgements	50

**Chapter 4. Influence of pH and Temperature on Struvite Purity and Recovery 51**

4.1	Introduction	51
4.2	Materials and Methods	53
4.2.1	Description of the full-scale wastewater treatment plant and centrate characterisation	53
4.2.2	Analytical methods	54
4.2.3	Struvite precipitate characterisation	55
4.2.4	Materials	55
4.2.5	Experimental set-up and procedure	55
4.2.6	Data processing and statistical analysis	56
4.3	Results and Discussion	58
4.3.1	Effect of pH and temperature on ions removal	58
4.3.2	Ions mass balance	60
4.3.3	Size and morphology of struvite crystals	61
4.4	Conclusions	63
4.5	Acknowledgements	64

**Chapter 5. Struvite recovery from municipal wastewater sludge dewatering centrate using a stirred tank and a fluidised bed reactor 65**

5.1	Introduction	66
5.2	Materials and Methods	67
5.2.1	Centrate from a conventional WWTP	67
5.2.2	Reactors design and operation	68
5.2.3	Experimental setup	70
5.2.4	Hydraulic evaluation	72
5.2.5	Analytical methods	72
5.2.6	Costs analysis	73
5.2.7	Calculations	74
5.3	Results and discussion	76
5.3.1	Hydraulic evaluation	76
5.3.2	Effect of phosphorus and ammonium concentration (C factor)	77
5.3.3	Effect of seed material (SM)	82
5.3.4	Effect of the aeration	84

---

5.3.5	Statistical model	84
5.3.6	Reactors comparison and nutrients mass balance (N and P)	85
5.3.7	Cost analysis	86
5.4	Conclusions	89
5.5	Acknowledgements	90
<b>Chapter 6. The determination of fertiliser quality of the formed struvite from a WWTP</b>		<b>91</b>
6.1	Introduction	92
6.2	Materials and Methods	92
6.2.1	Struvite production	92
6.2.2	Fertilisation trial (pot experiment)	93
6.2.3	Fertilisation trial calculations	95
6.2.4	Leaching Test	95
6.2.5	Leaching test calculations	96
6.2.6	Analytical Procedures	96
6.2.7	Statistical Analysis	97
6.3	Results and discussion	97
6.3.1	Struvite and biosolid characteristics	97
6.3.2	Fertilisation test	100
6.3.3	Leaching test	104
6.4	Conclusions	106
6.5	Acknowledgements	107
<b>Chapter 7. Conclusions and recommendations</b>		<b>108</b>
<b>References</b>		<b>111</b>
<b>ANNEXES</b>		<b>127</b>
Annex 1.	General Materials and Methods	127
	Analytical methods	127
	Main calculations	133
Annex 2.	Reactors design	137
	Preliminary tests on a laboratory scale	137
	Complete stirred tank Reactor (CSTR) design.	144
	Fluidised bed reactor (FBR) design	148
Annex 3.	Residence time distribution in CSTR and FBR reactors in ideal situation, undisturbed by the crystallisation process.	152
	Introduction	152
	Methodology	153
	RTD Results and discussion in ideal situation	156
	Conclusions	159
Annex 4.	Supplementary information to chapter 5	160

---

# Chapter 1. Introduction and objectives

## Highlights

- Due to the future food security emergency that will occur in the next 150 years owing to the scarcity and costs of phosphate rock, the emerging challenge is the effective recovery and reuse of phosphorus present in waste and wastewater, as fertiliser in the production of foods.
- The nutrients recovery pathway is made up of (1) nutrient accumulation, (2) nutrient release, and (3) nutrient extraction.
- Struvite is a kind of mineral that is precipitated by magnesium, ammonium, and phosphate ions in equal molar ratios and its crystallisation process is affected by a combination of physicochemical factors such as supersaturation, pH, temperature, mixing strength, and the presence of foreign ions.
- The recovery of nutrients such as struvite within a circular economy requires joint work on technical, social and political aspects.

## Abstract

The world may face a future shortage of phosphorus in the next 150 years, while the uncontrolled discharge of nutrients has caused severe eutrophication problems in water bodies. Therefore, different investigations have proposed physical-chemical and biological techniques to remove and recover nutrients; among them is the precipitation of struvite. Struvite is a kind of orthophosphate mineral formed in different classes of reactors, including CSTR and FBR reactor. Its crystallisation process depends on factors such as supersaturation, temperature, and pH. Although uncontrolled precipitation of struvite can cause technical problems in wastewater treatment plants, it has proven to be an eco-friendly fertiliser that can be used in a wide variety of crops. Obtaining struvite from wastewater is an excellent alternative to be applied in Latin American countries within a circular economy. However, the success of its application will largely depend on its articulation within the region's public policies and its reception by the community. Under this context, the research question, hypothesis, general objective and the specific objectives of this research were raised.

**Keyword:** eutrophication, phosphate rock, circular economy, anaerobic digestion.

## 1.1 Importance of nutrients recovery in WWTP

Excessive nitrogen (N) or phosphorus (P) loading to aquatic ecosystems leads to detrimental effects (such as algal overgrowth and reduced dissolved oxygen levels) that hinder the ability of water bodies to meet designated uses (Carey & Migliaccio, 2009). Wastewater treatment plants (WWTPs) are categorised as point sources of both N and P and are among the leading causes of eutrophication that negatively affect many natural water bodies. According to UNEP (1994) in Valsami-Jones (2005), between 41 and 53% of lakes and reservoirs in Europe and South America had eutrophication problems. Therefore, to minimise these problems, WWTPs should remove or recover P and N from the wastewater before returning to the environment (De-Bashan & Bashan, 2004).

Thus, in 1991 was proposed by European communities (EC) the establishment of the Urban Wastewater Directive that set discharge limits for some of the established sanitary determinants, e.g. biological oxygen demand (BOD) and suspended solids, as well as the nutrients, for rivers and the designated 'sensitive areas'. In the EC regulation, the permitted discharge concentrations are  $1 \text{ mg. L}^{-1} \text{ P}$  (10 000 – 100 000 Inhabitant Equivalent (IE)) or  $2 \text{ mg. L}^{-1} \text{ P}$  ( $> 100\ 000$  IE) (Council Directive 91/271/EEC). In some Latin American countries, maximum permissible limits for the discharge of nutrients to water bodies have also been established, between them are Ecuador ( $10\text{-}15 \text{ mg.L}^{-1}$  TKN and  $10 \text{ mg.L}^{-1}$  TP), Chile ( $10\text{-}75 \text{ mg.L}^{-1}$  TKN and  $2\text{-}15 \text{ mg.L}^{-1}$  TP), Argentina ( $15\text{-}35 \text{ mg.L}^{-1}$  TKN and  $1\text{-}2 \text{ mg.L}^{-1}$  TP in some provinces) and Mexico ( $15\text{-}60 \text{ mg.L}^{-1}$  TN and  $5\text{-}30 \text{ mg.L}^{-1}$  TP) (CONAGUA, 1997; Ministerio de ambiente Uruguay, 1998; MSGP, 2001; Republica de Ecuador, 2008). Meanwhile in others countries like Uruguay, Perú and Colombia, there are still no maximum permissible limits of nutrients in the regulation of wastewater discharges (Minambiente, 2015; Ministerio de ambiente Uruguay, 1998; MINAM, 2010).

Although N is widely available as  $\text{N}_2$ , its production is dependent on fossil fuels and may become scarce or expensive in the future, as do mineral sources of phosphorus. P is an essential nutrient, and it is a finite resource obtained mainly from rocks. The production of phosphorus-based fertilisers comes from a limited number of mines around the world, and there is no substitute for it in food production. There are about 7,000 million tons of phosphorus available in rocky deposits in the form of  $\text{P}_2\text{O}_5$ , and the population consumes 40 million and increases its demand by 1.5% each year. According to this, it is estimated that the sources of P can be exhausted between 70 and 150 years (Li et al., 2018; Mehta et al., 2015; Shu et al., 2006), however recent investigations show that in a very optimistic scenario global P requirement overtakes global P supply after 2045 (Nedelciu et al., 2020). Figure 1 noted the depletion year under different scenarios of ultimately recoverable P reserves, according to Li et al. (2018). In addition, as the world's P rock reserves are concentrated in a small number of geographical areas, the P shortage may cause geopolitical issues. Morocco, China, Algeria and the United States of America (USA) account for almost 85% of the world's reserves, with Morocco alone accounting for 77% (Cooper et al., 2011). Despite its considerable reserves and large production, the USA consistently must import phosphate rock; almost the entire stock must be imported from outside the continent, just like Asia and Europe. Latin America is also highly dependent on phosphate imports (Desmidt et al., 2015)( see Figure 2), and due to its high population growth rates, fertiliser requirement will increase in the region, reinforcing its dependence on imports in the coming decades (Nedelciu et al., 2020).

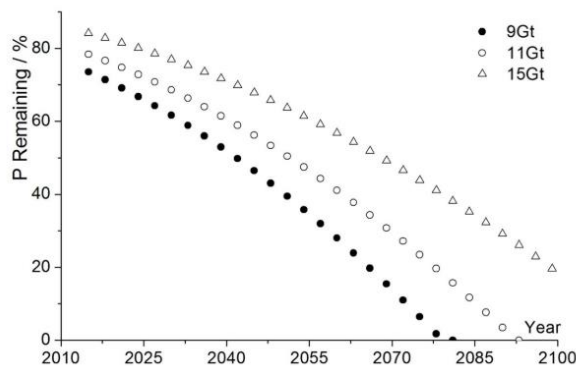


Figure 1. Trend analyses between depletion time and phosphorus reserves (Li et al., 2018)

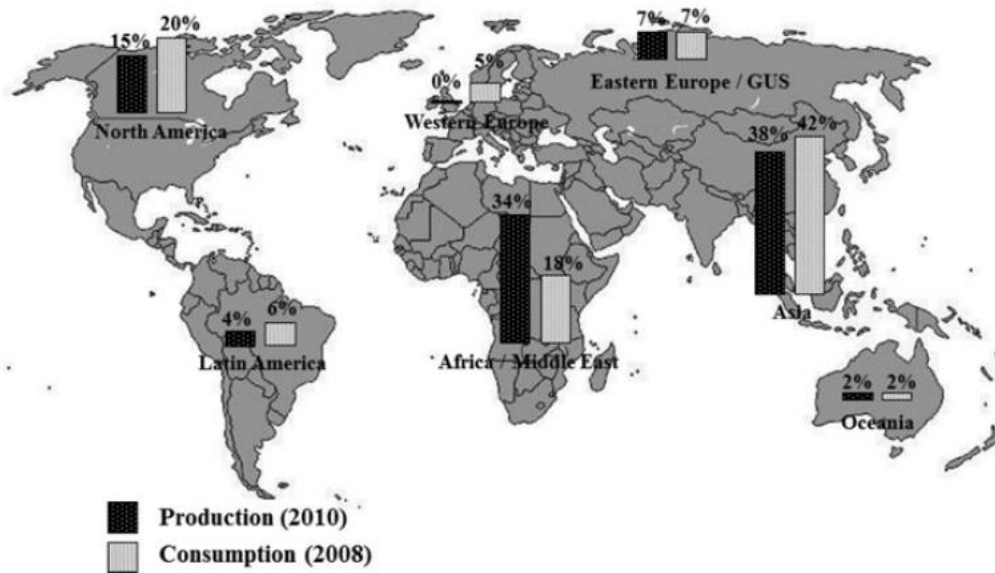


Figure 2. Global production and consumption of phosphorus. Data from U.S. Geological Survey, 2012 in Desmidt et al. (2015)

Additionally, the presence of N and P in the different liquid streams of a WWTP can cause problems in the treatment systems. On the one hand, if these nutrients are not eliminated, the concentration will increase in the waterline when the digested sludge dewatering supernatant (centrate) that has high nutrients concentration is returned to the treatment line, and this can reduce the efficiency in biological processes that have a BOD: N:P ratio as an effective operating criterion for aerobic processes of 100: 5: 1 (Uysal et al., 2010). On the other hand, in WWTPs that use enhanced biological phosphate removal (EBPR) and anaerobic digestion (AD) of sludge, the presence of these nutrients can cause uncontrolled growth of struvite, a phosphate precipitate that clogs and becomes embedded in sludge return lines and in pumps and valves associated, increasing pumping and maintenance costs and reducing the total capacity of the plant's piping system in terms of loss of hydraulic capacity and decrease in biological treatment capacity (Fattah, 2012; Uysal et al., 2010).

Therefore, the nutrients recovery from domestic and industrial WWTPs brings technical, environmental and economic benefits. It can represent a solution for the future world food security crisis since total phosphorus excreted by humans could meet 22% of the P demand (Mihelcic et al., 2011). Furthermore, implementing strategies to recover nutrients represents an excellent option for developing countries as the Latin American and Caribbean region (LACR), where 77% lacks access to safe sanitation. In this region there is an opportunity to increase sanitation access by building new treatment plants and simultaneously implementing resource recovery strategies in these facilities (Cardoso et al., 2019).

## 1.2 Principal techniques used for nutrients removal/ recovery in WWTP.

N can be removed from wastewater by physical-chemical and biological means; however, biological processes are the main techniques used to remove nitrogen from wastewater (Jenkins & Wanner,

2014). Among these processes are the Nitrification / Denitrification, Bio-increase, Nitration / Denitration processes and the ANAMMOX processes. Basically, these techniques differ in energy requirements, chemical demand, sustainability and operational complexity.

The most common methods for P removal are chemical precipitation and biological removal. The chemical precipitation of phosphorus is typically performed by adding the salts of di- and trivalent metal ions or lime that form precipitates of sparingly soluble phosphates. The chemicals can be added before the primary settling, during secondary treatment or as part of a tertiary treatment process. Chemical precipitation using salts of calcium (Ca), aluminium (Al), iron (Fe) and magnesium (Mg) is a desirable technology, as it is simple to operate and implement to achieve low P concentration (< 1mg P/L) in the effluent (Adelagun, 2016); however, it increases sludge volume, decreases the biodegradability of the sludge, and generates a sludge that is expensive to dispose of (Valsami-Jones, 2005).

The biological phosphate removal process is much more popular nowadays over chemical methods due to its simplicity, reduced chemical cost, less sludge production and several environmental benefits. The biological process involves removing phosphates by accumulating them with biomass (algae, bacteria, plants). Two major research areas of biological methods are the EBPR and wetland processes. The EBPR process consists basically of alternating conditions of an anaerobic zone followed by an aerobic zone that favours the cultivation of organisms called Polyphosphates Accumulating Organisms (PAOs) that help achieve the process by accumulating the poly-P reserves (Adelagun, 2016). In this process, approximately 90% of the incoming phosphorus load is incorporated into the sewage sludge (Desmidt et al., 2014). Among the limitations of this process are that it needs large bioreactors to establish anaerobic-aerobic conditions and large pumping capacities to enrich PAOs organisms (Valsami-Jones, 2005).

Although the removal of nutrients from wastewater is fundamental to reduce eutrophication problems in water bodies, in recent years, there has been a need to remove and recover the nutrients from WWTPs. The substantial difference between the traditional P removal and P-recovery from wastewater is that P removal aims at obtaining a P-free effluent by transferring P to sludge with chemical and biological processes. Meanwhile, P and N recovery aims at a P/N-containing product that can be reused either in agriculture or in P-industry (Desmidt et al., 2014).

There is a wide variety of physical, chemical and biological techniques for N and P recovery; however, their application is highly dependent on the existing treatment system. Since the efficiency of these techniques typically decreases with a lower nutrient concentration in the waste, Mehta et al. (2015) proposed a three-step framework for nutrient recovery: (1) nutrient accumulation, (2) nutrient release, and (3) nutrient extraction. The nutrients in dilute waste streams need to be accumulated so that subsequent release techniques can mobilise the nutrients for final recovery in the form of concentrated products for beneficial reuse (see Figure 3).



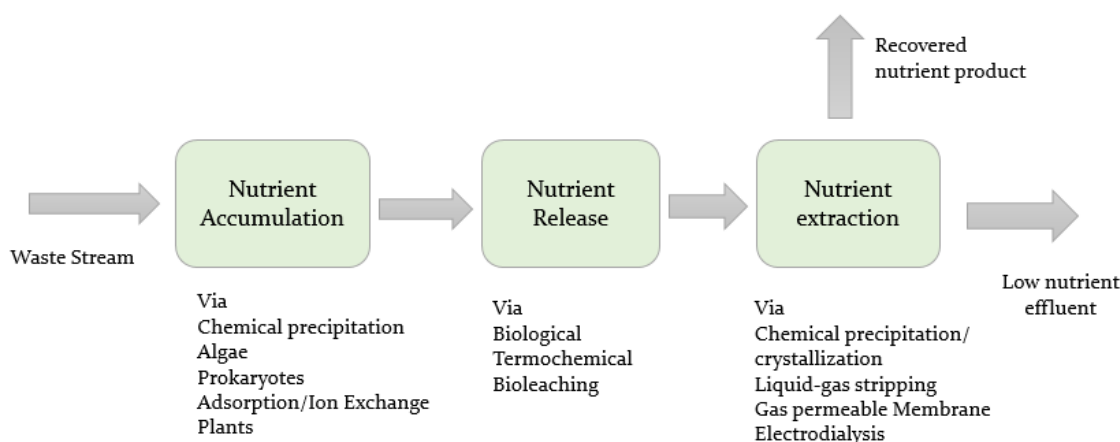


Figure 3. Nutrient recovery pathway. Adapted from Mehta & Batstone.(2013).

### 1.2.1 Technologies used for nutrient accumulation

Nutrient accumulation (nutrients removal) technologies collect soluble nutrients (N, P, and K) from waste streams with low nutrient concentrations ( $2\text{--}20\text{ mg L}^{-1}$ ). These techniques include Prokaryotic accumulation with PAOs organisms (using EBPR as was shown previously), purple non-sulphur bacteria and cyanobacteria, chemical accumulation via Precipitation, Adsorption/Ion-Exchange, Algae accumulation, Liquid-Liquid Extraction, Plant Accumulation (wetlands), Membrane Filtration and Magnetic Separation.

### 1.2.2 Technologies used for nutrient release

Once accumulated, nutrients must be either released or directly extracted into a recovered product. The principal nutrients release technics are Biological, Thermochemical and Bioleaching/Extraction. The most common biological release technique is anaerobic digestion. AD is used to stabilise wastes, organic solids destruction, pathogen destruction, and energy recovery from wastes in the form of bio-methane (Batstone & Jensen, 2011). In this process, organic matter is transformed into  $\text{CH}_4$  and  $\text{CO}_2$  by the action of different groups of bacteria. The main advantages of this process are the reduction in the volume of waste sludge and production (Marti et al., 2008).

The *Anaerobic Digestion* facilitates the release of nutrients from the biodegradable fraction of the waste. In this process, organic N is converted into ammonium, and organic P is hydrolysed to soluble P, with the extent of conversion depends on the conditions employed during digestion. Typically, the soluble P content in most municipally digested wastes, principally with EBPR, range from 50 to 500  $\text{mg L}^{-1}$ , and N is often five times higher than soluble P (Batstone & Jensen, 2011). This nutrient-rich side stream can be a feedstock for nutrient extraction/recovery techniques and the remaining particulate-bound nutrients and residual organics are recovered as biosolids. However, the phosphorus that is released in the anaerobic digester may precipitate as metal phosphates causing operational problems in the sludge line.

*Thermochemical processes* like thermal hydrolysis, wet oxidation, incineration, gasification, and pyrolysis can significantly reduce the bulk volume of wastes by destroying a large proportion of the carbon, and in the case of incineration, gasification, and pyrolysis, by evaporating off moisture. The

char/ash/oil produced from the thermochemical processes retains most P and K, but N is lost in the gas stream. The P recovery potential of this technique is very high (>90%) (Adelagun, 2016).

**Bioleaching** is a release technology that relies on the solubilisation of nutrients and heavy metals from solid substrates either directly by the metabolism of leaching microorganisms or indirectly by the products of metabolism. The major disadvantage of bioleaching technology is that the release efficiencies for N and P are low (<40%) as compared with that of unwanted heavy metals (>60%) (Pathak et al., 2009), creating a need for further processing of the leachate.

### 1.2.3 Technologies used for nutrient extraction

Once the nutrients are released, the next step is their extraction using physicochemical methods to recover the nutrients that were released into a soluble form (e.g., N–NH<sub>4</sub><sup>+</sup>, P–PO<sub>4</sub><sup>3-</sup>, and K–K<sup>+</sup>). The principal technics used are Chemical Precipitation/Crystallisation, Gas-Permeable Membrane and Absorption, Liquid–Gas Stripping and Electrodialysis (ED).

**Chemical precipitation** via crystallisation is a phase change process that converts previously dissolved components into a particulate, inorganic compound for separation from the liquid bulk. Struvite (MgNH<sub>4</sub>PO<sub>4</sub>·6H<sub>2</sub>O) crystallisation is a well-known example of this technique applied to recover N and P simultaneously from nutrient-rich streams. Alternative products like calcium phosphate, magnesium potassium phosphate, or iron phosphate can be produced similarly, depending on the composition of the waste and the added reagent chemicals. Calcium phosphates, as hydroxyapatite, are also an attractive form of phosphorus recovery because they can be directly comparable to phosphate rock (Vasconcelos, 2013).

**Gas-permeable membranes** can be used to recover N as ammonia from the liquid phase. In this process, ammonia is transferred by convection and diffusion from the liquid stream across a membrane. Ammonia volatilises through a hydrophobic membrane and is either condensed or absorbed into an acidic solution. Following ammonia recovery via membrane concentration, acids such as sulfuric acid are used to recover ammonium as ammonium sulphate ((NH<sub>4</sub>)<sub>2</sub>SO<sub>4</sub>). The NH<sub>4</sub>–N removal efficiency of a gas permeable process has been reported to be higher than 90% (EL-Bourawi et al., 2007). The main challenges to implementing this technology are the relatively low absorption rate per unit surface area and the high capital and operating costs per unit volume of waste streams being treated.

**Gas stripping** is a physiochemical process that involves the mass transfer of ammonia from the liquid phase to the gas phase. This process differs from gas-permeable membrane processing in that all constituents in the waste stream (not just ammonia) can exert their partial pressure, thus making the mass transfer less efficient. It is mainly applicable to situations where the effluent has a relatively high ammonia concentration (NH<sub>4</sub>–N > 2000 mg L<sup>-1</sup>). Recovery of the stripped ammonia occurs via condensation, absorption, or oxidation to produce a concentrated fertiliser product. Products from the gas stripping processes include ammonium sulphate ((NH<sub>4</sub>)<sub>2</sub>SO<sub>4</sub>), other ammonia salts, or a concentrated ammonia solution.

**Electrodialysis** is an extraction technology that selectively separates anions and cations across an ion-exchange membrane, driven by an applied electrical field between electrodes. Through this process, cations (K<sup>+</sup> and NH<sub>4</sub><sup>+</sup>) and anions (e.g., PO<sub>4</sub><sup>3-</sup>) are obtained separately in concentrated solutions. ED has the potential to recover all nutrients but is most applicable for N and K, as P can be effectively removed using other lower-cost methods.

Thus, there are many physical, chemical, and biological techniques used to accumulate, release, and extract nutrients. The recovery of P and N present in WWTPs can take place from the liquid phase (i.e. the effluent from a treatment unit such as the supernatant from a digester), sludge or ashes (originated after sludge incineration)(Cardoso et al., 2019). The main products of nutrient recovery are biomass, biosolids, char/ash, and chemical nutrient products.

As stated above, metals precipitation (with iron and aluminium) and bioaccumulation are widely applied to remove P in sewage treatment plants. Bioaccumulation techniques may have more advantages from a nutrient recovery and reuse perspective. In metals precipitation, P that is firmly bound to iron and aluminium precipitates is unavailable for crop growth and may require further processing steps that add to complexity and process cost. Nevertheless, recent research has shown that vivianite ( $\text{Fe}_3(\text{PO}_4)_2 \cdot 8\text{H}_2\text{O}$ ), the most important iron and phosphate phase in digested sewage sludge with high iron content, can be used in the electronics industry and agriculture with a high collection value (Wilfert et al., 2018; Y. Wu et al., 2019).

The combination of P removal via EBPR and P recovery as struvite and hydroxyapatite are appropriate sustainable technologies. The combination of these technologies, apart from being simple and easy to operate, implies reducing chemicals for precipitation, reducing the size of the treatment facility, and reducing the volume of effluent to be treated and consequently reducing costs (Adelagun, 2016).

Therefore, the recovery of nutrients from WWTPs has a high application potential. Since over 90% of all P-based products are associated with the agricultural sector, it is appropriate for extractive nutrient recovery options to target products to the agricultural sector. It is expected that in the short-to-medium term, the products from nutrient recovery will mainly offset treatment costs. However, as technologies mature and the value of nutrients increase in the longer term, the income from alternative fertiliser sales may become a significant driver for widespread technology adoption (Mehta & Batstone, 2013).

### 1.3 Struvite crystallisation

From a physical perspective, crystallisation is a state change from a liquid or gaseous phase to a solid with an organised structure called a crystal. It is a kinetic process, and as such, it requires a driving force called supersaturation. Precipitation processes (crystallisation by reaction) differ from classical crystallisation methods in the way in which supersaturation is achieved, since it does not result from an action on the physical properties of the solution but is obtained through a chemical reaction between two soluble components, resulting in a less soluble crystallised product (Pastor, 2008).


Struvite is a kind of orthophosphate mineral that is precipitated by magnesium, ammonium, and phosphate ions in equal molar ratios via the following reaction:



Struvite has low solubility in water, with a solubility constant of  $10^{-13.26}$  (Ohlinger et al., 1998). In contrast, it is readily soluble in acidic environments. Pure struvite is generally a white or transparent fine powder, but the morphology of struvite particles differs under various formation conditions and includes a needle-like shape, a cube-like shape, and irregular shapes (Zhang et al., 2009). According to the review of Rahman et al. (2013), the length of struvite particles varied from 15  $\mu\text{m}$  (Zhang et al., 2009) to 3.5  $\mu\text{m}$  (Adnan et al., 2003), however, recent investigations have found particle sizes up to 4.5  $\mu\text{m}$  (Muys et al., 2021). The main characteristics of struvite are presented in Table 1.

## Chapter 1. Introduction and objectives.

Table 1. Properties of struvite. Adapted from Le Corre et al. (2009).

Nature	Mineral salts
Chemical name	Magnesium ammonium phosphate hexahydrate
Formula	$\text{MgNH}_4\text{PO}_4 \cdot 6\text{H}_2\text{O}$
Composition	9.8 % Mg-7.3 % $\text{NH}_4$ - 38.8% $\text{PO}_4$ - 44.1% $\text{H}_2\text{O}$
Aspect	White glowing crystal
	Orthorhombic (*)
	
Structure	
Molecular weight	245.43 $\text{g}\cdot\text{mol}^{-1}$
Specific gravity	1.711 ( $\rho = 1.711 \text{ g}\cdot\text{cm}^{-3}$ )
Solubility	Low in water: 0.018 $\text{g}\cdot 100 \text{ ml}^{-1}$ at 25°C in water High in acids: 0.033 $\text{g}\cdot 100 \text{ ml}^{-1}$ at 25°C in 0.001 N HCl; 0.178 $\text{g}\cdot 100 \text{ ml}^{-1}$ at 25°C in 0.01 N HCl
Solubility constant	$10^{-13.26}$

\*Own source

### 1.3.1 Phases of struvite crystallisation

The development of struvite crystals occurs in two chemical phases: nucleation (primary and secondary) or crystal birth and crystal growth. Nucleation occurs when the constituent ions combine to form crystal embryos. Crystal growth continues until equilibrium is reached. The prediction of these mechanisms is complex since it is controlled by a combination of factors such as the initial state of the crystal, thermodynamics of the liquid-solid equilibrium, level of supersaturation, mass transfer phenomena between the solid and liquid phase and the kinetics of the reaction (Rahman et al., 2013; Wang et al., 2009).

Primary nucleation is divided into homogeneous and heterogeneous. The first refers to the appearance of nuclei within the supersaturated solution not influenced by any solid. The second occurs when there are solid foreign substances such as suspended dust or parts of the crystal itself (Pastor, 2006; Rahman et al., 2013).

The secondary nucleation refers to the formation of nuclei in a supersaturated solution when crystals of the solute are already present. In secondary nucleation, three mechanisms have been identified: surface, contact and apparent. The first refers to the formation of nuclei on the surface of the particles present; the second is produced by collisions between the same particles or the particles with the reactor, the third refers to crystallisers that have seed materials, where the fine crystals (detached by friction between crystals) are attached to the seed crystals by static electricity (Pastor, 2008). The secondary nucleation rate plays an essential role in controlling the final particle size distribution. The secondary nucleation rate is influenced by process parameters such as temperature, stirring speed, crystal content in the solution, and supersaturation (Mehta & Batstone, 2013).

Crystal growth corresponds to the development of crystals until the equilibrium is reached. The crystal growth determines the final size of the crystal according to the crystallisation kinetics (rate of growth). Although nucleation seems to be the most critical step in producing struvite crystals, the mechanisms involved in crystal growth are responsible for the final size and structure of the crystals, which are essential parameters in struvite recovery processes (Le Corre et al., 2009)

### 1.3.2 Main factors influencing crystallisation

Struvite crystallisation (nucleation and growth) is affected by a combination of physicochemical factors such as supersaturation, pH, temperature, mixing strength, and the presence of foreign ions. Supersaturation is the driving force for all crystallisation processes (Pastor et al., 2008). It significantly affects the induction time of crystallisation and the crystal growth rate (Le Corre et al., 2009).

Supersaturation is the state of a solution in which the concentration of the solute is more significant than its value at equilibrium (Rahman et al., 2013). In the case of struvite, considering that it contains three specific ions ( $Mg^{2+}$ ,  $NH_4^+$  and  $PO_4^{3-}$ ), its solute concentration can be defined by the ionic activity product (IAP). When the IAP is greater than the solubility product ( $K_{sp}$ ), the system is supersaturated, and the struvite can nuclear and grow, returning the system to equilibrium. The saturation index (SI) also allows describing the state of saturation of the aqueous phase. When  $SI < 0$ , the solution is sub saturated,  $SI = 0$  is in equilibrium and when  $SI > 0$ , the solution is supersaturated, and precipitation occurs spontaneously (Pastor et al., 2010).

The decrease of SI or solution pH promotes an increasing contribution of aggregation. With the growth of aggregates, cluster-cluster aggregation gradually starts to dominate the evolution process, giving rise to more fractal aggregates with a more elongated shape and rougher surface (Ye et al., 2014) ( see Figure 4).

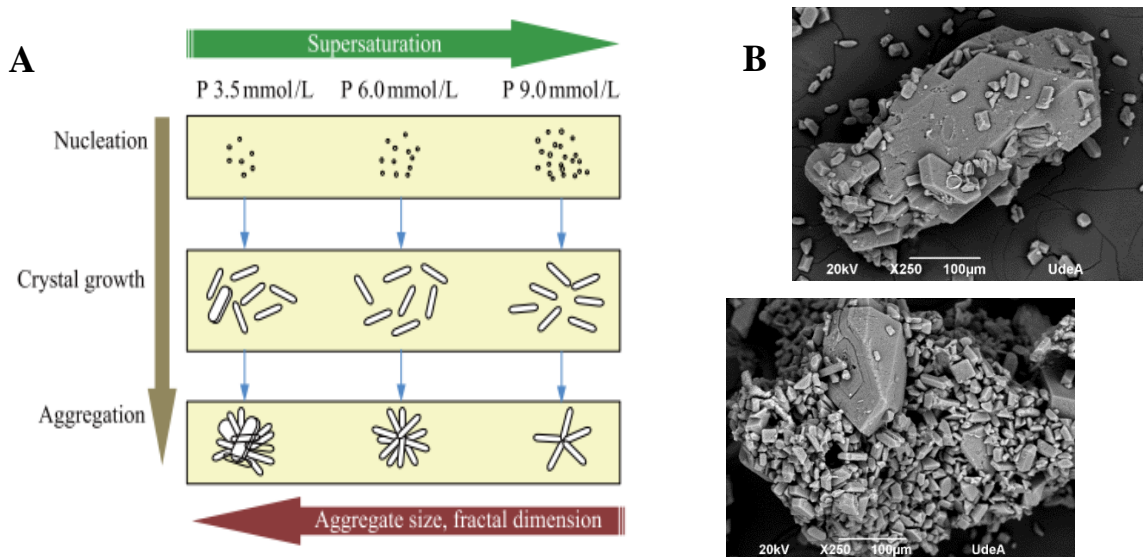


Figure 4. Schematic illustration for the formation of struvite aggregates at constant pH. (A) Taken from Ye et al. (2014) and B. Struvite crystals formed in this research.

Some studies consider that the main factor that affects struvite precipitation is the pH (the supersaturation increases with a rise in pH) it is because pH affects not only the amount of struvite

precipitation but also its purity, so it is a parameter to be optimised or adjusted by using a strong base or using air separation. Although struvite can form in a pH range of 7 to 11, the suitable pH range is 8.0 to 9.5 (Kim et al., 2017). According to Guadie et al.(2014), pH > 9.5 nitrogen removal increases mainly due to loss of ammonia by stripping instead of struvite formation.

Temperature and other ions in the solution, such as calcium ( $\text{Ca}^{2+}$ ), can also affect the crystallisation of struvite (Pastor et al., 2010). Temperature influences the struvite solubility product, and the presence of calcium can imply a competition between the precipitation of struvite and calcium phosphate (Wang et al., 2009). In solutions containing calcium, magnesium, ammonium, and carbonate, hydroxyapatite, calcium phosphate, calcite ( $\text{CaCO}_3$ ), and dolomite ( $\text{CaMg}(\text{CO}_3)_2$ ) may precipitate, which could reduce the efficiency of struvite nutrients recovery (Le Corre et al., 2007; Pastor et al., 2010). According to Acelas et al.(2015) Ca interfered in struvite precipitation only when this is in equal or greater molar ratios to Mg, while Al inhibited the production of struvite completely even at lower aluminium molar ratios to magnesium. For example, in this research, the co-precipitation of other amorphous compounds, mainly Al and Si, was observed together with the struvite crystals (Figure 5).

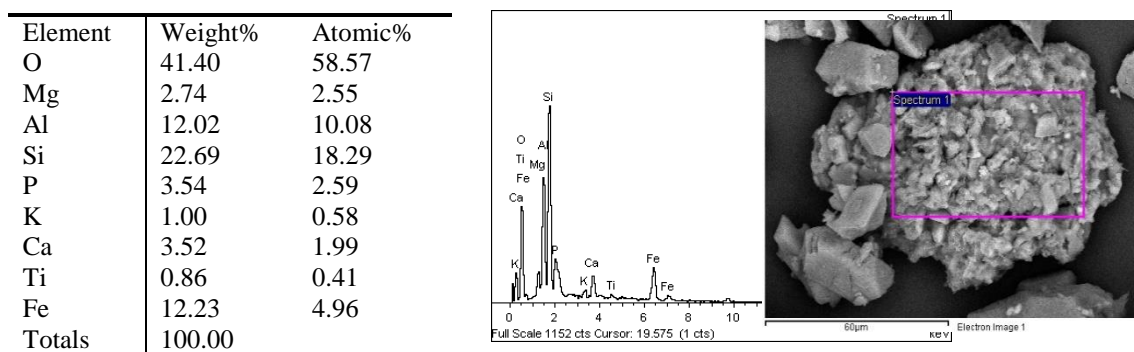


Figure 5. Co-precipitation of some metals with struvite crystals (SEM-EDX Analysis of this research).

### 1.3.3 Reactors used in the struvite crystallisation

The technologies developed for the recovery of struvite can be broadly classified as precipitation in a stirred reactor, precipitation in a fluidised bed reactor (FBR), and an air stirred reactor (Le Corre et al., 2009). FBRs are currently the most commonly investigated reactors for struvite crystallisation (Li et al., 2019).

FBRs and air-stirred reactors are essentially circular/cylindrical tanks that promote upward flow of the liquid by injecting feed through the bottom of the reactor (Fattah, 2012). They usually consist of a vertical column with the seed material inside on which the struvite will precipitate. Growth in aerated reactors will occur due to the interaction of the particles (agglomeration), while in FBR, it will be conducted by contact with the seed materials that constitute the initial seedbed (Le Corre et al., 2009).

The continuous stirred tank reactor (CSTR) is one of the most widely used industrially for crystallisation processes, mainly because it is a simple and flexible technology, easy to implement, and capable of absorbing fluctuations in operating conditions (Pastor et al., 2008); however, some authors consider that the FBR and the air-stirred reactor having the advantage of producing larger struvite particles (Shim et al., 2020) that improve its the efficiency of downstream processes like

settle ability, filtering and drying and favour its subsequent application as a fertiliser (Shaddel et al., 2019).

Currently, there are different patented technologies for the crystallisation of struvite. These reactors mainly differ in their mode of operation (continuous or discontinuous), type of waste (digested sludge, wastewater, centrate, etc.), place of application (industrial plant, WWTP), characteristics of the struvite obtained (fine or large particles) and type of Mg source used (MgCl, MgO, etc.).

CSTR reactors include PHOSPAQ™ and ANPHOS® processes, developed in the Netherlands and implemented in potato processing companies and NuReSys developed by the Belgian company Akwadok. The NuReSys process differs from the ANPHOS process since it is operated in continuous mode instead of a batch at a lower residence time. FBR reactors include Phosnix, The Ostara Pearl™ and Crystalactor® and between air-stirred reactor is Airprex®. The Phosnix process was developed in Japan by Unitika Ltd Environmental and Engineering Div. A crystal retention time of 10 days allows the growth of pellets between 0.5 and 1.0 mm in size, after which they are purged from the bottom of the reactor column. The Ostara Pearl process was developed at the University of British Columbia (Canada) and held a US Patent. The process has the advantage of allowing large struvite pellets from 1.5 to 4.5 mm in diameter. The Crystalactor was initially developed in the early 1980s by the Dutch consultancy and engineering company DHV to remove calcium (hardness) from drinking water, and the AirPrex® technology was developed and patented by the Berliner Wasserbetriebe after massive incrustations were found in the sludge dewatering lines of some WWTPs, downstream of anaerobic sludge digestion (Desmidt et al., 2014).

### 1.3.4 Main uses of struvite

Struvite has many uses, the most common being as a raw material for the fertiliser industry. Besides, it can be used as a material for cement, and if developed at low production costs, it could be used in the manufacture of detergents, cosmetics, and animal feed, all of which use phosphates (Wang et al., 2009). Struvite is an excellent fertiliser due to its low solubility in water and slow rate of release. Besides, it can be applied directly to soil (Guerra-Rodríguez et al., 2020).

Compared with other fertilisers of a commercial nature, struvite has several advantages. First, the plants can quickly incorporate the nutrients before they are leached, and therefore the application is less frequent. Second, impurities caused by heavy metals in recovered struvite are two to three orders of magnitude lower than commercial phosphate fertilisers (Bhuiyan et al., 2008; Ezquerro, 2010). Finally, the essential nutrients, phosphorus, nitrogen, and magnesium, are applied simultaneously (Bhuiyan et al., 2008).

### 1.3.5 Economic viability

Generally, wastewater contains less magnesium compared with phosphate and ammonium. Thus, it is necessary to supply a source of magnesium to promote the crystallisation of struvite. Besides, the reaction of struvite crystallisation causes a release of protons ions which could cause a pH drop. Therefore, an alkali source must be added to the crystallisation system to maintain the pH in a range suitable for struvite crystallisation (Crutchik et al., 2017). The use of magnesium sources such MgCl<sub>2</sub>, MgSO<sub>4</sub>, MgO, Mg(OH)<sub>2</sub> and alkali sources as NaOH can lead to high operating costs.

Costs of struvite production vary in each country due to the different prices of reagents, electricity, and transportation; for example, it is around \$140 per tonne in Australia and \$460 per tonne in Japan (Guo, 2010). The market value of struvite ranges from \$0 to \$1885 per tonne (Guo, 2010; Muys et al., 2021). In recent years, several studies based on struvite crystallisation have been carried out using

different low-cost magnesium sources to reduce the struvite production costs (Siciliano et al., 2020); however, according to Molinos-Senante et al. (2010), nutrient recovery from wastewater will be economically feasible by incorporating the benefits derived from avoiding the discharge of phosphorus to the natural environment. Eutrophication problems in waterways are estimated to cost \$2.2 billion in annual economic losses due to degraded environmental services (e.g. drinking water quality and recreation) (Bird, 2015).

In addition to the environmental benefits, the production of struvite brings with it internal benefits in the operation costs. Recovering 1 kg of struvite from a wastewater treatment plant will minimise sludge handling and disposal (Shu et al., 2006), prevent incrustation, reduce the cleaning, reduce centrifuges' maintenance, and improve the dewatering characteristics. Researchers estimate cost savings from \$ 500 to \$2500 for every 260 thousand gallons of wastewater treated with reduced maintenance and materials used to remove struvite scaling problems (Bird, 2015). Although currently, struvite is more expensive to produce than phosphate rock fertilizer, installation of a struvite recovery facility demonstrates positive economic returns when maintenance costs and environmental benefits are considered (Bird, 2015; Jia, 2014; Maaß et al., 2014).

### 1.4 Nutrient recovery within a circular economy

The circular economy (CE) is the concept in which products, materials (and raw materials) should remain in the economy for as long as possible, and waste should be treated as secondary raw materials that can be recycled to process and reuse (Ghisellini et al., 2016). CE distinguishes it from a linear economy based on the 'take-make-use-dispose' system, in which waste is usually the last stage of the product life cycle. CE promotes the sustainable management of materials and energy by minimising waste generation and reuses as secondary material (Neczaj & Grosser, 2018).

In December 2015, the European Commission adopted a Circular Economy Plan called "Closing the loop—an European Union (EU) action plan for the Circular Economy" (EU, 2015). It is a strategy to change the consumption model of European citizens towards a climate-neutral, circular economy, which would minimise the impact on the environment. This plan is mainly focused on reducing, recycling, and recovering waste, focusing on paper, ferrous metals, aluminium, glass, plastic, and wood. However, in context to the idea of "closing the loop", the circular economy can go beyond any sector, for instance, the wastewater treatment sector (Guerra-Rodríguez et al., 2020).

Colombia, for its part, launched in 2019 the first circular economy strategy in Latin America that seeks to guarantee sustainable consumption and production modalities through reducing the intensity in the use of materials and taking advantage of the opportunities of reuse and recycling (MADS, 2019). The reuse of wastewater, framed within resolution 1207 of 2014 (defines the allowable quality values for wastewater reuse), is within this national strategy.

In WWTPs, the objectives have generally been removing carbonaceous organic matter, suspended solids, chemical pollutants, excess nutrients and pathogens before disposing of the effluents to the environment (Tchobanoglous et al., 2015). However, recycling resources such as nutrients through recovery processes is an emerging objective due to environmental and economic motivations such as reducing drinking water consumption and generating revenue for the WWTPs (Mehta et al., 2015; Rao et al., 2017).

Nutrient recycling from WWTPs has a positive impact on the environment by reducing the demand for conventional fossil-based fertilisers and, consequently, the consumption of water and energy. It is possible to recover nutrient from raw wastewater, semi-treated wastewater streams and sewage sludge



(biosolids). Phosphorus recycling from wastewater, beyond directly land application, can be achieved through technical recycling from sewage sludge, wastewater, and ashes of incinerated sludge. Another option for nutrient recovery is urine separation from the main wastewater stream. It is estimated that about 70–80% of nitrogen and 50% of phosphorus is contained in urine, which can be theoretically recovered on the level of 70% using the urine-collecting system in toilets (Batstone et al., 2015). Figure 6 shows the general circular economy scheme applied to recycling and reusing waste generated in cities (including all nutrient-rich waste from a WWTP). The figure shows how from a circular economy model, WWTPs will be replaced by water resources recovery facilities (WRRF). In line with this, wastewater should not be considered a "waste" anymore but a resource (World Bank, 2019).

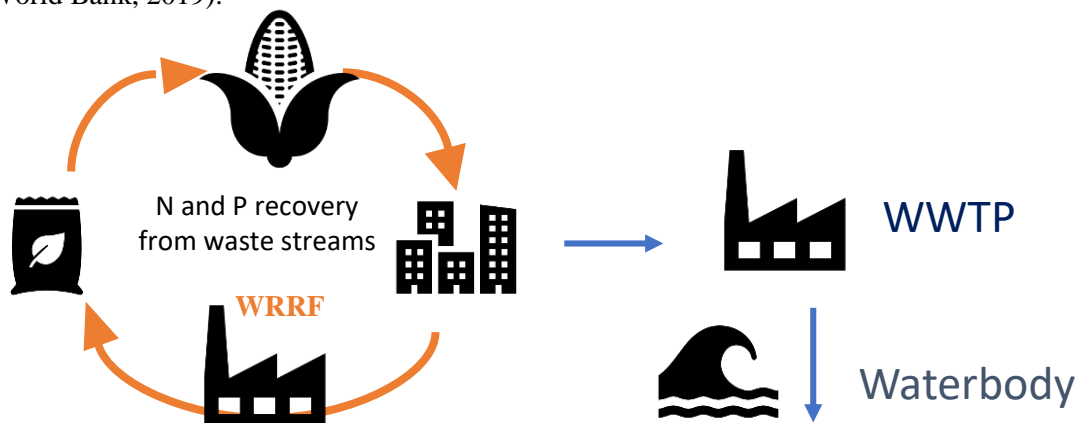


Figure 6. Circular economy model through nutrient recovery: orange lines (circular economy) and blue lines (linear economy). WRRF are water resource recovery facilities.

A transformation from linear nutrient flows towards a circular nutrient economy can serve numerous societal and environmental objectives. The replacement of mineral fertilisers with recycled ones can increase efficiency in the use of materials and energy for food production. If the quality of the recycled fertilisers can be guaranteed, the products can significantly enhance food safety (Valve et al., 2020).

Struvite has proven to be an excellent eco-friendly fertiliser due to its low solubility in water and low release rate that reduces the environmental impact that produces the traditional fertiliser (due they run off and accumulates in groundwater and surface waters, leading to eutrophication). Struvite also minimises nitrous oxide ( $N_2O$ ) emissions that is a greenhouse gas and may contribute to the destruction of the stratospheric ozone when converted to nitric oxide (Therogowda et al., 2019). Therefore, struvite, as eco-friendly fertiliser, can reduce the pressure on phosphate rock and be used in a circular economy, contributing to more sustainable fertiliser production.

In Europe, struvite is not yet recognised as fertiliser, and therefore a special admission of the national government is necessary to obtain status as fertiliser. If the national government does not give the special admission, struvite is considered a waste. Therefore, the distribution of the produced struvite as fertiliser in agriculture is often a bottleneck. Of the full-scale techniques, only the struvite products of Pearl and NuReSys (respectively Crystal Green and BioSTRU) are certified as fertilisers in the United States/United Kingdom and Belgium, respectively (Desmidt et al., 2014).

Recently in Colombia, in September 2020, the document CONPES 4004 was published, which covers the strategies in the 2020-2025 period for the application of the circular economy in the management of wastewater and drinking water services. National policies include increasing wastewater treatment,

analysing the use of by-products, improving conditions for reuse, and encouraging community participation (DNP et al., 2020). However, due to the few studies on nutrient recovery in the region, struvite is not within the country's strategies, and it is not considered a fertiliser within the NTC 5167 fertiliser Colombia standard (ICONTEC, 2011).

According to Cardoso et al.(2019), the principal current barriers related to P and N recovery implementation on WWTP are: economic, political, institutional, social and technical. Between economic aspects are the uncertainties in return on investment and the low cost of phosphate rock and fertilisers. The political aspects are: No common interest; the integrated approach is missing concerning recycles per country; fertiliser regulations involving implementing P recovery technologies; regulations on installing P recovery technologies; recovered P product guidelines. The social aspects are: negative public opinion due to the uncertainties of health issues; safety concerns; low awareness among farmers about struvite. The technical aspects are product safety is unclear; low solubility of struvite; struvite is not a stand-alone product; negative chemical characteristics of struvite; low maximum recovery yield.

Therefore, the recovery of nutrients such as struvite within a circular economy requires joint work on technical, social and political aspects. The transformation to nutrient recycling cannot be created, or its benefits attained, without careful tailoring of policy mixes that restrict inefficient nutrient use and generate demand for recycled fertilisers (Valve et al., 2020). Further studies regarding its technical feasibility in developing countries such as Colombia and greater educational strategies for the acceptance of products recovered from waste are essential aspects to consider.

### 1.5 Problem statement and research objectives

The LACR still faces significant problems in sanitation; approximately 77% of the population lacks safe sanitation. Therefore, the work in the region has focused mainly on expanding sanitation coverage and not on implementing strategies for the removal or recovery of nutrients and energy from wastewater. However, the world may face a future shortage of phosphorus in the next 70 to 150 years (Li et al., 2018), whereas the uncontrolled discharge of nutrients has caused serious eutrophication problems in water bodies. Therefore, different physical-chemical and biological techniques to remove and recover nutrients have been proposed over the years; among them is the precipitation of struvite. Although uncontrolled precipitation of struvite can cause technical problems in WWTPs, it has proven to be an eco-friendly fertiliser used in a wide variety of crops.

Besides, previous research has shown that in environmental terms, it is better to remove and recover nutrients in a WWTP than only to remove them (Burgos, 2018). It is due to lower environmental impacts associated with eutrophication and ecotoxicity of freshwater. It reduces the impacts caused due to the implementation of a biological nutrient removal system that demands high levels of energy and increases greenhouse gas emissions. Also, by-products such as struvite and biosolids reduce the impacts generated by the production of synthetic fertilisers (Burgos, 2018).

Then, the nutrients recovery from domestic WWTPs brings technical, environmental and economic benefits, and it can represent a solution for the future world food security crisis and an excellent option for developing countries as Colombia, where despite the low level of sanitation, the percentage of treated wastewater has increased by 34.6% from 2002 to 2017 and will reach 68.6% by 2030 (CRA & Minvivienda, 2019).

While the crystallisation of ammonium struvite has been widely studied worldwide, research conducted in LACR has been limited, so it is considered necessary to evaluate the possibility of recover nutrients as struvite in the current and future conditions of a WWTP located in this region. Therefore, this research will evaluate the struvite crystallisation process applied to the thickening and dewatering sludge supernatants (centrate) from the first secondary type treatment plant in Colombia, the San Fernando WWTP (Itagui, Colombia).

### 1.5.1 Research question and hypothesis

This doctoral thesis aims at bringing innovation and knowledge on the recovery of essential macronutrients (phosphorus, nitrogen and magnesium) from waste streams, specifically, the sustainable recovery of struvite fertiliser from real sludge thickening and dewatering centrates of a WWTP. Therefore, the proposed research question is:

*Is it possible to recover P and N from the centrates of a conventional activated sludge WWTP via struvite precipitation?*

We raised several research hypotheses to answer this question:

- In a conventional activated sludge WWTP, a significant fraction of phosphorus and nitrogen remains in the sludge thickening and dewatering centrates.
- The stirring speed improves the efficiency and quality of the precipitated struvite in a continuous stirred tank reactor.
- There are an optimal pH and temperature value that improves the efficiency of nutrient recovery through struvite crystallisation and improves the quality of the precipitated product.
- It is technically feasible to recover nutrients such as struvite from centrates with low P concentrations.
- Aeration applied to struvite crystallisation reactors reduces the amount of NaOH required, and the seed material improves the efficiency of nutrient recovery and the size of the precipitated product.
- The type of reactor used to crystallise struvite (CSTR or FBR) influences the efficiency of the process and the quantity and quality of the recovered product.
- The struvite obtained from a conventional WWTP applied to a conventional crop presents yield efficiencies comparable or superior to other commercial fertilisers.
- The struvite obtained from sludge dewatering and thickening centrates act as a slow-release fertiliser.

### 1.5.2 Objectives

The present work has been mainly focused on evaluating the technical feasibility of a recovery system of macronutrients (N and P) in the liquid fraction (centrate) from the sludge dewatering and thickening of a WWTP in Colombia using the struvite crystallisation process.

This PhD thesis is outlined according to the objectives and hypothesis in various chapters and are all connected to achieve the main goal of sustainable recovery of struvite from the centrate of a WWTP.

The specific objectives of the PhD are as follows:

1. Characterise the nitrogen and phosphorus fluxes by developing a mass balance in the different treatment stages of the selected WWTP (chapter 2).
2. Evaluate the effect of operating variables (stirring speed, pH, temperature, P concentration, seed material and aeration) and the type of reactor (CSTR and FBR) on the efficiency of the

struvite crystallisation process applied to real centrates in terms of quantity and quality of nutrients recovered (chapters 3,4 and 5).

3. Evaluate the quality of the produced struvite as fertiliser compared with biosolid and commercial fertilisers (chapter 6).

## 1.6 Thesis Context

The Ph.D. student was beneficiary of the COLCIENCIAS grant-647 and the ENLAZA MUNDOS program 2017 for the partial funding of your research internship and this work was funded principally by the Grupo de investigación en gestión y modelación ambiental-GAIA research group from Universidad de Antioquia and partially by the Grupo interdisciplinario de estudios moleculares-GIEM group also from Universidad de Antioquia, Bio resource Systems research group from University of Leeds and IRTA research institute under CERCA Program and the Consolidated Research Group TERRA (ref. 2017 SGR 1290), both from the Generalitat de Catalunya, as well as INIA support, from Gobierno de España, through the research project PIONER (ref. RTA2015-00093-00-00).

This thesis is a compendium of five published, sent and unpublished articles to different indexed journals. Most of the chapters have been presented at different national and, international congresses, chapter 3 and 6 have already been published and chapter 4 has already been submitted to an international journal. The list of conferences and the publications that have been made are presented below.

### 1.6.1 Congresses

1. González, C., Camargo-Valero, M.A., Molina, F., Fernández, B. Effect of stirring speed on the formation of struvite crystals using centrates from a sewage sludge anaerobic digester. *XIII Taller y Simposio Latinoamericano de Digestión Anaerobia*. 21 al 24 de octubre de 2018, Medellín, Colombia
2. González-Morales, C., López, D., Acevedo, C., Peláez, C. & Molina-Pérez, F. Cristalización de estruvita: Una oportunidad para recuperar nutrientes de las aguas residuales. *EXPORESIDUOS 2018-X* Feria y seminario internacional Gestión integral de residuos sólidos y peligrosos. 14-16 noviembre 2018, Medellín-Colombia.
3. González-Morales, C., Camargo-Valero, M., Fernández, B., López, D., Peláez, C. & Molina-Pérez, F. Effect of temperature and stirring speed on struvite precipitation using real centrates from sewage sludge anaerobic digesters. *16<sup>TH</sup> IWA World conference on anaerobic digestion*. 23-27 June 2019, The Netherlands.
4. González C, Fernández B, Molina F, López D, Peláez C, Camargo-Valero M. Nutrients Recovery from Wastewater by Struvite precipitation: Influence of pH and Temperature. In: *3<sup>Rd</sup> IWA Resource Recovery Conference*. 8-12 september, Venice, Italy; 2019:586-587.
5. González-Morales, C. “Recuperación de Macronutrientes (N Y P) de Los Centrados de Deshidratación de Una PTAR.” *II Encuentro Nacional de Estudiantes de DOCTORADO EN INGENIERÍA*, edited by Minciencias, 16-18 de septiembre, ACOFI, Bogotá, Colombia, 2020, pp. 225–32.
6. ---. “Recuperación de Nutrientes de Las Aguas Residuales Mediante Cristalización de Estruvita.” *I Congreso Internacional Para El Tratamiento y Reuso de Efluentes Industriales*, APETRAMA; CITREA SAC; ITAMA SAC, 23 al 26 de septiembre de 2020, Lima, Perú.

7. González-Morales, Carolina, et al. “Nutrients Recovery (N and P) as Struvite from Digested Sewage Sludge Using a Continuous Crystallization.” *Latin American Meetings on Anaerobic Digestion*, vol. Chile Sess, 22<sup>th</sup> and 29<sup>th</sup> October and 5<sup>th</sup> and 12<sup>th</sup> November, 2020, pp. 5–8.
8. González, C., Molina, F., Fernández, B., Camargo-Valero, M.A., Peláez, C. The determination of fertiliser quality of the formed struvite from a WWTP centrate. **2<sup>nd</sup> Latin American and Caribbean young water professional conference**. 8<sup>th</sup>-12<sup>th</sup> November 2020, Manizales, Colombia.

## **1.6.2 Publications**

Peer-reviewed papers publications presented as chapters (3 and 6) of this PhD thesis, and the candidate PhD contribution is listed below:

González-Morales, C., Camargo-Valero, M. A., Molina-Pérez, F. J., & Fernandez, B. (2019). Effect of the stirring speed on the struvite formation using the centrate from a WWTP. *Revista Facultad de Ingeniería*, 92(92), 9–17. <https://doi.org/http://dx.doi.org/10.17533/udea.redin.20190518>

**Author’s contribution:** Experimental design and performance. Data monitoring and operation. Writing the paper.

C. González, B. Fernández, F. Molina, M. A. Camargo-Valero, C. Peláez; The determination of fertiliser quality of the formed struvite from a WWTP. *Water Sci Technol* 15 June 2021; 83 (12): 3041–3053. doi: <https://doi.org/10.2166/wst.2021.162>

**Author’s contribution:** Experimental design and performance. Data monitoring and operation. Writing the paper

## Chapter 2. Nutrient mass balance (N, P) and recovery potential in San Fernando WWTP

### Highlights

- The steady-state mass balance applied to the San Fernando WWTP allowed observing the nutrients behaviour inside the WWTP. The overall N and P mass balances present relative errors of 6.67% and 28%, respectively.
- The centrate recirculation represented 17% of influent TKN-N loading and 14 % of influent P loading.
- The low concentration of orthophosphates found in the centrates ( $<17 \text{ mg P. L}^{-1}$ ) could limit the precipitation of struvite in a conventional WWTP with secondary treatment. However, under a process of biological removal of P, nutrients recovery as struvite precipitation could be feasible.

### Abstract

Recycling resources such as nutrients through recovery processes is an emerging trend in Waste Water Treatment Plants (WWTPs) due to environmental concerns and economic incentives. In this regard, struvite crystallisation is one of the most widely used methods for the simultaneous recovery of nitrogen (N) and phosphorus (P), suitable to produce fertilisers. This trend is still incipient in Latin America and the Caribbean region (LACR), where investigations on this subject are limited due to a focus on expanding sanitation coverage and the existence of few WWTPs with the capacity to remove nutrients. However, resource recovery approaches can provide benefits beyond the wastewater treatment sector, improving the sustainability of wastewater treatment operations and generating revenue for the utility provider. Therefore, this study evaluated the potential to recover nutrients as struvite in the San Fernando WWTP (Colombia), using a nutrient mass balance (N, P) through the plant internal liquid and sludge flows. Results show that in this conventional WWTP with secondary treatment, the sludge thickening and dewatering supernatant (F9 and F13, respectively) are the liquid streams with the highest concentration of N and P, and their recirculation represents 17 and 14% of the initial loading of N and P in the influent, respectively. Although the orthophosphate concentration in both centrates was relatively low ( $12.9$  and  $17.5 \text{ mg PO}_4^{3-}\text{-P. L}^{-1}$ ) and the struvite precipitation could be limited, further studies are required at the laboratory level to assess its technical feasibility. Besides, under the future P biological removal in the WWTP, struvite precipitation could represent an economically and environmentally sustainable source of nutrients.

**Keywords:** nutrients recovery; struvite; centrate; nutrients loading

**Note:** This manuscript will be submitted to a national journal.

## 2.1 Introduction

The objectives of WWTPs have generally been the removal of carbonaceous organic matter, total suspended solids (TSS), chemical pollutants, excess nutrients and pathogens before disposing of the effluents to the environment (Tchobanoglous et al., 2015). However, recycling resources such as nutrients through recovery processes is an emerging goal due to environmental and economic

motivations such as reducing drinking water consumption and generating revenue for the wastewater treatment works (Mehta et al., 2015).

In the LACR, nutrient removal and recovery strategies in wastewater have been limited, mainly because 77% of the population remains without access to improved sanitation and only 20% of wastewater is treated (Cardoso et al., 2019; WSP, 2013). However, there is an opportunity to increase sanitation access by building new treatment plants and upgrading existing plants with the simultaneous implementation of nutrient recovery strategies in these facilities.

The main motivations for recovering and removing nutrients from WWTP are: the reduction of nutrient discharges into water bodies to avoid eutrophication and human health issues (Cárdenas & Sánchez, 2013); the avoidance of a future shortage of phosphorus for fertiliser production in the next 100-150 years (Mehta et al., 2015; Shu et al., 2006); and the solution of operational issues caused by recirculation of nutrients in WWTPs.

In Colombia, for instance, the Porce II reservoir that receives the wastewater from the Aburrá Valley (Antioquia-Colombia) presents hypereutrophic conditions ( $P > 0.1 \text{ mg}\cdot\text{L}^{-1}$ ), which have generated an excessive increase of algae and aquatic macrophytes (*Eichhornia crassipes*) (Palacio et al., 2016). Besides, there are no policies in the country that restrict the discharge of nutrients to water bodies (Minambiente, 2015). However, sanitation coverage has increased, from 237 WWTP in 2004 to 682 in 2017 (CRA, 2019), and the country plans to build new WWTP that will include removal of nutrients, as the San Nicolás Valley WWTP and the upgrading process in San Fernando WWTP (Itagui-Antioquia) with a possible process of biological N and P removal (Martínez, 2017).

Phosphorus can be recovered as struvite ( $\text{MgNH}_4\cdot 6\text{H}_2\text{O}$ , MAP), hydroxyapatite ( $\text{Ca}_{10}(\text{PO}_4)_6(\text{OH})_2$ , HAP), sewage sludge and sewage sludge ash. However, P recovery as struvite is very promising and preferred due to its value as agricultural fertiliser comparable in performance to commercial fertilisers. Struvite crystallisation also helps to reduce chemical inputs in WWTPs as it reduces sludge generation, handling and transport when recovered in a granular form. Struvite is a slow-release fertiliser, requiring less frequent applications, showing decreased nutrient loss via surface run-off and containing low amounts of heavy metals and pathogens (Adelagun, 2016; Doyle & Parsons, 2002).

The recovery of nutrients as struvite has been widely studied in WWTP with Enhanced Biological Phosphate Removal (EBPR) because in this type of process, more than 95% of P is transferred to the sludge, and about 20% of that amount appears in the centrate generated by dewatering of the digested sludge (Jenkins & Wanner, 2014). Unfortunately, the continuous recirculation of the dewatering centrate/filtrate reduces the efficiency of phosphorus removal, increases operating costs, and in some cases, results in increased nutrient concentrations in the final effluent (Holloway et al., 2007; Yuan & Kim, 2017). Also, some of these WWTPs have reported encrustation by uncontrolled struvite precipitation that increases pumping and maintenance cost and reduces the plant's overall capacity due to losses in hydraulic capacity (Fattah, 2012).

Few studies report the recovery of nutrients through struvite precipitation from centrates in WWTPs without EBPR, mainly due to the lower nutrient concentration. Nevertheless, Fattah et al. (2008) reported over 77% of phosphate recovery by struvite precipitation from centrate with filter press of a secondary wastewater treatment plant, while Kumar et al. (2013) reached 83% of P removal by struvite precipitation from wastewater with low orthophosphate concentration ( $22 \text{ mg P}\cdot\text{L}^{-1}$ ).

Given the importance of nutrient recovery from wastewater to improve the sustainability of WWTPs and the lack of research in this field in developing countries, this research aims at evaluating the

potential recovery of nutrients as struvite from a conventional WWTP by developing a mass balance of N and P over all the plant's liquid and solid flows.

Mass balancing applied to a conventional activated sludge WWTP allowed estimating the nutrient loads in all the flows of the WWTP, determining the main exit routes of nutrients, defining the possibility of recovering nutrients such as struvite under current and future conditions of the WWTP, and proposing possible modifications in the WWTP for the more significant technical feasibility of a recovery process.

## 2.2 Materials and Methods

### 2.2.1 Description of the full-scale wastewater plant

The San Fernando WWTP (SF-WWTP) is in Itagüí-Colombia and is operated by the EPM group. San Fernando is the first secondary-type WWTP built in the country. This plant treats a mixture of domestic and industrial wastewater coming from a population equivalent (p.e.) of 700,000 inhabitants, that corresponds approximately to 20% of the wastewater generated in the metropolitan area of the Aburrá Valley (south side: Itagüí, Envigado, Sabaneta and La Estrella municipalities) (Figure 7). The treated effluent discharge into the Medellín River. The WWTP started operations in May 2002 with an installed capacity of 1.8 m<sup>3</sup>/s. However, today the plant treats around 1.36 m<sup>3</sup>/s. The design load is 32.7 tons of BOD<sub>5</sub>.day<sup>-1</sup> and 59.1 tons.day<sup>-1</sup> of TSS and currently removes an average of 26.5 tons.day<sup>-1</sup> of BOD<sub>5</sub> and 35.1 tons. d<sup>-1</sup> of TSS.

SF-WWTP water line consists of a pre-treatment (screening and de-sanding), primary treatment (primary sedimentation) and secondary treatment by activated sludge and secondary sedimentation to remove organic matter. In the sludge line, the secondary sludge goes through a centrifugal thickener for concentration. Afterwards, primary and secondary sludges mix before anaerobic digestion (AD) in two digesters of 8700 m<sup>3</sup> per unit. The digested sludge is stored and finally dewatered by centrifugation. The biogas generated in the anaerobic digestion process produces electricity that supplies an average of 30% of the plant's total electric demand. The supernatants from the sludge dewatering and thickening (centrates) are recirculated back to the water line before grit removal (Figure 8).

Currently, SF-WWTP is being upgraded with an improvement of its primary and biological treatments. An anaerobic reactor will be added to the current line (Bio-P), and a new line will be included with a Bardenpho five stages system (Martínez, 2017).



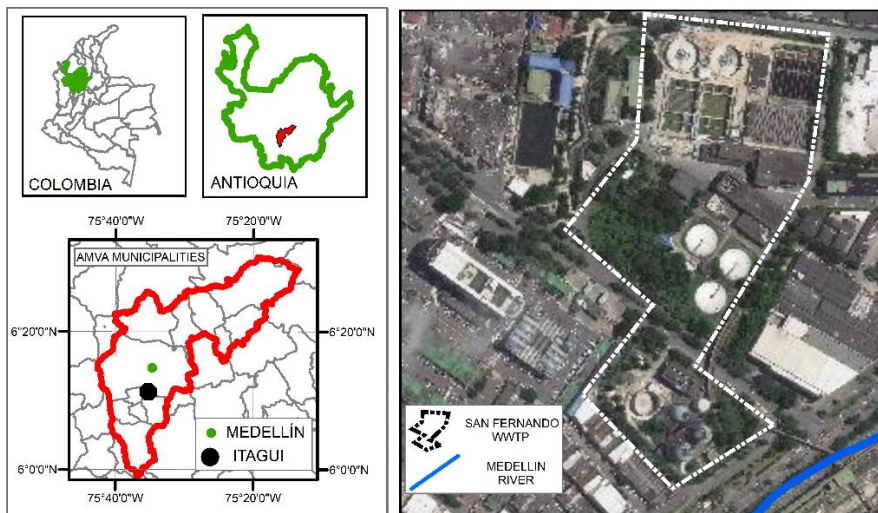


Figure 7. Location of San Fernando WWTP. Note: AMVA stands for the metropolitan area of Aburrá valley in Spanish.

### 2.2.2 Analytical methods

The WWTP was monitored during three intensive sampling campaigns (under three hydrological scenarios) since the sewerage system is of the combined type (wastewater and rainwater). The first set of measurements was performed during the 6th, 12th and 24th of October 2016 (matching a rainy season). The second set on the 2nd and 12th December 2016 (matching low rains). The third set was conducted on 31st January and 8th February 2017 (a dry season during La Niña conditions). 8-h time composite samples were taken from 15 wastewater and sludge flows identified in the WWTP (see Figure 8). The sampling frequency was 1.5 h.

Components in the wastewater and sludge were measured according to standard methods (APHA, 2017). Ammonium nitrogen ( $\text{NH}_4\text{-N}$ ) and total Kjeldahl nitrogen (TKN) were determined using the Kjeldahl method (standard code: 4500-NH<sub>3</sub>-Norg B), total phosphorus (TP) and ortho-phosphate ( $\text{PO}_4^{3-}\text{-P}$ ) using the ascorbic acid method (standard code: 4500-P E) and nitrites using the colourimetric method (standard code: 4500-NO<sub>2</sub>B). The solution pH and electrical conductivity were measured by an IQ Scientific Instrument pH/ conductivity meter (WTW Cond 3110). In the centrates (flows 9 and 13),  $\text{Mg}^{2+}$ ,  $\text{Ca}^{2+}$ ,  $\text{K}^+$ ,  $\text{Al}^{3+}$ ,  $\text{Fe}^{+2}$ ,  $\text{Ni}^{+2}$ ,  $\text{Pb}^{+2}$ ,  $\text{Cr}^{+2}$  and  $\text{Na}^+$  concentrations were determined by atomic absorption spectrometry (Thermo Scientific iCE 300 SERIES) (SM 3111B-D). Total solids (TS), TSS, total volatile solids (TVS) were determined by gravimetry (SM 2540), alkalinity by titrimetric method (SM 2320-B), COD and BOD by closed-flow and incubation method, respectively (SM5220-D).

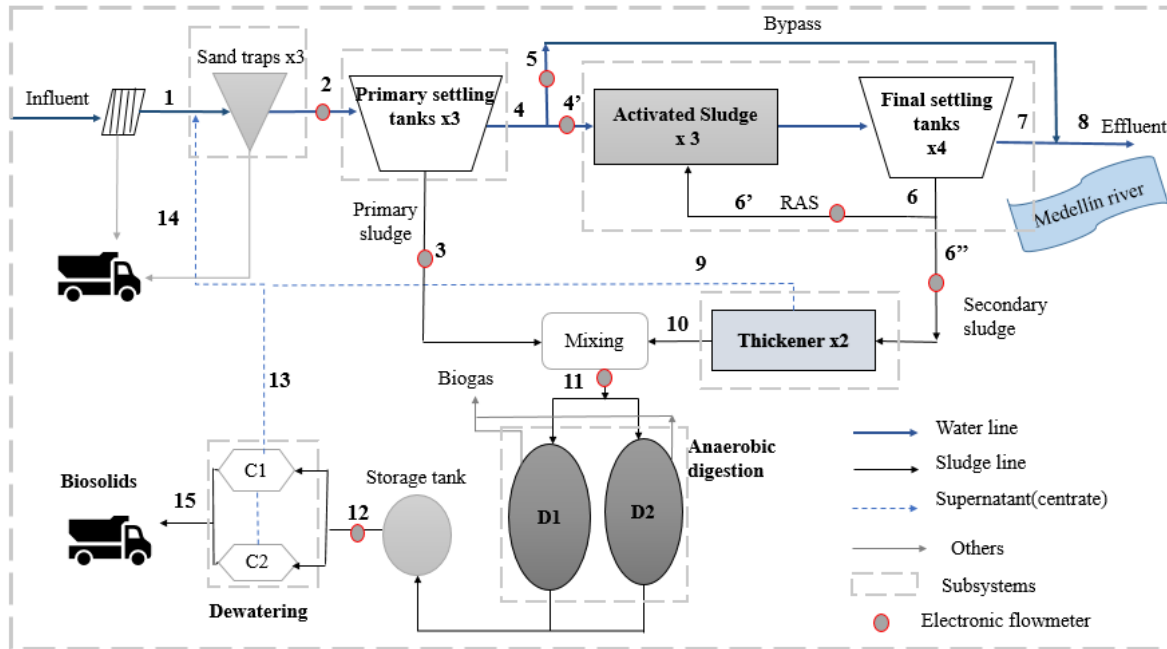


Figure 8. Flow diagram of full-scale SF-WWTP processes.

### 2.2.3 Mass balance calculation

A 'steady-state mass balance was developed in the overall system (the WWTP) and the subsystems (pre-treatment, primary settling tanks, activated sludge, thickener, anaerobic digestion and sludge dewatering) as is shown in Figure 8. In the overall system, the influent is the input (flow 1), and the outputs are the effluent and the biosolid. An additional output could be given in N mass balance due to the volatilisation of ammonium; however, this was not quantified.

According to Puig et al.(2008), phosphorus is a suitable parameter for mass balance evaluation since TP only follows the wastewater flows and does not leave the system via the gas phase. In this case, flow, TP and TKN mass balance were developed considering a stationary close system; this means that there is no mass transfer in the time interval studied, and there is no accumulation (Veverka & Madron, 1997).

TKN and TP mass balance were calculated by multiplying the mean concentration of TKN and TP of the 7-sampling campaigns by average daily flow rates. Some flow rates were measured in situ (2, 3, 4', 5, 6', 6'', 11 y 12) with an electronic flowmeter, but others were determined by the flow balance (1, 4, 6, 7, 8, 9, 10, 13 y 14) considering that  $Q_{in} = Q_{out}$ . The bypass (F5) composition was obtained from the mass balance between the primary settling effluent (F4) and activated sludge influent (F4'); meanwhile, the mixture of the centrates (F14) was calculated from the mass balance between centrates 9 and 13. The relative error for each subsystem was calculated as a percentage of the relation between the difference among measured and calculated values and the measured value (nutrient loading). The coefficient of variation (CV), expressed as a percentage, was defined as the ratio of the standard deviation to the mean. Figure 8 shows the WWTP configuration with the electronic flowmeter points marked with grey dots.

## 2.3 Results and discussion

### 2.3.1 Flows characterisation

The results of the measurement campaign are presented in Table 2. The overall in and outflow measurements were done to close the overall flow balance (**Figure 8**). High standard deviation values (SD) and high values of the CV were observed, especially in the biosolid flow (F15), indicating the high variability of the measurements. It was caused by the influent dynamics (domestic and industrial wastewater inputs and variation of flows due to seasonal changes).

**Table 2.** Measured data used for mass balance evaluation. Mean $\pm$ SD. Primary settling (PS), Secondary settling (SS), Thickener (T), Anaerobic digestion (AD), TP-CV and TKN-CV are the variation coefficient of TP and TKN concentration, respectively.

Flow	Units	PO <sub>4</sub> <sup>3-</sup> -P	TP	TP-CV (%)	TKN	TKN-CV (%)	NH <sub>4</sub> -N	Nitrites
Influent 1	mg/L	2.61 $\pm$ 0.92	7.20 $\pm$ 3.53	49	60.70 $\pm$ 10.65	18	21.25 $\pm$ 10.27	0.08 $\pm$ 0.07
In-PS 2	mg/L	3.54 $\pm$ 0.51	6.94 $\pm$ 2.09	30	59.09 $\pm$ 6.78	11	32.36 $\pm$ 6.78	0.08 $\pm$ 0.1
out-PS 3*	mg/Kg	-	6610 $\pm$ 3752	57	14198 $\pm$ 9624	68	4525 $\pm$ 2918	-
out-PS 4	mg/L	2.93 $\pm$ 0.97	5.79 $\pm$ 1.58	27	59.54 $\pm$ 9.62	16	41.17 $\pm$ 5.65	0.03 $\pm$ 0.01
out-SS 6*	mg/Kg	-	17403 $\pm$ 2815	16	83713 $\pm$ 17888	21	23146 $\pm$ 17888	-
out-SS 7	mg/L	0.60 $\pm$ 0.42	1.36 $\pm$ 0.82	61	49.97 $\pm$ 16.75	34	36.48 $\pm$ 7.94	0.06 $\pm$ 0.04
Effluent 8	mg/L	1.38 $\pm$ 0.68	2.95 $\pm$ 0.83	28	58.34 $\pm$ 15.47	27	36.64 $\pm$ 6.78	0.04 $\pm$ 0.04
centrate 9	mg/L	12.88 $\pm$ 9.62	38.53 $\pm$ 9.62	56	230.22 $\pm$ 63.28	27	51.77 $\pm$ 13.88	0.08 $\pm$ 0.06
out-T 10*	mg/Kg	-	15520 $\pm$ 5356	35	44997 $\pm$ 19007	42	15625 $\pm$ 2973	-
in-AD 11*	mg/Kg	-	9092 $\pm$ 4089	45	26093 $\pm$ 12829	49	6395 $\pm$ 4801	-
out-AD 12*	mg/Kg	-	14199 $\pm$ 1947	14	21922 $\pm$ 4877	22	22633 $\pm$ 3554	-
centrate 13	mg/L	17.50 $\pm$ 8.95	43.80 $\pm$ 8.95	29	1073 $\pm$ 266	25	771.4 $\pm$ 246.2	0.14 $\pm$ 0.06
Biosolid 15*	mg/Kg	-	7045 $\pm$ 6554	93	24696 $\pm$ 21009	85	9744 $\pm$ 1409	-

\*results on a dry basis. **Note:** In 2016, the mean BOD<sub>5</sub> concentrations in the affluent and effluent were 271 and 70 mg. L<sup>-1</sup>, respectively; meanwhile, COD concentrations were 730 and 194 mg. L<sup>-1</sup> (Information provided by SF-WWTP).

The results show that SF-WWTP presents a minimum reduction in TKN concentration (approx. 4 %) but an essential reduction of TP (59%). As explained previously, SF-WWTP was designed for the biological removal of organic matter, and in its initial design, the removal of nutrients was not considered. During secondary biological treatment, microorganisms use P for cell synthesis and energy transport. Consequently, between 10 and 30% of the P present is eliminated from the wastewater (Metcalf & Eddy, 1995). However, SF-WWTP has a sludge age of 2 days (high rate activated sludge); therefore, the synthesis of biomass is more significant than in a conventional activated sludge process (sludge age between 4-10 days; Von Sperling (2007)), which in turn may be the cause of further removal of P.

Due to this P and N removal, it could be feasible to recover these nutrients from some of the WWTP sludge flows, for example, from the thickening and dewatering sludge centrates (flows 9 and 13), the digested sludge (F12) or the biosolids (F15). The most common use of the biosolid is as a fertiliser, used directly or after a composting process, but its use may be limited due to the concentration of pathogens and heavy metals (Bedoya-Urrego et al., 2013). Considering the advantages of struvite to

recover nutrients, this research evaluated its recovery potential from thickening and dewatering sludge centrates of SF-WWTP.

To assess the potential to recover nutrients as struvite or as other possible precipitate, the centrates were characterised in terms of heavy metals, BOD<sub>5</sub>, COD, solids, pH, alkalinity and temperature. Table 3 summarises the main characteristics of the centrates. In addition, values of the Saturation Index (SI) for the most common precipitates in the anaerobic digestion (AD) process, according to Çelen et al.(2007), Hallas et al. (2019) and Marti et al.(2008), were calculated using the software visual Minteq v3.1. The SI describes the saturation state of the aqueous phase composition versus different solids that can precipitate. When SI = 0, the solution is in equilibrium; when SI < 0, the solution is undersaturated and no precipitation occurs; when SI > 0, the solution is supersaturated, and precipitation occurs spontaneously. Therefore, the SI values serve to evaluate the effect of the solution conditions on the tendency and extent of the precipitation, according to the following equation:

$$SI = \text{Log} \frac{IAP}{K_{sp}}$$

where IAP represents the ion activity product, and K<sub>SP</sub> represents the thermodynamic solubility product (Liu, 2018; Ye et al., 2016).

According to the characterisation of centrates (Table 3), the concentrations of K, Ca, Al, Mg, ammoniacal N and TKN were lower in the thickener centrate (F9) than in the centrate from digested sludge dewatering (F13). TP, Orthophosphate, BOD<sub>5</sub>, COD and solid concentration were similar in both flows, but alkalinity, pH and temperature were higher in the flow 13 (Table 3). The high variability observed in the concentrations of the centrates, especially Al, Ca and Mg, may be due to the contribution of industrial wastewater to the WWTP.

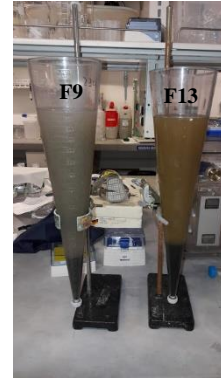
The difference in the centrates is due to the characteristics of the AD process that facilitates the mobilisation of nutrients from the organic matter to the liquid phase (Romero et al., 2016). In turn, complex organic N compounds are transformed to NH<sub>4</sub><sup>+</sup>-N in the digester as protein is degraded (Barat et al., 2009; Möller & Müller, 2012). However, the activated sludge has relatively low degradability in comparison with the primary sludge. The P release to the liquid phase occurs mainly in sludge that has a pre-treatment before anaerobic digestion (Carrère et al., 2010), or in the sludge from EBPR systems, where metal cations are taken up and stored as polyphosphates (Poly-P) inside the bacterial cells. During the AD, these Poly-P are released to the liquid phase by hydrolysis (Barat et al., 2009).

Regarding the SI, in F9 flow, struvite, dolomite and calcite presented a negative SI but hydroxyapatite (HAP) and amorphous calcium phosphate (ACP) presented a positive SI (Table 4). HAP is thermodynamically stable but has low formation speed and requires precursors as ACP to be formed first, which may explain its highest SI (Vasconcelos, 2013). Therefore, considering the low ACP SI in F9 (0.16), it is highly unlikely that both minerals can precipitate in this flow.

The positive SI for all the precipitates evaluated in F13 flow means that it is thermodynamically possible the precipitation of the evaluated minerals, due to the higher Mg, Ca, ammoniacal N and orthophosphate concentrations in F13 flow in comparison with F9. However, struvite SI in F13 is low (0.18) due to the low Mg and orthophosphate concentration, therefore its precipitation could be limited and it might not be economically feasible (minimum 50-60 mg. L<sup>-1</sup> of PO<sub>4</sub>-P according to Cornel and Schaum (2009)).

Table 3. Centrates characterisation

Measurements	Units	F9	F13
Ortho-phosphate	mg PO <sub>4</sub> <sup>3-</sup> -P. L <sup>-1</sup>	12.88 ± 9.62	17.50 ± 8.95
Ammoniacal N	mg NH <sub>4</sub> -N. L <sup>-1</sup>	51.77 ± 13.88	771.44 ± 246.24
Total phosphorus	mg P.L <sup>-1</sup>	38.53 ± 21.51	43.80 ± 12.54
Total Kjeldahl N	mg N.L <sup>-1</sup>	230.52 ± 63.19	1073.30 ± 63.19
Nitrites	mg NO <sub>2</sub> <sup>-</sup> -N. L <sup>-1</sup>	0.08 ± 0.06	0.14 ± 0.06
Total COD	mg O <sub>2</sub> . L <sup>-1</sup>	2696.67 ± 901.48	3478.33 ± 656.46
BOD <sub>5</sub>	mg O <sub>2</sub> . L <sup>-1</sup>	830.55 ± 716.17	865.28 ± 620.17
Al <sup>3+</sup>	mg Al. L <sup>-1</sup>	0.70 ± 1.21	0.23 ± 0.08
K <sup>+</sup>	mg K.L <sup>-1</sup>	23.46 ± 5.31	103.25 ± 35.63
Ca <sup>2+</sup>	mg Ca. L <sup>-1</sup>	46.59 ± 44.14	89.36 ± 95.42
Mg <sup>2+</sup>	mg Mg. L <sup>-1</sup>	14.35 ± 13.89	33.81 ± 32.44
TS	mg TS. L <sup>-1</sup>	1941.29 ± 943.99	2075.29 ± 893.24
Settling solids	mL.L <sup>-1</sup>	53.67 ± 38.48	10.74 ± 22.16
VS	mg VS. L <sup>-1</sup>	1661.79 ± 492.46	1624.43 ± 486.32
DS	mg DS. L <sup>-1</sup>	612.29 ± 168.17	789.07 ± 269.15
SS	mg SS. L <sup>-1</sup>	1885.42 ± 789.79	1791.67 ± 916.95
Temperature	°C	25.37 ± 0.83	32.33 ± 1.81
pH	-	7.01 ± 0.44	7.81 ± 0.41
Alkalinity	mg CaCO <sub>3</sub> . L <sup>-1</sup>	323.2 ± 139.4	4121.49 ± 259.63



Although the SI of the other precipitates is higher than struvite SI (Table 4), the high ammoniacal N concentration in this flow (mean 771.44 mg NH<sub>4</sub>-N. L<sup>-1</sup>) and the slow-forming kinetics of the precipitates evaluated (Çelen et al., 2007; Hallas et al., 2019) could reduce the probability of its formation. Furthermore, SF-WWTP has not reported yet issues of uncontrolled precipitation of struvite or other precipitates, which proves its improbable formation under the current conditions. Nonetheless, under the addition of a Mg source, the struvite SI will increase and the reaction will probably be possible, as was reported by Fattah et al.(2008) and Kumar et al.(2013).

Table 4. Saturation Index values (SI) in the centrates (Flows 9 and 13)

Mineral	F9	F13
Struvite	-1.991	0.176
Dolomite	-1.197	2.71
Hydroxyapatite (HAP)	7.605	10.981
Amorphous calcium phosphate (ACP)	0.165	2.262
Calcite	-0.245	1.589

### 2.3.2 Mass balance calculations

The strong dynamics in the influent characteristics and the full-scale operational conditions of the WWTP can cause a strong negative effect on the reliability of the measurements (Puig et al., 2010).

Furthermore, erroneous data could be detected after manually checking a conservative balance (i.e. TP balance) (Puig et al., 2008). Therefore, after the measurement campaign, we performed a manual and rigorous check to identify gross errors such as wrong labels in the database, wrong samples (method or place) or mistakes in laboratory measurements. After the gross error detection, in the study, we calculated the TP, TKN and flow balance based on the average of the seven campaigns (although the last two campaigns were in dry weather, the reduction in the influent flow was only 10%, allowing the averaging of nutrients and flow balance with the seven campaigns). Figure 9 and Figure 10 show the results of these calculations (abbreviations are explained in Table 2).

From the flow balance, we found that an average flow of  $1.25 \text{ m}^3 \cdot \text{s}^{-1}$  entered to primary treatment, from which 2.8% came from the centrate recirculation (F14). 84% of the secondary sludge was recirculated to the activated sludge process and only 16% was taken to the sludge treatment line. The bypass line represented 34% of the input flow and the thickener centrate (F9) flow rate was five times higher than that of the dewatering centrate (F13).

According to the P mass balance in SF-WWTP, the centrate (F14) represented less than 14% of the P loading that entered the primary settler. 43% of the initial P loading (influent) was removed in the activated sludge process, 30% was removed in the primary settling and 31% of this loading was accumulated in biosolids. 41% of the influent's P load left through the effluent (F8) and the bypass (F5) represented the 64% of this effluent loading. Although the P concentration of the dewatering centrate (F13) was slightly higher than that of the thickening centrate (F9) (see Table 3), the mass of P from F13 was 3.5 times less than that of F9, mainly due to its lower flow rate.

TKN mass balance shows that the centrate represented 17% of the N loading that entered the primary settler. The activated sludge process only removed 13.6 % of influent N loading, while 11.3% accumulated in biosolids. 95% of the influent's N load left through the effluent (F8) and the bypass (F5) represented the 34% of this effluent loading. Due to the high concentration of TKN in the F13, the N loading in the two centrates was very similar, although the flow rate of the F13 was much lower than that of the F9.

The RE of the overall P mass balance was 27.87%. The RE for each subsystem in P mass balance was less than 25% and the maximum relative errors occurred in the dewatering, thickening and activated sludge processes (Table 5). The overall N mass balance RE was 6.67 % and the maximum RE occurred in the thickening process (27%) (Table 6). These errors were mainly due to the normal variability of the data in the SF-WWTP. According to Puig et al., (2008) application of mass balances on WWTP data is difficult because the process is dynamic, and the variability of the influent loading is unknown. Even more, as reported by Meijer et al., (2002), mass balances on a WWTP never can be closed perfectly since measurements are never 100% accurate.

**Chapter 2.** Nutrient mass balance (N, P) and recovery potential in San Fernando WWTP

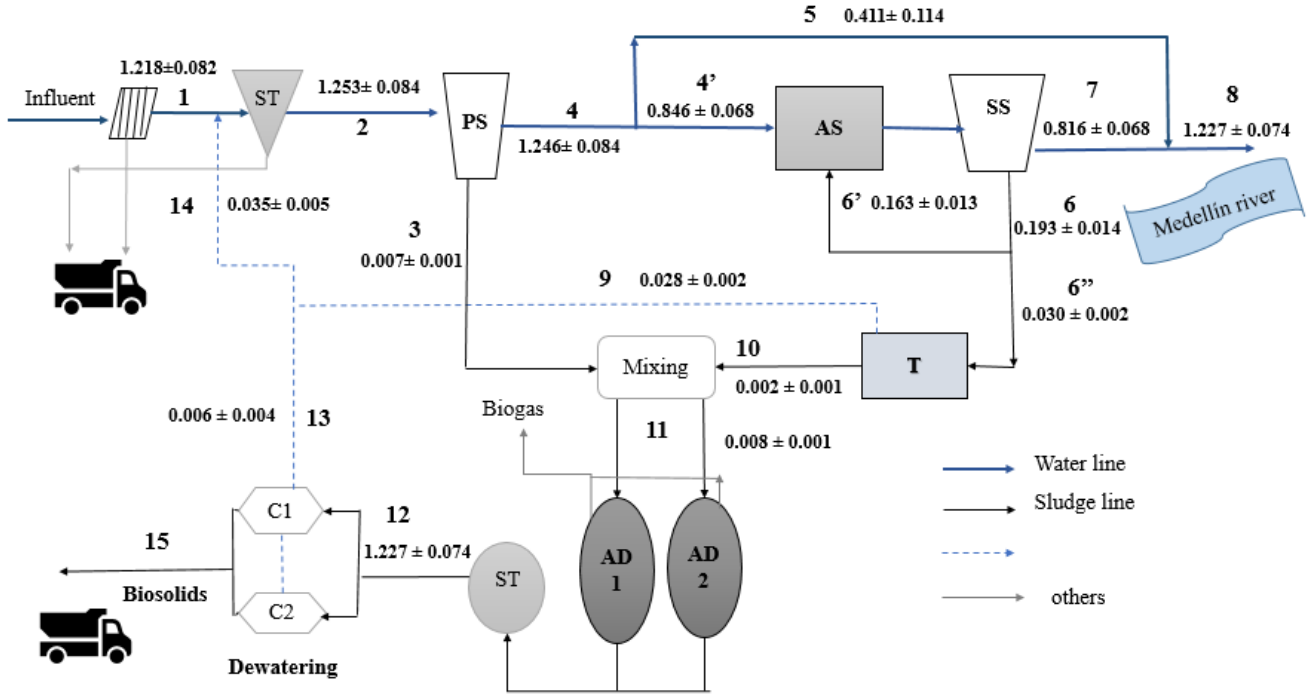


Figure 9. Mean flow balance in San Fernando WWTP (m<sup>3</sup>/s).

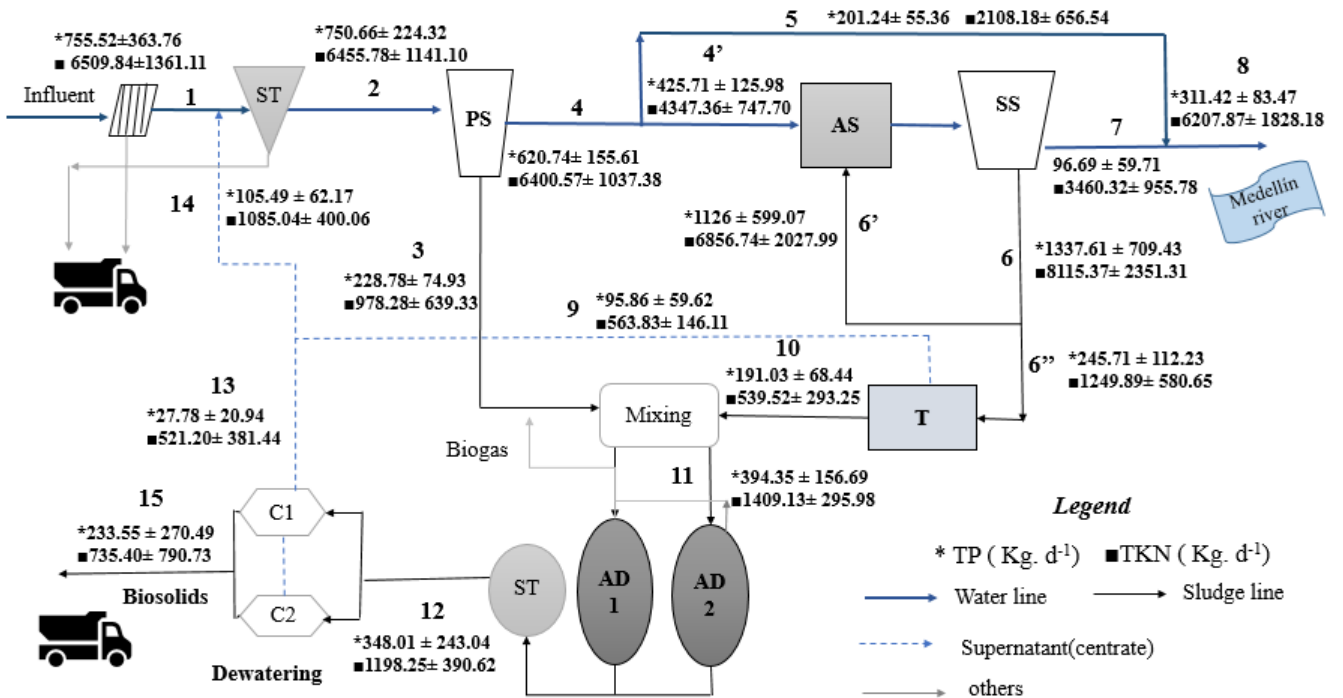


Figure 10. Nutrient mass balance in San Fernando WWTP. Nutrients loading (N, P) in each flow (Kg.d<sup>-1</sup>).

Table 5.Relative error (RE) in TP mass balance. PL is Phosphorus loading

Process	measured P loading (KgP.d <sup>-1</sup> )	Balance 1	calculated P loading 1 (KgP.d <sup>-1</sup> )	Balance 2	calculated P loading 2 (KgP.d <sup>-1</sup> )	RE 1 (%)	RE2 (%)
Influent	755.52	PL1=PL2-PL14	645.17			15	
Primary settling	750.66	PL2=PL4+PL3	849.52	PL2=PL1+PL14	861.01	-13	-15
Activated Sludge	425.71	PL4'=PL7+PL6"	342.40	PL4'=PL4-PL5	419.50	20	1
Effluent	311.42	PL8=PL7+PL5	297.93			4	
Thickener	191.03	PL10=PL6"-PL9	149.85	PL10=PL11-PL3	165.56	22	13
Anaerobic digestion	394.35	PL11=PL12	348.01	PL11=PL3+PL10	419.81	12	-6
Dewatering	348.01	PL12=PL13+PL15	261.33			25	

Table 6. Relative error (RE) in TKN mass balance. NL is Nitrogen loading

Process	measured value (KgN.d <sup>-1</sup> )	Balance 1	calculated value 1 (KgN.d <sup>-1</sup> )	Balance 2	calculated value 2 (KgN.d <sup>-1</sup> )	RE 1 (%)	RE2 (%)
Influent	6509.84	NL1=NL2-NL14	5370.74			17	
Primary settling	6455.78	NL2=NL4+NL3	7378.85	NL2=NL1+NL14	7594.88	-14	-18
Activated Sludge	4347.36	NL4'=NL7+NL6"	4710.21	NL4'=NL4-NL5	4292.40	-8	1
Effluent	6207.87	NL8=NL7+NL5	5568.50			10	
Thickener	539.52	NL10=NL6"-NL9	686.05	NL10=NL11-NL3	430.85	-27	20
Anaerobic digestion	1409.13	NL11=NL12	1198.25	NL11=NL3+NL10	1517.79	15	-8
Dewatering	1198.25	NL12=NL13+NL15	1256.60			-5	

The comparison of nutrient loadings for N and P in the different flows of the SF-WWTP shows that, in the influent, TKN loading is 8.6 times higher than the TP loading, while in the effluent this difference is 20 times higher. The maximum N and P loadings were present in the secondary sludge (F6) and the minimum in F13 (Figure 11). Although the main exit route of N and P was the effluent (F8), a significant accumulation of both nutrients occurred in the biosolids (F15).

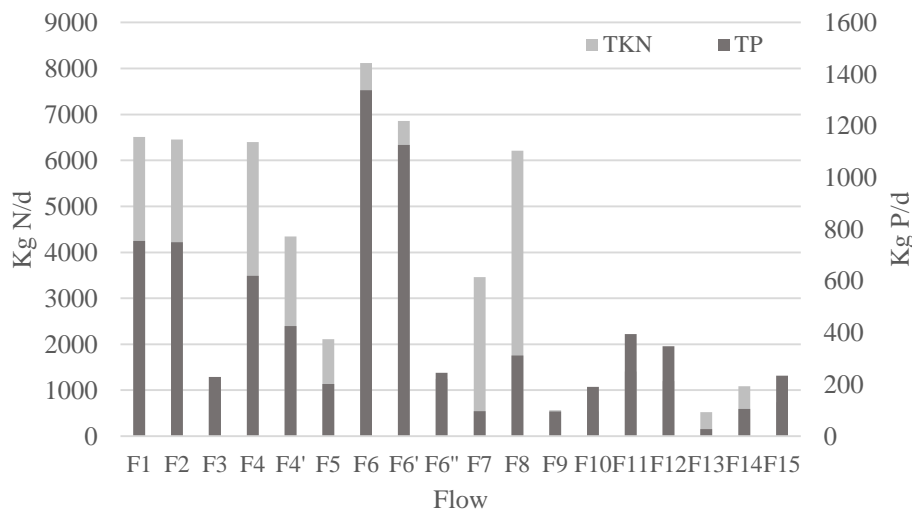


Figure 11. Nutrient loading in the flows of the San Fernando WWTP.



### 2.3.3 Comparison with other WWTP

Although in Colombia there are few WWTPs with tertiary treatment, in Europe the phosphate discharges must be limited due to an increasingly stringent regulation (permitted discharge concentrations between 1-2 mg. L<sup>-1</sup>-Council Directive 91/271/EEC), to protect surface waters from eutrophication. Therefore, in addition to the P removed by conventional treatment, approximately another 50% of the incoming phosphorus load has to be removed under different physicochemical or biological processes (Desmidt et al., 2014).

It has been proven that in WWTPs with biological phosphorus removal it is possible to recover nutrients from the liquid and sludge phase by struvite crystallisation (Desmidt et al., 2014; Romero-Güiza et al., 2016), but there are few studies that explore this possibility in WWTPs with another type of treatment. Therefore, in this research, we evaluated the nutrients loading at the influent and effluent of two WWTPs with chemical precipitation of P (La Llagosta in Barcelona-Spain and Esholt in Bradford-UK), and compared them with the SF-WWTP. The dewatering sludge concentrates of both WWTPs were also characterised to assess the potential to recover nutrients from these flows in comparison with some of the concentrates reported in the literature (Jia, 2014; Munch & Barr, 2001). The main results are presented in Table 7 and Table 8.

Table 7. Principal characteristics of affluent (In) and effluent (Out) from La Llagosta, Esholt and San Fernando WWTPs.

Value	La Llagosta		Esholt		San Fernando	
	In	Out	In	Out	In	Out
Q (m <sup>3</sup> . s <sup>-1</sup> )	0.33		3.24		1.22	
COD (mg O <sub>2</sub> . L <sup>-1</sup> )	400	54	704.4	46.4	730*	194*
TKN (mg N.L <sup>-1</sup> )	66.2	29	60.4	1.8	60.7	58.34
TP mg (P L <sup>-1</sup> )	8.1	1.1	6.4	1	7.2	2.95
Kg (P.d <sup>-1</sup> )	240	29	2022	452	755.5	311.4
Kg (N d <sup>-1</sup> )	1747	765	15594	30729	6510	6208

\*average for the year 2016(information provided by the WWTPs).

Table 8. Principal characteristics of sludge dewatering concentrate of the three WWTP evaluated, and some WWTPs reported in the literature.

Concentration (mg. L <sup>-1</sup> )	La Llagosta		San Fernando	Bolivar WWTP*	Others**
	Llagosta	Esholt	Fernando	WWTP*	Others**
K <sup>+</sup>	97	111	103.25	28.6	-
Ca <sup>+2</sup>	235	91	89.36	38	-
Mg <sup>+2</sup>	68	32	33.81	43	7-26
TP	10	12	43.8	-	110
PO <sub>4</sub> <sup>3-</sup> -P	3	2.5	17.5	235	44-293
TKN	891	1390	1073.3	-	-
NH <sub>4</sub> <sup>+</sup> -N	878	1080	771.44	643	500-820
TSS	77	512	1791.67		140-270

\*Taken from Jia (2014);\*\* taken from Munch & Barr (2000).

La Llagosta and Esholt WWTPs perform P removal by chemical precipitation, and only Esholt has a nitrification-denitrification process for the biological removal of N. Both present a high percentage of P removal (88 and 78%, respectively) and Esholt has a higher efficiency of N removal (80%). The Esholt flow rate is 2.6 times higher than that of SF-WWTP and 9.7 times higher than La Llagosta (Table 7). The influent TKN and TP concentrations were similar in the three WWTPs (mean 7.2 mg. L<sup>-1</sup> TP-P and 62 mg TKN-N L<sup>-1</sup>) and corresponds to the typical values found in wastewater (Qiu & Ting, 2014; Rojas, 2009). The main differences in the centrates are the higher Ca and Mg concentration in La Llagosta (due to the local water hardness), the highest TSS concentration in SF-WWTP (possibly due to the low dose of polymer applied in sludge dewatering), and the lowest orthophosphate concentration in Esholt and La Llagosta (due to the chemical precipitation of P that reduced the soluble P in the centrate). The main difference between the centrates of the WWTP evaluated with those of some WWTP with biological removal of nutrients is the lower concentration of soluble phosphorus.

Consequently, it is not possible to recover nutrients as struvite from the sludge dewatering centrate of a WWTP with P chemical precipitation due to the low soluble P concentration. This type of WWTP can explore alternative phosphate recovery options. One innovative method that has gained attention is phosphorus recovery as vivianite (Fe<sub>3</sub>(PO<sub>4</sub>)<sub>2</sub>· 8H<sub>2</sub>O) that is predominant in digested sludge from plants where iron is used for phosphate removal (Wilfert et al., 2018). The advantages of this process are its natural ubiquity, easy accessibility, efficiency to prevent iron chlorosis in calcareous soils and foreseeable economic value, but its current development stage is at its infancy, and further studies are required (Cardoso et al., 2019; ESPP, 2020).

## 2.4 Conclusions

The nutrient mass balance of N and P in SF-WWTP allowed observing the dynamics of nutrients in their different flows. Despite the variability of the data, the relative errors for each subsystem were below 25%. The overall TKN balance presented a RE of 6.67 %; however, TP overall mass balance presented a RE of 28% due to the dynamics of this nutrient in the WWTP and to the high variability of the data. Results show that SF-WWTP has a minimal removal of N (4%) but an important removal of P (59%), mainly due to the low sludge age used in the WWTP (2 days).

The highest N and P loadings occurred in the secondary sludge, with a significant percentage of removal of both loadings by primary settling (30% of P and 15% of N, respect to influent mass). The N loading in the two centrates was similar (mean 540 Kg d<sup>-1</sup>), while the P loading in the thickener centrate was higher than in the dewatering centrate (PL9=3.5 times PL13) due to its higher flow rate. The centrate recirculation (F14) represented 17% and 14 % of initial TKN-N and TP-P loading, respectively. For biological treatment processes, which have an effective criterion of BOD: N:P ratio of 100:5:1, the increase in N and/or P due to the centrate recirculation will decrease treatability efficiency (Fattah, 2012). Therefore, it is vital to determine the amount of nutrient recycled on a regular basis, looking for solutions to maximise the recovery of these nutrients.

The characterisation of centrates showed that, under current conditions in SF-WWTP, struvite precipitation could be limited due to a low orthophosphate concentration (mean 17.5 mg PO<sub>4</sub><sup>3-</sup>-P. L<sup>-1</sup>). However, some research has reported struvite crystallisation processes even at low P concentrations (20- 60 mg PO<sub>4</sub><sup>3-</sup>-P. L<sup>-1</sup>) (Fattah et al., 2008; Uysal et al., 2010; Kumar et al., 2013), for which a further study is required to evaluate its technical feasibility under such conditions. In

addition, other techniques may increase the accumulation of nutrients in the centrates such as EBPR process, sludge acid digestion, and sludge pre-treatment.

Moreover, in WWTPs with P chemical precipitation, nutrients recovery as struvite would not be technically possible because precipitation of P prevents the release of orthophosphates in the anaerobic digestion ( $< 2 \text{ mg PO}_4^{3-}\text{-P. L}^{-1}$ ). Therefore, other recovery technics (i.e., the use of vivianite) can be explored in this type of WWTPs.

Nonetheless, the projected improvements of the biological removal of N and P in the SF-WWTP may foster the economic and environmental feasibility of struvite crystallisation, since a greater accumulation of nutrients, such as polyphosphates, in the biological process, will allow greater solubilisation of nutrients in anaerobic digestion and higher contents of P and Mg in the sludge dewatering centrate. The combination of P removal via EBPR and P recovery as struvite implies a reduction of chemicals for precipitation, reduction of the size of the treatment facility, and reduction of the volume of effluent to be treated and consequently a reduction of costs (Adelagun, 2016). Therefore, the recovering of nutrients from the SF-WWTP would set an example towards greater environmental sustainability in similar WWTPs in Colombia and Latin America.

## 2.5 Acknowledgements

The authors thank SF-WWTP for facilitating sample collection and the EPM group for providing the information necessary for this research; the GAIA and GIEM groups from Universidad de Antioquia, especially L.F Montoya, M. Gómez, A. Hurtado and the colleagues who conducted chemical analyses and sampling collection; IRTA and Leeds University for their technical support and La Llagosta and Esholt WWTP for facilitating sample collection. C. González received funding from Minciencias, Colombia (National Doctorates call 647-2014) to conduct this research as part of her doctoral studies.

## **Chapter 3. Effect of the stirring speed on the struvite formation using the centrate from a WWTP.**

### **Highlights**

- The particle size of struvite crystals decreased with higher stirring speeds ( $G > 312 \text{ s}^{-1}$ )
- Largest particle size can be obtained at stirring speeds ranging from 100 to 200 rpm, equivalent to a velocity gradient between 79 and  $188 \text{ s}^{-1}$ .
- Struvite was obtained even under no stirring conditions, but the total amount recovered increased with the increment in stirring rates.

### **Abstract**

The formation of struvite ( $\text{MgNH}_4\text{PO}_4 \cdot 6\text{H}_2\text{O}$ ) for nutrient recovery in wastewater treatment plants has been widely investigated; however, little attention has been paid to the effect of stirring speeds on the resulting particle size, which could affect its agronomic value as a slow-release fertiliser. In this study, struvite formation from the centrate of sewage digestate was performed under six stirring speeds (0, 100, 200, 300, 400, 500 rpm). The resulting struvite crystals were characterised using X-ray diffraction and scanning electron microscopy with energy-dispersive X-ray spectroscopy. The average particle size of struvite crystals increased from  $55 \mu\text{m}$  at 0 rpm to  $127 \mu\text{m}$  at 100 rpm and  $128 \mu\text{m}$  at 200 rpm. Further increments in stirring speeds resulted in smaller crystal sizes. These results indicated that the largest particle size could be obtained at stirring speeds ranging from 100 to 200 rpm, equivalent to a velocity gradient between 79 and  $188 \text{ s}^{-1}$ , as there was no statistically significant difference between mean values ( $t$ -test,  $p < 0.05$ ). The optimum stirring speed range reported herein can be used to set operational conditions for struvite crystallisation with the benefit of producing large crystals and reducing energy consumption in stirring tanks.

Keywords: Wastewater, Phosphorus recovery, Struvite crystallisation, Velocity gradient (G), Sustainable development

**Note:** This article was presented as poster in *XIII Taller y Simposio Latinoamericano de Digestión Anaerobia*. 21 al 24 de octubre de 2018, Medellín, Colombia and has already been published in the journal Revista Facultad de Ingeniería- Universidad de Antioquia; ISSN (online): 2422-2844 (<https://revistas.udea.edu.co/index.php/ingenieria/article/view/337569>).

## 3.1 Introduction

Phosphorus (P) and nitrogen (N) are the main nutrients causing eutrophication that lead to biodiversity loss and water quality problems (Guadie et al., 2014; Ye et al., 2014). However, although an excess of phosphorus is problematic, modern agriculture is highly dependent on phosphorus fertiliser, which is derived from phosphate rock, a non-renewable resource with global reserves expected to be depleted within the following 50–100 years (Doyle & Parsons, 2002), making a serious problem for its contribution to agricultural and industrial development.

Both problems, phosphorus source depletion and eutrophication, can be tackled at the same time by the application of technologies aimed at recovering nutrients from wastewater streams (Morales et al., 2013). For example, the centrate from anaerobic digesters in Wastewater Treatment Plants (WWTPs), which is an N- and P-rich stream produced after sewage digestate dewatering, with concentrations between 750-1,500 mg N L<sup>-1</sup> for nitrogen and 40-400 mg P L<sup>-1</sup> for phosphorus compounds. Those figures are typical of WWTP using enhanced biological nutrient removal (EBNR) processes (Fattah, 2012; Jordaan, 2011), which represents a good opportunity to recover nutrients from domestic wastewater. A technique proven to be a successful method to recover phosphorus from phosphorus-rich streams is the precipitation of struvite (MgNH<sub>4</sub>PO<sub>4</sub>·6H<sub>2</sub>O) (Battistoni et al., 2002). Struvite is an effective, slow-release fertiliser that can be used to close the nutrient loop in between waste production and agriculture, as it simultaneously recovers N and P from waste effluents (Li et al., 2019; Muhmood et al., 2019).

Hence, struvite offers multiple benefits, including limited negative impacts from agricultural runoffs into freshwater bodies, when compared with traditional chemical fertilisers. In fact, N losses have been reported to be considerably lower in struvite-treated soils than in soils receiving chemical fertilisers (Muhmood et al., 2019). Struvite can also reduce nitrous oxide emissions and the need for phosphate rock, thus creating a more sustainable environment in line with a wider circular economy approach.

To date, various kinds of reactors have been developed at laboratory, pilot and full scales showing great potential in recovering struvite from waste streams, among them are: fluidised bed reactor (FBR), airlift reactor and continuously stirred tank reactor (CSTR) (Le Corre et al., 2009; Rahman et al., 2013). FBR is the most commonly used due to its ability to produce struvite pellets of large size, high crushing strength and purity (Ye et al., 2016); however, its operation requires high flow rate and energy for mixing to ensure that the bed is continuously fluidised, so different efforts have been made to reduce energy demand and minimise losses of fine particles remaining in solution (Battistoni et al., 2005). Guadie et al. (2014) used a novel cone-inserted fluidised bed reactor for reducing unwanted crystal loss, while Le Corre et al. (2007) used stainless steel meshes to reduce the losses of fine particles in the effluent; Wang et al. (2017) conducted an economic analysis in FBR reactor using different Mg sources. On the other hand, in airlift reactors air increases the pH by CO<sub>2</sub> stripping and creates an internal recycle flow that allows crystals to grow until a critical particle size (Tarragó et al., 2016); however, the costs of energy used in aeration can be considerably high. The stirred reactor or CSTR is one of the simplest and most effective technologies to produce struvite (Pastor, 2006; Ronteltap et al., 2010), although the mixing force and the reactor hydrodynamics are significant factors that contribute to the formation of struvite crystals (Crutchik et al., 2017; Dhakal, 2008).

In a stirred reactor, hydraulic shear forces can break struvite crystals into smaller fractions, which ultimately affect the resulting size of the precipitates (Dhakal, 2008). These fine precipitates are more

### Chapter 3. Effect of the stirring speed on the struvite formation using the centrate from a WWTP.

---

likely to be washed out with the effluent, decreasing the recovery of precipitates. Therefore, in order to optimise P-recovery efficiency after crystallisation, it is beneficial to aim for larger particle sizes (Ronteltap et al., 2010). In addition, larger struvite particles will have a longer effect on soils, increasing the absorption of nutrients from plants and crops (Tarragó et al., 2016).

The effect of stirring speed on struvite formation and particle size has been little investigated. Liu et al.(2013) showed that mixing rates and contact time increase phosphorus removal efficiency, while Cerrillo et al.(2014) found that the maximum particle size decreased when the mixing speed was increased from 100 to 200 rpm. These results agree with the work reported by Kim et al.(2009) indicating that in struvite precipitation processes, removal patterns of nitrogen and phosphorus from the solution increased logarithmically as a response to the increment of  $Gt_d$  values – i.e., the product between mixing intensity/velocity gradient ( $G$ ) and mixing duration ( $t_d$ ); however, the individual effect of  $G$  on particle size at speeds between 0 and 500 rpm is yet unknown. Therefore, it is important to evaluate the effect of stirring speed and mixing intensity in a wide range of velocity gradients ( $G$ ) to optimise the amount of energy needed in these reactors to obtain high percentages of P and N recovery and larger particles sizes of struvite precipitates.

Thus, the main objective of this study was to evaluate the effect of stirring speed on struvite precipitation using the centrate from a conventional municipal WWTP. The removal of nutrients and the particle size were assessed to obtain the optimum stirring range for a struvite mixing reactor.

## 3.2 Materials and methods

### 3.2.1 WWTP

Centrate samples were collected in the municipal WWTP of La Llagosta, located in the Catalonia autonomous community, province of Barcelona, Spain, at  $41^{\circ} 30'12.62''$  N and  $2^{\circ} 12'5.12''$  E (Figure 12), which has a treatment capacity of  $43,000 \text{ m}^3 \cdot \text{d}^{-1}$  and a population equivalent (p.e) of 358,000 inhabitants. This WWTP has a conventional system for the treatment of a blend of domestic and industrial wastewaters, which comprises pre-treatment, primary settlement, and activated sludge units followed by a final secondary settling with chemical precipitation (Figure 13). The process can remove 56% TKN and 86% TP for the raw municipal wastewater.

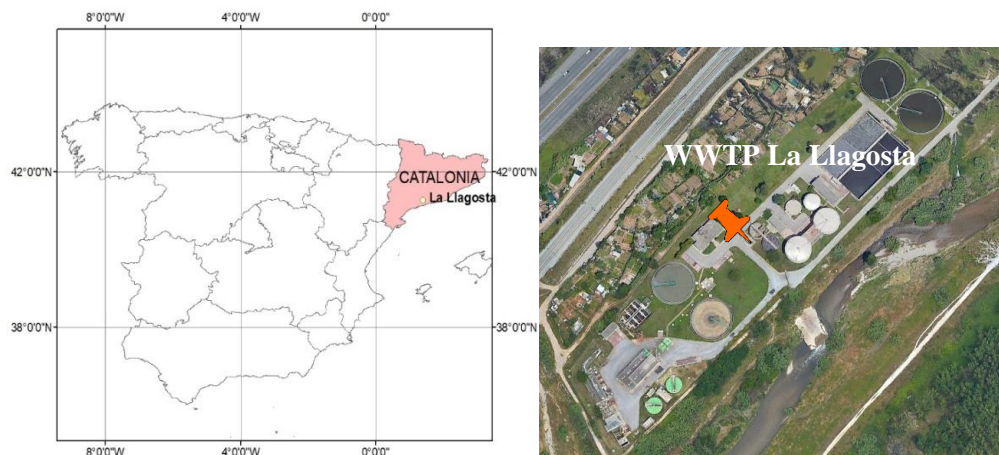


Figure 12. Localisation of La Llagosta WWTP (Spain)

### Chapter 3. Effect of the stirring speed on the struvite formation using the centrate from a WWTP.

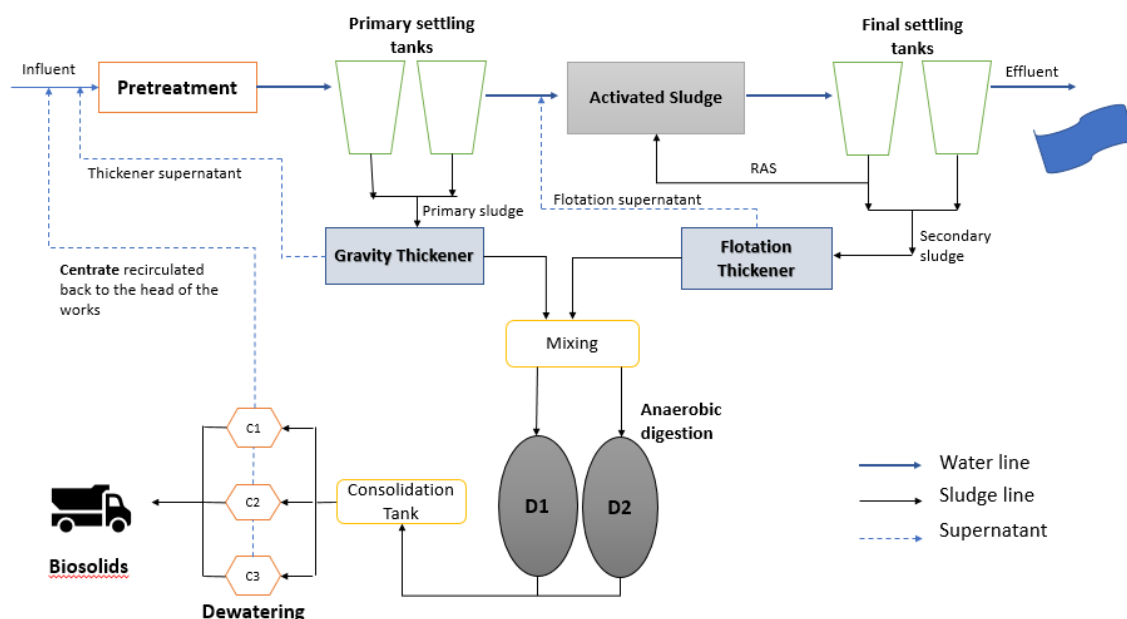


Figure 13. La Llagosta WWTP (Barcelona, Spain)

### 3.2.2 Analytical methods

Centrate samples were analysed at IRTA facilities (Caldes de Montbui, Spain). Cations ( $\text{Ca}^{2+}$ ,  $\text{Mg}^{2+}$ ,  $\text{K}^{+}$ ) and anions ( $\text{P-PO}_4^{3-}$ ) concentrations were analysed by ionic chromatography using a Metrohm 790 IC equipped with a Metrosep C4 150/4.0 column and a Metrohm 861 Advanced Compact IC equipped with a Metrosep A Supp 5-250 column and an 853  $\text{CO}_2$  suppressor, respectively. Total solids (TS), total suspended solids (TSS), volatile solids (VS),  $\text{NH}_4^+\text{-N}$ , TKN, TP and total alkalinity concentrations were determined according to Standard Methods (APHA et al., 2017). The appearance of the precipitates was analysed by using a scanning electron microscope (SEM, ZEISS EVO@MA 10) coupled to an energy dispersive X-ray microanalysis detector (EDX-Oxford, Inca) at Universidad Aut3noma de Barcelona (Cerdanyola, Spain). Meanwhile, the crystalline nature of precipitates was determined by X-ray diffraction (XRD, X'Pert Powder of Panalytical), using Cu K-alpha radiation. The XRD patterns were recorded in the scanning range of 2-theta from  $10^\circ$  to  $60^\circ$ . Data were collected and processed using High-score-plus software. Identification of the phase peaks was accomplished by comparing the observed XRD patterns with a standard of struvite compiled by the International Centre for Diffraction Data (ICDD), the crystallography open database and the Powder Diffraction File (PDF) (ICDD, 2001). Crystal sizes were measured using ImageJ (1.51J8) software (Rasban, 2016) by making 120 measurements of the length of the crystals for each sample.

### 3.2.3 Methods

Due to the characteristics of the centrate,  $\text{MgCl}_2 \cdot 6\text{H}_2\text{O}$  and  $\text{NaH}_2\text{PO}_4$  were added to balance the P: N: Mg molar ratio to 1:6:1.7 ( $\text{P} = 300 \text{ mg P-PO}_4^{3-}/\text{L}$ ). This molar relationship was chosen because higher N:P molar ratio improves the precipitation of struvite instead of amorphous calcium and magnesium phosphates (Capdevielle et al., 2013; Rodrigues, 2014), while Mg: Ca higher than 2:1 have the same effect (Acelas et al., 2015). Although struvite can precipitate at a wide range of pH values (7.0-11.5) (Hao et al., 2008), many investigations agree that the optimum pH value is around 9 (Cerrillo et al.,

2014; Pastor, 2008), for that reason, NaOH in solution was added to reach pH 9. The principal conditions of the experiments are listed in Table 9.

### 3.2.4 Experimental setup

A standard jar tester with six paddles was used for struvite precipitation. Jars consist of 1L cylindrical glass vessels with 130 mm internal diameter. The flat paddles at the end of each stirrer shaft, which were made of stainless steel with a length of 7.6 cm and a height of 2.5 cm. The stirring device included a tachometer and a rev controller to adjust mixing rates ranging from 0 to 300 rpm. For the testing of mixing rates higher than 300 rpm, the same paddles were coupled to a laboratory stirrer. Mixing intensity ( $G$ ) values tested in this study varied from 0 to  $591 \text{ s}^{-1}$ . The applied  $G$  value was calculated based on the interaction between mixing rates of flat paddles and the corresponding velocity gradient based on a work previously reported (Cornwell & Bishop, 1983), which found that the velocity gradient has a linear correlation to the impeller speed.

Table 9. Test conditions

Parameter	Values
pH	9
Temperature ( $^{\circ}\text{C}$ )	12
Duration (h)	3
Volume (L)	1
Reagents used	$\text{MgCl}_2 \cdot 6\text{H}_2\text{O}$ and $\text{NaH}_2\text{PO}_4$
mg $\text{P-PO}_4^{3-} \text{ L}^{-1}$	300
mg $\text{Mg}^{2+} \text{ L}^{-1}$	389
mg $\text{N-NH}_4^+ \text{ L}^{-1}$	825
mg $\text{Ca}^{2+} \text{ L}^{-1}$	261
<i>Molar ratios</i>	
$\text{N-NH}_4^+ / \text{P-PO}_4^{3-}$	6.1
$\text{Mg}^{2+} / \text{P-PO}_4^{3-}$	1.7
$\text{Mg}^{2+} / \text{Ca}^{2+}$	2.5
Stirred speed (rpm)	0, 100, 200, 300, 400, 500
Replicates	2

The applied mixing duration ( $t_d$ ) was 3 hours in the six-stirring speeds tested (0, 100, 200, 300, 400 and 500 rpm) followed by 16 hours without stirring to achieve greater sedimentation of particles and, therefore, a more significant recovery of the precipitate (Figure 14). After 16 hours without stirring, the solutions were filtered using  $1.2 \mu\text{m}$  membrane filters. In order to avoid struvite thermal decomposition that occurs above  $55^{\circ}\text{C}$  (Bhuiyan et al., 2008), the precipitates were air-dried at ambient temperature for 24 hours. Filters were weighed with and without the precipitate to calculate net struvite production; the TSS concentration from the centrate was also considered to calculate the total mass of struvite.

Considering that phosphate is the limiting reagent in this reaction, the maximum amount expected of struvite was calculated by multiplying the mmols of phosphate present in the centrate by the molecular weight of struvite.



**Chapter 3.** Effect of the stirring speed on the struvite formation using the centrate from a WWTP.

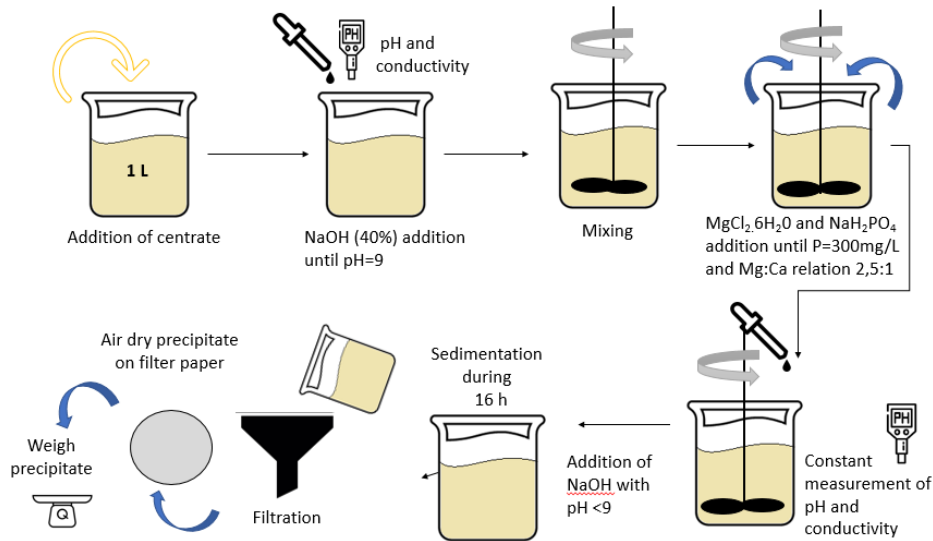


Figure 14. Experimental procedure for struvite precipitation

### 3.3 Results and discussion

The characterisation of centrate samples reported the following mean values: pH = 8.3; reactive phosphorus = 1 mgP-PO<sub>4</sub><sup>3-</sup> L<sup>-1</sup>; ammonium = 825 mgN-NH<sub>4</sub><sup>+</sup> L<sup>-1</sup>; calcium = 261 mgCa<sup>2+</sup> L<sup>-1</sup>; total suspended solids = 116 mg TSS L<sup>-1</sup>; and total alkalinity = 3.1 gCaCO<sub>3</sub> L<sup>-1</sup>.

Struvite was obtained even under no stirring conditions, but the total amount recovered increased with the increment in stirring rates. Higher removal of NH<sub>4</sub><sup>+</sup> was found because of increasing stirring speeds (Figure 15 and Table 10), which could be due to NH<sub>3</sub> volatilisation. This did not affect struvite formation since the recovered struvite precipitate was between 89 and 112% of the maximum amount calculated from the composition of centrate samples (Figure 15). In contrast, the Mg<sup>2+</sup> removal increased between 0 and 100 rpm but later decreased as the stirring speeds increased, being slightly higher than the maximum that could be achieved by struvite precipitation (Figure 15). In this case, high Mg<sup>2+</sup> removals at different speeds may be due to the precipitation of other Mg precipitates, such as Mg(OH)<sub>2</sub> since the excess mass of external magnesium source can rapidly react with OH<sup>-</sup> ions in the solutions to produce these amorphous products (Kim et al., 2009).

Table 10. Removal efficiencies (%), struvite similarity score XRD (%) and SEM-EDX results

Stirring Speed (rpm)	Velocity gradient (s <sup>-1</sup> )	Removal Efficiency (%)*				mass of crystals (g)	XRD Score (%)	SEM-EDX (%)**		
		Mg	Ca	N	P			Mg	P	Ca
0	0	72.3	41.8	16.8	>95	2,1	97	14.9	18.5	0.6
100	79	85.1	56.7	19.0	>95	2,4	88	14.6	17.6	0.6
200	188	81.8	69.7	23.9	>95	2,5	90	13.8	16.4	1.6
300	312	73.5	45.2	24.5	>95	2,5	97	14.9	17.2	1.4
400	447	67.6	63.6	28.5	>95	2,6	87	14.3	15.4	1.8
500	591	68.1	57.9	28.7	>95	2,6	82	14.5	31.0	1.4

\*regarding the initial content in the soluble phase; \*\* percentage of total atoms

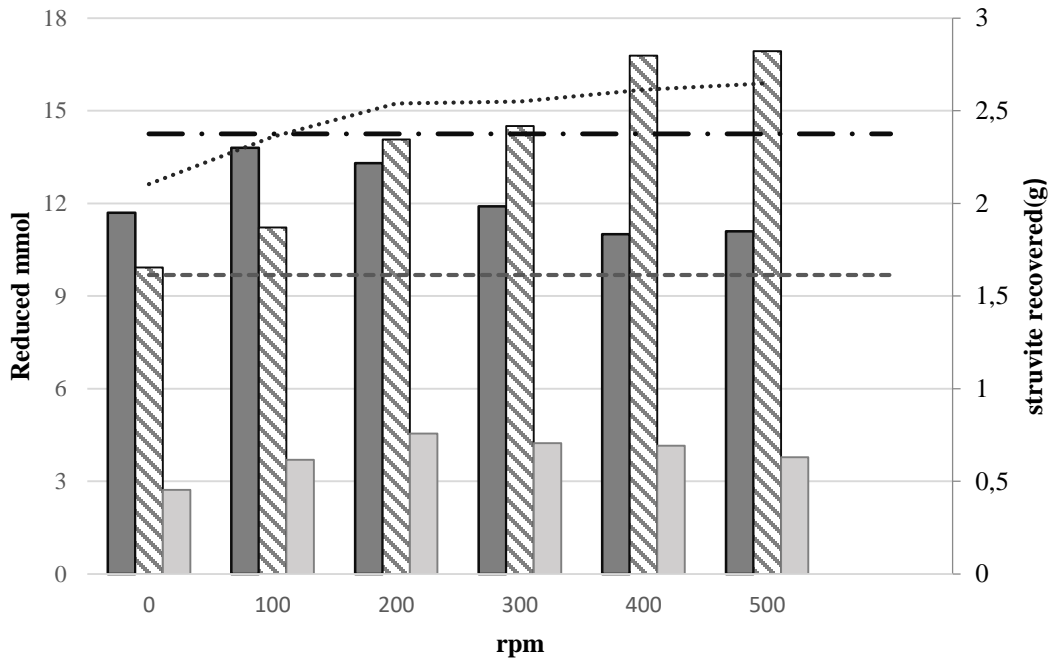


Figure 15. Reduced Mg, Ca and N (mmol) and recovered crystals depending on the stirring speed-velocity gradient. Symbols: ■ Mg, ■ Ca, ▨ N, ..... Mass of crystals (g) — · · max struvite(g) ---- Max mmol Mg and N

The  $\text{Ca}^{2+}$ ,  $\text{Mg}^{2+}$  and N removal from the soluble phase was between 2.73 and 4.55 mmol  $\text{Ca}^{2+}$ , between 11.0 and 13.8 mmol  $\text{Mg}^{2+}$  and between 9.9 and 16.9 mmol N- $\text{NH}_4^+$ . The  $\text{Ca}^{2+}$  removal may be due to the formation of calcium carbonates like calcite ( $\text{CaCO}_3$ ) and monohydrocalcite ( $\text{CaCO}_3 \cdot \text{H}_2\text{O}$ ), more favoured in comparison with the formation of calcium phosphate (Crutchik et al. 2017; Rodrigues 2014).

As reported in Figure 15, there was no direct relationship between the removal of  $\text{Mg}^{2+}$  and  $\text{Ca}^{2+}$ . This is because the initial high magnesium content enhances the phosphate reaction with  $\text{Mg}^{2+}$  rather than  $\text{Ca}^{2+}$  (Jaffer et al., 2002), thereby reducing the interference due to the formation of  $\text{Mg}^{2+}$  and  $\text{Ca}^{2+}$  precipitates such as dolomite ( $\text{CaMg}(\text{CO}_3)_2$ ) and favours the formation of struvite.

High stoichiometric  $\text{NH}_4^+ : \text{PO}_4^{3-}$  ratio ( $\approx 4.7$ ) favour the struvite precipitation (Crutchik et al. 2017); however, the mass of crystals above the maximum expected for struvite at stirred speeds between 200 rpm and 500 rpm (Figure 15) may be due to the formation of other precipitates not detected in the XRD, since the agitation possibly favours other reactions.

Despite finding greater removal of N and  $\text{Mg}^{2+}$  than the maximum expected by struvite precipitation, it was found by X-ray diffraction that the main product obtained at all stirred speeds was struvite, finding similarities between 82 and 97% with the standard of struvite (Score in Table 10 and Figure 16). The SEM-EDX analyses confirmed the presence of Mg and P in the precipitates, with a minimum presence of Ca (Table 10 and Figure 17).

**Chapter 3.** Effect of the stirring speed on the struvite formation using the centrate from a WWTP.

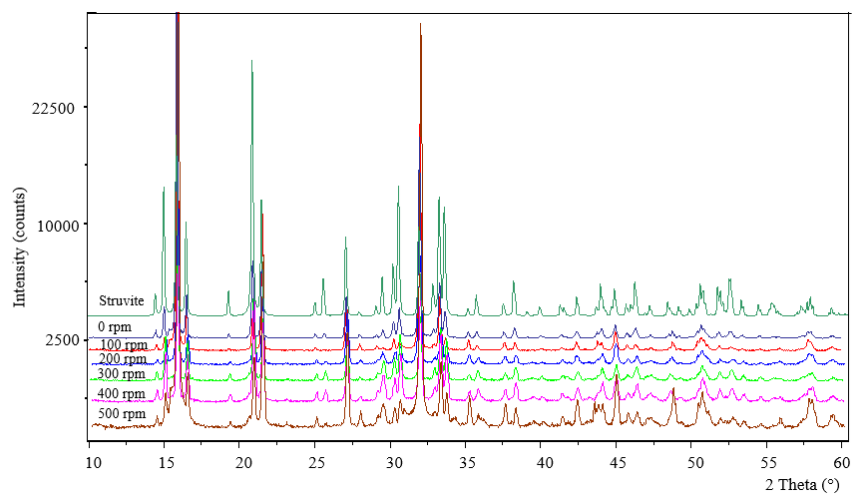


Figure 16. XRD of precipitates at different stirred speeds and standard struvite (line in dark green).

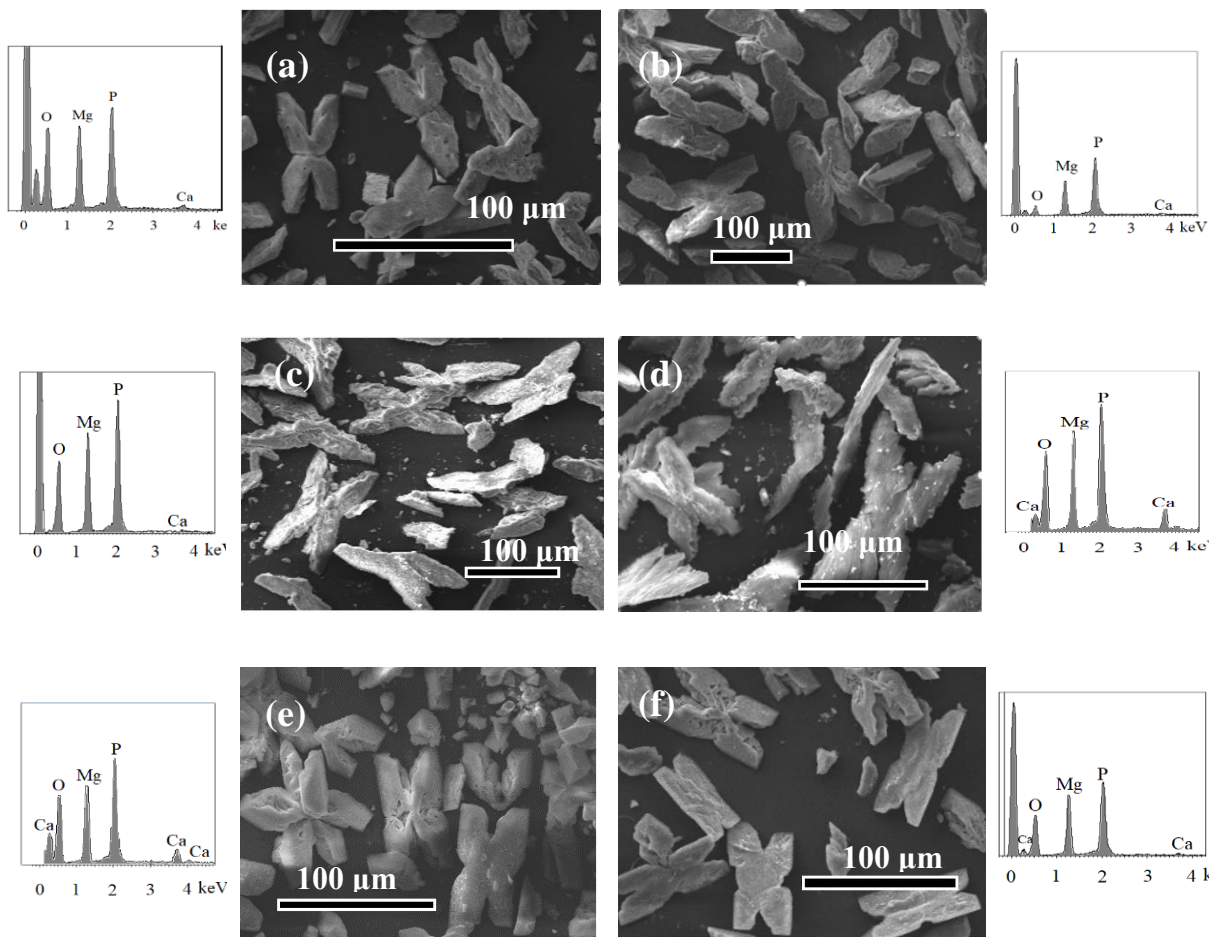


Figure 17. SEM images and EDS analysis of struvite crystals obtained working with different stirring speed: (a) 0 rpm, (b) 100 rpm, (c) 200 rpm, (d) 300 rpm, (e) 400 rpm and (f) 500 rpm.

Although Pastor (2008) concluded that the degree of agitation of the system could exert a considerable influence on the crystalline habit (external appearance of the crystals), similar crystal shapes were observed in this work – i.e., stars, X shapes and needles (Figure 17). The last shape, needles, are the most reported in by researchers, including Crutchik et al.(2017).

The attained data in this work confirmed the strong influence of stirring speeds on particle size distribution. The largest mean particle size was found at 200 rpm (128  $\mu\text{m}$ ; Figure 18) and the smallest size at 0 rpm (55  $\mu\text{m}$ ). According to *t*-student tests, there were no statistically significant differences between the particle size of 100 and 200 rpm ( $p > 0.05$ ); however, there were statistically significant differences between the particle size of 0 and 100 rpm, and 100 and 500 rpm ( $p < 0.05$ ). Therefore, the largest particle sizes were between 100 and 200 rpm, which corresponds to a *G* value between 79 and 188  $\text{s}^{-1}$ . According to Capdevielle et al. (2013), high mixing rates harm struvite crystal sizes due to struvite dissolution and crystal break, thus, although the mixing effect enhances mass transfer rates (Kim et al., 2009) and therefore the particle size, stirring speeds higher than 200 rpm were detrimental to the struvite crystallisation process.

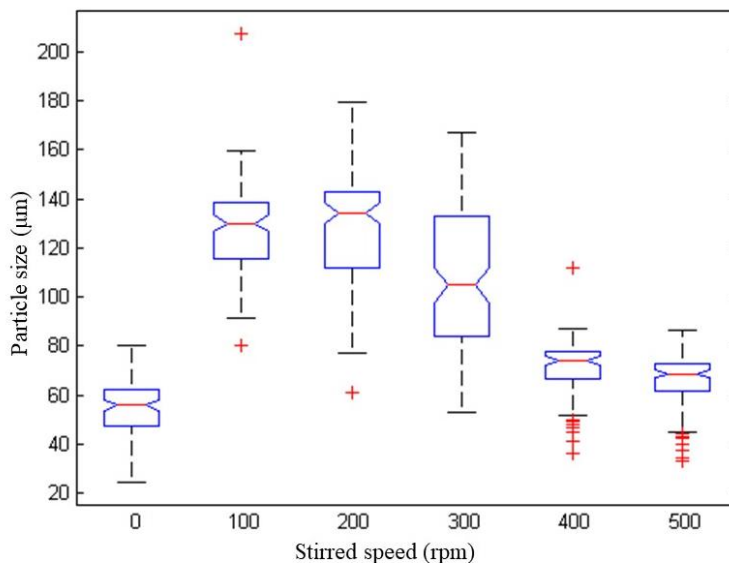


Figure 18. Distribution of particle size of struvite crystals at different stirring speeds.

### 3.4 Conclusions

The struvite formation is affected by the stirring speed. The largest mean particle size of 128  $\mu\text{m}$  was obtained at 200 rpm – i.e., equivalent to a *G* of 188  $\text{s}^{-1}$ . The particle size of struvite crystals decreased with higher stirring speeds. Although the velocity gradient improves mass transfer rates of ions in the solution to support better crystal growth, high *G* values beyond the optimal can revert this effect, reducing the size of crystals formed or disfavours their growth rates.

The P removal was not affected by stirring speeds, while the N removal increased with stirring speed achieving at 500 rpm a removal of 7 mmol more than the maximum possible by the sole formation of struvite. In this case, the agitation may favour the volatilisation of N in the form of  $\text{NH}_3$  (Ariyanto et

al., 2017). Although this did not affect the formation of struvite by the high contents of  $\text{N-NH}_4^+$  in the centrate, it implied an increased emission and a potentially higher environmental risk.

Although the removal of Mg appears to be influenced by the stirring speed, the precipitation of other salts was minimal compared to the struvite precipitation, according to XRD. Therefore, a stirring speed range between 100 and 200 rpm ( $79 \text{ s}^{-1} < G < 188 \text{ s}^{-1}$ ) is recommended for struvite crystallisation with the benefit of producing large crystals, reducing energy consumption in stirring tanks and reducing the volatilisation of ammonia nitrogen.

### 3.5 Acknowledgements

The authors thank J. R. Navarro, L. Tey and E. Muñoz from IRTA, for their technical support and the La Llagosta WWTP for facilitating sample collection. C. González thanks Colciencias National Doctorates 647-2014 and Enlaza Mundos for the financial support for her PhD Internship. IRTA thanks the financial support of CERCA Program and the Consolidated Research Group TERRA (ref. 2017 SGR 1290), both from the Generalitat de Catalunya, as well as INIA support, from Gobierno de España, through the research project PIONER (ref. RTA2015-00093-00-00).

## Chapter 4. Influence of pH and Temperature on Struvite Purity and Recovery

### Highlights

- An ion balance was compared with the SI of different minerals to establish the possible precipitates formed at different pH and temperatures.
- Temperatures of 33°C and 40 °C are not recommended because at 33 °C the amount of amorphous material increases and at 40 °C ammonia volatilisation induces losses.
- A pH of 9 is recommended for the formation of struvite, considering a more effective removal of P, greater particle size, and greater purity of the product obtained.

### Abstract

Precipitation of struvite crystals ( $\text{MgNH}_4\text{PO}_4 \cdot 6\text{H}_2\text{O}$ ) from wastewater streams is a process aimed to simultaneously recover nitrogen (N) and phosphorus (P) for reuse as fertilisers in agriculture. Struvite crystallisation is controlled by pH, saturation index, temperature and the presence of other soluble ions (e.g.,  $\text{Ca}^{2+}$ ,  $\text{Mg}^{2+}$ ,  $\text{CO}_3^{2-}$ ). This work studies the effect of pH and temperature on phosphorus and nitrogen removal via struvite precipitation and the quality of the product obtained (i.e., crystal size, morphology and purity). Struvite was precipitated in batch reactors from the supernatant produced during anaerobic sludge dewatering (centrate) at a wastewater treatment works, under controlled pH (8, 9 and 10) and temperature (25, 33 and 40 °C) conditions. Optimal process conditions were determined for P removal as struvite, reduction of co-precipitation with Ca and the increase in particle size of struvite precipitates. The results showed that temperatures of 33°C and 40°C are not recommended for struvite precipitation – i.e., at 33°C the amount of amorphous struvite material increases, and at 40°C ammonia losses are induced by volatilisation. At all pH-tests, P removal efficiency was > 93%, but the highest phosphate content and purity as struvite were obtained at pH 9.0. The optimum pH and temperature for the formation of large crystals (84 µm) and high purity (>70%) of struvite precipitates were 9 and 25 °C, respectively. **Keywords:** centrate; nutrient recovery; struvite crystallisation; saturation index (SI).

**Note:** One part of this article was presented as poster presentation at the *3<sup>rd</sup> IWA Resource Recovery Conference*. 8-12 September, Venice (2019), Italy; 2019:586-587. The article was submitted to the Sustainability journal (ISSN: 2071-1050).

### 4.1 Introduction

Phosphorus (P) is considered as a non-renewable resource and is irreplaceable in crop and livestock production; intensive production of P fertilisers from phosphoric rocks is contributing to a fast depletion of commercial and affordable phosphorus global reserves. Therefore, the recovery of P from waste streams like sewage and sewage sludge at wastewater treatment works (WWTPs) would provide a more sustainable option to P fertiliser supply and would contribute to reduce impacts from

P shortages in the future. The recovery of P in the form of struvite ( $\text{MgNH}_4\text{PO}_4 \cdot 6\text{H}_2\text{O}$ ) is often achieved from P-rich waste streams like sludge dewatering liquor and digester supernatant at WWTPs (Liu & Qu, 2017).

Struvite is a white crystalline mineral composed of magnesium, ammonium and phosphate (MAP) in an equal molar ratio (1:1:1). This mineral can potentially be used as an eco-fertiliser, competing against traditional fertilisers only if its crystallisation process is well controlled. Struvite is considered a slow-release fertiliser ideal for agriculture, as it reduces nutrient run-off and subsequent impact on water bodies (Guadie et al., 2014).

Wastewaters with a high concentration of N and P are a suitable source for nutrient recovery via struvite precipitation. Recently, struvite has been recovered from different types of wastewaters, such as swine wastewater, digester supernatant, industrial wastewater, agro-industrial wastes and anaerobic digester effluents (Rahman et al., 2013). During the anaerobic digestion of sewage sludge in WWTPs,  $\text{NH}_4^+$ -N,  $\text{PO}_4^{3-}$ -P and other nutrients ( $\text{Mg}^{2+}$ ,  $\text{K}^+$ ,  $\text{Ca}^{2+}$ ) are released from the solids into the liquid phase. This makes the supernatant from digested sludge dewatering (centrate) a great source for potential recovery of nutrients via struvite precipitation, particularly in WWTPs with enhanced biological phosphate removal (EBPR) (Batstone & Jensen, 2011)

Struvite precipitation is controlled by pH, saturation index, temperature and the presence of other ions such as calcium ( $\text{Ca}^{2+}$ ), magnesium ( $\text{Mg}^{2+}$ ) and carbonates ( $\text{CO}_3^{2-}$ ) that can inhibit or reduce struvite formation, depending on their relative concentrations (Tansel et al., 2018). Various researchers have investigated the effect of pH as a function of struvite recovery efficiency. Most of them have reported a pH range between 7 and 11 for struvite crystallisation (Siciliano et al., 2020; Tansel et al., 2018), demonstrating that pH has a significant effect on the growth rate and size of struvite crystals. An increase in pH causes an increase in supersaturation and a subsequent increase in the growth rate of struvite (Le Corre et al., 2009). Other works have reported that high pH values increase the density of nuclei population yielding heterogeneous and smaller crystals (Rahman et al., 2013).

In addition, it has been suggested that the concentration of  $\text{Mg}^{2+}$ ,  $\text{NH}_4^+$  and  $\text{PO}_4^{3-}$  ions depends on pH, controlling the solubility of struvite that decreases as the pH increases reaching a minimum solubility at pH values between 9.0 and 10.7 (Doyle et al., 2000; Snoeyink & Jenkins, 1980). Thus, various research works have demonstrated that the increase in pH enhances P and N removal and recovery (Rahman et al., 2013). Although high pH has been reported to increase P recovery efficiency, it promotes the precipitation of magnesium and calcium phosphate making it a less-valuable product (Rahman et al., 2013; Yan & Shih, 2016). No consensus has been achieved regarding the optimal pH to obtain high removal efficiency of P and N and high quality of struvite as the crystallisation product (Moulessehoul et al., 2017; Siciliano et al., 2020); however, such differences likely lie on the different compositions of wastewaters (Li et al., 2019).

Calcium interference on struvite precipitation has been extensively investigated with inconclusive results. It has been suggested that  $\text{Ca}^{2+}$  could interfere in the crystallisation process of struvite by promoting the formation of calcium phosphate (Bouropoulos & Koutsoukos, 2000), but it has been also suggested that such interference depends on alkalinity or molar ratios of N:P and Ca: Mg (Capdevielle et al., 2013; Le Corre et al., 2005). Other works have reported an increase on the kinetics rate for the formation of struvite when  $\text{Ca}^{2+}$  is present (Hallas et al., 2019), and although fast Ca-phosphate precipitation can be dominant at the beginning of the reaction, a high thermodynamic driving force of struvite precipitation could drive the re-dissolution of Ca-ions from the Ca-phosphate compounds favouring a higher purity crystallisation of struvite (Lee et al., 2013). Other investigations have confirmed the presence of  $\text{CaCO}_3$  and  $\text{Ca}_3(\text{PO}_4)_2$  together with struvite; however, the presence

of  $Mg^{2+}$ ,  $PO_4^{3-}$  and dissolved organic compounds can decrease the rate of precipitation of  $CaCO_3$  (Le Corre et al., 2005; Li et al., 2016).

Temperature has a relatively less significant effect on struvite precipitation than pH, ionic composition or ionic saturation conditions (Ariyanto et al., 2017); however, it strongly influences the growth rate and the efficiency of phosphate removal (Moussa et al., 2011). Struvite solubility and ionic speciation are sensitive to temperature (Crutchik & Garrido, 2016; Tansel et al., 2018). It is known that the solubility of struvite increases with temperature reaching a specific value after which the solubility decreases; however, no agreement has been reached on this value suggested to be 30, 35 or 50°C (Bhuiyan et al., 2007; Doyle & Parsons, 2002; Webb & Ho, 1992).

Besides temperature, pH and the presence of other ions, supersaturation is an inclusive parameter that should be considered in the operation of struvite precipitation process because it considers the effect of several factors (struvite constituent ions, ionic strength, pH and temperature) (Shaddel et al., 2019), affecting morphology and particle size that are important factors for the potential use of struvite as a fertiliser.

Given the current disagreement in literature regarding process conditions leading to high nutrient removal efficiency and high quality struvite precipitation, this work evaluates the influence of pH, temperature and saturation index (SI) on struvite precipitation (quantity and quality) to find the best conditions for P and N removal from, a real complex medium, the centrate from the dewatering of digested sewage sludge. The best pH and temperature condition favouring the maximum efficiency of struvite recovery was evaluated, along with an ion mass balance ensuring the optimal N: Mg: P: Ca molar ratios. The quality of the precipitate formed was assessed by X-ray diffraction (XRD), whilst the morphology and size of struvite crystals were identified and quantified using scanning electron microscopy (SEM).

## 4.2 Materials and Methods

### 4.2.1 Description of the full-scale wastewater treatment plant and centrate characterisation

The Yorkshire Water's Esholt WWTP (Bradford, West Yorkshire, UK) treats 280,000 m<sup>3</sup>/d of domestic and industrial wastewater from municipalities located in Bradford and the west part of Leeds serving 760,000 PE. The wastewater treatment process comprises pre-treatment and primary settlement, activated sludge combined with nitrogen (N) removal via nitrification-denitrification and chemical treatment for phosphorus (P) removal (Figure 19). This process removes 97% of total Kjeldahl nitrogen (TKN) and 84% of total phosphorus (TP). Sludge from primary and secondary treatment is stabilised in anaerobic digesters. The clarified stream produced after dewatering the digested sludge (centrate) (Table 11) was used to recover TP as struvite. Centrate samples were stored at 4°C soon after sampling until used in struvite precipitation tests.

The centrate from Esholt WWTP is a complex matrix with the typical characteristics shown in Table 11 (reported as mean values). Despite the low P concentration found due to the absence of an enhanced biological P removal process, it was decided to use this centrate for struvite precipitation tests because it represents the typical complex matrix of real digested waste activated sludge (P concentrations in the centrate were adjusted, see Table 12).



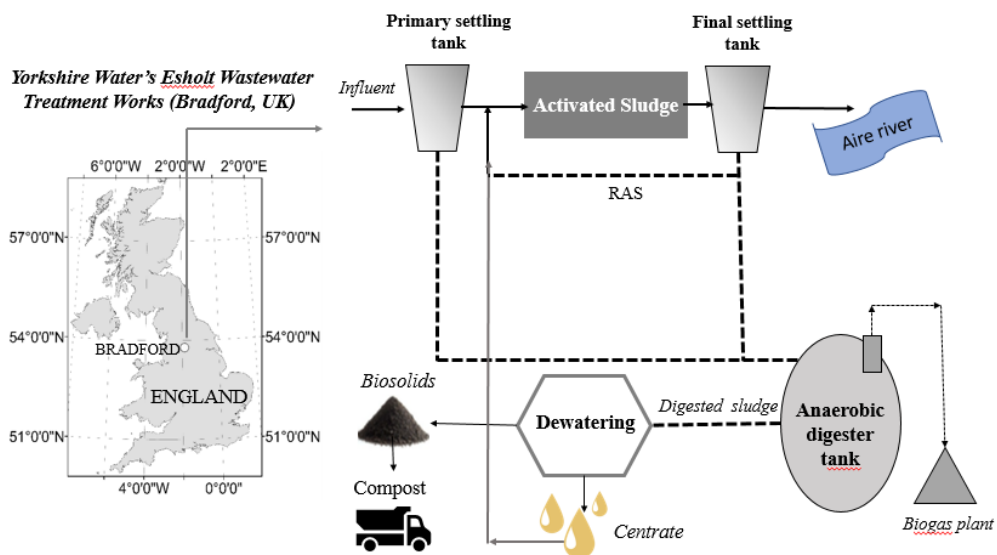


Figure 19. Esholt WWTP (Bradford, England). Adapted from Yulistyorini, (2016)

Table 11. Characteristics of digested sludge sampled from Esholt WWTP

Parameters	Units	Concentration
NH <sub>4</sub> <sup>+</sup> -N	mg N/L	1,080
TKN-N	mg N/L	1,560
K <sup>+</sup>	mg/L	111
Ca <sup>2+</sup>	mg/L	92
Mg <sup>2+</sup>	mg/L	32
PO <sub>4</sub> <sup>3-</sup> -P	mg P/L	2.5
TP	mg P/L	12
TSS	mg/L	512
VSS	mg/L	324
Alkalinity	mg CaCO <sub>3</sub> /L	4,587
Conductivity	mS/cm	8.7
pH	-	7.8

### 4.2.2 Analytical methods

The concentration of Ca<sup>2+</sup>, Mg<sup>2+</sup> and K<sup>+</sup> was quantified by ionic chromatography (Metrohm 850 Professional IC with a Metrosep C4 100/4.0). The content of total suspended solids (TSS) and volatile suspended solids (VSS) in the centrate, and ammonium content (NH<sub>4</sub><sup>+</sup>-N) in struvite precipitates, were determined according to Standard Methods (APHA et al., 2017); struvite precipitates were dissolved in acid (HCl 0.1 M) before distillation for ammonium characterisation. Further analyses to determine the content of NH<sub>4</sub><sup>+</sup>-N, TKN-N, TP, and PO<sub>4</sub><sup>3-</sup>-P in solution were conducted following standardised methodologies developed by HACH®, for use in an automated water analysis Laboratory robot (AP3900 MULTI, Laboratory Robot, HACH): tests LCK 302 and 305 (ammonium), APC350 and APC350o (total phosphorus and orthophosphate), and APC238 (Total Kjeldahl Nitrogen).

### 4.2.3 Struvite precipitate characterisation

The morphology of struvite precipitates was identified by scanning electron microscopy (SEM; ZEISS EVO®LS 15, INCA analyser). The crystalline nature and the semi-quantitative composition (purity) were determined by X-ray diffraction (XRD; Bruker D2 Phaser), using a struvite pattern (PDF number 01-071-2089 and 01-077-2303); data processing was conducted by using DIFRACC SUITE EVA, High Score Plus 3.0e software and the Crystallography Open Database. Crystal size was quantified using ImageJ software (Rasban, 2016), measuring 60 crystals per sample on average.

### 4.2.4 Materials

In all experiments, magnesium chloride hexahydrate ( $\text{MgCl}_2 \cdot 6\text{H}_2\text{O}$ ) was added to meet a molar ratio Mg: Ca >2 and Mg: P >1, which were selected based on data reported by Li et al. (2016) and Liu et al. (2008). They found struvite crystals with high purity and high phosphorus recovery when using these molar ratios. The concentration of  $\text{PO}_4^{3-}\text{-P}$  in centrate samples was adjusted to 120 and 300 mg P/L, using sodium dihydrogen phosphate ( $\text{NaH}_2\text{PO}_4$ ), for pH and temperature (T) tests, respectively. Both initial phosphate concentrations in centrate samples are typical from WWTPs with enhanced biological phosphorus removal (EBPR) (Cabanelas et al., 2013; Jia, 2014). The P concentration in T-tests (300 mg P/L) was deliberately higher than in pH-tests (120 mg P/L) in order to produce a sufficient amount of struvite precipitate for subsequent characterisation. This was considered due to the fact that T-tests were carried out in smaller reactors (1 L) than those used in pH-tests (2 L). The pH of the tested centrate samples was adjusted to 8, 9 and 10 using a 1 M sodium hydroxide (NaOH) solution. All chemical reagents used were analytical grade.

### 4.2.5 Experimental set-up and procedure

Experimental conditions for pH-tests and T-tests are reported in Table 12, and a description of the experimental procedure is presented in Figure 20.

Table 12. Experimental conditions of pH and temperature (T) trials.

Conditions	pH trials	temperature trials(T)
pH	8,9,10	9
Temperature (°C)	20	25,33,40
Stirring speed (rpm)	85	100
Velocity gradient ( $\text{s}^{-1}$ )	79	79
Volume (L)	2	1
Replicates	2	2
Molar ratios		
Mg/Ca	2.3	7.1
N/P	21.6	8.6
Mg/P	1.3	1.7
Concentration		
$\text{PO}_4\text{-P}$ (mg/L)	120	300
$\text{NH}_4\text{-N}$ (mg/L)	1,172	1,172
Mg (mg/L)	125	387
K (mg/L)	111	111
Ca (mg/L)	91.5	91.5
TSS (mg/L)	512	202

The velocity gradient ( $G$ ) was used to control mixing conditions and set at  $79\text{ s}^{-1}$ , following a previous study in which the largest particle size of struvite precipitates was obtained when  $G$  values ranged between  $79$  and  $188\text{ s}^{-1}$  (González et al., 2019). The pH-tests were conducted in a standard jar tester (PB-900 Phipps & Bird), with acrylic plastic jars of  $2.0\text{ L}$ , at room temperature ( $20^\circ\text{C}$ ) and at stirring speed of  $85\text{ rpm}$  ( $G = 79\text{ s}^{-1}$ ) for three pH levels (8, 9 and 10). Then, T-tests were conducted at pH 9 and three temperature levels ( $25$ ,  $33$ , and  $40^\circ\text{C}$ ) in cylindrical glass vessels of  $1\text{ L}$ , submerged into a water bath with temperature control. In T-tests, the centrate was centrifuged to reduce the concentration of total suspended solids (TSS) and to obtain a struvite with fewer impurities.

All tests were performed by duplicate over 3 hours of reaction time. Although the time required to begin struvite nucleation varies between 10 and 45 minutes (Crutchik & Garrido, 2016), a longer reaction time was chosen to form large crystals (Liu et al., 2018). The sedimentation time was 10 hours to increase particle recovery. Precipitates were separated by vacuum filtration using a  $0.45\text{ }\mu\text{m}$  pore size filter (fibreglass) and air-dried at room temperature (Figure 20).

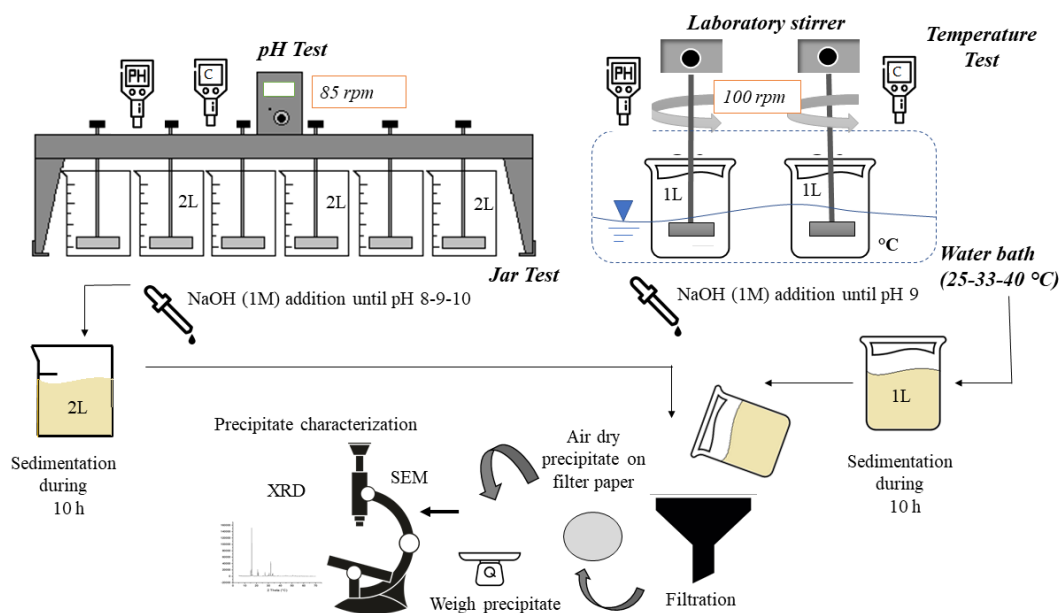


Figure 20. Experimental procedure for struvite precipitation in pH and temperature tests.

### 4.2.6 Data processing and statistical analysis

ANOVA one factor analysis was performed for pH and Temperature tests to assess statistically significant differences between each level of the variables tested (differences exist in at least one pair of data if  $p < 0.05$ ).

The thermodynamic Visual MINTEQ 3.1 software (U.S. Environmental Protection Agency) was used to calculate the saturation index ( $SI$ ) of other compounds that can precipitate under the experimental conditions: (i) when  $SI = 0$ , the solution is in equilibrium; (ii) when  $SI < 0$ , the solution is undersaturated, and no precipitation occurs; (iii) when  $SI > 0$ , the solution is supersaturated, and precipitation occurs spontaneously.  $SI$  was calculated using Equation 1, where  $IAP$  is the ion activity

product and  $K_{SP}$  is the solubility product constant, of the selected solid substance dissolving in the aqueous solution.

$$SI = \log \frac{IAP}{K_{SP}} \quad \text{Equation 1}$$

Visual MINTEQ version 3.1 was also used in this study to predict concentrations of species in the aqueous solution. The modelling process was based on the concentrations of chemical species reported in Table 12.

The quantity precipitated in each trial was calculated as the amount of TSS formed. Therefore, it was calculated as the final weight of the precipitate minus the initial amount of TSS in the solution. The mass balance per test was calculated on a mmol basis. The concentrations of  $Mg^{2+}$ ,  $PO_4^{3-}$ -P,  $Ca^{2+}$  and  $K^+$  precipitated were calculated based on the difference between their initial and final molar concentration in solution. The amount of  $NH_4^+$ -N contained in the precipitates was calculated by multiplying the precipitate mass (g) by its N content (% , dry weight). An N molar mass balance was calculated in all tests to find the amount (mmol) of N volatilised ( $NH_3$ -N), according to Equation 2, where each term is reported as molar mass (Capdevielle et al., 2013).

$$(NH_3 - N)_{\text{volatilized}} = (NH_4 - N)_{\text{initial-liquid}} - (NH_4 - N)_{\text{final liquid}} - (NH_4 - N)_{\text{final solid}} \quad \text{Equation 2}$$

According to Li et al., (2016), ammonia nitrogen can be used as a proxy element to calculate the struvite content in the total solid product since struvite is the only possible precipitate containing ammonia nitrogen. However, considering that struvite has an N: P: Mg molar ratio of 1: 1: 1, in this research, the number of precipitated mmoles of struvite ( $nMAP$ ) in each test was assumed as the lowest value between the precipitated mmoles of  $Mg^{2+}$ ,  $PO_4^{3-}$ -P and  $NH_4^+$ -N; therefore, the quantity of ions that did not precipitate as struvite were calculated as the difference between the mmoles of MAP and the mmoles precipitated of each ion. The percentage of phosphate as struvite ( $P_{MAP}$ ; Equation 3) was calculated as the ratio of  $nMAP$  and the initial mmoles of  $PO_4^{3-}$ -P in the solution (Capdevielle et al., 2013).

$$P_{MAP}(\%) = \frac{n \text{ MAP}}{(PO_4 - P)_{\text{initial}}} \times 100 \quad \text{Equation 3}$$

The struvite purity was calculated as the percentage of struvite in the final solid precipitate using Equation 4, where  $M_{struvite}$  is the molar mass of struvite (245 g/mol), and  $m_{product}$  is the final precipitated mass (g) obtained in each test (Ye et al., 2016).

$$\text{Purity}(\%) = \frac{n \text{ MAP} \cdot M_{\text{struvite}}}{m_{\text{product}}} \times 100 \quad \text{Equation 4}$$

## 4.3 Results and Discussion

### 4.3.1 Effect of pH and temperature on ions removal

Previous researchers have studied the effect of pH on P removal by struvite precipitation and demonstrated that P removal efficiency increased as the pH increases between 7.0 and 11.5 (Liu et al., 2018) because of the lower solubility of struvite at higher pH values (Doyle & Parsons, 2002). However, we found similar Mg and P removal as struvite at the three pH conditions evaluated (i.e., pH 8, 9 and 10) at high concentrations (7.9 mmol; calculated from the initial mmol of P in the solution; Figure 21a). Removal of Ca and N increased as the pH increased (Figure 21a), explained by the formation of calcium carbonates ( $\text{CaCO}_3$ ) and calcium phosphates ( $\text{Ca}_3(\text{PO}_4)_2$ ). Ammonium removal can be explained as a combination of precipitation and volatilisation processes, the latter favoured under well mixing conditions at higher pH levels. The percentage of volatilised  $\text{NH}_3\text{-N}$  was 13, 22 and 54% of total initial ammonium concentration for pH 8, 9 and 10, respectively (Table 13). These values agree with data from model simulation runs using Visual MINTEQ, which predicted an increase in  $\text{NH}_3(\text{aq})$  with increasing pH (4, 30 and 76 % for pH 8,9 and 10, respectively).

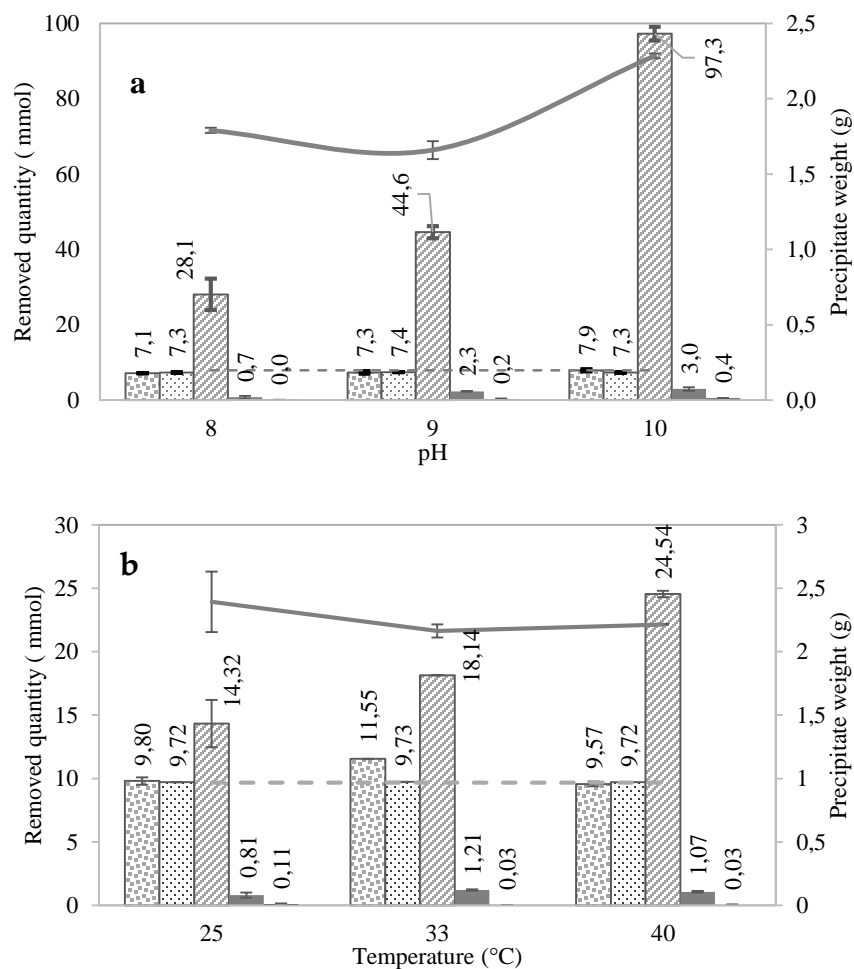


Figure 21. Removed Mg, P, N and Ca quantities from the solution and recovered mass as a precipitate in the pH (a) and T (b) trial. Symbols: Mg, P, N, Ca, K — precipitate mass, — — maximum quantity (mmoles) that can precipitate as struvite.

## Chapter 4. Influence of pH and Temperature on Struvite Purity and Recovery

In pH-tests, the  $\text{PO}_4^{3-}$ -P removal efficiency was  $> 92\%$ , the K removal efficiency was  $< 7\%$  (Table 13), and the Ca precipitation was minimal in all the experiments (Figure 21). The Mg removal efficiency was similar in all the experiments (pH 8, 9 and 10) based on the statistical analysis of experimental data (Anova;  $p$ -value: 0.11). The  $P_{\text{MAP}}$  was higher at pH 9 and 10 than at pH 8 (Table 13), the precipitate mass was higher at pH 10 and the purity was higher at pH 9, indicating that possibly at pH 8 and 10, other products in addition to struvite co-precipitated. The best relation between  $P_{\text{MAP}}$  and purity was reached at pH 9, where  $SI$  almost reached the optimum value of 2.4 for P removal (Ghosh et al., 2019).

In T-tests, the most effective removal of Mg and Ca occurred at  $33\text{ }^\circ\text{C}$  (Figure 21b). This temperature also corresponds to the mean centrate temperature after sludge dewatering and the maximum struvite solubility (Bhuiyan et al., 2007), meaning that part of the struvite-precursor ions are dissolved and available to form other salts like farringtonite ( $\text{Mg}_3(\text{PO}_4)_2$ ), magnesite ( $\text{MgCO}_3$ ) or calcium phosphate ( $\text{Ca}_3(\text{PO}_4)_2$ ). In addition,  $P_{\text{MAP}}$  and purity decreased in comparison with results at  $25$  and  $40\text{ }^\circ\text{C}$ .

Due to a lower TSS concentration and higher phosphate concentration (Table 12), the purity ( $> 87\%$ ) and phosphorus removal efficiency ( $> 99.5\%$ ) was higher in T-tests than in pH-tests (Table 13). The  $\text{NH}_4^+$ -N removal also increased with increasing temperature (Table 13), with an increased volatilisation of  $\text{NH}_3 - \text{N}$  of 5, 12 and 17% total initial ammonium concentration for 25, 33 and  $40\text{ }^\circ\text{C}$ , respectively. This is consistent with model simulations using Visual MINTEQ that showed an increase in the percentage of  $\text{NH}_3$  (aq) as the temperature rose: 30, 42 and 54% total initial ammonium concentration at 25, 33 and  $40\text{ }^\circ\text{C}$ , respectively.

Table 13. Removal efficiency per ion, precipitate quality (mass and richness; particle size). Abbreviations: PMAP, percentage of phosphate as struvite; SI, saturation index; T, temperature trial;  $\text{NH}_3$ -NVol, N volatilised. Note: \*Percentage of the corresponding initial soluble ion concentration. \*\*Score denotes similarity between X-ray diffraction profiles of pure struvite and obtained precipitates (see Figure 23). \*\*\*SI of MAP was calculated by a mathematical model (see Figure 22)

T ( $^\circ\text{C}$ )		20	20	20	25	33	40	ANOVA	
pH		8	9	10	9	9	9	$p$ -value	
Parameter		pH trial			T trial			pH	T
Removal efficiency* (%)	$\text{Mg}^{2+}$	68.6 $\pm$ 0.1	70.4 $\pm$ 3.0	<b>75.8<math>\pm</math>3.0</b>	60.8 $\pm$ 1.5	71.6 $\pm$ 0.1	59.3 $\pm$ 1.2	0.118	<b>0.004</b>
	$\text{Ca}^{2+}$	15.9 $\pm$ 7.8	50.6 $\pm$ 0.5	<b>64.5<math>\pm</math>10.0</b>	35.2 $\pm$ 9.1	52.7 $\pm$ 2.3	46.5 $\pm$ 2.9	<b>0.014</b>	0.109
	$\text{PO}_4^{3-}$ -P	92.7 $\pm$ 0.3	93.9 $\pm$ 0.0	92.8 $\pm$ 0.4	99.5 $\pm$ 0.1	<b>99.8<math>\pm</math>0.1</b>	99.6 $\pm$ 0.0	<b>0.029</b>	0.037
	$\text{NH}_4^+$ -N	16.8 $\pm$ 2.5	26.6 $\pm$ 1.0	<b>58.1<math>\pm</math>1.1</b>	18.6 $\pm$ 2.4	23.5 $\pm$ 0.0	31.8 $\pm$ 0.3	<b>0.0003</b>	<b>0.006</b>
	$\text{NH}_3$ -NVol	13.1 $\pm$ 2.5	22.2 $\pm$ 1.1	<b>53.7<math>\pm</math>1.1</b>	5.4 $\pm$ 1.2	12.8 $\pm$ 0.7	18.7 $\pm$ 0.3	<b>0.0003</b>	<b>0.001</b>
	$\text{K}^+$	0.7 $\pm$ 1.0	3.1 $\pm$ 4.5	<b>7.1<math>\pm</math>0.2</b>	3.9 $\pm$ 1.5	0.9 $\pm$ 0.2	0.8 $\pm$ 1.4	0.261	0.192
	$P_{\text{MAP}}$ (%)	78.4 $\pm$ 0.5	92.7 $\pm$ 4.0	92.8 $\pm$ 0.4	<b>99.6<math>\pm</math>0.1</b>	85 $\pm$ 1.8	98.1 $\pm$ 2.0	<b>0.002</b>	0.071
MAP	Purity (%)	56	<b>70</b>	56	93	87	<b>98</b>	-	-
precipitates	Score** (%)	55	<b>87</b>	68	72	66	<b>74</b>	-	-
	Mass (g)	1.8 $\pm$ 0.0	1.7 $\pm$ 0.1	<b>2.3<math>\pm</math>0.0</b>	<b>2.4<math>\pm</math>0.2</b>	2.2 $\pm$ 0.1	2.2 $\pm$ 0.0	<b>0.001</b>	0.359
	SI***	1.71	2.55	2.80	<b>3.19</b>	3.11	3.07	-	-
	size ( $\mu\text{m}$ )	72 $\pm$ 30.2	<b>84<math>\pm</math>25.6</b>	46 $\pm$ 8.7	44 $\pm$ 7.2	58 $\pm$ 15.6	52 $\pm$ 8.6	<b>0.008</b>	<b>0.007</b>

### 4.3.2 Ions mass balance

The experiments (T and pH tests) were modelled using Visual MINTEQ 3.1 software to determine the saturation index (*SI*) of potential precipitates (Figure 22). According to the current literature (Capdevielle et al., 2013; Le Corre et al., 2005; Li et al., 2016) and the molar mass balance developed in this research (), five compounds were considered as possible precipitates: (a) struvite, (b) amorphous calcium phosphate ( $\text{Ca}_3(\text{PO}_4)_2$ ; ACP), (c) calcite ( $\text{CaCO}_3$ ), (d) magnesite ( $\text{Mg}_3(\text{PO}_4)_2$ ) and (e) farringtonite  $\text{Mg}_3(\text{PO}_4)_2$ . Amorphous calcium phosphate  $\text{Ca}_3(\text{PO}_4)_2$  (ACP) and calcite  $\text{CaCO}_3$  were considered as probable precipitates, but struvite kinetics formation is likely to be faster than ACP. The presence of  $\text{Mg}^{2+}$ , phosphates and dissolved organic compounds could decrease the rate of calcite precipitation. Magnesite precipitates are usually in negligible quantities in anaerobic digestion centrates and farringtonite  $\text{Mg}_3(\text{PO}_4)_2$  can be principally formed at higher pH (Çelen et al., 2007) (Figure 22).

Low amounts of potassium were removed in all experiments (<7%) indicating that potassium struvite ( $\text{MgKPO}_4 \cdot 6\text{H}_2\text{O}$ ) was not formed and explained by the high ammonium concentration in the experiments and no predicted by the model (Uysal & Kuru, 2013). Other solids as dolomite  $\text{CaMg}(\text{CO}_3)_2$ , hydroxyapatite  $\text{Ca}_{10}(\text{PO}_4)_6(\text{OH})_2$  (HA) or huntite  $\text{Mg}(\text{CaCO}_3)$  were not considered as possible precipitates, based on their slow-forming kinetics (Çelen et al., 2007; Hallas et al., 2019) and on the duration of these tests. Neither newberyite  $\text{MgHPO}_4 \cdot 3\text{H}_2\text{O}$  was considered because it only precipitates at  $\text{pH} < 6$  when high concentrations of magnesium and phosphorus are present (Hallas et al., 2019).

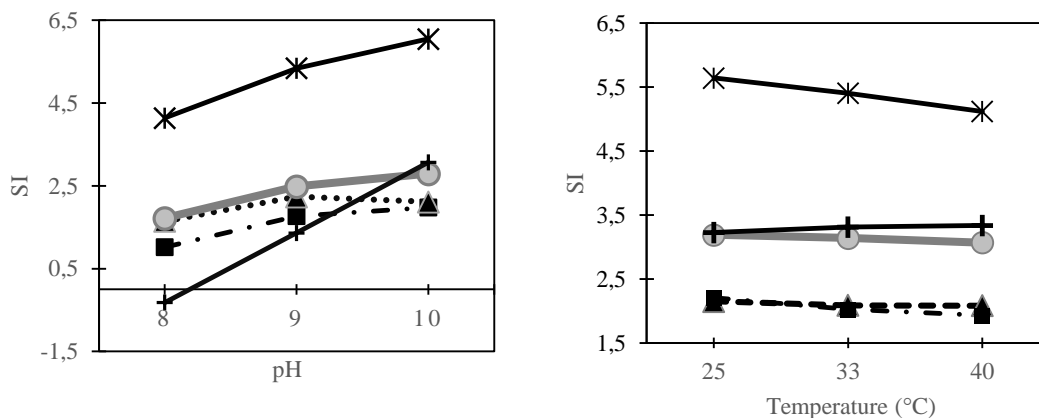


Figure 22. Saturation index (*SI*) calculated with Visual MINTEQ software for expected precipitates at (a)  $\text{pH} = 8, 9$  and  $10$ ; (b) temperature =  $25, 33$  and  $40$  °C. Symbols: ●— Struvite  $\text{MgNH}_4\text{PO}_4 \cdot 6\text{H}_2\text{O}$ , —■— Magnesite  $\text{MgCO}_3$ , ···▲··· Calcite  $\text{CaCO}_3$ , —■— Farringtonite  $\text{Mg}_3(\text{PO}_4)_2$ , —\*— Amorphous calcium phosphate  $\text{Ca}_3(\text{PO}_4)_2$ .

Considering that struvite has a N: P: Mg molar ratio of 1: 1: 1, the maximum moles of struvite that could be precipitated in each test was quantified as the lowest value between the precipitated mmoles of  $\text{Mg}^{2+}$ ,  $\text{PO}_4^{3-}$ -P and  $\text{NH}_4^+$ -N (Table 14). According to the results, the least amount of struvite and calcium phosphates appeared at  $\text{pH} 8$ , likely due to their higher solubility at this  $\text{pH}$  (Yan & Shih, 2016b). Other Mg and P non-struvite precipitates formed at this  $\text{pH}$  probably because of the oversaturation of  $\text{Ca}_3(\text{PO}_4)_2$  and  $\text{MgCO}_3$  (Figure 22; Table 14).

The maximum amount of struvite that could precipitate at both pH 9 and 10 was 7.3 mmol; however, at these conditions is where the highest concentrations of Ca and Mg also precipitate (Table 13 and Table 14). Although the *SI* of  $\text{Ca}_3(\text{PO}_4)_2$  increased with the pH (Figure 22), the most feasible Ca-precipitate at pH 10 is  $\text{CaCO}_3$  since high alkalinity levels favour its formation (Vasconcelos, 2013). Additionally, at high alkalinity values,  $\text{HCO}_3^-$  and  $\text{CO}_3^{2-}$  can bond  $\text{Mg}^{2+}$  ions, which leads to the formation of stable aqueous phases of  $\text{MgCO}_3$ ,  $\text{Mg}(\text{HCO}_3)_2$ , and, therefore, can reduce the availability of this constituent for struvite nucleation (Siciliano et al., 2020). Both  $\text{MgCO}_3$  and  $\text{CaCO}_3$  presented high *SI* value at pH 10 (Figure 22).

In temperature tests, the least amount of precipitated struvite and the maximum quantity of Mg, Ca and P in non-struvite precipitates occurred at 33 °C (Table 14). According to calculated *SI* values,  $\text{CaCO}_3$ ,  $\text{Mg}_3(\text{PO}_4)_2$  and  $\text{Ca}_3(\text{PO}_4)_2$  can be taken as impurities in the precipitate. Regarding  $\text{NH}_4^+$ -N removal at 25 and 40°C, it has been reported that a small amount could be removed as  $\text{NH}_4\text{OH}$  (Tansel et al., 2018) (<0.5 mmol), however this is very unlikely. In fact, the model in Visual MINTEQ did not predict  $\text{NH}_4^+$ -N precipitates other than struvite, in agreement with the findings of Li et al.(2019).

Table 14. Ion balance in precipitates, including struvite, and non-struvite precipitates.

Test conditions		Quantity of total and individual ions in the precipitates (mmol)										
		Total precipitates and MAP <sup>1</sup>						non-struvite precipitates (see Figure 22)				
T (°C)	pH	Mg <sup>2+</sup>	Ca <sup>2+</sup>	NH <sub>4</sub> <sup>+</sup> -N	PO <sub>4</sub> <sup>3-</sup> -P	K <sup>+</sup>	MAP <sup>1</sup>	Mg <sup>2+</sup>	Ca <sup>2+</sup>	NH <sub>4</sub> <sup>+</sup> -N	PO <sub>4</sub> <sup>3-</sup> -P	K <sup>+</sup>
20	8	7.1	0.7	6.2	7.3	0.0	6.2	0.9	0.7	0.0	1.1	0.0
20	9	7.3	2.3	7.4	7.4	0.2	7.3	0.0	2.3	0.1	0.1	0.2
20	10	7.9	3.0	7.4	7.3	0.4	7.3	0.6	3.0	0.1	0.0	0.4
25	9	9.8	0.8	10.1	9.7	0.1	9.7	0.1	0.8	0.4	0.0	0.1
33	9	11.5	1.2	8.3	9.7	0.0	8.3	3.3	1.2	0.0	1.4	0.0
40	9	9.6	1.1	10.1	9.7	0.0	9.6	0.0	1.1	0.5	0.1	0.0

<sup>1</sup> MAP is the maximum amount of struvite (mmol) that precipitated in each test.

### 4.3.3 Size and morphology of struvite crystals

In all tests, MAP precipitation was favoured compared to other Mg and Ca precipitates confirmed by XRD analysis (Figure 23). Results from the High Score plus software used to process XRD data, the corresponding scores were calculated for all precipitates determining how well their XRD profiles match with struvite standards, where a high score indicates a better match. According to the results, the maximum score of 87% was found at pH 9. The peaks of the diffraction patterns could be assigned to struvite in all sets of conditions between pH 8 and 10 increasing progressively in crystallinity (Figure 23; Table 13). No other crystalline phases were identified demonstrating that the amount recovered from other precipitates is minimal. In T-tests, the diffraction patterns from the solids of experiments at 25°C, 33°C and 40°C also showed the presence of struvite, but in lower degree of crystallinity compared to that of the test at pH 10.



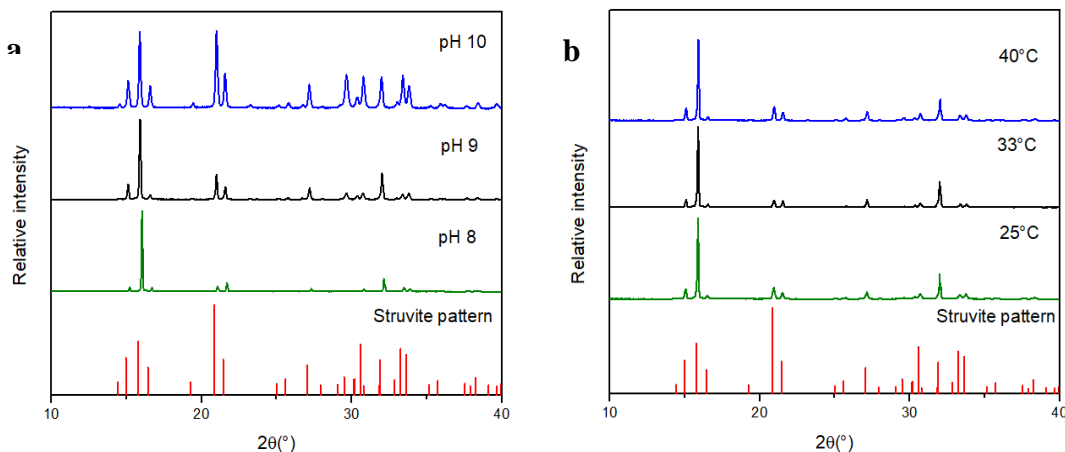


Figure 23. X-ray diffraction (XRD) diagram of precipitates obtained in the pH (a) and temperature (b) tests.

The purity of the final product is essential for the successful and economic recovery of MAP crystals; a high product purity would improve both the product's effectiveness for end-use application and the market price. The high TSS content of centrates and the moderate concentration of ions in solution, such as  $\text{Ca}^{2+}$ ,  $\text{K}^+$  and  $\text{CO}_3^{2-}$ , could affect the purity of the formed struvite (Li et al., 2016; Zhang et al., 2012). However, the high N:P molar ratio of the centrate and the molar ratios  $\text{Mg}:\text{Ca} > 2$  and  $\text{Mg}:\text{P} > 1$  improved the precipitation of struvite over others precipitates as calcium and magnesium phosphate (Capdevielle et al., 2013).

Product quality also includes the struvite morphology and particle size distribution, as these are all relevant characteristics for the end-use product. Particle size is an essential characteristic during crystallisation, larger particle sizes of struvite are of particular interest for applications as fertiliser since the MAP released from this mineral is slow because of the lower surface area to volume ratio (Li et al., 2016). In pH-tests, the largest mean particle size was obtained at pH 8 (72  $\mu\text{m}$ ) and pH 9 (84  $\mu\text{m}$ ), meanwhile the largest mean particle size was obtained at 33  $^{\circ}\text{C}$  (58  $\mu\text{m}$ ) in T-tests (Figure 24 and Table 13). An increase in the saturation ratio increases the nominal weight of fines since a higher *SI* level results in a higher nucleation rate than the crystal growth rate (Ghosh et al., 2019). Therefore, due to the higher struvite *SI* at pH 10 (2.8) and temperature 25 $^{\circ}\text{C}$  (3.19), the mean particle size was smaller in these two tests (Figure 24c-d). Although *SI* is lower at pH 8 than at pH 9, the particle size did not show significant differences (ANOVA;  $p$ -value > 0.05), possibly because the reaction rates are lower at pH 8, and the reaction time was not enough to obtain the maximum particle size.

All the obtained particle sizes were smaller than those sizes previously reported to facilitate a low release of P and N in crops (>1 mm) (Rahman et al., 2013). This may be related to the presence of Ca, to the high *SI* produced by the high concentration of ammonium in the centrate and to the low reaction time in the tests (3h)(Shaddel et al., 2019; Stratful et al., 2001; Tarragó et al., 2016).

In the crystallisation process, settling velocity is an essential factor in ensuring efficient solid-liquid separation and obtaining a more significant recovery of nutrients. The settling velocity is strongly dependent on the sizes and morphology of the precipitates. According to Shaddel et al.(2019), the bigger crystals settle faster for all morphologies; also, among different morphologies, the bipyramidal crystals have the highest settling velocity for all crystal sizes, followed by X-shape and the dendritic crystals.

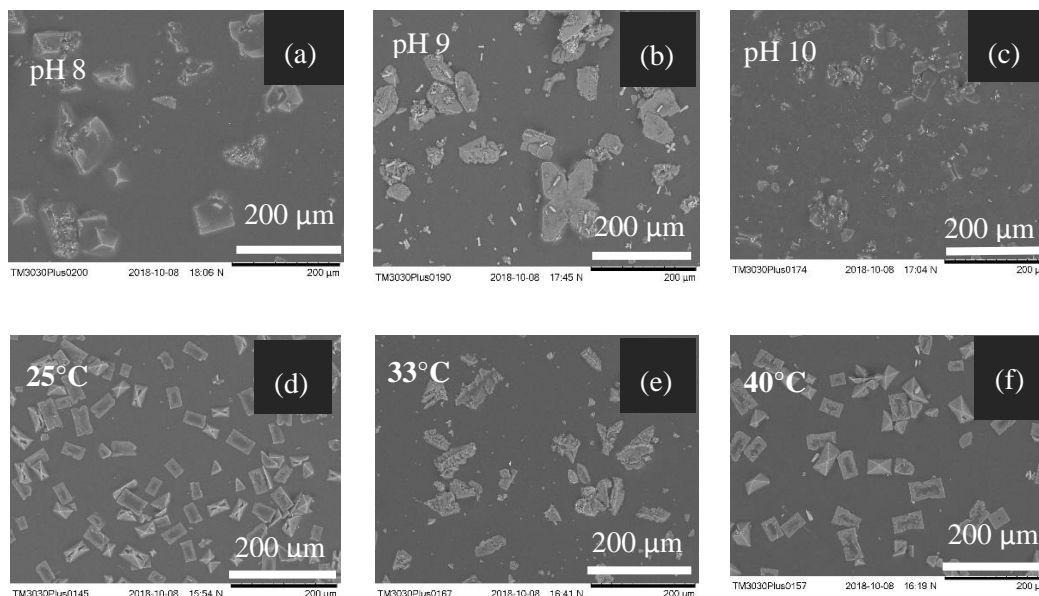


Figure 24. SEM images of precipitates obtained in pH (a, b,c) and temperature (d, e, f) trials. pH 8,9,10 at  $T=20^{\circ}\text{C}$  (a,b,c, respectively);  $T$  25, 33,  $40^{\circ}\text{C}$  at pH 9 (d,e,f, respectively).

At pH 8, a plate crystal morphology predominately formed in comparison to that at pH 9-10. A more dendritic crystal with a less defined X-shape morphology was obtained at pH 10, exhibiting particle agglomeration that can be explained by the high  $SI$  at this pH condition. As previously reported,  $SI$  have a significant impact on the morphology of crystals with low  $SI$  (1.56) yielding plate-shaped crystals and high  $SI$  ( $> 2.69$ ) forming needle-shaped crystals with sharper edges (Ghosh et al., 2019; Shaddel et al., 2019). The struvite morphologies obtained in this work at 25 and  $40^{\circ}\text{C}$  showed a well-faceted structure, with a bipyramidal appearance while at  $33^{\circ}\text{C}$  a combination of different morphologies were obtained likely because of the presence of Ca and Mg in the system. According to Liu & Qu (2017), an increasing N:P molar ratio increases the crystal size and the crystal shape changes from a triangular prism to an irregular X shape; however, the latter is considered an undesirable morphology for its use as fertiliser as it is not compatible with current farming practices for fertiliser spreading and transport, for which a granulated material is often preferred. In this work, the best-operating conditions to obtain a pure struvite crystals with a higher sedimentation rate were at pH 9 (high N:P molar ratio, 21.6:1) and  $40^{\circ}\text{C}$ .

## 4.4 Conclusions

The influence of pH and temperature on struvite precipitation (MAP removal) efficiency and purity from a real complex centrate, from the dewatering of digested municipal sludge, was investigated. In all conditions tested, P-removal was favourable with an efficiency higher than 93%; however, to obtain struvite with higher purity and larger particle size, that allows a slower release of nutrients in its application as a fertiliser, the recommended conditions are a pH 9 and  $40^{\circ}\text{C}$  linked to a system in which any ammonium lost due to volatilisation is also recovered (i.e., acid solution absorption) to avoid its release to the environment.

The purity of struvite was influenced by the presence of  $Mg^{2+}$ ,  $Ca^{2+}$ ,  $PO_4^{3-}$  and the TSS content of the initial centrate, as well as by pH and temperature. Although the high concentration of ammoniacal N in the centrate favours the purity of the struvite obtained, such purity was strongly reduced at pH 8 and 10, and at a temperature of 33 ° C. A pH 8 could favour the precipitation of Ca and Mg compounds, such as  $Ca_3(PO_4)_2$  and  $MgCO_3$ , whereas the most feasible Ca-precipitate is  $CaCO_3$  at pH 10 since high alkalinity levels favour its formation. The temperature of 33 ° C, which is typical of sludge dewatering supernatants (by centrifuge), is not recommended to precipitate struvite, since the solubility of struvite is maximum at this temperature and therefore, the precipitation of other compounds such as  $CaCO_3$ ,  $Mg_3(PO_4)_2$  and  $Ca_3(PO_4)_2$  is favoured.

Under more practical conditions, the recommended process conditions for P recovery as struvite precipitates from the digester supernatant (centrate) from a WWTP are pH 9 and 20-25 °C, this is mainly based on the high P recovery as MAP, the purity of the crystals (70-93%), the lower precipitation of impurities, reduction in the operation cost ( by not increasing the centrate temperature to 40 ° C) and acceptable ammonia losses due to volatilisation and lower temperatures.

### 4.5 Acknowledgements

The authors thank David Elliot, Lucy Leonard and Christian Aragon from the School of Civil Engineering, University of Leeds; Celia Segura and Marlene Mendoza from IRTA; and GAIA group from Universidad de Antioquia for their technical support, as well as Yorkshire Water's Esholt WWTW for facilitating sample collection. C. González thanks Colciencias and Enlaza Mundos for the financial support for her PhD Internship. IRTA thanks the financial support of CERCA Program and INIA through the research project PIONER (ref. RTA2015-00093-00-00).

## **Chapter 5. Struvite recovery from municipal wastewater sludge dewatering centrate using a stirred tank and a fluidised bed reactor**

### **Highlights**

- It is technically feasible to recover N&P as struvite from centrates with low phosphorous concentration (30-120 mg P-PO<sub>4</sub><sup>3-</sup>), using a continuous crystalliser under CSTR and FBR configuration.
- Aeration applied to the CSTR struvite crystalliser increased the fine particulate losses in the effluent.
- Struvite granules as seed material can increase the quantity, purity and size of struvite precipitates.
- The average ammonia loss by the effluent and volatilisation in both reactors was 35% and 16% respectively under tested conditions, due to the high N/P molar ratio of the centrates (>19) and the high pH (9) during struvite precipitation.

### **Abstract**

Struvite precipitation is one of the most widely used and studied techniques to recover nutrients from wastewater treatment plants, including feedstocks like sewage sludge, sludge ash or wastewaters. However, investigations in Latin America are still incipient. In this work, the effect of saturation index (SI), seed material (SM) and aeration on the quantity and quality of struvite precipitates were evaluated, carrying out the crystallisation process in an aerated and continuous Complete Stirring Tank Reactor (CSTR) and a Fluidised Bed Reactor (FBR). A real centrate from anaerobically digested sewage sludge, from a conventional WWTP secondary treatment, was used as raw material with their P concentration modified to simulate WWTPs centrate coming or not from biological P removal units (30-120 mg P-PO<sub>4</sub><sup>3-</sup>). The results showed high efficiency of phosphate (PO<sub>4</sub><sup>3-</sup>-P) precipitation (>85% incoming PO<sub>4</sub><sup>3-</sup>-P), being >63% of precipitated PO<sub>4</sub><sup>3-</sup>-P as struvite (PMAP) with a mean purity >73%. Nonetheless, due to a high N: P molar ratio in the centrate, a high percentage of ammonia loss by the effluent and volatilisation was found (35% and 16% incoming N-NH<sub>4</sub><sup>+</sup>, respectively) in both reactors. These results indicate the feasibility of recovering nutrients as struvite from centrates with a low P concentration, using a CSTR and FBR crystalliser; however, it is recommended to couple this process with a system aimed at recovering N from volatilised ammonia, as well as an after-treatment for the removal and/or recovery of N from the reactors effluent.

**Keywords:** Struvite crystallisation, CSTR, FBR, nutrients recovery

**Note:** One part of this article was presented as **Oral presentation** at the *Latin American Meetings on Anaerobic Digestion*, vol. Chile Sess, 22<sup>th</sup> and 29<sup>th</sup> October and 5<sup>th</sup> and 12<sup>th</sup> November, 2020, pp. 5–8.

## 5.1 Introduction

Struvite or MAP (magnesium ammonium phosphate) crystallisation is one of the most widely used methods to recover nutrients from Wastewater Treatment Plants (WWTPs); however, the investigations in Latin America, and the Caribbean region (LACR) have been limited, mainly because the main concern is improving sanitation coverage (nearly 77% of the population in LACR lacks safe sanitation; Cardoso et al., 2019). In addition, LACR has a limited number of WWTPs with tertiary treatment for nutrient removal (FAO, 2017) devoted to nutrients (N and P) recovery.

Although uncontrolled struvite precipitation can cause significant operational problems in WWTPs (Marti et al., 2008), it brings the opportunity to recover nutrients from wastewater if produced under controlled conditions. Due to its slow-releasing characteristics, struvite is considered an eco-friendly fertiliser because the plant can uptake most of the N without any waste, reducing N loss through leaching and volatilisation in comparison with traditional fertilisers like the urea (Rahman et al., 2013). However, the quantity and quality of struvite precipitates depend on many factors, including pH, P:N: Mg molar ratio, in-reactor saturation index (SI), temperature, P concentration, the use of seed material (SM), and the hydrodynamics of the reactor (mixing conditions) used for their formation (Li et al., 2019).

Several articles have been published regarding the effectiveness of the struvite crystallisation process in recovering phosphorus from wastewaters. However, the effects of some variables as type of reactor, SI, SM and aeration are inconclusive.

In crystallisation, SM acts as a template in which further accumulation of crystallising material takes place. Seed controls nucleation by providing surface area and thus reducing the induction period for crystal development (Kataki et al., 2016). Compared to struvite seed addition, lower crystallisation rates and higher induction time are reported for non-struvite seed (Ali & Schneider, 2005). Some investigations reported the insignificant effect of seed on struvite crystallisation (Rahaman et al., 2008) while some others report enhancement of recovery and size growing using struvite seeds (Liu et al., 2008; Tang and Ma 2016).

According to Adnan et al. (2003), the formation of struvite crystals mainly depends on the degree of SI of the inlet solution that is a function of pH, as well as on the concentration of magnesium, ammonium, and phosphate. Both nucleation and crystal growth rates scale with supersaturation; thus, the reaction times for completing the precipitation shorten under high supersaturation. On the one hand, crystal size is determined dominantly by supersaturation due to its strong effect on the nucleation rate, so low supersaturation levels result in slow reaction kinetics but also in large size crystals with a lower content of fine particles (Shaddel et al., 2019). On the other hand, Ping et al. (2016) proved that increasing PO<sub>4</sub>-P concentration resulted in larger average diameter and higher purity of struvite pellets. Therefore, the combined effect of P concentration and saturation index on the size and purity of struvite crystals constitute an open field in research.

NaOH is generally used to adjust the pH; however, its chemical dosage increases the ionic strength of a solution and thus might also increase the struvite dissolution potential (Li et al., 2019). Therefore, aeration is another alternative to adjust the pH. Aeration strips carbon dioxide and thus alters the carbonate chemistry of the liquors, increasing pH (Doyle & Parsons, 2002) and, according to Fattah et al. (2010), it has been shown to reduce the caustic chemical addition by over 50%, depending on operational conditions. Pastor et al. (2010) also showed that, although aeration can clean struvite

crystals from suspended solids, it can also increase the loss of phosphorus with the effluent of the reactor and promote ammonium volatilisation.

The efficiency of different types of reactors has been evaluated in the literature. However, Completely Stirred Tank Reactors (CSTR) and up-flow Fluidised Bed Reactors (FBR) are the most commonly used either on a laboratory, pilot or full scale (Agrawal et al., 2018). The hydrodynamic conditions in the precipitation reactor can also affect the size and quantity of the produced particles strongly (Valsami-Jones, 2005) because they play an important role in preventing local supersaturation (Ali, 2005) and the hydraulic shear forces can affect the size of the precipitates (Crutchik et al., 2017). However, few studies compare the efficiency of these two types of reactors in terms of quantity and quality of the recovered struvite.

Thus, this work aims to evaluate the technical feasibility of struvite precipitation from centrates with low P concentration ( $<120 \text{ mgPO}_4^{3-}\text{-P/L}$ ) and high ammonium concentration ( $>400 \text{ NH}_4\text{-N/L}$ ), usually found in conventional WWTP with secondary treatment, focusing on operational parameters such as SI, aeration and SM on struvite crystallisation. We studied the efficiency of the process in two types of reactors (CSTR and FBR), considering phosphorus removal from the centrate (recovery percentage), as well as the quality of the final product. Finally, an evaluation of the operating costs of both reactors is carried out under the experimental conditions to know the economic viability of the process, considering only the sale price as an economic benefit.

## 5.2 Materials and Methods

### 5.2.1 Centrate from a conventional WWTP

Centrate produced by dewatering anaerobically digested sludge was collected from San Fernando WWTP in Itagui (Antioquia - Colombia) in which a conventional activated sludge process is used for wastewater treatment, while anaerobic digestion is used for sludge treatment. A thickening process concentrates secondary sludge. The primary and secondary sludges are combined afterwards in the anaerobic digester. The digested sludge is finally dewatered, using centrifugal equipment. The main characteristics of the centrate are shown in Figure 15. For the experiments, approximately 120 L of centrate were collected in 25 L plastic cans and refrigerated at  $4^\circ\text{C}$  to prevent further degradation. The centrate used in the tests was diluted with distilled water (40/100) and the concentrations of P, N and Mg were adjusted to ensure the experimental conditions (Table 16). The centrate was diluted to have enough to run the 24 tests in each reactor.

Table 15. Composition of the centrate from San Fernando WWTP. Samples were taken between September 2016 and June 2019 (\* mean of three/four values, \*\* mean of five/ seven values and the others are a mean of twelve).

Parameter	Mean concentration (mg/L, except for pH and temperature)	Parameter	Mean concentration (mg/L)
PO <sub>4</sub> -P	22 ± 14	TS	2524± 990
NH <sub>4</sub> -N	826 ± 238	TSS	1612 ± 802
Mg	33 ± 23	DS	1260 ± 770
Ca	68 ± 66	VS	1923 ± 717
K	109 ± 38	Fe*	0.34 ± 0.44
Al	0.36 ± 0.19	Cr*	N. Q
TP	43 ± 15	Ni*	N. Q
TKN	1069 ± 249	Pb*	N. Q
Alkalinity (CaCO <sub>3</sub> ) **	3553 ± 729	Na*	80 ± 64
COD (O <sub>2</sub> ) **	3478 ± 708	Sulphates*	62 ± 3
BOD(O <sub>2</sub> ) **	867 ± 566	Nitrates*	77 ± 2
pH*	7.6 ± 0.5	Fluoride*	N. Q
Temperature (°C) *	33.3± 0.6	Chlorides *	116 ± 19

NQ are non-quantifiable parameters.

## 5.2.2 Reactors design and operation

Two different reactors, a CSTR and an FBR, were used during the experiments. The CSTR was made in acrylic, had a working volume of 5L and was designed according to Regy et al. (2002), with separate reaction and sedimentation zones. The reaction zone was equipped with four baffles to prevent the formation of vortex effects during mixing. This reactor was operated in continuous mode for the liquid phase (centrate), which enters in the mixing zone and flows out at the top of the settler (see Figure 25). The settling zone is located above the reaction zone and is cone-shaped with an angle of 45° between the two zones. This part is also equipped with a baffle to guide the flow. The number of baffles (4) in the reaction zone was different from the number of impeller blades (2) to reduce the risk of entering in resonance (Valsami-Jones, 2005). The reactor was equipped with two stainless steel meshes dimensioned to fit in the upper reactor baffle (1) and conical section (2), both in the sedimentation zone. Both meshes were made of woven wire stainless steel 0.212 mm hole, 0.152 mm wire (mesh 70-AISI 304) to act as a seed material to grow struvite and maximise its recovery (Doyle et al., 2002).

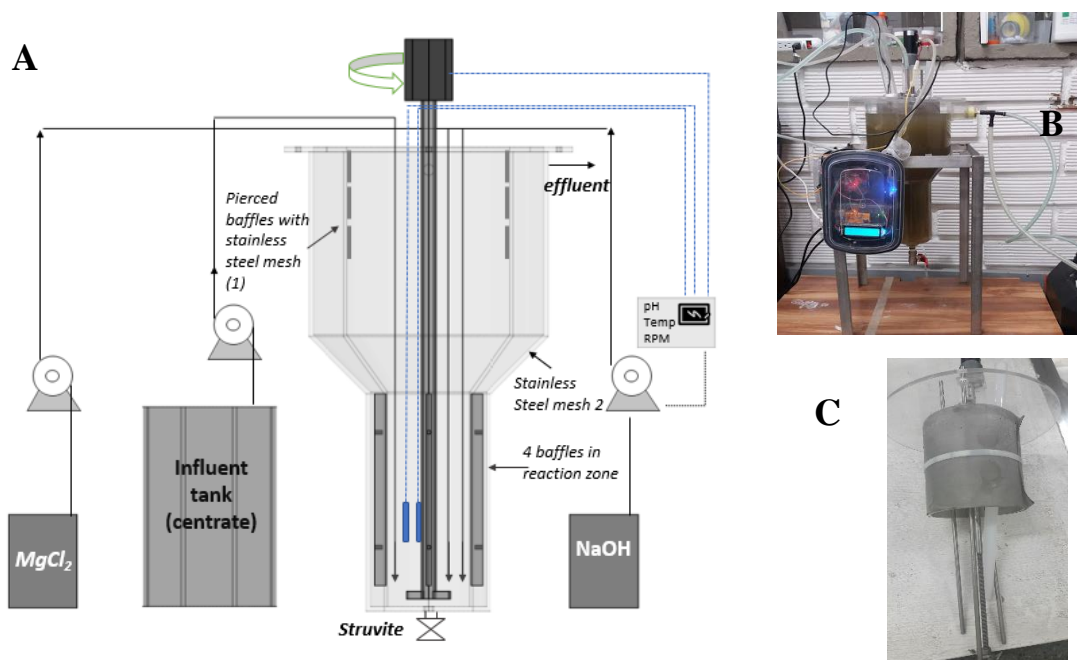


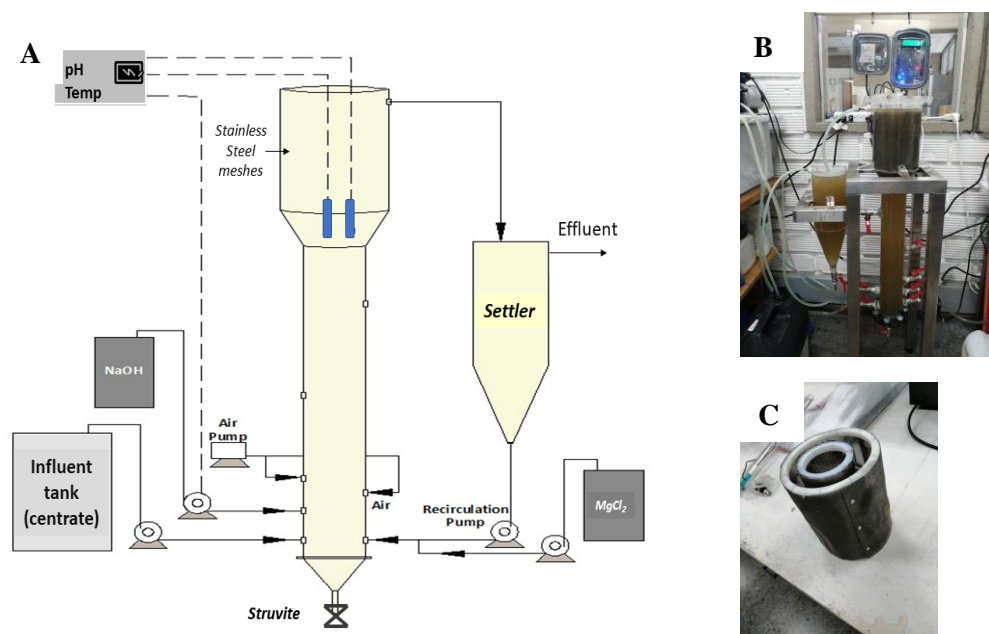
Figure 25. CSTR Reactor. A. Scheme, B. Photo of the reactor, C. Detail of the stainless-steel mesh in the baffling part.

The struvite crystallisation system is composed of four stainless steel injection tubes connected to an air pump and three peristaltic pumps for dosing the dewatering sludge centrate (9 mL/min), MgCl<sub>2</sub>·6H<sub>2</sub>O (2.3 mL/min), and 1M NaOH (1.1 mL/min) to maintain the pH at the desired value. The alkali pump was controlled by a microcontroller (ATmega 2560) arranged on an Arduino board where pH and temperature sensors, LCD and DC motor for stirring were connected.

The FBR was designed after the concept of the fluidised bed reactor by Valsami-Jones (2005), Suleiman et al. (2013) and Yates and Lettieri (2016). The reactor of 6.5 L (useful volume) was made in acrylic, with two different parts: bottom (volume 2.5 L, diameter 80mm), and top (volume 2.8 L, diameter 140 mm). The parts of the reactor are joined with conically shaped structures at an angle of 45° in order to reduce the crystal loss at each junction (Guadie et al., 2014).

Since the bottom diameter is smaller than the upper one, as the liquid flows upwards, its flow velocity decreases and leads to the segregation of the crystals formed. While large crystals are accumulated at the bottom, finer particles flow out from the reactor and are recycled back with the effluent through the external settler of 2.2 L, using a peristaltic pump (Figure 26). The reactor was also equipped with two concentric stainless steel meshes dimensioned to fit in the top part to use them as a substrate to grow struvite (Le Corre et al., 2007) ( Figure 26B and C).





**Figure 26.** FBR reactor. A. Scheme, B. Photo of the reactor, C. Detail of the stainless-steel meshes.

Influent and reagents solutions were supplied to the FBR at the bottom ports, using peristaltic pumps at a rate of 13 mL/min for centrate and 2.3 mL/min for  $\text{MgCl}_2 \cdot 6\text{H}_2\text{O}$ . A pH probe was introduced in the top part to control and maintain the pH constant during the crystallisation process, using the same control system of the CSTR tests. The NaOH (1M) application rate was 5 mL/min (dosage applies only at pH below 9). The up-flow velocity was 2.6 cm/min in the bottom and 0.85 cm/min in the top part to ensure fluidisation of the bed and avoid the elutriation of finer particles (20  $\mu\text{m}$ ). The recirculation rate ( $Q_r$ ) was 114 mL/min, and the recycle ratio (RR) was 85%. (RR defined as the quantity of the recycled flow/the quantity of the total up-flow stream). More information on the design of the reactors can be found in the general annexes section (Annex 2. Reactors design) of this thesis.

### 5.2.3 Experimental setup

The experiments were conducted using a factorial design of order  $3 \times 2^2$  (levels -1, 0, +1 for one factor and level -1 and 1 for two factors). Common statistical tools, such as analysis of variance, F-test and the Student's t-test, were used to define the most important process variables affecting struvite crystallisation. The factorial experimental design methodology involves changing all variables from one experiment to the next. The reason for this is that variables can influence each other, and the ideal value for one of them can depend on the values of the others (Montgomery, 2004). Three operation factors were analysed: phosphorus and ammonium concentration (in pairs of P and N were 30-400, 70-800 and 120-1000 mg  $\text{PO}_4^{3-}\text{-P} \cdot \text{L}^{-1}$  and mg  $\text{NH}_4^+\text{-N} \cdot \text{L}^{-1}$ , respectively), aeration (with and without) and seed material (with and without). According to the results obtained by previous one-factor design experiments (see chapters 3-4 and González et al., 2019) pH, temperature and stirring speed were fixed at 9, 25 °C and 200 rpm ( $G \ 155 \ \text{s}^{-1}$ ). Experimental conditions are shown in Table 16.

**Chapter 5.** Struvite recovery from municipal wastewater sludge dewatering centrate using a stirred tank and a fluidised bed reactor

Table 16. Experimental conditions.

C	Factor		P and N concentration		Aeration rate (L-Air min <sup>-1</sup> )		SM g/L	Struvite SI	Molar relation P: N: Mg
	Aeration	SM	mg P-PO <sub>4</sub> <sup>3-</sup> /L	mg N-NH <sub>4</sub> <sup>+</sup> /L	CSTR	FBR			
-1	1	1	30	400	0.45	1.3	1	1.34	1:33:2.1
-1	1	0	30	400	0.45	1.3	0	1.34	1:33:2.1
-1	0	1	30	400	0	0	1	1.34	1:33:2.1
-1	0	0	30	400	0	0	0	1.34	1:33:2.1
0	1	1	70	800	0.45	1.3	1	2.04	1:25:1.4
0	1	0	70	800	0.45	1.3	0	2.04	1:25:1.4
0	0	1	70	800	0	0	1	2.04	1:25:1.4
0	0	0	70	800	0	0	0	2.04	1:25:1.4
1	1	1	120	1000	0.45	1.3	1	2.40	1:19:1
1	1	0	120	1000	0.45	1.3	0	2.40	1:19:1
1	0	1	120	1000	0	0	1	2.40	1:19:1
1	0	0	120	1000	0	0	0	2.40	1:19:1

\* The experiments were conducted randomly to guarantee the independence of the data.

\*\* C is the level of P and N concentration.

The CSTR and FBR systems were operated in a semi-continuous mode. All experiments were conducted at ambient temperature (23°C) over 7 hours and repeated two times to ensure reproducibility of the results. Effluent samples were collected at constant intervals, the first sample after 1 hour and later ones every 2 hours. Four effluent samples were collected for each experimental run to observe the variation of conductivity, PO<sub>4</sub><sup>3-</sup>-P and NH<sub>4</sub>-N over time. The struvite pellets were not harvested until the end of a cycle. The crystals could settle for 7 hours once all the pumps were switched off, and the crystals were removed by opening the bottom valve.

The significant factors affecting the different response variables were determined with an analysis of variance (ANOVA). From the P values—defined as the smallest level of significance that leads to rejection of the null hypothesis—it appears that the main effect of each factor and the interaction effects are statistically significant when P < 0.05. The statistical analysis was performed using the R software package (R project for statistical computing, <http://www.rproject.org> and statgraphics software <https://statgraphics.net/>).

The aeration was 0.45 L-Air min<sup>-1</sup> for the CSTR, and was 1.3 L-Air min<sup>-1</sup> for the FBR, lower than the used by Cerrillo et al.(2014) and Jordaan (2011). The level of aeration in both reactors was chosen to avoid or reduce the loss of fines by the effluent. The FBR required a slightly higher aeration rate for bubble formation because the water column is higher in this reactor. The aeration flow rate of the air pump was measured with a thermal dispersion flow meter (One Omega Drive- Model # FVL-1608A-I).

The SM was synthetic struvite produced in a jar test, adding 1 g L-reactor<sup>-1</sup> as recommended by Ali & Schneider (2005) and Liu et al. (2008). To produce the amount of struvite necessary for all tests, two jar tests of 6 glasses each (2L) were performed at 3.16 mol PO<sub>4</sub><sup>3-</sup>-P. L<sup>-1</sup>, 7.58 mol NH<sub>4</sub><sup>+</sup>-N. L<sup>-1</sup> and 2.84 mol Mg. L<sup>-1</sup>, maintaining the optimal molar ratio Mg: PO<sub>4</sub><sup>3-</sup>: NH<sub>4</sub><sup>+</sup> of 0.9:1:2.4 as suggested by Pastor et al.(2008). The tests were conducted at an ambient temperature, pH 9, a reaction time of 2 hours and a velocity gradient G of 80 s<sup>-1</sup> (120 rpm), according to previous results (see chapter 4).

Struvite was chosen as SM due to the similarity of its lattice structure between seed and mother crystal that improves the integration process of newly born crystals onto the seed surface. Also, struvite has reported higher crystallisation rates and lower induction time compared to non-struvite seeds (Ali & Schneider, 2005; Kataki et al., 2016).

The struvite SI (1.34, 2.04 and 2.32), was calculated using MINTEQ 3.1 software, accounting for three phosphates (30, 70 and 120 mg P-PO<sub>4</sub><sup>3-</sup> L<sup>-1</sup>) and ammonium (400, 800 and 1000 mg N-NH<sub>4</sub><sup>+</sup> L<sup>-1</sup>) initial concentrations in centrates. These P and N contents correspond to the range found in centrates from WWTPs with EBPR (40-350 mg PO<sub>4</sub><sup>3-</sup>-P, 400-1340 mg NH<sub>4</sub>-N) (Guo, 2010; López, 2017) and without EBPR (3.5-50 mg P-PO<sub>4</sub><sup>3-</sup>, 400-1100 mg NH<sub>4</sub>-N). To attain such values, the phosphate content of real centrate samples, collected in a conventional WWTP (San Fernando, Itagui, Colombia), was adjusted with NaH<sub>2</sub>PO<sub>4</sub>·H<sub>2</sub>O. Besides, MgCl<sub>2</sub>·6H<sub>2</sub>O was used to balance the P:N: Mg molar ratio to 1:33:2.1, 1:25:1.4 or 1:19:1. Finally, Mg: Ca and the Mg: P molar ratios were always >2.5 and never <1, respectively, in order to reduce the formation of Ca precipitates and favour the formation of struvite (Li et al., 2016; Shih & Yan, 2016).

### 5.2.4 Hydraulic evaluation

The hydrodynamic conditions in a precipitation reactor can affect the size and quantity of the produced particles (Valsami-Jones, 2005) strongly since they play an essential role in preventing local supersaturation (Ali, 2005). For this reason, in this work, the flow of both reactors was characterised by the residence times distribution (RTD) model, whose purpose is to describe how mass transport occurs inside a reactor that works continuously (Levenspiel, 1986). To evaluate the hydraulic behaviour of the reactors, the trend curve analysis, the Wolf-Resnick model and the model of wholly mixed reactors in series were applied (CEPIS, 2004; Levenspiel, 1986; Wolf & Resnick, 1963).

The RTD was determined experimentally by injecting a pulse of a tracer (NaCl) into each reactor, and then the tracer concentration (E) was measured in the effluent stream as a function of time (Fogler, 2008), by determining water conductivity. Previously, a calibration curve was performed to relate the NaCl concentration to the water conductivity. The tests lasted 28 and 26 hours in the CSTR and FBR reactors, respectively, to guarantee a time greater than three times the average theoretical hydraulic retention time of each reactor (CEPIS, 2004). Further details of the test can be found in Annex 3. Residence time distribution in CSTR and FBR reactors of this thesis.

### 5.2.5 Analytical methods

Centrate characterisation was performed in terms of chemical oxygen demand (COD), alkalinity (Alk), pH, phosphorus, nitrogen, metals and solids, among others, as shown in Table 15. Effluent samples were characterised in terms of total phosphorus (TP), orthophosphate (PO<sub>4</sub><sup>3-</sup>-P), ammonium (NH<sub>4</sub><sup>+</sup>-N), calcium (Ca) and potassium (K). Suspended solids (SS) were determined in the feed solution of each test. Water conductivity and temperature were measured with a conductivity meter (WTW cond 3110), pH was verified with a pH meter (IQ Scientific Instrument).

At the end of each experiment, the precipitates were filtered and dried at room temperature for 24 hours. Then they were weighed on an analytical balance. To analyse the struvite purity, 0.3 ± 0.01 g pellets were dissolved in 10 mL of H<sub>2</sub>SO<sub>4</sub>, then ammonium concentration in the precipitates was determined with the Kjeldahl method (SM 4500). All the analyses were performed by Standard Methods (APHA, 2017).

Two samples of the precipitate obtained in each reactor were characterised by their total organic carbon (TOC) content, using the sulphochromic oxidation method following the ISO 14235 standard (ISO, 1998), as a tool to evaluate the organic matter content in the product obtained.

The morphology and particle size of the precipitate obtained in each test were determined using an inverted microscope BOECO BIB100 at 4,10,20 and 40 X objectives with a digital camera B-CAM 16 megapixel 1 / 3.33" Panasonic CMOS sensor. The viewing software used was Boeckel B-View x64 Windows XP / Vista / 7/8/10 compatible version. After calibrating the image scale, the sizes of at least 100 particles were measured for each test using the Image J software. The morphology of some crystal was also analysed by a scanning electron microscopy (SEM, JEOL JSM 6490 LV). The elemental analysis of these samples was developed with an X-ray Microscope-EDX (INCA PentaFETx3 Oxford Instruments).

Some struvite samples were also examined by X-ray diffraction (XRD) on an XPert PANalytical Empyrean Series II diffractometer with a PIXcel 3D detector 2012 model, using Cu K-alpha radiation. The XRD patterns were recorded in the scanning range of 2-theta from 10°–60°. A small angular step of 2-theta = 0,0220° and a fixed counting time of 90 s was used. Data were collected and processed using High Score Plus 3.0 software. Identification of the phase peaks was accomplished by comparing the observed XRD patterns to that of standard struvite compiled by the Joint Committee on Powder Diffraction and Standards (ICDD,2001). More information about the analytical methods used can be found in Annex 1. General Materials and Methods of this thesis.

## 5.2.6 Costs analysis

The economic analysis was based on the experimental results. The main cost factors affecting the economy of struvite crystallisation are magnesium and alkali sources (Crutchik et al., 2017) , Therefore, we do not consider investment costs such as direct cost (storage tank, reactors, etc.) and equipment, and only we analysed the cost of chemicals and energy. Struvite sales were considered as a potential income.

The market value of struvite ranges from € 0 to € 1590 per ton (Guo, 2010; Muys et al., 2021). According to Muys et al. (2021) struvite is currently mainly marketed at values between €0–100 per ton, but also at prices of €350 per ton (Phoshorgreen) to €1000 (Pearl) per ton. Due to the high variability of the sale price of struvite, two possible sale scenarios were considered: €168 (\$COP 760,000) per ton (mean value commonly reported in papers) and €1590(\$COP 7,163,000) per ton (the highest value found). Currently, the highest value is unlikely considering that in the local market, the similar fertiliser Diammonium Phosphate -DAP (N:P:K;18:46:0) is approximately COP 3,000,000.ton<sup>-1</sup> (Tierragro Company).

### 5.2.6.1 Reagents costs

Reagents cost used in the calculation of operating cost were taken from Crutchik et al.(2017) and Yetilmezsoy et al. (2017) (Table 17). It was because of the variability of the high prices in the country's current situation (global pandemic and social demonstrations in Colombia). The cost analysis was carried out under the three PO<sub>4</sub><sup>3-</sup>-P concentrations evaluated in the tests. Aeration and seed material conditions were not considered in this analysis. Reagent requirements in each reactor was calculated according to the mass of reagents used in each test, the volume of treated water (0.009 and 0.0142 m<sup>3</sup> in CSTR and FBR, respectively) and the mean precipitated P. The cost of use two low-cost magnesium sources (MgSO<sub>4</sub>.7H<sub>2</sub>O and Mg(OH)<sub>2</sub>) under the same test conditions was also considered to compare the results. The same efficiency in the P precipitation was assumed for this

comparison. The consumption of NaOH was taken as zero for the use of Mg(OH)<sub>2</sub> because this reagent has the advantage of also raising the pH (Munch & Barr, 2001) and equal to the tests for the use of MgSO<sub>4</sub>·7H<sub>2</sub>O.

Table 17. Reagents consumptions and costs

Reagent/P concentration (mg/L)	Reagent requirements in each reactor (Kg/m <sup>3</sup> centrate)						Costs (1€=4500 \$COP)	
	CSTR			FBR			€/Ton	\$ COP/Kg
	30	70	120	30	70	120		
MgCl <sub>2</sub> ·6H <sub>2</sub> O	0.21	0.43	0.67	0.36	0.58	0.76	656.25	2953.13
NaOH	0.65	0.64	0.78	0.58	0.87	1.00	437.50	1968.75
Mg(OH) <sub>2</sub>	0.06	0.12	0.19	0.10	0.17	0.22	350.00	1575.00
MgSO <sub>4</sub> ·7H <sub>2</sub> O	0.25	0.52	0.81	0.43	0.70	0.91	437.50	1968.75

### 5.2.6.2 Energy costs

In the mixing power calculations, the selected velocity gradient was 79 s<sup>-1</sup>, according to the result found in Chapter 3 (González-Morales et al., 2019). The centrate temperature was selected as 25°C, due to the high recovery and precipitate purity found at this temperature in Chapter 4. To determine the engine power and electricity costs required for the industrial static mixer, dynamic viscosity was calculated by using the Poiseuille's and the safe mixing power equations (for temperatures between 0 °C and 100 °C) as shown in Equation 9 and Equation 10 (Yetilmezsoy et al., 2017). The safe mixing power was obtained as PSF =0.85 kW for a full-scale fertiliser plant based on these equations

The energy consumed by the centrate, Mg and NaOH pumps was calculated according to the power required by each selected pump. Considering the mean centrate flow in the WWTP (126 m<sup>3</sup> / h) and the mean consumption of MgCl<sub>2</sub> and NaOH solutions in the tests (reagents/m<sup>3</sup>), the flow for the three pumps were selected as 126 m<sup>3</sup>/ h, 14 m<sup>3</sup>/ h and 2 m<sup>3</sup>/ h, respectively for CSTR reactor and 126 m<sup>3</sup>/ h, 9 m<sup>3</sup>/ h and 1.8 m<sup>3</sup>/ h, respectively for FBR reactor. A flow rate of 880 m<sup>3</sup>/h was selected for the recirculation pump in the FBR system to maintain the same ratio of influent to recirculation flow. According to the flow rates, possible pumps were chosen for each solution (from the Homecenter, Evans and New dose companies). The electricity price of 532.8 \$ COP/kW h (0.118 €/kW h) was chosen according to the energy price in Itagui municipality for the first semester of 2021.

### 5.2.7 Calculations

Process efficiency was calculated based on phosphorus and nitrogen removal from the solution. Two types of phosphorus efficiencies were calculated according to Pastor et al. (2008): precipitation efficiency (PP) and recovery efficiency (PR).

**Precipitation efficiency (%):** PP is calculated as the percentage of the soluble phosphorus (SP) entering the reactor that precipitates, according to Equation 5.

$$PP(\%) = \frac{(PO_4^{3-}-P)_{INF}-(PO_4^{3-}-P)_{EFF}}{(PO_4^{3-}-P)_{INF}} * 100 \quad \text{Equation 5}$$

**Recovery efficiency:** PR considers both precipitation and crystal growth efficiency. It is obtained as the percentage of the total phosphorus (TP) entering the reactor that is not lost with the effluent (Equation 6).

$$PR(\%) = \frac{(TP)_{INF} - (TP)_{EFF}}{(TP)_{INF}} * 100 \quad \text{Equation 6}$$

Where the (PO<sub>4</sub><sup>3-</sup>-P) and (TP) are the concentrations of SP and TP and the sub-scripts "INF", and "EFF" represent influent and effluent, respectively.

The difference between precipitation efficiency and recovery efficiency corresponds to the fine crystals lost in the effluent of the reactor.

**Purity:** the percentage of struvite gives the product purity in the final solid precipitate since struvite is the target compound. Considering that struvite is the only precipitate containing ammonia nitrogen (Bing Li et al., 2016), it can be used as a proxy element to calculate the struvite content in the total solid product, which is determined by Equation 7.

$$Purity (\%) = \frac{n_N * M_{Struvite}}{m_p} * 100 \quad \text{Equation 7}$$

where n<sub>N</sub> are the moles of nitrogen in the precipitate, M<sub>Struvite</sub> is the molar mass of struvite (245.4 g/mol), and m<sub>P</sub> is the mass (g) of the total precipitates.

**P<sub>MAP</sub>:** P was supposed to form struvite, calcium phosphate and other precipitates, so the percentage of phosphate as struvite in the precipitate is calculated according to Equation 8.

$$P_{MAP(\%)} = \frac{n_{MAP}}{n_{SP}} * 100 \quad \text{Equation 8}$$

where n<sub>MAP</sub> are the moles of struvite (n<sub>MAP</sub>=n<sub>N</sub>) and n<sub>SP</sub> are the moles of soluble phosphorus in the precipitate that is calculated according to the difference of SP concentration between the influent and effluent.

**Saturation:** The saturation index (SI) is an indicator of how likely a solid precipitate at aqueous phase conditions. Precipitation occurs when the ionic product of a salt exceeds the solubility limit (Crutchik et al., 2013). An SI < 0 means the solid is under saturated and will remain as such in solution. An SI > 0 means the solid is supersaturated or at potentially precipitating conditions. The struvite SI values and the theoretical yield for each solution were calculated for all the experiments, using the equilibrium speciation model Visual MINTEQ ver. 3.1 professional software (Gustafsson, 2013). More information about SI can be found in Annex 1. General Materials and Methods of this thesis.

**Mixing power:** The energy used for the stirring system in the CSTR reactor was calculated with the following equations.

$$\nu = \frac{0.0179}{1 + 0.03368(T) + 0.000221(T)^2} * \left(10^{-4} \frac{m^2}{cm^2}\right) \quad \mu = \nu * \frac{\tau}{g} \quad \text{Equation 9}$$

$$P = \mu \cdot G^2 \cdot V \cdot \left(9.807 \frac{N}{kgf}\right) \cdot \left(10^{-3} \frac{kW}{W}\right) \quad P_{SF} = P \cdot (SF) \quad \text{Equation 10}$$

where  $\nu$  is the kinematic viscosity ( $m^2/s$ );  $T$  is the wastewater temperature ( $^{\circ}C$ );  $g$  is the specific weight ( $\gamma=1000 \text{ kgf}/m^3$ );  $g$  is the acceleration of gravity ( $9.807 \text{ m}/s^2$ );  $G$  is the velocity gradient ( $s^{-1}$ );  $\rho$  is the specific mass ( $101.97 \text{ kgf s}^2/m^4$ );  $\mu$  is the dynamic viscosity ( $\mu= 0.0000921774 \text{ kgf s}/m^2$  for  $T= 25 \text{ }^{\circ}C$ );  $V$  is the volume of struvite tank (herein  $126 \text{ m}^3$ );  $P$  is the required mixing power (kW, where  $1 \text{ kW}=1000 \text{ watts (W)} = 1000 \times N \cdot m/s$ );  $SF$  is the safety factor (herein  $SF$  is considered as 1.2); and  $P_{SF}$  is the safe mixing power (kW).

## 5.3 Results and discussion

### 5.3.1 Hydraulic evaluation

The hydrodynamic behaviour of CSTR and FBR reactors was characterised at macroscopic scale by measurements of Residence Time Distribution (RTD), using NaCl as the tracer. According to the trend curve method, both reactors have a predominance of mixed flow and presence of hydraulic short circuits. The hydraulic behaviour of both reactors is similar (**Figure 27**); however, the first concentration of NaCl detected in the CSTR occurs at 40 min while in the FBR occurs at 4 min. The up-flow velocity explains this difference in the FBR that is higher than the up-flow velocity in the CSTR. Also, according to Valsami-Jones (2005), the CSTR acts as a perfectly mixed reactor (mixing zone) followed by a plug flow (sedimentation zone).

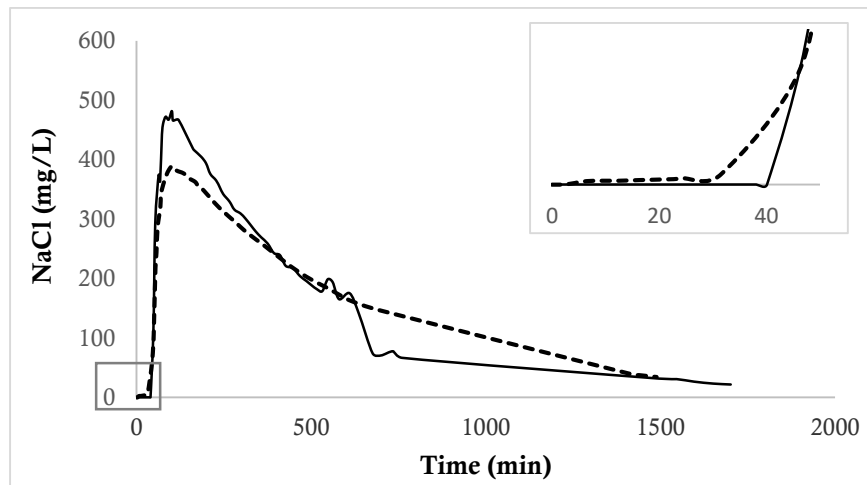


Figure 27. Residence time distribution of CSTR (—) and FBR (----) reactors

The Wolf- Resnik method was also used to determine the hydrodynamic behaviour of both reactors. The results indicate that, in the CSTR and FBR reactors, the perfect mixing predominates (75 and 92%, respectively) (Table 18). The high percentage of plug flow in the CSTR (25%) can be due to its large sedimentation zone that represents about 78 % of its total volume. Meanwhile, high flow recirculation in the FBR increases the percentage of perfect mixing despite its elongated geometry (Levenspiel, 1986). Besides, the high percentage of dead zones in both reactors (59-65%) is due to

**Chapter 5.** Struvite recovery from municipal wastewater sludge dewatering centrate using a stirred tank and a fluidised bed reactor

the volume of the sedimentation zone, which can reduce the effective volume of the reactors and their efficiency (CEPIS, 2004). However, this zone is essential in both reactors to decrease the loss of the finest particles.

**Table 18.** Main results of the reactors hydrodynamic behaviour.

Parameter	CSTR	FBR
Trend curve method		
short circuits	✓	✓
mixed flow	✓	✓
Wolf-Resnick method		
Plug Flow (%)	25	8
Perfect mixing (%)	75	92
		65a
Dead zones (%)	59	(46b)

a. Considering all the system 8.7 L, b considering only the FBR reactor (6.5L)

The real hydraulic retention time (HRT) was calculated according to Levenspiel (1986) and was compared with the theoretical HRT. The results show that the real HRT was slightly lower than the theoretical HRT in both reactors (7.98 and 8.37 h vs 8.38 and 10.59 h for the CSTR and FBR reactors, respectively). The useful volume was also lower than the real one, obtaining a volume of 4.7 L for CSTR ( $V_{real}=5L$ ) and of 6.87 L for FBR ( $V_{real}=8.7 L$ ).

### 5.3.2 Effect of phosphorus and ammonium concentration (C factor)

The tested CSTR and FBR reactors successfully crystallise struvite, achieving mean phosphorus precipitation of 85% and 89 % and mean phosphorus recovery of 68% and 71%, respectively (Table 19). The recovery efficiency is affected by the level of supersaturation obtained in each reactor, which could increase the production of fine crystals. These fine run-offs decrease the value of recovery efficiency, thereby increasing the difference between the two efficiencies (Pastor et al., 2008).

Table 19. Results of the principal experimental factorial design (volatilised nitrogen – Nv; recovery mass-mp).

SI	Factor			Reactor (% except for mp)											
				CSTR						FBR					
				PP	PR	Purity	PMAP	Nv	mp(g)	PP	PR	Purity	PMAP	Nv	mp(g)
1.34	-1	1	1	81.3	59.0	98.1	83.4	11.1	6.1	86.1	67.4	81.7	65.3	14.1	8.3
	-1	1	0	83.9	57.6	69.8	72.2	16.3	1.9	87.2	68.1	76.6	67.7	12.2	2.9
	-1	0	1	77.9	60.9	95.0	76.2	13.1	5.8	92.6	67.0	80.2	76.6	14.8	10.6
	-1	0	0	79.9	66.5	76.4	40.9	21.4	1.1	87.1	53.5	67.0	56.7	8.7	2.8
	0	1	1	88.2	72.9	97.5	80.3	16.8	7.7	87.0	72.1	85.3	59.7	19.3	9.7
2.04	0	1	0	86.9	60.9	68.4	58.3	11.7	3.1	95.4	83.1	75.3	63.1	22.5	5.9
	0	0	1	87.1	71.9	96.1	79.7	10.9	7.9	93.6	78.7	80.8	72.4	18.4	13.0
	0	0	0	82.5	58.8	82.0	51.2	18.2	2.6	90.3	75.2	85.7	64.9	18.1	5.2
2.40	1	1	1	88.0	71.1	93.7	74.1	14.1	10.1	88.4	71.7	86.9	68.8	18.5	15.3
	1	1	0	83.5	67.3	76.2	70.6	15.3	6.4	82.4	76.8	69.1	47.5	22.6	7.8
	1	0	1	91.8	81.1	88.8	84.8	17.0	10.8	87.0	68.9	86.2	74.2	16.3	16.6



**Chapter 5.** Struvite recovery from municipal wastewater sludge dewatering centrate using a stirred tank and a fluidised bed reactor

Factor				Reactor (% except for mp)											
				CSTR						FBR					
SI	C	A	SM	PP	PR	Purity	PMAP	Nv	mp(g)	PP	PR	Purity	PMAP	Nv	mp(g)
	1	0	0	88.9	82.1	71.4	58.3	18.0	5.6	87.0	73.9	70.4	58.0	21.2	10.7
	Mean			85.0	67.5	84.5	69.2	15.3	5.7	88.7	71.4	78.8	64.6	17.2	9.1
	Deviation			5.6	9.9	12.1	15.2	4.3	3.1	5.6	9.1	8.4	10.4	4.4	4.4

\*Experiment in duplicate, an average of two values

\*\* C is the level of P and N concentration; A is the aeration; SM is the seed material factor

In the CSTR, both PP and PR increased with increasing struvite SI (mean 81%, 86%, 88% and 61%, 66%, 75% initial SP and TP with SI 1.34, 2.04 and 2.40, respectively), because a higher SI implies a higher chemical potential for crystallisation and, consequently, a higher phosphorus recovery (Shaddel et al., 2019). Differences between SI 1.34 and SI 2.40 ( $p < 0.05$ ) were found statistically significant.

In the FBR, the highest PP and PR were found in SI 2.04 (92 and 77 % initial SP and TP, respectively) and statistically significant differences were only found in PR ( $p < 0.05$ ) between SI 1.34 and the other two levels evaluated (2.04 and 2.40) (Figure 28). In both reactors, the minimum mean phosphorus recovery was found in SI 1.34 and was slightly lower in the CSTR (61% and 64% initial TP), possibly because the recirculation flow in the FBR increases the recovery of finer particles.

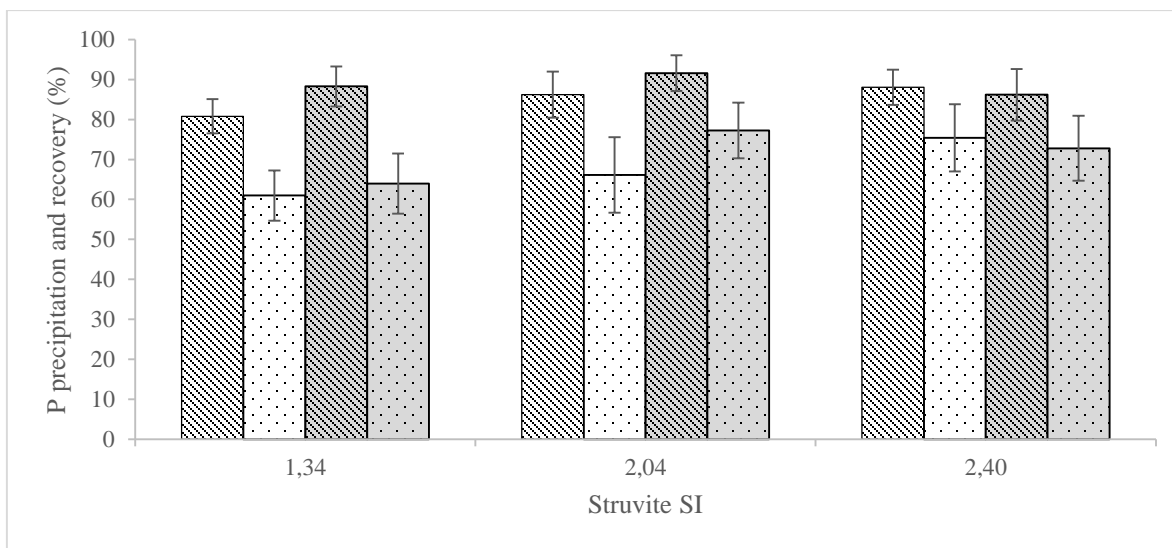


Figure 28. Assessment of continuous struvite production. Mean phosphorus recovery (PR) and PO<sub>4</sub><sup>3-</sup>-P precipitation (PP) at different saturation index (SI), reported as a percentage (% initial TP and SP) PP in CSTR, PR in CSTR, PP in FBR and PR in FBR. Lines represent the standard deviation.

Although in the CSTR the phosphate precipitation at SI 1.34 presented statistically significant differences concerning SI 2.40, the high precipitation at SI 1.34 (81 % initial SP with a minimum value of 78%) means that, even with low initial P concentrations (30 mg P-PO<sub>4</sub><sup>3-</sup> L<sup>-1</sup>), it is possible to achieve a P precipitation >78% (68% P<sub>MAP</sub>). This is consistent with the results found for the FBR (minimum value of 84% PP at 30 mg P-PO<sub>4</sub><sup>3-</sup> L<sup>-1</sup>).

**Chapter 5.** Struvite recovery from municipal wastewater sludge dewatering centrate using a stirred tank and a fluidised bed reactor

The precipitate purity and  $P_{MAP}$  were not affected by the initial phosphorus and ammonium concentrations (mean purity of 84% and 79 % and mean  $P_{MAP}$  of 69% and 65% for CSTR and FBR, respectively). However, Ca removal (%) increased with the increasing of the C factor.

According to Desmidt et al. (2013), Ca interferes with struvite in wastewater with low phosphate (<35 mg/L). However, we found higher Ca removal at 120 mg P- $PO_4^{3-}$  L<sup>-1</sup> than at 30 mg P- $PO_4^{3-}$  L<sup>-1</sup> (24.7% vs 10 % and 32.6% vs 8.4 % initial Ca concentration for CSTR and FBR, respectively). This result is likely due to the initial calcium concentration that was lower at -1 C level (30mg Ca / L) than at 0 and 1 levels (50 and 57 mg Ca / L), even though an Mg / Ca ratio greater than 2.5 and a Mg/P  $\geq 1$  were ensured in all tests to promote struvite formation (Li et al. 2019; Zhang et al., 2017). Therefore, it could be concluded that the concentration of Ca interferes with struvite formation even at medium P concentrations (< 120 mg P- $PO_4^{3-}$  L<sup>-1</sup>) and high Mg/Ca and N/P molar relations.

Nevertheless, the composition of precipitates was confirmed as struvite with XRD diffractograms (Figure 29A). SEM-EDX analyses confirmed the presence of Mg and P in the precipitate, with a minimum presence of Ca (< 1.3 atomic %) (Figure 29 B). The Ca removal from the soluble phase may be due to the formation of others precipitates as Ca phosphates (TCP =Ca<sub>3</sub>(PO<sub>4</sub>)<sub>2</sub> and hydroxyapatite) and Ca carbonates as calcite, dolomite and huntite. In addition, due to the high alkalinity of the centrates (approx. 2500 mg CaCO<sub>3</sub>/L), the precipitation of other carbonates as magnesite and vaterite can also be favoured (Capdevielle et al., 2013; J. Liu, 2018; L. Pastor et al., 2010). EDX analysis confirmed that, in the FBR, other metals as Al and Si precipitated but in minimal amounts (<0.4%). More detail on the SEM, EDX and XRD images of the precipitates obtained in this article can be found in Annex 4. Supplementary information to chapter 5.

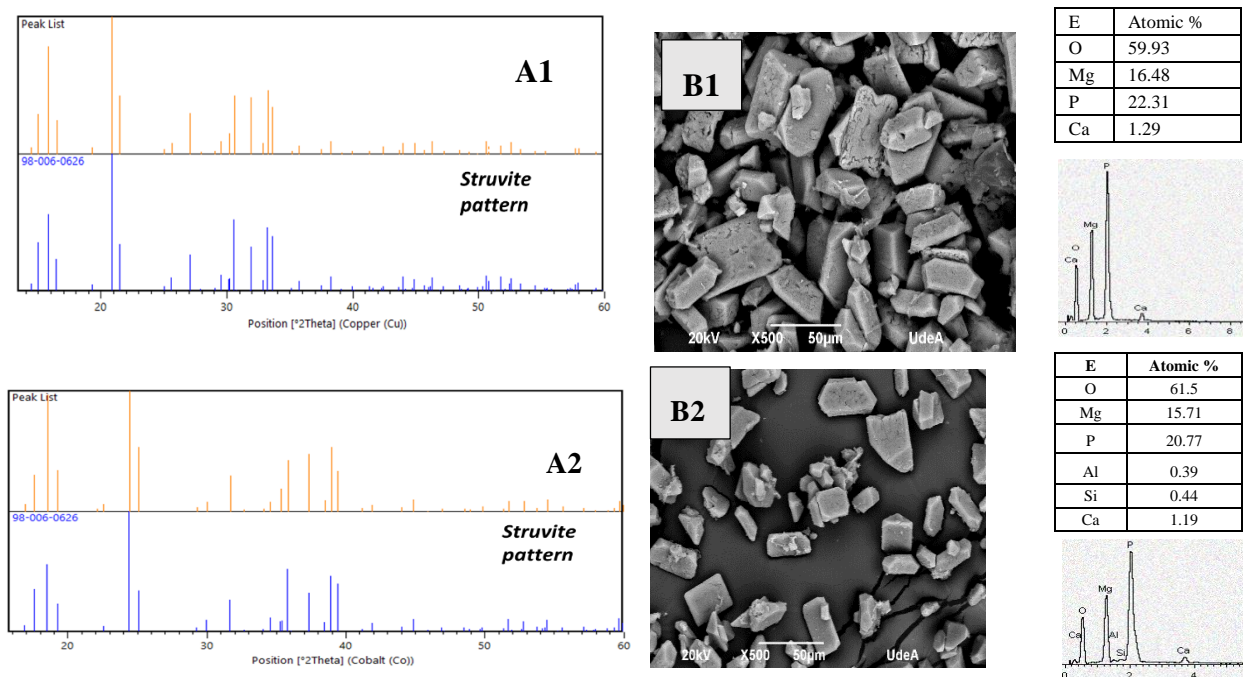


Figure 29. (A) XRD diffractograms and SEM-EDX analysis. (A-1) CSTR reactor (A-2) FBR reactor. (B) Images by SEM-EDX of struvite crystals with SI of 2.4, without SM and with aeration: (B-1) CSTR; (B-2) FBR reactor. \* Other diffractograms are presented in the annexe section.

The SI of all possible precipitates was calculated with the Visual MINTEQ software V 3.1 (some precipitates were discarded due to their low formation velocity, such as hydroxyapatite (Hallas et al., 2019)). The main results are presented in Figure 30. The maximum SI of magnesite, dolomite and calcite occurred at the middle C level. The maximum SI of TCP and struvite occurred at the high C level (maximum concentration of N and P). Therefore, it is possible that the Ca removal, which increased as the P concentration increased, is mainly due to the formation of small amounts of TCP, although this did not significantly affect the purity of the material (mean purity of 76-78 % and  $P_{MAP}$  72-62 % at 120 mg P- $PO_4^{3-}$  L<sup>-1</sup> for CSTR and FBR, respectively).

The suspended solids present in the centrate (mean 460 mg TSS. L<sup>-1</sup>) and the formation of the possible solids present in Figure 30 that were not detected on the XRD analysis, could slightly reduce the purity of the precipitate. The presence of organic matter in the struvite was confirmed with TOC measures (mean 25.6 g TOC. Kg<sup>-1</sup>). Small traces of metals were also detected in the analysed precipitates (one for each reactor): < 0.2 Al, < 1.5 Na, < 0.1 Fe, < 0.00004 Cr, <0.000138 Ni % weight.

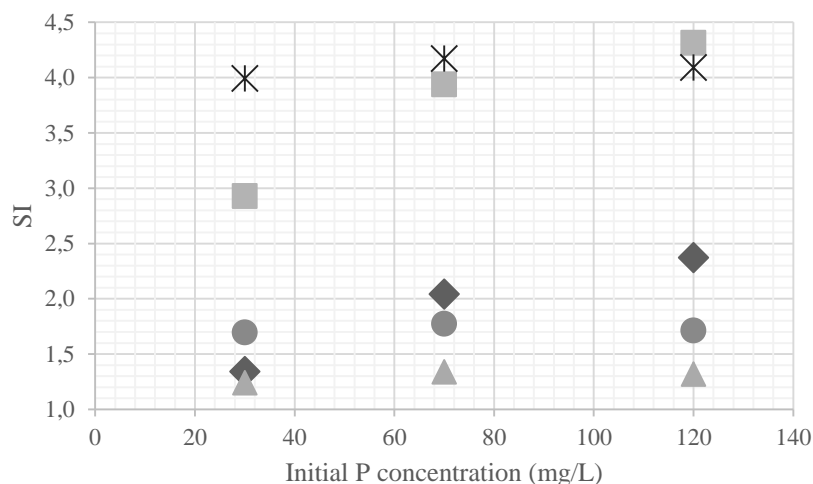
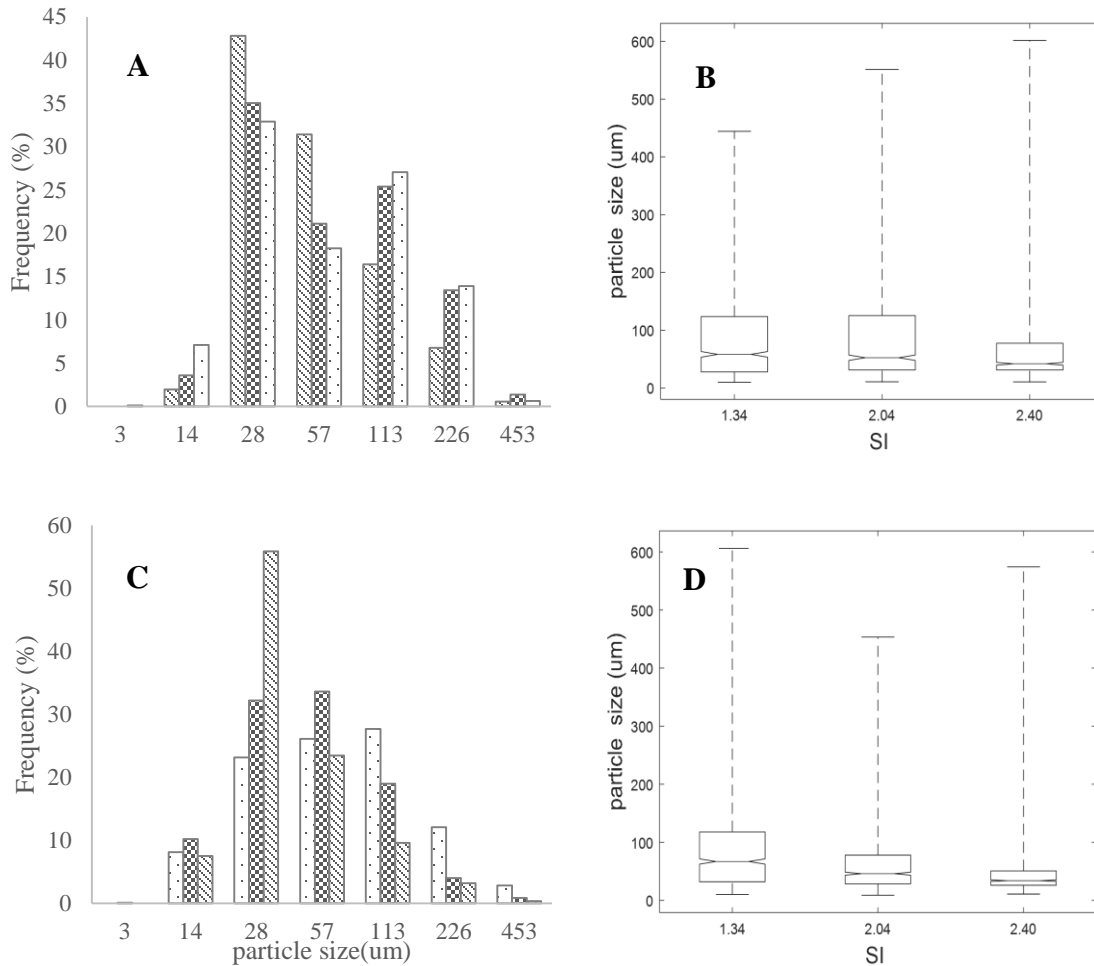


Figure 30. SI of five precipitates (■ TCP, ◆ struvite, ▲ magnesite, ✕ dolomite and ● calcite) at different  $PO_4^{3-}$ -P,  $NH_4^+$ -N and Mg concentrations (C levels -1, 0, 1).

Particle size was also affected by the initial N and P concentrations because as the inlet  $PO_4$ -P and N- $NH_4$  concentration increased, the supersaturation in both reactors also increased (Figure 30). According to Mehta and Batstone (2013), increasing initial supersaturation may boost nucleation rates that produce a higher number of smaller particles. Such rapid nucleation is unwanted, as this may produce fine crystals which are often washed out with treated effluent, affecting the quality of the treated effluent as well as the economic viability of the process (Crutchik et al., 2017).

The frequency of particle size and the particle size distribution of each reactor was determined (Figure 31). The results show that the smallest size and the highest homogeneity of particles occur at the highest SI (mean particle size 65  $\mu$ m and 49  $\mu$ m for CSTR and FBR, respectively) (Figure 31). Kruskal-Wallis Test and T-test for samples with unequal variances were applied to compare the medians and means between the particles' size at different SI. Tukey HSD was applied to determine which means were significantly different from each other. Significant statistical differences were found among the medians of 1.34, and 2.04 SI with 2.4 SI for the CSTR and differences among the medians of three SI evaluated for the FBR ( $p < 0.05$ ).

Thus, the increase in P and N concentrations produced a decrease in the mean particle size due to the increase in the struvite SI. However, the most significant difference found between PP and PR occurred at the lower struvite SI (20 and 24% at 1.34 SI vs 12.7 and 12.3 % at 2.4 SI for CSTR and FBR, respectively) and significant statistical differences were found between 1.34 and 2.4 SI at a significance level of 5% and 10 % for CSTR and FBR, respectively. It may be because the sizes are much more heterogeneous at 1.34 SI and, despite having a larger mean size, the proportion of small particles (0-20  $\mu\text{m}$ ) is higher (7.2%) in comparison with the proportion at SI 2.4 (1.9%) (**Figure 31A**).



**Figure 31.** Particle size distribution at different SI. (A-B) CSTR reactor. (C- D) FBR reactor. Adopted diameter ranges are 3  $\mu\text{m}$  (1-10  $\mu\text{m}$ ), 14  $\mu\text{m}$  (10–20  $\mu\text{m}$ ), 28  $\mu\text{m}$  (20–40  $\mu\text{m}$ ), 57  $\mu\text{m}$  (40–80  $\mu\text{m}$ ), 113  $\mu\text{m}$  (80–160  $\mu\text{m}$ ), 226  $\mu\text{m}$  (160–320  $\mu\text{m}$ ), 453  $\mu\text{m}$  (320–640  $\mu\text{m}$ ). 1.34 SI, 2.04 SI and 2.4 SI.

The FBR presented a similar proportion of small particles at different SI (**Figure 31C**). This result may be because, at a higher upward velocity, the smallest particles produced at the lowest SI failed to collect at the end of the test and were quickly washed out by the reactor effluent. These results disagree with Ping et al. (2016) that affirm that increasing  $\text{PO}_4\text{-P}$  concentration improves the struvite

pellet size, possibly because high concentrations of P reduce the number of fine particles. However, due to the simultaneous increase in N and therefore in the struvite SI, the average size of particles produced at the higher C level (2.4 SI) was reduced.

As expected, the final mass of recovered struvite increased with increasing P and N concentration (3.7, 5.3 and 8.2 g for CSTR and 6.1, 8.4 and 12.6 g for FBR at 1.34, 2.04 and 2.4 SI respectively). In the FBR reactor, the volume of NaOH (mL) used to maintain pH at nine also increased with SI (204, 308 and 355 mL for 1.34, 2.04 and 2.4 SI), while in the CSTR no significant differences were found (mean 155 mL).

### **5.3.3 Effect of seed material (SM)**

Regarding the effect of the SM (synthetic struvite), it was found that seeds help to increase the particles size (CSTR 118 and 32  $\mu\text{m}$  with and without SM; FBR 101 and 38  $\mu\text{m}$  with and without SM; see Figure 32A and C), quantity (CSTR 3.9 and 3.4 g with and without SM; FBR 6.9 and 5.9 g with and without SM) and purity of precipitated struvite (CSTR 87 and 60 % with and without SM; FBR 84 and 74 % with and without SM respectively).

Since the SM presents larger particle sizes (mean 158 and 89  $\mu\text{m}$  for CSTR and FBR reactors, respectively) than those presented in the tests without SM (mean 33 and 38  $\mu\text{m}$  for CSTR and FBR reactors, respectively), a cumulative frequency analysis was performed to determine the SM real effect on the crystal growth. The results in the FBR reactor show that the frequency of larger particles is higher in tests with SM than in the synthetic struvite used as SM, confirming that the SM increased the particle size obtained (Figure 32-D).

However, in the CSTR, this effect is not exact because the synthetic struvite used as SM presented larger particle sizes than those presented in all tests (with and without SM; see Figure 32-A), but the particle size of the tests with SM was larger than the size of a cumulative mean (according to the mean proportion between SM and precipitated struvite) between the SM and the test without it (Figure 32B).

Therefore, it could be concluded that the SM does increase the size of the crystals obtained by acting as a nucleus on which further accumulation of crystallising material takes place and by providing a surface area that results in higher crystal accumulation (Kataki et al., 2016; Yu, Geng, Ren, Wang, & Xu, 2013).

To determine the amount of struvite solids that precipitated onto the seeds, the granules were weighed before and after each experiment. The mass of crystal generated in each experiment was defined as the difference between the weigh after the experiment and the SM weight (1 g/L affected by a loss percentage equal to the difference between PP and PR) and settleable suspended solids weight (g). Although precipitation and recovery did not show significant differences concerning the SM, the results show that SM increased the amount of precipitated struvite, the  $P_{MAP}$  and the struvite purity in both reactors, in agreement with the findings of other authors (Liu et al. 2008; Shaddel et al. 2020).

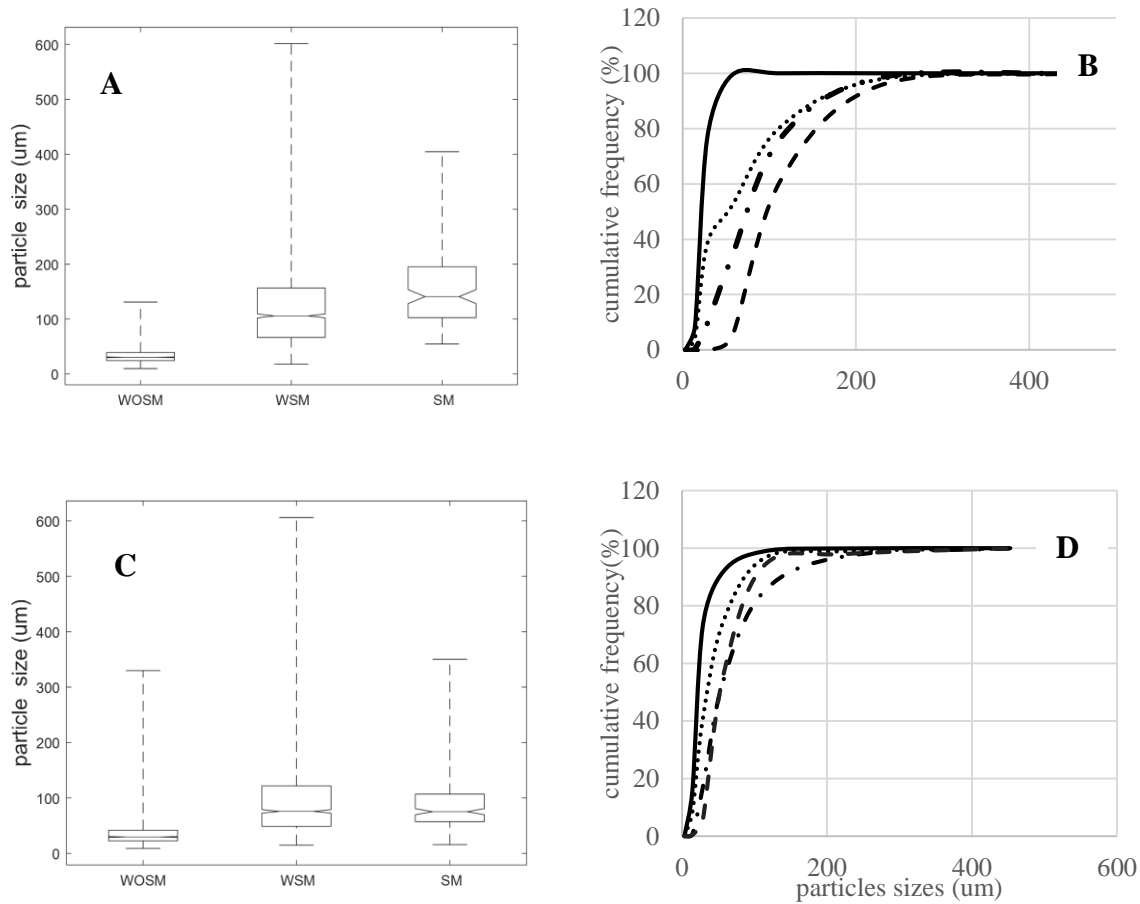


Figure 32. Effect of SM on particle size distribution. (A-B) CSTR reactor. (C-D) FBR reactor. — Without SM (WOSM), - · - with SM (WSM), - - - SM and ..... Mean.

Moreover, SM did not improve the reaction speed. This latter finding contrasts with previous works (Agrawal et al., 2018; Tang & Ma, 2016), possibly because the first measurement of P in the effluent was done after 1 hour of reaction while the increase in the P removal rate rapidly occurred within the first minutes; so after 1 hour the system was very close to equilibrium, and the change in P removal overtime was minimal ( Figure 33).

Stainless steel meshes used as a complement to improve crystal growth presented low agglomeration rates. Although some studies have found a good affinity of struvite with stainless steel (for instance, Doyle et al. (2002) and Le Corre et al. (2007) found high accumulation rates and retention of fines particle in two concentric stainless meshes), in this study the average amount of struvite collected in the meshes used in both reactors was less than 9% of the harvested precipitate. However, a more significant agglomeration of crystals was observed in the aluminium screws of the meshes, possibly due to its greater roughness.

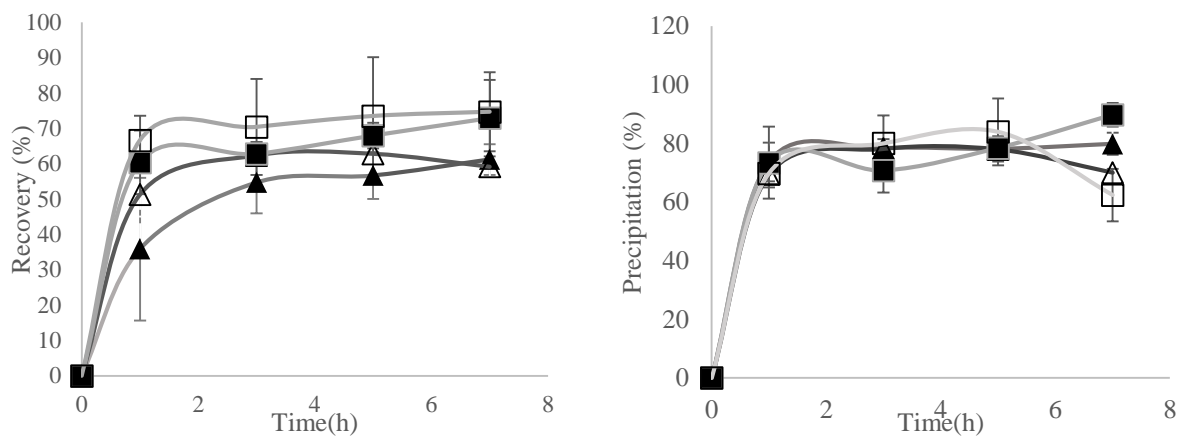


Figure 33. P precipitation and recovery in CSTR reactor. ▲ 1.34 SI with SM, △ 1.34 SI without SM, ■ 2.4 SI with SM, □ 2.4 SI without SM.

### 5.3.4 Effect of the aeration

Aeration applied to the CSTR did not significantly affect the quantity or quality of precipitated struvite, with no statistically significant differences found in ammonia volatilisation nor the purity of the precipitated material. However, aeration increased the fine particle loss in the CSTR effluent (also registered by a higher difference between the percentage of precipitation and recovery).

Meanwhile, aeration applied to the FBR reactor reduced the amount of precipitated struvite (5.6 and 7.2 g with and without aeration) and the percentage of  $P_{MAP}$  (60 and 67 % with and without aeration), slightly increased the ammonia volatilisation (18 and 16 % with and without aeration;  $p=0.06$ ) and increased the amount of struvite collected in the stainless steel meshes (11.2 and 5.6 % in the big mesh and 7.2 and 4.4 % in the small mesh with and without aeration). Aeration slightly reduced the amount of NaOH required to maintain pH at 9 (270 mL vs 309 mL, with and without aeration) due to  $CO_2$  stripping, but the difference was not statistically significant ( $p>0.05$ ).

Aeration did not have a good effect on struvite precipitation at the rates evaluated in both reactors. Aeration could help in ammonia volatilisation, could reduce the amount of struvite recovered and did not significantly reduce the NaOH required to keep pH constant at 9. The small pH increase by air stripping can be attributed to the buffering effect of the high alkalinity of the centrate (Ackerman & Jordaan, 2015).

### 5.3.5 Statistical model

Few significant interactions were found between the analysed factors (C, aeration and SM) for the different response variables. The amount of precipitate recovered, the N in the precipitate and the volatilised N, presented interaction between the factors, however, the precipitated N did not meet the assumption of normality and homogeneity of variances in the residuals. Using the R software, the coefficients of the interaction model with the coded variable were found, and the ANOVA analysis of variance was performed to find out if the effects were statistically significant ( $p\text{-value}<0.1$ ). According to the interactions that were found significant, the regression model with coded variables

for precipitate recovered and % N<sub>v</sub> (in FBR reactor) was written as Equation 11, Equation 12 and Equation 13.

$$\begin{aligned} \text{Precipitate CSTR(g)} & \hspace{15em} \text{Equation 11} \\ & = 1.06970 + 1.50500[\text{SI0}] + 4.50828[\text{SI1}] + 0.79605[\text{A}] \\ & \quad + 4.69165[\text{SM}] - 0.47220[\text{A}][\text{SM}] \end{aligned}$$

$$\begin{aligned} \text{Precipitate FBR(g)} & \hspace{15em} \text{Equation 12} \\ & = 2.76405 + 2.43775[\text{SI0}] + 7.89732[\text{SI1}] + 0.16243[\text{A}] + 7.78649 [\text{SM}] \\ & \quad + 0.49617[\text{SI0}][\text{A}] - 3.01232[\text{SI1}][\text{A}] + 0.01263[\text{SI0}][\text{SM}] \\ & \quad - 1.87423[\text{SI1}][\text{SM}] - 2.36955[\text{A}][\text{SM}] - 1.60431[\text{SI0}][\text{A}][\text{SM}] \\ & \quad + 3.90452[\text{SI1}][\text{A}][\text{SM}] \end{aligned}$$

$$\begin{aligned} \text{N volatilization FBR(\%)} & \hspace{15em} \text{Equation 13} \\ & = 8.6544 + 9.4911[\text{SI0}] + 12.5949[\text{SI1}] + 3.57 [\text{A}] + 6.13 [\text{SM}] \\ & \quad + 0.7451[\text{SI0}][\text{A}] - 2.2251[\text{SI1}][\text{A}] - 11.0980[\text{SI1}][\text{SM}] - 5.8917[\text{SI0}][\text{SM}] \\ & \quad - 4.2185[\text{SM}][\text{A}] \end{aligned}$$

Where, SI0 = 1 when SI is 2.04 and 0 otherwise; SI1=1 when SI is 2.40 and 0 otherwise; A=1 when aeration level is 1 (with) and 0 when aeration level is -1(without); SM=1 when SM level is 1 (with) and 0 when SM level is -1(without).

According to Equation 11 and Equation 12 for both reactors, precipitate recovery increases with the SI, because higher P and N concentrations increase the struvite recovery potential. The precipitate recovery also increased with the SM and slightly with the aeration at low SI (in FBR). The adjusted R-squared precipitate model was 0.9758 for the CSTR and 0.945 for FBR reactor. N volatilisation was also affected by the factors evaluated, but only in the FBR reactor, possibly due to its geometry and its higher up-flow velocity. SI and aeration increased the ammonium volatilisation, but the interaction between SI and SM reduced it. The adjusted R-squared N<sub>v</sub> model was 0.7258.

### 5.3.6 Reactors comparison and nutrients mass balance (N and P)

Both reactors presented high percentages of P precipitation. In the CSTR, P-precipitates accounted for 85% of initial P-PO<sub>4</sub><sup>3-</sup>, the effluent lost 6%, and 9% remained soluble in the reactor. In the FBR, P-precipitates accounted for 88.6 % of initial P-PO<sub>4</sub><sup>3-</sup>, the effluent lost 4.2%, and 7.2% remained soluble in the reactor.

According to the N mass balance in both reactors, N-precipitates accounted for only 4.3 % and 3.8 % of initial N-NH<sub>4</sub><sup>+</sup>, 15.5 % and 17.2 % of initial N-NH<sub>4</sub><sup>+</sup> were lost via NH<sub>3</sub> volatilisation, 37.2 % and 33 % were lost by the effluent, and 43 and 46 % remained soluble in CSTR and FBR reactors, respectively (see Figure 34).



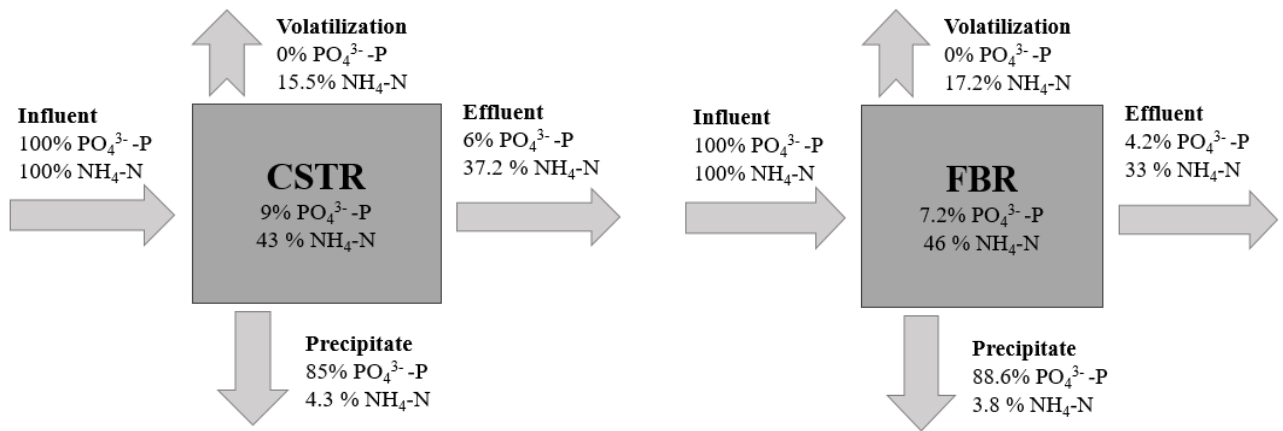


Figure 34. Mass balance of nutrients in CSTR and FBR reactors

The reactors were also compared in terms of percentage of P precipitation and recovery, purity,  $P_{MAP}$ ,  $NH_3$  volatilisation, the difference between precipitation and recovery, amount of product recovered per unit of inlet P and particles sizes. The results show that  $P_{MAP}$  (mean 72%),  $NH_3$  volatilisation (mean 16% initial  $NH_4$ ), the quantity of product recovery (mean 6g precipitate/g P), the loss of fines (mean difference PP-PR 17.4%) and PR (mean 69.4 % initial P) did not present statistically significant differences between the reactors. Nevertheless, PP (Figure 34) and particles sizes were slightly higher in the FBR (33 and 38  $\mu m$  without SM for CSTR and FBR, respectively) but the purity of its precipitates was slightly lower (84.5 and 78.8 % for CSTR and FBR, respectively).

The two reactors evaluated have very similar efficiencies in terms of quantity and quality of the recovered product. The closest hydraulics to perfect mixing in the FBR reactor (92%), which allows a more homogeneous distribution of supersaturation, could favour the formation of struvite by forming precipitates with larger particles sizes. Although the FBR reactor produced more significant P precipitation and particle with larger sizes, a greater proportion of impurities have probably precipitated. However, N precipitation and Ca removal did not show statistically significant differences between the two reactors (t-test  $p > 0.05$ ).

Due to the high  $N-NH_4^+$  concentration concerning the  $P-PO_4^{3-}$  concentration in the sludge dewatering centrate ( $N:P$  molar relation  $> 19$ ), the amount of N losses by the effluent and by volatilisation is high ( $> 50\%$  initial N) compared to the high P precipitation efficiency in both reactors ( $> 85\%$ ). Therefore, it is recommended to link the crystallisation system applied to centrates with low P concentrations to an  $NH_3$  recovery system to minimise N-losses (e.g., absorption tower) and an effluent post-treatment (i.e. nitrification-denitrification system) to minimise environmental impacts.

### 5.3.7 Cost analysis

Initially, the amount of precipitated P and struvite produced was calculated according to the results found in the tests. As shown in Table 20, the amount of phosphorus and struvite precipitated increases as the P concentration increase. According to the efficiencies found under the test conditions, the struvite production per  $m^3$  of centrate is similar for both reactors, and the annual struvite production at the San Fernando WWTP will vary between 184 and 736 tons.

**Chapter 5.** Struvite recovery from municipal wastewater sludge dewatering centrate using a stirred tank and a fluidised bed reactor

Table 20. Struvite production

Reactor	CSTR			FBR		
	30	70	120	30	70	120
Production/P concentration (mg/L)						
Precipitated P (Kg P/m <sup>3</sup> centrate)	0.02	0.06	0.11	0.03	0.06	0.1
<b>Struvite production</b>						
Kg/m <sup>3</sup> centrate	0.17	0.31	0.67	0.2	0.39	0.65
Kg/100 m <sup>3</sup> wastewater influent	0.48	0.89	1.92	0.57	1.11	1.86
Kg/d	504	941	2016	596	1171	1959
Ton/year	184	343	736	218	428	715

In the CSTR reactor the energy consumed by the industrial static mixer is minimal ( approximately 9% of the total energy) compared to the pump's energy. However, the power consumed by the pumps in the FBR reactor is ten times higher than in the CSTR reactor, mainly due to the recirculation pump, which requires greater power due to its high flow. Therefore, energy costs to produce struvite were higher in the FBR than in the CST reactor (Table 21).

Table 21. Energy consumption and costs. Note: Consumption was calculated considering 24 hours of operation.

Energy	Units/Reactor	CSTR		FBR
		Pumps	Industrial static mixer	Pumps
Consumption	kWh	205.9	20.5	1995.6
	(kWh/m <sup>3</sup> )	0.068	0.007	0.660
	(kWh/ Kg precipitate P) *	2.8-1.1-0.6	0.28-0.11-0.06	25-10-6
Costs	(kWh/Kg struvite) *	0.4-0.2-0.1	0.04-0.02-0.01	3.34-1.70-1.01
	\$ COP/m <sup>3</sup>	36.28	3.61	351.61
	\$ COP/Kg precipitate P*	1497-601-343	149-60-34	13273-5483-3360
	\$ COP/Kg struvite*	217-117-54	22-12-5	1783-908-543

\*Values for 30, 70 and 120 mg P.L<sup>-1</sup>, respectively.

The consumption and cost of the reagents increased with the increase in the P concentration because the higher the P concentration, the greater consumption of reagents is required to produce more struvite (Table 17; Figure 35 A-B). According to the price of the reagents (Table 17), the total expenses for chemical costs were evaluated and compared with the energy costs under the three P concentration scenarios in the two reactors ( CSTR and FBR). The results showed that under a struvite price value of 760\$COP.Kg<sup>-1</sup> cannot obtain economic income from its sale since its production price would be higher than its sale price. However, under a struvite sale price of 7160 \$COP. Kg<sup>-1</sup>, a concentration of 120 mg P/L, would be favourable to obtain financial gain. In the FBR reactor, the profit would be only \$COP 88 per m<sup>3</sup> of centrate; meanwhile, in the CSTR reactor, it could be \$ COP 1200 per m<sup>3</sup> of centrate (Figure 35 A-B).

**Chapter 5.** Struvite recovery from municipal wastewater sludge dewatering centrate using a stirred tank and a fluidised bed reactor

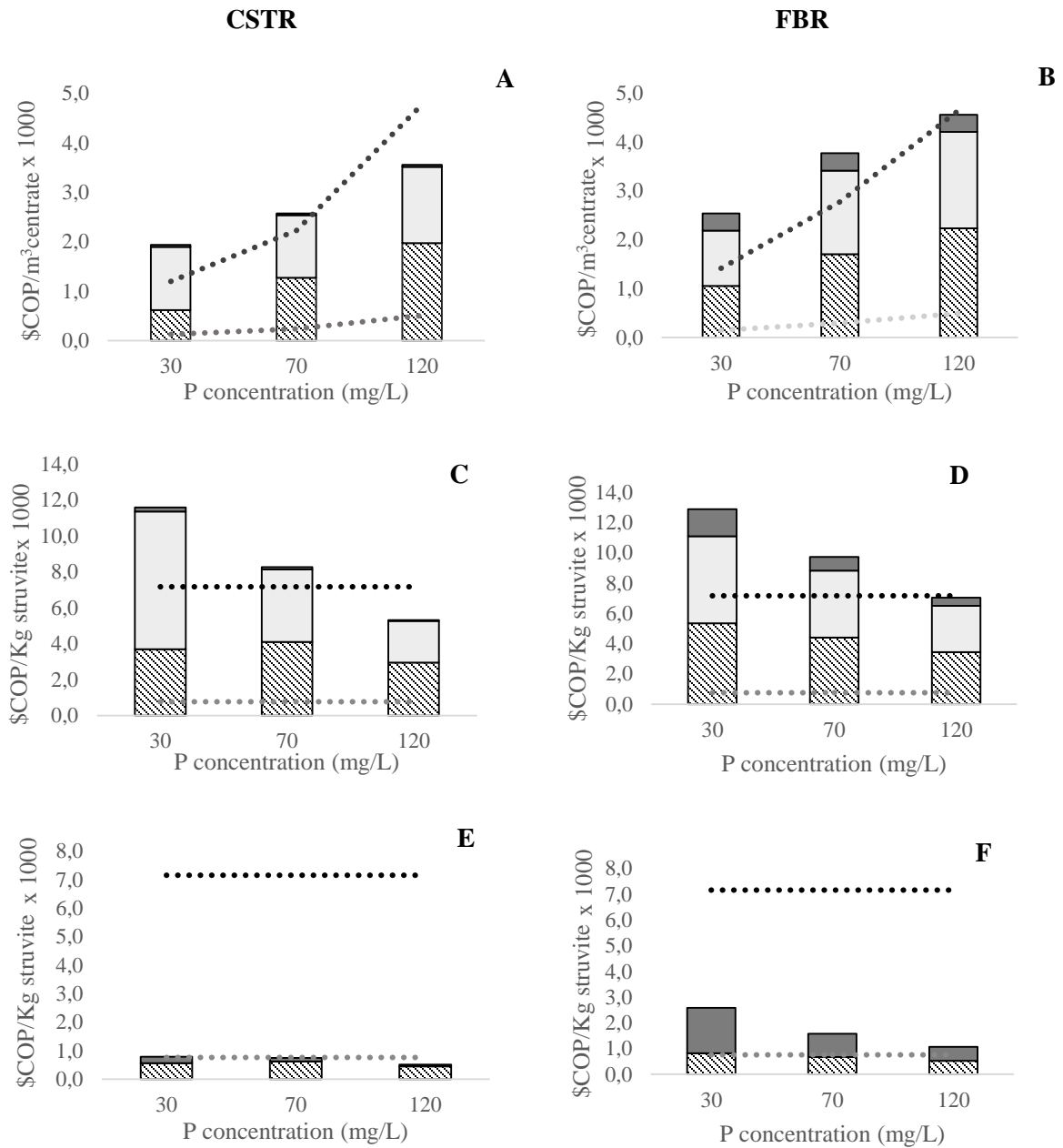


Figure 35. Costs and revenues in the struvite production. **A and B** \$COP/m<sup>3</sup> in the CSTR an FBR reactor, respectively. **C and D** \$COP/Kg struvite in the CSTR an FBR reactor, respectively. **E and F** \$COP/Kg struvite in the CSTR an FBR reactor under addition of Mg (OH)<sub>2</sub> as a source of magnesium.

**Symbols:** Cost of NaOH and Mg cost of Energy ; Revenue 1 (760 \$COP/Kg struvite) and ..... Revenue 2( 7163 \$COP/Kg struvite) .....

Considering 1€ = 4500 \$COP. Producing one Kg of struvite decreased with the increase of P concentration due mainly to reducing the reagents consumption. This agrees with what was reported by Dockhorn (2009), and Desmidt et al.(2013) that found wastewater containing low phosphate concentrations (<50 mg L<sup>-1</sup> PO<sub>4</sub>-P) needed disproportionately large chemical additions. The incomes at 120 mgP/L (struvite sale price of

7160 \$COP. Kg<sup>-1</sup>) were 1837 and 136 \$COP. Kg<sup>-1</sup> for CSTR and FBR reactors, respectively (Figure 35 C-D). Additionally, it was observed that the cost of energy in both reactors is minimal compared to the cost of reagent consumption ( a mean of 1.58 and 10 % of the total cost in CSTR and FBR reactors, respectively).

The use of low-cost magnesium sources, such as seawater, brine or industrial grade MgO or Mg(OH)<sub>2</sub>, can significantly reduce the operating costs (Crutchik et al., 2017). Assuming the same struvite production and the same experimental conditions, the use of Mg(OH)<sub>2</sub> could significantly reduce the operating costs of the process, mainly due to its low cost (reduction of 84% in the Mg cost per Kg struvite). According to the results, under all P concentrations, income would be obtained with the highest sale price of struvite in both reactors, and even a positive balance would be obtained in the CSTR reactor at 120 mg P / L with the lowest struvite price evaluated (income of 150 \$COP. Kg<sup>-1</sup>) (Figure 35 E-F).

Therefore, Mg(OH)<sub>2</sub> can be a good source of Mg to improve the economic viability of the process; however it can be less efficient in terms of NH<sub>4</sub><sup>+</sup> and phosphorus removal; also the pH value and the Mg:P molar ratio cannot be controlled independently of each other which could interfere with process control (Siciliano et al., 2020; Wu & Bishop, 2004). MgSO<sub>4</sub>.7H<sub>2</sub>O as an Mg source also can be an option to reduce the operational cost (reduction of 19% in the Mg cost per Kg struvite); however, the costs of the process would continue to be higher than the sale price.

In addition to changing the source of Mg, the pH control system could be optimised to reduce the additional application of NaOH and thus reduce operating costs. Nevertheless, according to Maaß et al.(2014), the revenues account for only about 4% of the total benefits of the struvite production in a WWTP. Between the benefits of a struvite system in a WWTP are the reduction of electricity consumption, reduction of aeration cost for nitrogen removal, benefits related to a lower phosphorus content in dried biosolids, improvement of dewatering characteristics, preventions of incrustations and reduction of cleaning; minimizing struvite scale decreases pumping, operational, pipe replacement, and labour costs (Bird, 2015; Maaß et al., 2014; Shu et al., 2006).

Thus, evaluating only the internal operating costs and the benefits generated by the sale of struvite, the system may be economically viable at a minimum concentration of 120 mgP / L using a CSTR reactor and selling the product at a value of \$ COP 7160.Kg<sup>-1</sup>. However, if the internal benefits are incorporated in the WWTP in addition to the environmental benefits derived from avoiding the discharge of phosphorus into the natural environment, the net benefit obtained may be positive; that is, the process may be profitable (Molinos-Senante et al., 2010). Additionally, over time, the price of phosphate rock and fertilisers will increase, which will improve the economic profitability of struvite production.

## 5.4 Conclusions

Struvite precipitation from sludge dewatering centrate by a simple continuously operated CSTR, and by an FBR reactor is feasible with a dissolved phosphate removal efficiency of >85%. A higher struvite SI and a higher initial concentration of P favours phosphorus precipitation and recovery. Nevertheless, the crystallisation of struvite from centrates with low P concentration (30 mg PO<sub>4</sub><sup>3-</sup>P L<sup>-1</sup>) is technically feasible since the phosphate precipitation, P<sub>MAP</sub> and purity were >85 %, >69 % and >73 %, respectively. The effect of aeration and SM inclusion (synthetic struvite and stainless steel meshes) was evaluated. Aeration is not recommended in CSTR and FBR crystallises since it favours

the loss of fine particles in the CSTR effluent, whereas in the FBR reactor it increases the  $\text{NH}_3$  losses and reduces the amount of struvite recovered. In addition, due to the low aeration rates used ( $<1.3$  mL/min) and to the high alkalinity of the centrate, aeration did not significantly reduce the amount of NaOH used. Meanwhile, synthetic struvite used as SM can improve the quantity and quality of struvite precipitates, increasing the purity and size of the crystals. A more significant effect on increasing crystal size was observed in the FBR reactor, possibly because the seed material had a smaller particle size and, according to Ariyanto et al.(2014), the smaller the added crystal nucleus is, the faster is the rate of crystal growth. However, seed material is energy and cost-intensive process, so additional work is needed to assess the economic feasibility to implement this approach at a large scale.

Both reactors showed very similar efficiencies in terms of P precipitation and recovery, quantity and purity of the recovered product. Although the FBR had larger particle sizes than the CSTR (33 and 38  $\mu\text{m}$  without SM), the particle sizes in both reactors are small, mainly due to the high supersaturation of the centrates, so it is considered necessary to evaluate their direct use as fertiliser (for the possibly significant release of nutrients) or as a raw material in the production of fertilisers to consider the sustainability of the process. The cost analysis showed that the operational costs of struvite production rely on phosphorus concentration and decrease with increasing phosphorus concentration. Furthermore, under the conditions of the tests, phosphorus concentrations should be above  $120 \text{ mg P-PO}_4^{3-}\cdot\text{L}^{-1}$  to obtain a positive economic balance but at a high struvite selling price (COP  $7160\cdot\text{Kg}^{-1}$ ). It is necessary to evaluate the economic viability of the process in future research, but considering all the internal and external costs and benefits of the process, mainly the environmental benefits.

## 5.5 Acknowledgements

The authors would like to thank the School of Environment at Universidad de Antioquia, for providing lab space to conduct the experiments; the GAIA Research Group and the students Cristian Camilo Acevedo and Carolina Giraldo from the Faculty of Engineering for their technical support; and EPM and San Fernando WWTP for facilitating sample collection, especially to Andrea González. This research was partially funded by Colciencias under the Beca Doctoral # 647-2014 awarded to the first author.

## **Chapter 6. The determination of fertiliser quality of the formed struvite from a WWTP**

### **Highlights**

- Heavy metal concentrations metals in the struvite from the centrate of a WWTP were below the threshold limits.
- P uptake and apparent P recovery efficiency by grass was significantly higher in two struvite treatments than in the commercial fertilisers tested.
- N and P leaching depend on particle size. Smaller crystals can produce greater N uptake by the grass but more significant N losses by leaching.
- The use of struvite and biosolids as fertilisers represent a sustainable alternative for the recovery of nutrients in a WWTP.

### **Abstract**

Struvite from nutrient-rich wastewaters has been identified as a potential substitute for commercial mineral fertilisers, with the added benefit of reducing threats to global food security by prolonging phosphate rock reserves. A fertilisation test using grass (*Brachiaria brizantha Marandú*) and a sand column leaching test was conducted to determine the agronomic effectiveness of struvite precipitates produced from the supernatant of dewatered sewage sludge (centrate) from a municipal WWTP. The performance of this struvite as a fertiliser was compared with biosolids (or digested sludge from the same WWTP) and commercial fertilisers (Urea and Triple15). Results show that the concentration of heavy metals in struvite was lower than in biosolids and below the limits of Colombian and European regulations for fertilisers. Struvite increased the grass uptake of N and P, resulting in crop yields comparable to those of the other treatments tested. Struvite use as an effective slow-release fertiliser is highly dependent on the size of crystal particles, based on a lower P loss but a high N loss in sand columns; the N loss was higher than in the commercial fertilisers tested, due to the small particle size of struvite. Therefore, struvite represents a suitable opportunity to recover nutrients from municipal sewage sludge, facilitating the plant assimilation of its available P and N.

**Keywords:** nutrients recovery; struvite; centrate; crop yield.

**Note:** This article was presented as **Oral presentation** at the **2nd Latin American and Caribbean young water professional conference**. 8th-12th November 2020. and **has already been published** in the journal *Water Sci Technol* 15 June 2021; 83 (12): 3041–3053. doi: <https://doi.org/10.2166/wst.2021.162>

## 6.1 Introduction

World phosphorus (P) reserves are expected to decline within the next 70 to 150 years (Li et al. 2018). Wastewaters contain a high amount of phosphorus (Rahman et al., 2013), being its recovery a new source to the global phosphorus fertiliser supply. Secondary phosphate sources, such as struvite ( $\text{MgNH}_4\text{PO}_4 \cdot 6\text{H}_2\text{O}$ ) recovered from wastewaters, have the potential to reduce the pressure on phosphate rock mining while contributing to a more sustainable fertiliser production (Talboys et al., 2016).

Struvite releases nutrients at a slower rate compared to other fertilisers, which makes it an eco-friendly fertiliser that facilitates the incorporation of nutrients by plants before being rapidly leached and reduces the frequency of application, since phosphate ( $\text{PO}_4^{3-}$ ), nitrogen (N) and magnesium (Mg) can be absorbed simultaneously without using any other artificial components. Struvite has 2 to 3 times lower heavy metal impurities than commercial fertilisers (Bhuiyan et al., 2008). Furthermore, struvite can reduce greenhouse gas emissions (mainly nitrous oxide) because plants can take up most of the N after its application, avoiding other biological transformations of N into the soil (Lee et al., 2009).

However, the utilisation of struvite as a fertiliser can be highly dependent on the size of its crystal particles (Warmadewanthi et al., 2019): an increase in size ( $> 1 \text{ mm}$ ) leads to a slower fertiliser release rate due to a lower surface to volume ratio. In addition, struvite with large crystal sizes is easier to handle, transport, and apply (Bing Li, Ming, et al., 2019).

The characteristics (morphology, size and quality) of struvite precipitates rely on the nature of the crystallisation process used, mainly the hydrodynamic behaviour and operational conditions in crystallisers (Le Corre et al., 2009). To date, different reactors have been examined for efficient phosphorus recovery by struvite crystallisation, such as continuous stirred tank (CSTR) or fluidised bed reactors (FBR) (Rahman et al., 2013), having both reactors high recovery efficiencies ( $>60\%$ ) depending on the P source (i.e., the type of wastewater).

Many studies have evaluated the potential of struvite as a fertiliser using synthetic struvite or granular struvite (commercial struvite fertiliser with high particles sizes, for example, Crystal Green<sup>TM</sup>) (Degryse et al., 2017; Hall et al., 2020), but few have compared the agronomic effectiveness of resulting struvite from a WWTPs under different hydraulic conditions. Therefore, this research aims to assess the agronomic efficiency of struvite precipitates (obtained from the supernatant of dewatered sewage sludge or centrate from a municipal WWTP) compared to biosolids (obtained from the same WWTP and usually disposed on land, which are considered an effective fertiliser by beneficially recycling organic matter and nutrients and improving soil quality (Lu et al., 2012)), and two common commercial fertilisers tested in parallel (Urea and Triple15).

## 6.2 Materials and Methods

### 6.2.1 Struvite production

Enough quantity of a real sludge dewatering centrate was collected in San Fernando WWTP (Itagui, Colombia), stored in jars at four °C, for the production at laboratory scale of two-real struvites (SR1 and SR2) in a CSTR-type (5 L of working volume) and FBR-type (6.5 L of working volume) crystallisers, respectively. The quantity and quality (composition and size) of the struvite crystals

obtained in both reactors were similar at seven h of reaction time <sup>(1)</sup>; therefore, to increase the crystal particle sizes (> 100 µm) in one of the reactors, the crystallisation time in the CSTR reactor was increased to 5 d, while in the FBR reactor it remained at seven h. <sup>(2)</sup>. The main characteristics of the centrate used and the process performance (removal efficiency) are shown in **Table 22**.

Table 22. Performance of the struvite recovery process in lab-scale crystallisers.

Parameter	Units	Influent		Removal efficiency (%)	
		CSTR*	FBR*	CSTR	FBR
N-NH <sub>4</sub> <sup>+</sup>	mg L <sup>-1</sup>	1228.40	1123.85	19.09	33.27
TP	mg L <sup>-1</sup>	146.38	125.77	77.81	89.01
P-PO <sub>4</sub> <sup>3-</sup>	mg L <sup>-1</sup>	91.33	121.77	87.46	95.09
Ca	mg L <sup>-1</sup>	62.21	59.68	40.36	63.24
K	mg L <sup>-1</sup>	121.27	130.00	28.00	22.73
Al	mg L <sup>-1</sup>	NQ.	NQ.		

Abbreviations: NQ. - not quantifiable. Notes: \*Centrate from San Fernando WWTP (Colombia).

The concentration of orthophosphate, Ca and K of the centrate was adjusted using NaH<sub>2</sub>PO<sub>4</sub>.H<sub>2</sub>O, MgCl<sub>2</sub>.6H<sub>2</sub>O, CaCl<sub>2</sub>.2H<sub>2</sub>O and KCl reactive grade (EMSURE® and Mallinckrodt chemicals), respectively, before the entrance to reactors. The pH inside each reactor was brought up to 9, using a NaOH 1 M solution and a peristaltic pump connected at an Arduino controller. At the end of each test, effluent samples were filtered with coffee filters (stilo café #4; Stilotex S.A). The solid collected on filters was retained to be dried for 24 hours at room temperature and then, stored for its characterisation and X-ray diffraction (XRD) analysis.

Synthetic struvite (SS) was precipitated using a Jar tester (6 beakers of 2 L each one), fixing a stirring speed of 120 rpm and a constant pH of 9 (NaOH 1M added). Reactants NH<sub>4</sub>Cl, NaH<sub>2</sub>PO<sub>4</sub>.H<sub>2</sub>O and MgCl<sub>2</sub>.6H<sub>2</sub>O reagents (EMSURE® and JT Baker) were added to distilled water to achieve an optimal molar Mg: PO<sub>4</sub>: NH<sub>4</sub> relation of 0.9:1:2.4 (Pastor et al., 2008). After 3 hours, the stirring was stopped, and a settling period of 60 minutes was maintained to ensure that solids precipitated. The content of each beaker was then filtered with coffee filters (stilo café #4; Stilotex S.A). The solid precipitate, collected on filters, was also retained to be dried at room temperature for 24 hours and then, stored at room temperature (22 °C) for its characterisation.

## 6.2.2 Fertilisation trial (pot experiment)

The fertiliser values of synthetic struvite (SS) and real struvites SR1 obtained in CSTR and SR2 obtained in FBR were compared to the values of biosolids (Bio) or digested sludge obtained from the same WWTP, a mixture 90:10 (in % weight) of biosolids and SR1 struvite (Mix) and two commercial fertilisers for grass, Urea (U) and Triple 15 (T15) (both provided by Abonamos S.A.S company, Colombia). The biosolid, with a humidity of 67 % weight, was dried at room temperature for one week and then crushed before application.

The experiment was arranged as a completely randomised design with three replications per product. A control treatment or pot without N and P fertilisation was included. Eight sets of three pots, or a total of 24 plastic pots, were prepared. Each plastic pot had 13 cm surface diameter and approximately 10 cm of working depth. Grass (*Brachiaria Brizantha Marandú*) was cultivated for 90 days in pots

<sup>1</sup> See section 5.4(conclusions) of Chapter 5 for more details.

<sup>2</sup> See section 5.2.3 of Chapter 5 for more details.



**Chapter 6.** The determination of fertiliser quality of the formed struvite from a WWTP

(0.01327 m<sup>2</sup>) filled with sand (river sand from Depósitos Chagualo Company, Colombia) for ensuring an inert material. The sand was chosen as the substrate because it has a minimum organic matter content, which reduces biological activity that might interfere with the N analyses, drains well and thereby is well suited for fertilisation tests.

For a medium to high production of grass, the fertiliser Bio is usually applied to attain 120 kgN ha<sup>-1</sup> (Bernal & Espinosa, 2003); in this work and considering the characteristics of Bio, the dose was 5.64 gP m<sup>-2</sup> (Table 23) and it was used to calculate the equivalent quantity of other fertilisers. The lonely exception was T15, which was applied to obtain a 2.46 gP m<sup>-2</sup> dose because an analytical mistake during its analysis: it was initially considered to have 15% TP; however, it has 15% of P<sub>2</sub>O<sub>5</sub>-P, equivalent to 6.54% TP. For the Urea, that has no phosphorous, the criterium was to match the N dose of struvite SR1. Table 23 summarizes the dose per product.

Table 23. Fertilisation trial: applied product and equivalent P and N doses.

Treatment	Fertiliser per pot (t ha <sup>-1</sup> )	P dose (g P m <sup>-2</sup> )	N dose (g N m <sup>-2</sup> )
SR1	0.52	5.64	2.55
SR2	0.56	5.64	2.50
Bio	4.50	5.64	12.02
Mix	2.55(0.25 SR1-2.3 Bio)	5.64	7.34
U	0.06	0	2.64
T15	0.38	2.46	5.64
SS	0.37	5.64	1.62

Figure 36 is a scheme of the pot experiment procedure. The pot trial test was performed at room temperature, inside a greenhouse facility in Universidad de Antioquia (Medellin, Colombia). In each pot, 1.5 g of grass seeds (150 seeds per pot) were planted within the top 1.0 cm of sand (day 1). All fertilisers were applied in their solid form directly on the soil 15 days after sowing seeds. In addition, 60 mL of tap water per pot was added every two days.

After 27 days, the plants were harvested for the first time from each pot and weighed before and after drying (in an oven at 105 °C for 24 hours) to determine their fresh and dry weight. After five days (day 32), the same dosage of fertiliser per pot was applied. After 44 days (day 76), the plants were harvested again and weighed to estimate fresh and dry matter yield.

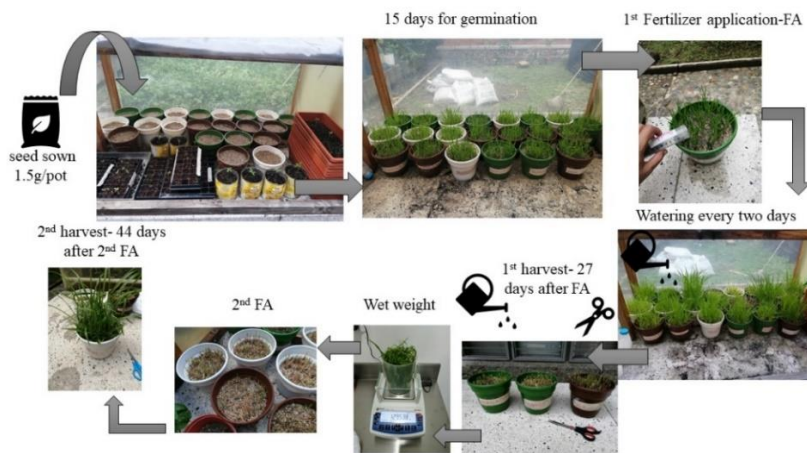


Figure 36. Steps of the fertilisation trial (pot experiment)

### 6.2.3 Fertilisation trial calculations

The agronomic efficiency (AE;  $\text{kg kg}^{-1}$ ) is defined as the economic production obtained per unit of nutrient applied (N or P). It can be calculated by Equation 14, according to Fageria (2009) and Szymanska et al., (2019). Agronomic efficiency was calculated for P (AEP) and N (AEN). In Equation 14, dry matter yield (DMY) was defined as the amount of total dry matter per pot ( $\text{kg pot}^{-1}$ ), the sub-indices T and C denote "treatment" and "control" (without fertiliser), respectively, and  $N_a$  is the quantity of P or N applied per pot.

$$AE(\text{kg kg}^{-1}) = ((\text{DMY})_T - (\text{DMY})_C) / N_a \quad \text{Equation 14}$$

The apparent recovery efficiency (ARE; %) is defined as the quantity of nutrient uptake per unit of nutrient applied. It can be calculated by Equation 15, according to Fageria (2009). In Equation 15, G is the nutrient (N or P) uptake into leaves of the fertilised pot (kg), the sub-indices T and C denote "treatment" and "control" (without fertiliser), respectively, and  $N_a$  is the quantity of P or N applied per pot. This index was calculated for P (APR) and N (APN). The N or P uptake (G) was calculated by multiplying the DMY of the biomass by the respective P or N content of the biomass.

$$ARE(\%) = ((G)_T - (G)_C) / N_a \times 100 \quad \text{Equation 15}$$

### 6.2.4 Leaching Test

The N and P loss of SR1, SR2, and biosolids (Bio) was investigated from November to December of 2019, and was compared with the leaching loss of commercial U and T15 fertilisers, by performing a leaching test. Ten columns filled with sand (river sand from Depósitos Chagualo Company, Colombia) were used, two per fertiliser (Figure 37). Each column was prepared in a 30-cm high PVC tube with an internal diameter of 10.16 cm, a cross-sectional area of  $0.008 \text{ m}^2$  and an outlet stop valve at the bottom for leachate collection. The sand used in each column was initially washed in a bucket with HCl and tap water to remove traces of nutrients, and organic matter that the sand could have. Later, the sand was washed with tap water until a pH 6.8 (pH of the tap water) was obtained in the leachate; then the cleaned sand was distributed between all columns, supported by a metal mesh. The sand columns were saturated with distilled water before the beginning of the experiment and maintained at room temperature ( $25^\circ\text{C}$ ).

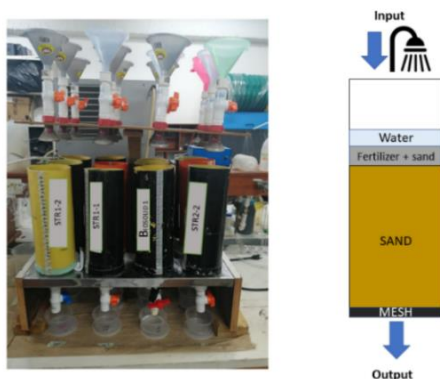


Figure 37. Leaching Test. Left: Image of the experimental setup. Right: scheme of a leaching column.

During day 1, the sand was mixed with the corresponding fertiliser in the superficial layer (0-3 cm), to achieve a value of 5.64 g-TP m<sup>-2</sup>. Only in the U treatment (that has no P), the dose was 2.54 g-TN m<sup>-2</sup> (same N-dosage than in SR1 treatment). These amounts are equivalent to a fertilisation dosage between 20.6 to 129.17 kg N ha<sup>-1</sup> (Table 24).

Table 24. Leaching test: applied product and equivalent P and N doses.

Column or Treatment	Applied product (g per column)	Applied TP (g-TP m <sup>-2</sup> )	Applied TP (mg-TP)	Applied TN (g N-NH <sub>4</sub> <sup>+</sup> m <sup>2</sup> )	Applied TN (mg- N-NH <sub>4</sub> <sup>+</sup> )
SR1	0.42	5.64		2.55	20.65
SR2	0.45	5.64	45.73	2.50	20.33
U	0.05	0		2.55	20.65
T15	0.70	5.64		6.00	48.60*
Bio	3.66	5.64		12.05	97.68

\*The applied TN on T15 is of 104.64 mg

Irrigation with distilled water was done for 29 days (4 weeks): a shower system, installed at the top of each column, allowed a slow and uniform water flow (100 mL per column and irrigation) twice per week. Sampling was also done twice a week, always 24 hours after irrigation, by opening the stop valve and using 200 mL plastic containers. Nine leachate samples were collected per column during the whole experiment. The collected volume and the TN and TP concentrations in leachates were periodically measured to calculate the cumulative mass loss.

### 6.2.5 Leaching test calculations

The mass of nutrients in each irrigation was calculated as the multiplication between the concentration of P or N and the volume collected in each irrigation. The cumulative mass (TN or TP) loss in leachates was calculated as the sum of the masses of N and P collected in each irrigation. The total loss of N or P was calculated according to Equation 16, and the N or P loss rate was calculated according to Equation 17..

$$\text{Total Lost N or P (\%)} = \frac{\sum_{i=1}^9 \text{nutrient mass}}{\text{Applied mass of Nor P}} * 100 \quad \text{Equation 16}$$

$$N \text{ or } P \text{ loss rate (mg. g}^{-1}. d^{-1}) = \frac{\sum_{i=1}^n (\text{nutrient mass } i / \Delta T)}{(\text{Applied mass of N or P}) * n} \quad \text{Equation 17}$$

Where  $i$  is the number of irrigations ( $i$  is between 1 and 9),  $\Delta T$  are the days between irrigations ( $\Delta T = T_{i+1} - T_i$ ) and  $n$  is the total number of irrigations ( $n=9$ ). The applied mass of TP or TN is 45.73 mg P and between 17 and 104 mg N, depending on the treatment.

### 6.2.6 Analytical Procedures

Struvite, biosolid and the commercial fertilisers (U and T15) were characterised by their heavy metal concentration, using microwave-assisted digestion in accordance to EPA 3052, and using a flame atomic absorption spectrophotometer (ThermoScientific iCE 300 SERIES spectrophotometer) in accordance to Standard Methods (SM 3111B, SM 3112, SM 3114C) (APHA, 2017). Ammonium concentration in the precipitates and biosolid was determined using Kjeldahl method (SM 4500), while total nitrogen (TN) and total phosphorus (TP) were calculated according to the Colombian

technical standard for fertilisers (NTC 234 and NTC 370, respectively) (ICONTEC, 1996, 2011). The microbiological analysis of SR1 and the biosolid was conducted following the NTC 4574 Colombian standard. The microbiological analysis was not performed in SR2 due to the small amount of sample that was available to perform the fertilisation and leaching tests.

The mineral compositions of struvite samples SR1 and SR2 were determined by X-ray fluorescence (XRF) analyses (Thermo ARL Optim'X WDXRF). SR1 and SR2 were also examined by X-ray diffraction (XRD) on an XPert PANalytical Empyrean Series II diffractometer with a PIXcel 3D detector 2012 model, using Cu K-alpha radiation, for struvite identification. Struvite sizes were determined by making at least 100 measurements of particles, observed under an inverted microscope (BOECO BIB100) and using the *ImageJ* program (<https://imagej.nih.gov/ij/>). Struvite samples were also analysed with an X-ray Microscope-EDX (INCA PentaFETx3 Oxford Instruments) to observe their morphologies and verify their composition.

In the fertilisation test, the TN and TP content in grass leaves was determined using analytical methods (Kjeldahl and spectrophotometry; ICONTEC, 1996, 2011). The gravimetry technique of the Colombian technical standard of products for the agricultural industry was used (NTC 5167; ICONTEC, 2011) to determine the humidity and ash content (% fresh and dried weight) in the harvested grass. Humidity was determined by maintaining the sample at 70 °C for 24 hours, while the sample was dried in the muffle at 650 °C for 4 hours for ash determination. The dry matter (DM) was calculated with the humidity and the wet weight. In the leaching test, the content of TN and TP in leachates was determined by the Kjeldahl and spectrophotometric methods, respectively, using the Colombian technical standard for fertilisers (ICONTEC, 1996, 2011).

### **6.2.7 Statistical Analysis**

One-way analysis of variance (ANOVA) was conducted to determine statistically significant differences between treatments (at  $p < 0.05$ ). Homogeneous groups for the examined treatments were determined by Fisher's least significant difference (LSD) multiple-comparison test. Statistical analyses were conducted using the Stat graphics v 4.1 software.

## **6.3 Results and discussion**

### **6.3.1 Struvite and biosolid characteristics**

Struvite precipitates were characterised in terms of macro and micronutrients, as well as heavy metals (Table 25 and Table 26). The results showed a high concentration of N, P and Mg in the SR1 and SR2, with minimum presence of other nutrients and heavy metals. Considering that N only precipitates as struvite during the real struvite production, the purity of the precipitate was determined by relating the moles of N to the moles of struvite (precipitate weigh/struvite molecular weight). Thus, the purity of the precipitate was 86.1, 78.7 and 77.7 % for SR1, SR2 and SS, respectively. The XRD analysis was also used to characterise the purity of struvite, finding that all test materials (SR1, SR2 and SS) were mainly composed of struvite, with a similarity to the struvite pattern of 97, 90 and 59%, respectively, according to high score software. EDX analysis was also used in SR1 and SR2 precipitates to corroborate its composition (Figure 38).

**Chapter 6.** The determination of fertiliser quality of the formed struvite from a WWTP

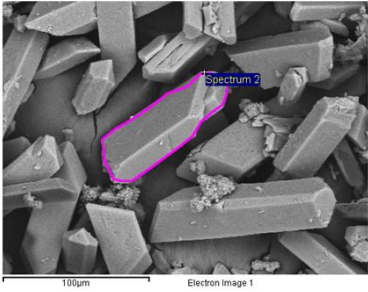
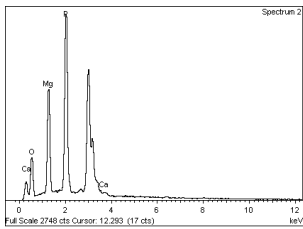
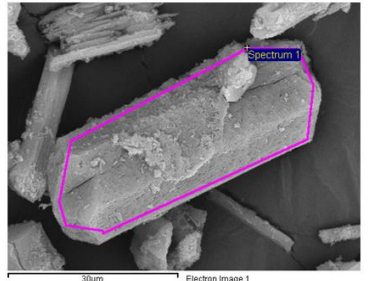
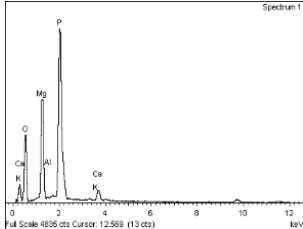
Struvite	SEM image	Element	Weight (%)	Atomic (%)	EDX
SR1		O	36.99	52.22	
		Mg	20.56	18.69	
		Al	0	0	
		P	41.80	29.83	
		K	0	0	
		Ca	0.66	0.36	
SR2		O	45.97	60.31	
		Mg	18.99	16.40	
		Al	0.31	0.24	
		P	31.54	21.38	
		K	0.37	0.20	
		Ca	2.81	1.47	

Figure 38. EDX of struvite (top) SR1 and (bottom) SR2, including the atomic composition. SEM images at 500X and 2000X for SR1 and SR2, respectively.

Struvite precipitates, biosolids and commercial fertilisers were compared using the Colombian Technical Standards (NTC 5167) and European regulation (EU 2019; ICONTEC 2011) for fertilisers. The concentration of heavy metals in struvite precipitates was lower than in biosolids (Table 26). Thus, although heavy metals can be incorporated into the crystal lattice or adsorbed to the surface of the struvite (which decreases its quality) (Muhmood et al., 2019), the concentration of heavy metals was low in all precipitates evaluated and below the permissible limits to be applied as a fertiliser, except for Cr in SR1 (with 3 mg-Cr kg<sup>-1</sup>). Biosolids fitted the permissible limits for organic and organic-mineral fertilisers, except for 19,000 mg-Zn kg<sup>-1</sup> and 87.2 mg-Cr kg<sup>-1</sup>, which are higher than the limit set by the European Union (800 and 2 mg kg<sup>-1</sup>, respectively). SS, U and T15 presented minimum concentrations of heavy metals, below permissible limits.

Table 25. Characteristics of struvites, biosolid and commercial fertilisers (Urea and Triple 15)

Parameter (units)*	SR1	SR2	SS	Biosolids	Urea	Triple15
Struvite purity (%)	86.1	78.7	77.7	-	-	-
Mean particle size (µm)	112.88	26.9	89.2			
Mix. Particle size (µm)	39.27	10.89	15.6			
Max. particle size (µm)	271.49	60.31	350.2	>200	NM	NM
Density (g cm <sup>-3</sup> )	1.6	NM	1.9	0.64	0.77	NM
Conductivity (dS m <sup>-1</sup> ) **	0.65	NM	-	0.18	NM	0.0078
DM % wm	98	98	98	95	98	98
TN (%)*	6.07	-	-	2.81	46.94	15
NH <sub>4</sub> -N (%)*	5.02	4.59	4.53	2.81	46.94	7.08
TP-P (%)*	11.11	10.35	15.6	1.32	0	6.68
K (%)*	0.05	0.49	NQ	0.06	0	12.45
Mg (%)*	5.77	6.86	7.79	0.79	0	2.14
Ca (%)*	1.12	2.1	0.01	0.16	0.01	1.66

**Chapter 6.** The determination of fertiliser quality of the formed struvite from a WWTP

Parameter (units)*	SR1	SR2	SS	Biosolids	Urea	Triple15
Al (%)*	NQ	0.22	0	3.71	0	0.07
Mn (%)*	NQ	NQ	NQ	0.01	NQ	0.01
Na (%)*	0.06	1.56	0.05	NQ	0.04	NQ
Fe (%)*	0.09	0.1	NQ	0.15	0	0.15
C-org (%)*	1.52	1.46	NM	19.68	NM	5.1
Salmonella (presence- absence / 25g)	absent	NM	NM	absent	NM	absent
Enterobacteriaceae (cfu g-1)	0	NM	NM	0	NM	NQ

Abbreviation: NQ. - Not quantifiable; NM – not measured. Note: \*All percentages are expressed on dried weight. \*\* Conductivity was measured in an extract (1/200) of each material.

Table 26. Concentration of heavy metals in precipitates produced in this study (pH 9.0) and biosolid from San Fernando WWTP, as well as allowable limits for heavy metals in fertilisers (Colombia and European regulations).

Component	Fertiliser						Legal limit (organic)		Legal limit (org-min)	
	Biosolid	STR1	STR2	SS	U	T15	EU	Col	EU	Col
Cr (mg kg <sup>-1</sup> )	87.2	3	0.4	NQ	NQ	33.61	2	1200	2	1200
Ni (mg kg <sup>-1</sup> )	92.2	3.969	1.38	NQ	NQ	10.97	50	420	50	420
Pb (mg kg <sup>-1</sup> )	30.1	NQ	NQ	NQ	NQ	NQ	120	300	120	300
Cd (mg kg <sup>-1</sup> )	1.751	<0.003	NM	NQ	NQ	NQ	1.5	39	-	39
Hg (mg kg <sup>-1</sup> )	<0.01	NQ	NQ	NQ	NQ	NQ	1	17	1	17
As (mg kg <sup>-1</sup> )	<0.1	NM	NM	NM	NM	NM	40	41	40	41
Zn (mg kg <sup>-1</sup> )	19000	20	89	NQ	NQ	695.87	800	-	1500	-
Cu (mg kg <sup>-1</sup> )	293.2	25.8	167	122.35	NQ	NQ	-	-	600	-

Abbreviation: NQ. - Not quantifiable.

Particle sizes and struvite morphology were determined using inverted microscopy. The largest mean particle size of 112 µm was found in SR1, and the smallest mean particle size of 26 µm was found in SR2 (Table 25). According to Shaddel et al.(2019), the size and morphology of the crystal are mainly influenced by the supersaturation (SI), but according to Tarragó et al.(2016), it is also influenced by the reaction time. Consequently, the mean size of SR1 was higher in comparison to the mean size of SR2 due to the high reaction time (5 days), despite presenting similar supersaturation levels (SI of 2.4 in both crystallisers). Furthermore, some particles from SS showed an X-shape morphology that can be considered as an intermediate evolutionary stage between the well-faceted and dendrite crystals or as an implicit boundary between slow and rapid growth (Prywer et al., 2012). X-shaped particles can have less settling velocity than bipyramidal crystals and, therefore, can be less easy to recover in a crystallisation reactor (Shaddel et al., 2019).

In addition, a microbiological analysis was performed on struvite SR1 and Biosolids. Microbiological analysis was not done in SR2 because there was not enough sample to do the analysis. Salmonella (absent / in 25 g) and Enterobacteriaceae (0 cfu g<sup>-1</sup>) were absent in both materials. It was expected because some pathogens, as some Enterobacteriaceae, are negatively charged; so owing to electrostatic repulsion, they will not be able to adsorb onto struvite particles at the alkaline pH 9 of the struvite crystallisation process (Michen & Graule, 2010; Muhmood et al., 2019). In the case of

Biosolid, Bedoya-Urrego et al. (2013) found the presence of *Salmonella* in all the samples and a highly variable concentration of Enterobacteriaceae ( $> 3,000 \text{ cfu g}^{-1}$ ) in the biosolid of this WWTP, pointing out that this material cannot be used as a fertiliser. Probably the previous drying process of the biosolids (8 days in the open air) favoured the absence of these microorganisms in the biosolids used during the tests.

### 6.3.2 Fertilisation test

The highest ( $3.9 \pm 1.6 \text{ gDW pot}^{-1}$ ) and the lowest ( $1.7 \pm 0.1 \text{ gDW pot}^{-1}$ ) crop yields were obtained with T15 and in the control treatment, respectively ( $P < 0.05$ ), after the first harvest (Figure 39A). Although this yield, in general, decreased after the second grass collection, except in pots fertilised with Mix, again the highest crop yield was reached in T15 treatment. This result may be due to the applied dose of N and K in T15 pots ( $5.64 \text{ g N.m}^2$  and  $4.68 \text{ g N.m}^2$ ; Table 23, Table 25), and its accumulation (N uptake), was higher than in the other treatments (Figure 39B). According to Fageria (2009), N accumulation is one of the most critical factors for improving the yield of field crops.

T15 presented the highest N uptake of  $52 \pm 16 \text{ mg N pot}^{-1}$  (Figure 39B). The N uptake of SR2 treatment did not show significant differences for T15, despite having a lower N percentage (Table 25). SR1 and SS presented lower N uptake (in the first harvest) than T15, which could be related to the particle size. Degryse et al. (2017) found that the rate of nutrient release from struvite is determined by the size of crystals and Nelson (2000), analysing the effect of struvite with different sizes, showed an increase in N uptake of ryegrass as the size of the crystals decreased. Therefore, it is possible that the low particle size of struvite in SR2 (mean size of  $26.9 \mu\text{m}$ ) conditions the highest N uptake in comparison with the other struvites tested (mean size  $> 89 \mu\text{m}$ ).

The P uptake by the grass was higher after SR1, SS and SR2 treatments than in the control or other treatments (Figure 39C). These results proved that the P contained in struvite is highly available for plants, may be due to the presence of Mg, which has a synergistic effect on the dissolution of P in soil solutions (González-Ponce et al., 2009). These results agree with those found by Ryu & Lee (2016), where P and Mg concentration in the tissue of lettuce cultivated with struvite was much higher than the concentration in lettuce cultivated with commercial fertiliser.

The P uptake in SR1 and SS treatments was higher than in SR2 treatment, which could also be related to the particle size. Suarez (1971 and 1973) and Guerrero (2013) found that tomato utilisation of P from triple superphosphate increased sharply when the particle size increased from 0.5 to 6 mm (in diameter). So, it is possible that higher particle sizes in struvite increased P accumulation during the grass fertilisation.

The highest amount of ashes in the first harvest was found in T15, SR2 and Bio treatments (Figure 39D). A high correlation was found between the amount of ash and the biomass (DW), with Pearson coefficients of 0.95 and 0.88 for first and second harvest, respectively.

The agronomic efficiency (AEN, AEP) and the apparent recovery efficiency (APR, ANR) were calculated with the consideration of differing N doses in the treatments and of a P dose that was slightly lower in T15 (Table 23), (Figure 40). The results show that the highest APR was attained after the first harvest in SR1 treatment and after the second harvest in SR1 and SS treatments:  $11.5 \pm 3.8$ ,  $14.7 \pm 4.4$  and  $15.7 \pm 5.5 \%$ , respectively. Biosolid and Mix reached the lowest APR:  $< 3.14 \%$  in the first harvest (Figure 40A). The highest ANR was attained in the first harvest of SR2 treatment and in the second harvest of treatments SR1 and SR2:  $100 \pm 37$ ,  $123 \pm 48$  and  $93 \pm 7 \%$ , respectively. The lowest ANR was also found in the first harvest of treatments Bio and Mix:  $< 12.6\%$  (Figure 40B).

The results suggest that plants efficiently used the nitrogen and phosphorus contained in struvite, since the highest values of apparent recovery efficiency were found in the struvite treatments. The mixture between struvite and biosolids did not show favourable N and P uptakes nor biomass production.

Regarding the agronomic efficiency, T15 treatment reached the highest AEP of  $69 \pm 48$  and  $33 \pm 20$   $\text{kg kg}^{-1}$  in the first and second harvests, respectively. Also, the grass harvested firstly in the SR2 treatment presented the highest AEN ( $61 \pm 18$   $\text{kg kg}^{-1}$ ); however, grass of the second harvest in SR2 treatment was minimum. Crop yields depend on many factors, including climatic conditions and the presence of 17 essential nutrients for optimal growth and development (Fageria, 2009). Therefore, the crop yield of grass could be affected by the small traces of nutrients (present in the sand used as substrate) and by a higher contribution of K in the T15 treatment. However, struvite treatments presented an efficient use of N to biomass production, comparable or even higher than commercial fertilisers (U and T15) (Figure 40D). The results indicate that struvite, although slightly soluble in water ( $0.18$   $\text{g L}^{-1}$  at  $25$  °C; Le Corre et al.(2009)), is as effective as highly soluble commercial P fertilisers (solubility  $>950$   $\text{g L}^{-1}$  at  $25$  °C for Urea and T15 fertilisers; Nutrición de plantas SA) because the available P concentration in soil and the uptake of both P and N increased. These findings corroborate the usefulness of struvite obtained from real centrate as fertiliser, similarly to Talboys et al. (2016).



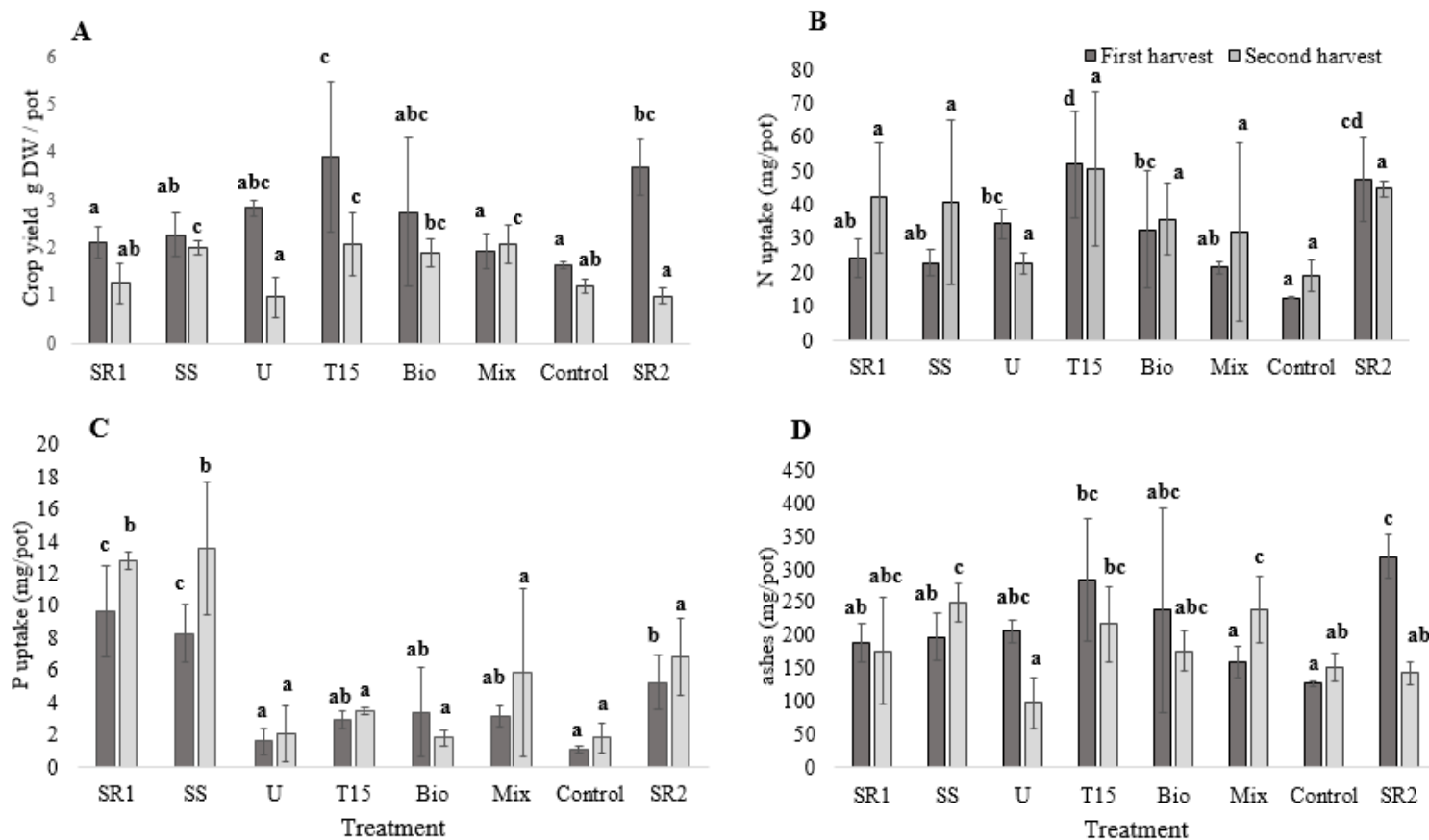


Figure 39. Crop yield, nutrients uptake and ash content, per harvest, in the fertilisation trial. (A) Grass yield (g DW per pot). (B) N uptake (mg per pot). (C) P uptake (mg per pot). (D) Ashes (mg per pot) in the grass. The standard deviation ( $n = 3$ ) within each treatment is indicated as the error bar. Letters (a–d) denote homogeneous groups; while within the same harvest, different letters indicate statistically significant differences according to the Fisher's least significant difference (LSD) multiple-comparison test at the 0.05 level. Abbreviations: DW, dried weight; SR1, SR2, struvites produced in CSTR and FBR crystallizers, respectively; SS, synthetic struvite; U, commercial urea; T15, commercial fertiliser; Bio, digested WWTP sludge; Mix, mixture of biosolids and struvite; C control (without fertiliser). Colours: dark and light grey bars denote the mean values after the first and second harvest, respectively.

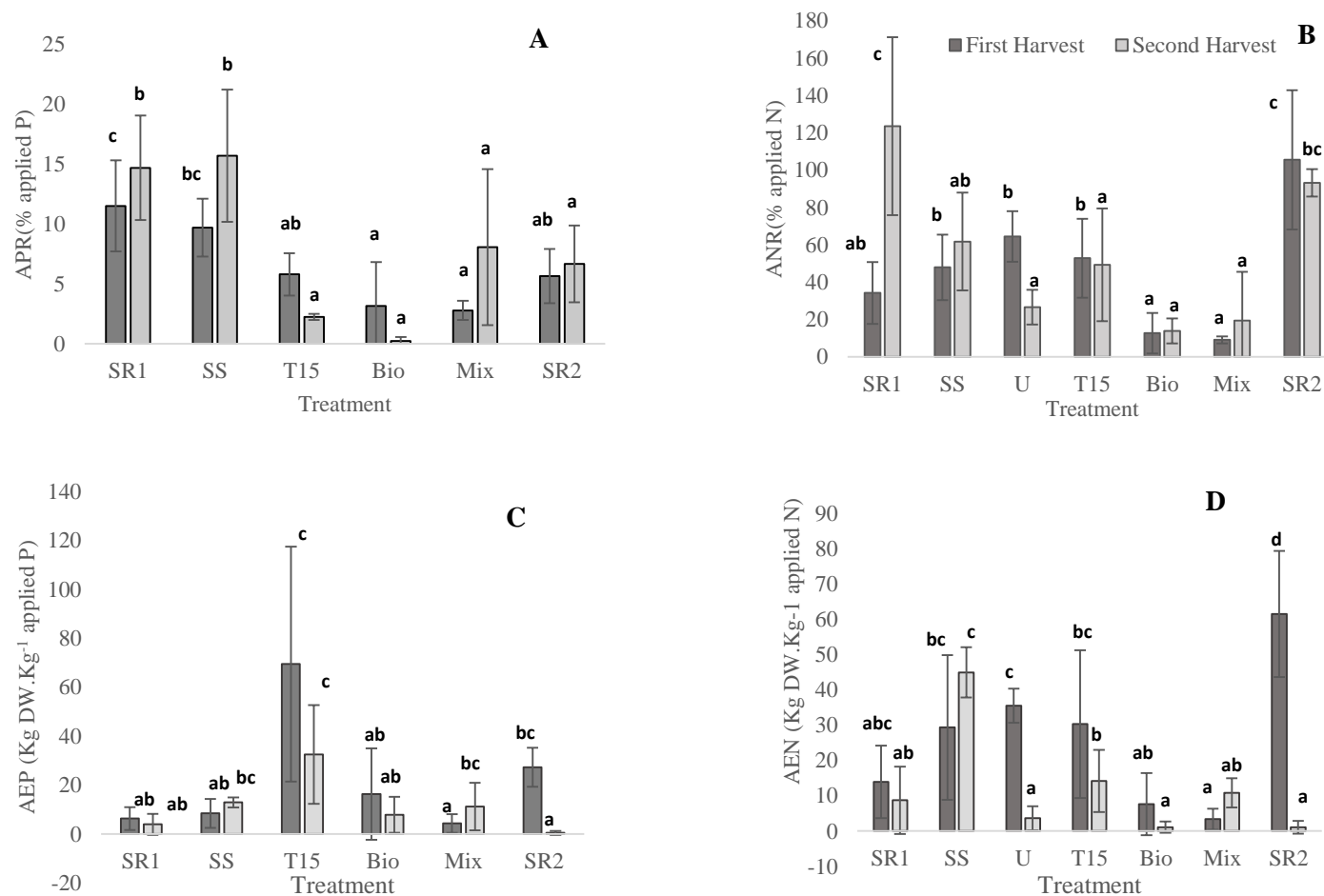


Figure 40. Phosphorus and nitrogen use efficiency, per harvest, in the fertilisation trial. Notes: The standard deviation ( $n = 3$ ) within each treatment is indicated as the error bar. Letters (a–d) denote homogeneous groups; while within the same harvest, different letters indicate statistically significant differences according to the Fisher's least significant difference (LSD) multiple-comparison test at the 0.05 level. Abbreviations: APR and ANR, apparent fertiliser nutrient P and N recovery, respectively; AEP and AEN, agronomic efficiency of applied P or N, respectively; DW, dried weight. Colours: dark and light grey bars denote the mean values after the first and second harvest, respectively.

### 6.3.3 Leaching test

The P leaching loss in SR1, SR2, T15 and Biosolid columns measured after each irrigation (9 irrigations) is shown in Figure 41A. In the second irrigation (3 days), P leaching from T15 reached the maximum value of 2.65 mg-P ( $79.5 \text{ mg} \cdot \text{L}^{-1}$ ), equivalent to 5.8 %applied-P. Meanwhile, the maximum P leaching value was attained in the third irrigation (7 days) in SR1 and SR2 columns, with values of 2.29 and 1.76 mg-P, respectively, being equivalent to 5.00 and 3.8 %applied-P, respectively. The P leaching loss from biosolid was slightly higher than the loss in struvites in the first two irrigations and presented its full release in the first irrigation. Therefore, SR1 and SR2 had better P slow-release properties than the other fertiliser tested, because the maximum P release was obtained only until after seven days.

The N leaching loss in all treatments is shown in Figure 42A. Nitrogen was rapidly washed out from the SR1 and SR2 treatment, whereas it was slowly leached from T15, Bio and U treatments. In the first irrigation, N leaching from SR1 and SR2 reached the maximum value of 5 and 7.8 mg-N, equivalent to 24 and 46 %applied-N, respectively. In U treatment, the maximum N leaching loss occurred in the third irrigation (7 days), equivalent to 3.9%. In the T15 and Bio columns, the maximum N leaching loss occurred in the second and third irrigation, equivalent to 1.8 and 1.6% applied-N, respectively. Therefore, biosolid had a better N slow-release property than the other fertilisers. The high N release in the first irrigation of SR1 and SR2 may be due to the small particle size of the struvite ( $<112 \mu\text{m}$ ) tested in this research (Rahman et al., 2013).

The P leaching pattern in all treatments was very similar in all columns. However, the accumulated loss of P in leachates (the sum of each irrigation leachate) was always higher in T15 columns, with a mean value of  $12.22 \pm 0.42 \text{ mg}$ , equivalent to  $26.7 \pm 0.92 \%$  applied-P (Figure 43B). Nevertheless, the accumulated loss of N in leachates was always higher in SR1 and SR2 columns (Figure 42B). The mean lost P in SR1, SR2 and Biosolid treatments was  $23.8 \pm 3.57$ ,  $24.5 \pm 0.29$ , and  $23.1 \pm 0.22 \%$  applied-P, respectively (Figure 43A). For the total nitrogen (TN), the average lost N for SR1, SR2, U, T15 and Biosolid treatments was  $38.8 \pm 28.1$ ,  $65.6 \pm 15.0$ ,  $19.6 \pm 1.3$ ,  $3.9 \pm 1.5$  and  $4.3 \pm 0.9 \%$  applied-N, respectively (Figure 43A). According to the European Standardisation Committee (CEN), a fertiliser may be described as slow-release if the nutrient or nutrients meet each of the following three criteria: no more than 15% released in 24 hours, no more than 75% released in 28 days and at least about 75% released at the stated release time (Trenkel, 2010). Therefore, since the irrigation was not done continuously and none of the evaluated products released more than 75% of the N and P at the time of the experiment, it was not possible to classify the products as slow-release fertilisers.

The average P leaching rate in this research was  $11.92 \pm 12.69$  and  $11.81 \pm 11.22 \text{ mg-P g}^{-1} \text{ d}^{-1}$  for STR1, STR2, while was  $14.23 \pm 16.94$  and  $12.51 \pm 15.87 \text{ mg-P g}^{-1} \text{ d}^{-1}$  for T15 and Biosolids, respectively (with respect to applied P). Meanwhile, the average N leaching rate was  $46.8 \pm 101$  and  $85.7 \pm 186 \text{ mg-N g}^{-1} \text{ d}^{-1}$  for STR1, STR2, while  $10.87 \pm 15.86$ ,  $3.27 \pm 4.67$  and  $2.07 \pm 2.95 \text{ mg-N g}^{-1} \text{ d}^{-1}$  for U, T15 and Biosolids, respectively (with respect to applied N). In addition to the high variability in the particle size of the struvite (Table 25), the high variability in the data occurs due to much higher leaching rates in the first irrigations than in the last ones. Reza et al. (2019) also found higher P than N leaching rates in the fertilisers tested. They found an average P leaching rate of 1.78 and 2.07 mg-P  $\text{g}^{-1} \text{ d}^{-1}$  and an average N leaching rate of 4.88 and 5.59 mg-N  $\text{g}^{-1} \text{ d}^{-1}$  for struvite and fused superphosphate (FSP), respectively. The lower leaching values of N and P found by Reza et al.(2019) can be due to the frequency of irrigation (once a week), the type of soil used (coarse sand and sandy soil) and the particle size of the struvite used. In addition, other researchers have reported that low P leaching from fertiliser might be due to the binding capacity of the P molecule with clay particles and

**Chapter 6.** The determination of fertiliser quality of the formed struvite from a WWTP

with other chemicals involved in P fixation such as Al, Fe and Ca (Chen et al., 2006; Sharpley, 1995). Therefore, the fixation of the P with mineral or organic compounds may have been lower due to the inert sand soil used in this experiment.

Some researchers have reported that nutrient leaching from struvite is lower than chemical fertilisers. Rahman et al.(2011) observed in a test of 7 weeks (one irrigation per week), P leaching of 0.03–0.37 % for struvite and 0.23–0.25 % (applied-P) for FSP. In the same way, Rahman et al.(2011) reported that leaching loss of N was higher in FSP-urea treatments (>6.47%) than in MAP-urea treatments (< 2.05%). In this work, the total lost N showed an opposite trend: the highest total N lost was presented in the treatments with struvite (>39%) and the minimum in T15 (3.9%) and Bio treatments (4.3%).

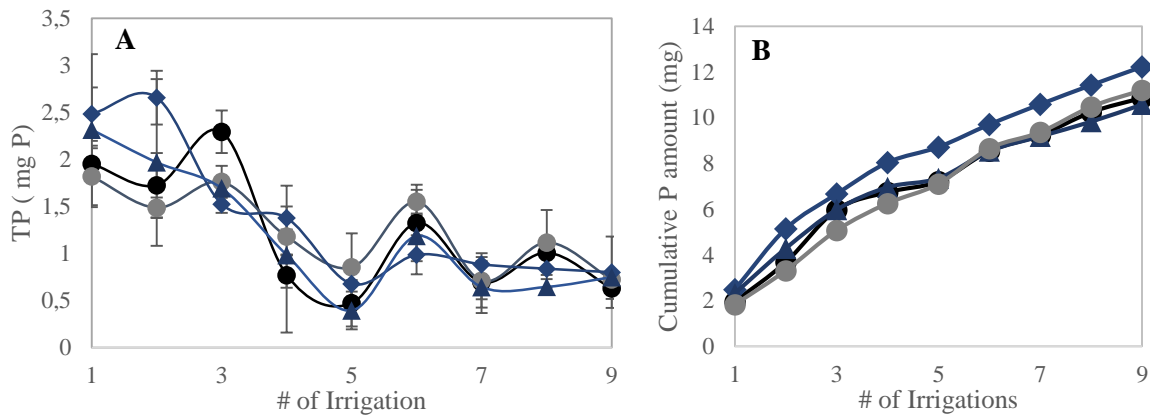


Figure 41. Leaching test. (A) Total P leaching loss measured after each irrigation. (B) Cumulative P amount in leachates. Symbols: ● SR1, ● SR2, ◆ T15 and ▲ Biosolid.

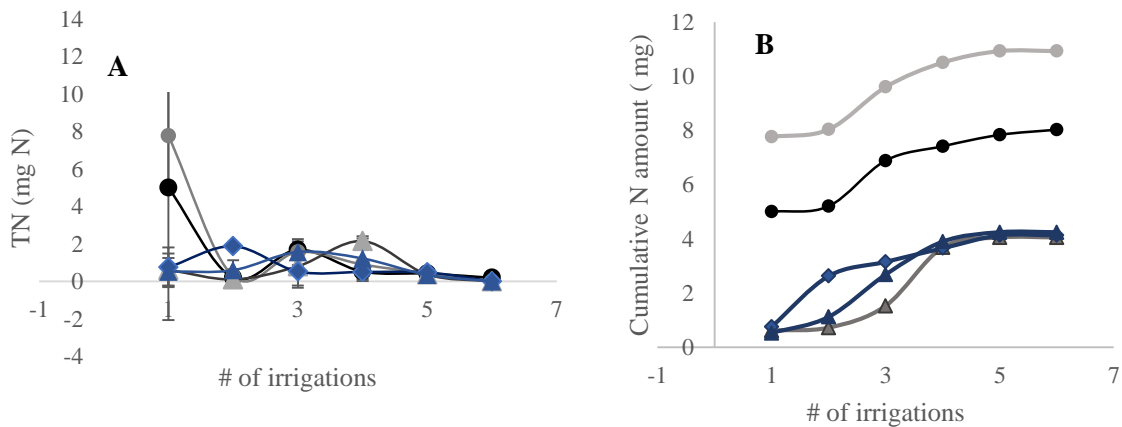


Figure 42. Leaching test. (A) Total N leaching loss measured after each irrigation. (B) Cumulative N amount in leachates. Note: After irrigation six, the content of N was not quantifiable. Symbols: ● SR1, ● SR2, ◆ T15 and ▲ Biosolid and ▲ U

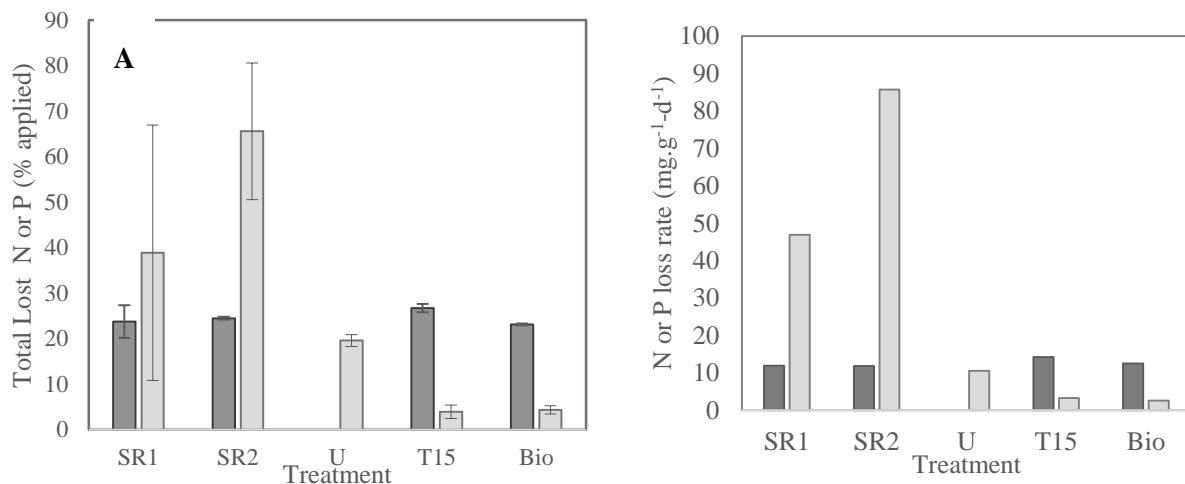


Figure 43. Leaching test. Lost nutrients in leachates. (A) Regarding the applied nutrient amount. (B) Mean nutrient loss rate (mg N-P.g<sup>-1</sup>-applied N-P.d<sup>-1</sup>). Symbols:  total P loss and  total N loss.

According to Degryse et al.(2017), struvite dissolution in soil depends on the particle size; the difference between granular or ground struvite can be explained by the increasing soil-fertiliser contact with decreasing particle size. When struvite is in granular form, diffusion of dissolved P from the particle surface into the soil becomes the rate-limiting process. Therefore, although most research reported that leaching pattern of struvite is slow and that nutrients are released for a more extended period compared with mineral fertilisers that can be completely leached out in the first 1–3 days (Ahmed et al.,2018), this research found that struvite with smaller particle size (<126µm) presented similar P leaching rate than a commercial NPK fertiliser (T15) and higher N losses than the two-commercial fertiliser tested (Urea and T15).

## 6.4 Conclusions

This study shows the application of real struvites (SR1, SR2), obtained from the centrate (supernatant of dewatered sewage sludge) of a conventional WWTP with high concentration of NH<sub>4</sub>-N, using two types of crystallisation reactor (CSTR and FBR) as fertiliser, based on data from fertilisation and leaching tests. The struvites were composed by N 4.5-4.9 %, P 10.3-13.8 %, Mg 5.6-7.6 %, Ca 1.10-2.06 %, and K 0.05-0.49 %. In addition, heavy metals were detected below the Colombian and European regulated limits for fertilisers, except for the slightly higher content of Cu. Salmonella and Enterobacteriaceae were not found in the precipitates.

In the fertilisation test, the commercial fertiliser (T15) had the maximum crop yield due to its high N content; however, it was found that P and N uptakes were higher in some of the struvites evaluated. The grass-grown with the struvite of higher particle size (89-113 µm) presented the highest apparent P recovery efficiency (11.5 ±3.8 and 15.7 ±5.5% in first and second harvests, respectively), meaning that the P of struvites is highly available to be absorbed by plants, even more than commercial NPK fertiliser (T15). Even more, the struvite with the smallest particle size (27 µm) presented the highest apparent N recovery efficiency in the first harvest (100 ±37%). Thus, real struvites showed greater

efficiencies in the absorption of N and P compared to the biosolid collected from the same WWTP and the commercial fertilisers tested (Urea and T15). The column leaching tests allowed to elucidate that P release from struvites and biosolid was slightly slower than the P release of the commercial fertiliser (T15). Nevertheless, N release was faster in struvite treatment than in Biosolid, T15 and Urea fertilisers. This release was increased with the use of the struvite with the smallest particle size ( $65 \pm 15$  % N losses).

Hence, struvites recovered from San Fernando WWTP could be an effective alternative to commercial fertilisers as they are readily available to the plants and, although the biosolid presented low nutrient recovery efficiency, the use of both can be a sustainable alternative for a WWTP. However, further studies are required to ascertain their potential eco-friendly application.

## 6.5 Acknowledgements

The authors would like to thank the Environmental School of Engineering Faculty, GIEM and GAIA groups from Universidad de Antioquia for providing the facilities to perform the experiments, especially to Acevedo M., Hurtado A. for their technical support and San Fernando WWTP for facilitating sample collection. Colciencias partially funded this research under the Beca Doctoral # 647-2014 awarded to the first author. IRTA thanks the financial support of CERCA Program (Generalitat de Catalunya) and INIA (Spanish Government) through the research project PIONER (ref. RTA2015-00093-00-00).

## Chapter 7. Conclusions and recommendations

This thesis focused on the recovery of nutrients through the precipitation of struvite from a side stream of the sludge of anaerobic digestion in a WWTP, called the sludge dewatering centrate. The thesis initially evaluated the applicability of struvite in the first WWTP with secondary treatment in Colombia, developing a steady-state mass balance that presented error percentages below 28%. Based on the low concentration of P found in the sludge of dewatered and thickened centrates and on future projections of the WWTP towards a process of biological nutrient removal, the thesis aimed at evaluating the factors that most influenced the process of crystallisation, including stirring speed, pH, temperature, SI, aeration, the addition of seed material and initial phosphorus concentration.

Two of the most commonly used reactors worldwide (CSTR and FBR) were designed and evaluated, using the actual centrate of the San Fernando WWTP as a matrix but modifying its phosphorus concentration to levels that included current and future operative conditions of the WWTP.

The precipitates obtained from the reactors were characterised and identified using scanning electron microscopy (SEM), X-ray diffraction, energy dispersive X-ray analysis (EDX), and chemical composition laboratory analysis. Finally, the quality of the products obtained as fertiliser was evaluated through a fertilisation and leaching test, comparing the precipitated struvite with other products, including the biosolid from the same WWTP, synthetic struvite (produced from reagents) and the commercial fertilisers' urea and triple 15.

The main results and conclusions respond to the hypotheses initially raised:

- In a conventional activated sludge WWTP, a significant fraction of phosphorus and nitrogen remains in the sludge thickening and dewatering centrates.

The mass balance developed in **Chapter 2** revealed that San Fernando WWTP removes approximately 60% of the TP, even though it is not designed to remove nutrients. This is mainly due to the low sludge age (2 days) and the high accumulation of these nutrients in the biosolids. Additionally, the recirculation of the centrates in the WWTP represents 17% and 14% of the initial load of TKN and TP, respectively. However, the average concentration of P in the thickening and dewatering sludge centrates were 12.9 and 17.5 mg PO<sub>4</sub><sup>3-</sup>-P. L<sup>-1</sup>, respectively, which can limit the formation of struvite. Nevertheless, under the future operative condition of the WWTP, which will include biological nutrient removal, this concentration is expected to increase.

- The stirring speed improves the efficiency and quality of the precipitated struvite in a continuous stirred tank reactor.

Regarding the effect of the stirring speed, it was observed in **Chapter 3** that the removal of N strongly increased with the increase in the stirring speed, mainly due to the volatilisation of ammonia; however, the P removal was similar in all the stirring speed evaluated. The optimal velocity gradient

(G) to obtain larger particle sizes with a higher agronomic value and reduce energy consumption and N volatilisation is between 79 and 188 s<sup>-1</sup>; higher or lower G will reduce the crystal size.

- There are an optimal pH and temperature value that improves the efficiency of nutrient recovery through struvite crystallisation and improves the quality of the precipitated product.

The results of **Chapter 4** indicated that high pH and temperature values tend to increase ammonium volatilisation and although the P removal was similar in all the temperatures and pH evaluated, the optimal struvite formation occurring around a pH of 9 and at 25°C, conditions that produced larger particle sizes, higher purity and lower volatilisation losses, which enhance the positive environmental impact of the process. The normal temperature of the centrates (33°C) is not recommended because at 33 °C, the amount of amorphous material increased due to the higher solubility of struvite.

- It is technically feasible to recover nutrients such as struvite from centrates with low P concentrations.

The tests conducted with the reactors in **Chapter 5** showed that it is technically feasible to recover nutrients such as struvite from centrates with low P concentrations (30 mg / L), finding soluble P removal efficiencies greater than 85% and precipitates purity greater than 73%. The economic viability could not be verified because the income produced by the sale of struvite was lower than the production costs (energy and chemicals), however the environmental and internal benefits could exceed the total costs.

- Aeration applied to struvite crystallisation reactors reduces the amount of NaOH required, and the seed material improves the efficiency of nutrient recovery and the size of the precipitated product.

Despite other research indicating that aeration can reduce NaOH's amount to maintain the pH at a given level, in this research (**Chapter 5**), no significant reductions in NaOH were observed due to aeration. However, there was an increase in losses of fine particles by the effluent. Besides, it was observed that the seed material did not increase the precipitation and recovery percentages but increased the size of the precipitated material, the amount of precipitated struvite, the P<sub>MAP</sub> and the struvite purity in both reactors evaluated.

- The type of reactor used to crystallise struvite (CSTR or FBR) influences the efficiency of the process and the quantity and quality of the recovered product.

When comparing the two reactors designed in this research (**Chapter 5**), no significant differences were observed in the process efficiency or the quality or quantity of the precipitated product. Although the FBR reactor seems to favour the particle size, the high saturation level of the centrates implied a small particle size in the products harvested from both reactors.

- The struvite obtained from a conventional WWTP applied to a conventional crop presents yield efficiencies comparable or superior to other commercial fertilisers.

According to **Chapter 6**, the precipitated products' characterisation indicated that most of the product was struvite with small traces of other Ca and Mg compounds, with a concentration of heavy metals below the concentration in the biosolids and below the limits allowed by Colombian and European regulations. The fertilisation tests indicated that although the highest (3.9 ± 1.6 gDW pot<sup>-1</sup>) crop yields were obtained with Triple 15, P and N are highly available in struvite to be absorbed by plants (grass *Brachiaria brizantha Marandú*), even more than in commercial fertilisers and biosolids. However, the



recovery of nutrients through the joint use of biosolids and struvite is a sustainable strategy that can be applied in municipal WWTPs.

- The struvite obtained from sludge dewatering and thickening centrates act as a slow-release fertiliser.

Although several investigations have classified struvite as a slow-release fertiliser, this investigation found ( **Chapter 6** ) that this characteristic is strongly dependent on crystal size. For small sizes, such as those obtained in this investigation, N's release was rapid, while the release of P took longer than the release of the other fertilisers tested.

Therefore, this research demonstrated that it is *possible to recover P and N from the centrates of a conventional activated sludge WWTP via struvite precipitation* only at P concentrations greater than 30 mg PO<sub>4</sub><sup>3-</sup>-P / L. Struvite with high purity degree (minimum concentration of heavy metals) can be obtained using a stirred tank or fluidised bed reactors, with minimal differences in the quality and quantity of the precipitate obtained.

Considering that it is technically and environmentally viable to recover nutrients as struvite from sludge dewatering centrates under the future operative conditions of the San Fernando WWTP, it is recommended for future research to conduct pilot-scale tests in the same WWTP to evaluate the efficiency of the production of struvite under variable concentrations of nutrients and to assess the economic feasibility of such production at large scales, including all the costs and the internal and external benefits.

## References

- Abd Mutalib, M., Rahman, M. A., Othman, M. H. D., Ismail, A. F., & Jaafar, J. (2017). *Scanning Electron Microscopy (SEM) and Energy-Dispersive X-Ray (EDX) Spectroscopy. Membrane Characterization*. Elsevier B.V. <https://doi.org/10.1016/B978-0-444-63776-5.00009-7>
- Acelas, N., Flórez, E., & López, D. (2015). Phosphorus recovery through struvite precipitation from wastewater: effect of the competitive ions. *Desalination and Water Treatment*, 54(9), 2468–2479. Retrieved from <http://www.tandfonline.com/doi/abs/10.1080/19443994.2014.902337>
- Ackerman, J. N., & Jordaan, E. M. (2015). Phosphorus removal from solids separated hog manure by air stripping Phosphorus Removal from Solids Separated Hog Manure by Air Stripping. *Canadian Biosystems Engineering*. Retrieved from [https://www.researchgate.net/publication/287284575\\_Phosphorus\\_removal\\_from\\_solids\\_separated\\_hog\\_manure\\_by\\_air\\_stripping](https://www.researchgate.net/publication/287284575_Phosphorus_removal_from_solids_separated_hog_manure_by_air_stripping)
- Adelagun, R. O. A. (2016). Chemical Science Review and Letters Technological Options for Phosphate Removal and Recovery from Aqua System: A Review. *Chem Sci Rev Lett*, 2016(18), 19–34.
- Adnan, A., Koch, F. A., & Mavinic, D. S. (2003). Pilot-scale study of phosphorus recovery through struvite crystallization – II: Applying in-reactor supersaturation ratio as a process control parameter. *Journal of Environmental Engineering and Science*, 2(6), 473–483. <https://doi.org/10.1139/s03-048>
- Agrawal, S., Guest, J. S., & Cusick, R. D. (2018). Elucidating the impacts of initial supersaturation and seed crystal loading on struvite precipitation kinetics, fines production, and crystal growth. *Water Research*, 132, 252–259. <https://doi.org/10.1016/j.watres.2018.01.002>
- Ahmed, N., Shim, S., Won, S., & Ra, C. (2018). Struvite recovered from various types of wastewaters: Characteristics, soil leaching behaviour, and plant growth. *Land Degradation and Development*, 29(9), 2864–2879. <https://doi.org/10.1002/ldr.3010>
- Ali, I. (2005). *Struvite Crystallization from Nutrient Rich Wastewater*. James Cook University. Retrieved from <https://researchonline.jcu.edu.au/148/2/02whole.pdf>
- Ali, I., & Schneider, P. A. (2005). Crystallization of Struvite from Metastable Region with Different Types of Seed Crystals Crystallization of struvite from metastable region with different types of seed crystal, (June 2014). <https://doi.org/10.1515/JNETDY.2005.007>
- Alvarez Cuenca, M., & Anthony, E. J. (1995). *Pressurized Fluidized Bed Combustion (Ryerson Po)*. Toronto: Springer-Science+Business Media, B. <https://doi.org/10.1007/978-94-011-0617-7>
- Andersen, J. M. (1976). An ignition method for determination of total phosphorus in lake sediments. *Water Research*, 10(4), 329–331. [https://doi.org/10.1016/0043-1354\(76\)90175-5](https://doi.org/10.1016/0043-1354(76)90175-5)
- APHA, AWWA, & WEF. (2017). *Standard Methods for the examination of Water and Wastewater*.

- (R. B. Baird, A. D. Eaton, & E. W. Rice, Eds.) (23rd editi). Washington, D.C: American Public Health Association. <https://doi.org/https://doi.org/10.2105/SMWW.2882.216>
- Ariyanto, E., Ang, H. M., & Sen, T. K. (2017). The Influence of Various Process Parameters on Dissolution Kinetics and Mechanism of Struvite Seed Crystals. *Journal of The Institution of Engineers (India): Series A*, 98(3), 293–302. <https://doi.org/10.1007/s40030-017-0212-4>
- Ariyanto, E., Sen, T. K., & Ang, H. M. (2014). The influence of various physico-chemical process parameters on kinetics and growth mechanism of struvite crystallisation. *Advanced Powder Technology*, 25(2), 682–694. <https://doi.org/10.1016/j.appt.2013.10.014>
- Barat, R., Bouzas, A., Marti, N., Ferrer, J., & Seco, A. (2009). Precipitation assessment in wastewater treatment plants operated for biological nutrient removal : A case study in Murcia , Spain, 90, 850–857. <https://doi.org/10.1016/j.jenvman.2008.02.001>
- Batstone, D. J., Hülsen, T., Mehta, C. M., & Keller, J. (2015). Platforms for energy and nutrient recovery from domestic wastewater: A review. *Chemosphere*, 140, 2–11. <https://doi.org/10.1016/j.chemosphere.2014.10.021>
- Batstone, D. J., & Jensen, P. D. (2011). Anaerobic Processes. *Treatise on Water Science*, 4(1), 615–639. <https://doi.org/10.1016/B978-0-444-53199-5.00097-X>
- Battistoni, P., De Angelis, A., Prisciandaro, M., Boccadoro, R., Bolzonella, D. (2002). P removal from anaerobic supernatants by struvite crystallisation: long term validation and process modelling. *Water Research*, 36, 1927–1938.
- Battistoni, P., Boccadoro, R., Fatone, F., & Pavan, P. (2005). Auto-nucleation and crystal growth of struvite in a demonstrative fluidized bed reactor (FBR). *Environ. Technol*, 26(9), 975–982. Retrieved from <https://www.ncbi.nlm.nih.gov/pubmed/16196406>
- Bayuseno, Athanasius P., & Schmahl, W. W. (2019). Thermal decomposition of struvite in water: qualitative and quantitative mineralogy analysis. *Environmental Technology (United Kingdom)*, 0(0), 1–7. <https://doi.org/10.1080/09593330.2019.1615558>
- Bayuseno, Athanasius Priharyoto, Perwitasari, D. S., Muryanto, S., Tauviqirrahman, M., & Jamari, J. (2020). Kinetics and morphological characteristics of struvite (MgNH<sub>4</sub>PO<sub>4</sub>·6H<sub>2</sub>O) under the influence of maleic acid. *Heliyon*, 6(3). <https://doi.org/10.1016/j.heliyon.2020.e03533>
- Bedoya-Urrego, K., Acevedo-Ruíz, J. M., Peláez-Jaramillo, C. A., & Agudelo-López, S. del P. (2013). Caracterización de biosólidos generados en la planta de tratamiento de agua residual San Fernando, Itagüí (Antioquia, Colombia). *Revista de Salud Publica*, 15(5), 778–790.
- Bernal, J., & Espinosa, J. (2003). *Manual de nutrición y fertilizacion de pastos*. IPNI-International plant nutrition institute. Retrieved from <http://nla.ipni.net/article/NLA-3058>
- Bhuiyan, M. I H, Mavinic, D. S., & Koch, F. A. (2008). Phosphorus recovery from wastewater through struvite formation in fluidized bed reactors: A sustainable approach. *Water Science and Technology*, 57(2), 175–181. <https://doi.org/10.2166/wst.2008.002>
- Bhuiyan, M. Iqbal H., Mavinic, D. S., & Koch, F. A. (2008). Thermal decomposition of struvite and its phase transition. *Chemosphere*, 70(8), 1347–1356. <https://doi.org/10.1016/j.chemosphere.2007.09.056>
- Bhuiyan, M I H, Mavinic, D. S., & Beckie, R. D. (2007). A solubility and thermodynamic study of struvite. *Environmental Technology*, 28, 1015–1026. <https://doi.org/https://doi.org/10.1080/09593332808618857>
- Bird, A. R. (2015). *Evaluation of the Feasibility of Struvite Precipitation from Domestic Wastewater as an Alternative Phosphorus Fertilizer Resource*. University of San Francisco.

- Bouropoulos, N. C., & Koutsoukos, P. G. (2000). Spontaneous precipitation of struvite from aqueous solutions. *Journal of Crystal Growth*, 213(3–4), 381–388. [https://doi.org/10.1016/S0022-0248\(00\)00351-1](https://doi.org/10.1016/S0022-0248(00)00351-1)
- Burgos, P. (2018). *EVALUACIÓN DE UN SISTEMA DE RECUPERACIÓN DE MACRONUTRIENTES (N Y P) EN UNA PLANTA DE TRATAMIENTO DE AGUAS RESIDUALES MEDIANTE ANÁLISIS DE CICLO DE VIDA*. Universidad de Antioquia.
- Cabanelas, I. T. D., Ruiz, J., Arbib, Z., Chinalia, F. A., Garrido-Pérez, C., Rogalla, F., ... Perales, J. a. (2013). Comparing the use of different domestic wastewaters for coupling microalgal production and nutrient removal. *Bioresource Technology*, 131, 429–436. <https://doi.org/10.1016/j.biortech.2012.12.152>
- Cánepa de Vargas, L. (2004). Manual III: Evaluación de plantas de tecnología apropiada. In Organización Panamericana de la Salud (Ed.), *Tratamiento de agua para consumo humano* (Centro Pan). Lima.
- Capdevielle, A., Sýkorová, E., Biscans, B., Béline, F., & Daumer, M. L. (2013). Optimization of struvite precipitation in synthetic biologically treated swine wastewater-Determination of the optimal process parameters. *Journal of Hazardous Materials*, 244–245, 357–369. <https://doi.org/10.1016/j.jhazmat.2012.11.054>
- Cárdenas, G., & Sánchez, I. (2013). Nitrógeno en aguas residuales: orígenes, efectos y mecanismos de remoción para preservar el ambiente y la salud pública. *Universidad y Salud*, 15(1), 72–88.
- Cardoso, M., Scholz, M., & Antunes, M. (2019). Phosphorus recovery from municipal wastewater treatment : Critical review of challenges and opportunities for developing countries. *Journal of Environmental Management*, 248(July), 109268. <https://doi.org/10.1016/j.jenvman.2019.109268>
- Carey, R. O., & Migliaccio, K. W. (2009). Contribution of wastewater treatment plant effluents to nutrient dynamics in aquatic systems. *Environmental Management*, 44(2), 205–217. <https://doi.org/10.1007/s00267-009-9309-5>
- Carrère, H., Dumas, C., Battimelli, A., Batstone, D. J., Delgenès, J. P., Steyer, J. P., & Ferrer, I. (2010). Pretreatment methods to improve sludge anaerobic degradability: A review. *Journal of Hazardous Materials*, 183(1–3), 1–15. <https://doi.org/10.1016/j.jhazmat.2010.06.129>
- Çelen, I., Buchanan, J. R., Burns, R. T., Bruce Robinson, R., & Raj Raman, D. (2007). Using a chemical equilibrium model to predict amendments required to precipitate phosphorus as struvite in liquid swine manure. *Water Research*, 41(8), 1689–1696. <https://doi.org/10.1016/j.watres.2007.01.018>
- Cerrillo, M., Palatsi, J., Comas, J., Vicens, J., & Bonmatí, A. (2014). Struvite precipitation as a technology to be integrated in a manure anaerobic digestion treatment plant – removal efficiency , crystal characterization and agricultural assessment. *J Chem Technol Biotechnol*, 90(July), 1135–1147. <https://doi.org/10.1002/jctb.4459>
- Cerrillo Moreno, M. (2012). Obtenció d'estruvita a partir de la fracció líquida digerida de purins de vaca, 162. Retrieved from <http://hdl.handle.net/2072/179786>
- Chen, G. C., He, Z. L., Stoffella, P. J., Yang, X. E., Yu, S., & Calvert, D. (2006). Use of dolomite phosphate rock (DPR) fertilizers to reduce phosphorus leaching from sandy soil. *Environmental Pollution*, 139(1), 176–182. <https://doi.org/10.1016/j.envpol.2004.12.016>
- CONAGUA. (1997). *Normas Oficiales Mexicanas NOM-001-SEMARNAT-1996 NOM-002-SEMARNAT-1996 NOM-003-SEMARNAT-1997*. (S. de M. A. y R. Naturales, Ed.). Coyoacán,

- México. Retrieved from <http://www.conagua.gob.mx/CONAGUA07/Publicaciones/Publicaciones/SGAA-15-13.pdf>
- Cooper, J., Lombardi, R., Boardman, D., & Carliell-Marquet, C. (2011). The future distribution and production of global phosphate rock reserves. *Resources, Conservation and Recycling*, 57(January), 78–86. <https://doi.org/10.1016/j.resconrec.2011.09.009>
- Cornel, P., & Schaum, C. (2009). Phosphorus recovery from wastewater: Needs, technologies and costs. *Water Science and Technology*, 59(6), 1069–1076. <https://doi.org/10.2166/wst.2009.045>
- Cornwell, D. A., & Bishop, M. M. (1983). Determining velocity gradients in laboratory and full-scale systems, 75(9), 470–475.
- CRA, & Minvivienda. (2019). *Regulación frente a tarifas por actividad del servicio-Tratamiento de vertimientos* (Documento de avance de análisis de impacto normativo) (Vol. 5). Bogotá. Retrieved from <https://www.cra.gov.co/documents/Documento-de-diagnostico-fase-2019.pdf>
- Crutchik, D., & Garrido, J. M. (2016). Kinetics of the reversible reaction of struvite crystallisation. *Chemosphere*, 154, 567–572. <https://doi.org/10.1016/j.chemosphere.2016.03.134>
- Crutchik, D., Sánchez, A., & Garrido, J. M. (2013). Simulation and experimental validation of multiple phosphate precipitates in a saline industrial wastewater. *Separation and Purification Technology*, 118, 81–88. <https://doi.org/10.1016/j.seppur.2013.06.041>
- Crutchik, D., Morales, N., & Garrido, J. M. (2017). Enhancement of struvite pellets crystallization in a full-scale plant using an industrial grade magnesium product, 3, 609–618. <https://doi.org/10.2166/wst.2016.527>
- Crutchik, Dafne, Rodrigues, S., Ruddle, D., & Garrido, J. M. (2017). Evaluation of a low-cost magnesium product for phosphorus recovery by struvite crystallization. *Journal of Chemical Technology and Biotechnology*, 93(4), 1012–1021. <https://doi.org/10.1002/jctb.5453>
- De-Bashan, L. E., & Bashan, Y. (2004). Recent advances in removing phosphorus from wastewater and its future use as fertilizer (1997-2003). *Water Research*, 38(19), 4222–4246. <https://doi.org/10.1016/j.watres.2004.07.014>
- Degryse, F., Baird, R., da Silva, R. C., & McLaughlin, M. J. (2017). Dissolution rate and agronomic effectiveness of struvite fertilizers – effect of soil pH, granulation and base excess. *Plant and Soil*, 410(1–2), 139–152. <https://doi.org/10.1007/s11104-016-2990-2>
- Departamento nacional de planeación (DNP), Ministerio de ambiente y desarrollo sostenible, & Ministerio de vivienda, ciudad y territorio. CONPES 4004-ECONOMÍA CIRCULAR EN LA GESTIÓN DE LOS SERVICIOS DE AGUA POTABLE Y MANEJO DE AGUAS RESIDUALES (2020). Colombia.
- Desmidt, E., Ghyselbrecht, K., Monballiu, A., Rabaey, K., Verstraete, W., & Meesschaert, B. D. (2013). Factors influencing urease driven struvite precipitation. *Separation and Purification Technology*, 110, 150–157. <https://doi.org/10.1016/j.seppur.2013.03.010>
- Desmidt, Evelyn, Ghyselbrecht, K., Zhang, Y., Pinoy, L., & Bruggen, B. Van Der. (2014). Global phosphorus scarcity and full-scale P-recovery techniques – a review. *Environmental Science and Technology*, 45(4), 336–384. <https://doi.org/10.1080/10643389.2013.866531>
- Desmidt, Evelyn, Ghyselbrecht, K., Zhang, Y., Pinoy, L., Van Der Bruggen, B., Verstraete, W., ... Meesschaert, B. (2015). Global phosphorus scarcity and full-scale P-recovery techniques: A review. *Critical Reviews in Environmental Science and Technology*, 45(4), 336–384. <https://doi.org/10.1080/10643389.2013.866531>
- Dhakal, S. (2008). A laboratory study of struvite precipitation for phosphorus removal from

- concentrated animal feeding operation wastewater, 86.
- Dockhorn, T. (2009). About the Economy of Phosphorus Recovery. In IWA Publishing (Ed.), *International Conference on Nutrient Recovery from Wastewater Streams* (pp. 145–158). Vancouver, Canada. [https://doi.org/ISBN 9781843392323](https://doi.org/ISBN%209781843392323).
- Doyle, J D, Oldring, K., Churchley, J., & Parsons, S. A. (2002). Struvite formation and the fouling propensity of different materials, *36*, 3971–3978.
- Doyle, J D, Philp, R., Churchley, J., & Parsons, S. A. (2000). ANALYSIS OF STRUVITE PRECIPITATION IN REAL AND SYNTHETIC LIQUORS, *78*(November).
- Doyle, James D., & Parsons, S. a. (2002). Struvite formation, control and recovery. *Water Research*, *36*(16), 3925–3940. [https://doi.org/10.1016/S0043-1354\(02\)00126-4](https://doi.org/10.1016/S0043-1354(02)00126-4)
- EL-Bourawi, M. S., Khayet, M., Ma, R., Ding, Z., Li, Z., & Zhang, X. (2007). Application of vacuum membrane distillation for ammonia removal. *Journal of Membrane Science*, *301*(1–2), 200–209. <https://doi.org/10.1016/j.memsci.2007.06.021>
- EU. (2015). Closing the Loop—An EU Action Plan for the Circular Economy. Brussels, Belgium. Retrieved from <https://eur-lex.europa.eu/legal-content/EN/TXT/?uri=CELEX:52015DC0614>
- European parliament. (2019). Legislation L170. *Official Journal of the European Union*, *170*(338), 1–127.
- European sustainable Phosphorus Platform-ESPP. (2020). Iron phosphorus workshop (online) (Vol. July 13-14, pp. 1–58). European Sustainable Phosphorus Platform (ESPP) and the Sustainable Phosphorus Alliance (SPA). Retrieved from <https://phosphorusplatform.eu/events/59-esp-activities/1975-esp-workshop-on-iron-phosphate-chemistry>
- Ezquerro, A. (2010). *Struvite precipitation and biological dissolution*. KTH-Water, Sewage and Waste technology.
- Fageria, N. . (2009). *The use of nutrients in crop plants*. (Taylor & Francis Group, Ed.), CRC Press. New York: CRC Press.
- FAO. (2017). *Reutilización de aguas para agricultura en América Latina y el Caribe*. (J. M. Sagasta, Ed.). Santiago de Chile: Organización de las Naciones Unidas para la Alimentación y la Agricultura (FAO). Retrieved from <http://www.fao.org/3/a-i7748s.pdf>
- Fattah, K. P., Zhang, Y., Mavinic, D. S., & Koch, F. a. (2010). Use of carbon dioxide stripping for struvite crystallization to save caustic dosage: performance at pilotscale operation Paper submitted to the Journal of Environmental Engineering and Science. *Canadian Journal of Civil Engineering*, *37*(9), 1271–1275. <https://doi.org/10.1139/L10-055>
- Fattah, Kazi P. (2012). Assessing Struvite Formation Potential at Wastewater Treatment Plants. *International Journal of Environmental Science and Development*, *3*(6), 548–552. <https://doi.org/10.7763/IJESD.2012.V3.284>
- Fattah, Kazi P., Mavinic, D. S., Koch, F. A., & Jacob, C. (2008). Determining the feasibility of phosphorus recovery as struvite from filter press centrate in a secondary wastewater treatment plant. *Journal of Environmental Science and Health - Part A Toxic/Hazardous Substances and Environmental Engineering*, *43*(7), 756–764. <https://doi.org/10.1080/10934520801960052>
- Fogler, H. S. (2008). Distributions of Residence Times for Chemical Reactors 13. In Pearson (Ed.), *Elements of Chemical Reaction Engineering* (4th Editio, pp. 867–944). University of Michigan. Retrieved from <http://www.umich.edu/~essen/html/byconcept/chapter13.pdf>
- Frost, R.L., Weier, M.L., Erickson, K. L. (2004). Thermal decomposition of struvite: implications for

- the decomposition of kidney stones. *Journal of Thermal Analysis and Calorimetry*, 76(3), 1025–1033. <https://doi.org/https://doi.org/10.1023/B:JTAN.0000032287.08535.b3>
- Galbraith, S. C., & Schneider, P. A. (2014). Modelling and simulation of inorganic precipitation with nucleation, crystal growth and aggregation: A new approach to an old method. *Chemical Engineering Journal*, 240, 124–132. <https://doi.org/10.1016/j.cej.2013.11.070>
- Ghisellini, P., Cialani, C., & Ulgiati, S. (2016). A review on circular economy: The expected transition to a balanced interplay of environmental and economic systems. *Journal of Cleaner Production*, 114, 11–32. <https://doi.org/10.1016/j.jclepro.2015.09.007>
- Ghosh, S., Lobanov, S., & Lo, V. K. (2019). Impact of supersaturation ratio on phosphorus recovery from synthetic anaerobic digester supernatant through a struvite crystallization fluidized bed reactor, 3330. <https://doi.org/10.1080/09593330.2018.1435734>
- González-Morales, C., Camargo-valero, M. A., Molina-Pérez, F. J., & Fernandez, B. (2019). Effect of the stirring speed on the struvite formation using the centrate from a WWTP. *Revista Facultad de Ingeniería*, 92(92), 9–17. <https://doi.org/http://dx.doi.org/10.17533/udea.redin.20190518>
- González-Ponce, R., López-de-Sá, E. G., & Plaza, C. (2009). Lettuce response to phosphorus fertilization with struvite recovered from municipal wastewater. *HortScience*, 44(2), 426–430. <https://doi.org/10.21273/hortsci.44.2.426>
- Guadie, A., Xia, S., Jiang, W., Zhou, L., Zhang, Z., Hermanowicz, S. W., ... Shen, S. (2014). Enhanced struvite recovery from wastewater using a novel cone-inserted fluidized bed reactor. *Journal of Environmental Sciences (China)*, 26(4), 765–774. [https://doi.org/10.1016/S1001-0742\(13\)60469-6](https://doi.org/10.1016/S1001-0742(13)60469-6)
- Guerra-Rodríguez, S., Oulego, P., Rodríguez, E., Singh, D. N., & Rodríguez-Chueca, J. (2020). Towards the implementation of circular economy in the wastewater sector: Challenges and opportunities. *Water (Switzerland)*, 12(5). <https://doi.org/10.3390/w12051431>
- Guerrero, R. (2013). Manual técnico. Propiedades Generales de los Fertilizantes. *Journal of Chemical Information and Modeling*, 53, 1689–1699. <https://doi.org/10.1017/CBO9781107415324.004>
- Guo, J. (2010). *Recovery of Nutrients from Anaerobic Digester Supernatant using Magnesium-Rich Waste Material*. RMIT University. Retrieved from <https://researchbank.rmit.edu.au/eserv/rmit:160617/Guo.pdf>
- Gustafsson, J. P. (2013). visual MINTEQ VER.3.1. Retrieved from <https://vminteq.lwr.kth.se/>
- Hall, R. L., Boisen Staal, L., Macintosh, K. A., McGrath, J. W., Bailey, J., Black, L., ... Williams, P. N. (2020). Phosphorus speciation and fertiliser performance characteristics: A comparison of waste recovered struvites from global sources. *Geoderma*, 362(December 2019), 114096. <https://doi.org/10.1016/j.geoderma.2019.114096>
- Hallas, J. F., Mackowiak, C. L., Wilkie, A. C., & Harris, W. G. (2019). Struvite Phosphorus Recovery from Aerobically Digested Municipal Wastewater, 1–12. <https://doi.org/10.3390/su11020376>
- Hao, X. D., Wang, C. C., Lan, L., & Von Loosdrecht, M. C. M. (2008). Struvite formation, analytical methods and effects of pH and Ca<sup>2+</sup>. *Water Sci. Technol.*, 58, 1687–1692. Retrieved from <https://www.ncbi.nlm.nih.gov/pubmed/19001726>
- Holloway, R. W., Childress, A. E., Dennett, K. E., & Cath, T. Y. (2007). Forward osmosis for concentration of anaerobic digester centrate. *Water Research*, 41(17), 4005–4014. <https://doi.org/10.1016/j.watres.2007.05.054>
- ICONTEC- Instituto Colombiano de Normas Técnicas. AGRICULTURAL INDUSTRY

- PRODUCTS. ORGANIC PRODUCTS USED AS FERTILIZERS AND SOIL AMENDMENTS. (2011). Colombia.
- ICONTEC. NTC 5167 (2011). Retrieved from <http://tienda.icontec.org/brief/NTC5167.pdf>
- ICONTEC - Instituto Colombiano de Normas Técnicas. FERTILIZERS. TEST METHOD FOR QUANTITATIVE DETERMINATION OF PHOSPHORUS., Pub. L. No. 073 PRODUCTOS PARA LA INDUSTRIA AGRÍCOLA, 18 (1996). Colombia.
- ICONTEC - Instituto Colombiano de Normas Técnicas. FERTILIZER. DETERMINATION OF TOTAL NITROGEN CONTENT, Pub. L. No. 073 PRODUCTOS PARA LA INDUSTRIA AGRÍCOLA, 12 (2011). Colombia.
- ISO. ISO 14235 Soil quality — Determination of organic carbon by sulfochromic oxidation (1998). Retrieved from <https://www.iso.org/obp/ui/#iso:std:iso:14235:ed-1:v1:en>
- Jaffer, Y., Clark, T. A., Pearce, P., & Parsons, S. A. (2002). Potential phosphorus recovery by struvite formation, 36, 1834–1842.
- Jenkins, D., & Wanner, J. (2014). *100 years activated sludge*. London: IWA Publishing.
- Jia, G. (2014). *Nutrient removal and recovery by the precipitation of magnesium ammonium phosphate*. The University of Adelaide.
- Jordaan, E. M. (2011). *Development of an aerated struvite crystallization reactor for phosphorus removal and recovery from swine manure*. University of Manitoba. Retrieved from [https://umanitoba.ca/faculties/afs/ncle/pdf/jordaan\\_elsie.pdf](https://umanitoba.ca/faculties/afs/ncle/pdf/jordaan_elsie.pdf)
- Kataki, S., West, H., Clarke, M., & Baruah, D. C. (2016). Resources , Conservation and Recycling Phosphorus recovery as struvite : Recent concerns for use of seed , alternative Mg source , nitrogen conservation and fertilizer potential. “*Resources, Conservation & Recycling*,” 107, 142–156. <https://doi.org/10.1016/j.resconrec.2015.12.009>
- Kim, Daegi, Min, K. J., Lee, K., Yu, M. S., & Park, K. Y. (2017). Effects of pH, molar ratios and pre-treatment on phosphorus recovery through struvite crystallization from effluent of anaerobically digested swine wastewater. *Environmental Engineering Research*, 22(1), 12–18. <https://doi.org/10.4491/eer.2016.037>
- Kim, Daekeun, Kim, J., Ryu, H. D., & Lee, S. I. (2009). Effect of mixing on spontaneous struvite precipitation from semiconductor wastewater. *Bioresource Technology*, 100(1), 74–78. <https://doi.org/10.1016/j.biortech.2008.05.024>
- Kostov, G., Angelov, M., Mihailov, I., & Stoeva, D. (2011). Development of combined models to describe the residence time distribution in fluidized-bed bioreactor with light beads. *Procedia Food Science*, 1(December), 770–775. <https://doi.org/10.1016/j.profoo.2011.09.116>
- Kumar, A., Das, A., Goel, M., Ravi Kumar, K., Subramanyam, B., & Sudarsan, J. S. (2013). Recovery of nutrients from wastewater by struvite crystallization. *Nature Environment and Pollution Technology*, 12(3), 479–482.
- Le Corre, K. S., Valsami-Jones, E., Hobbs, P., Jefferson, B., & Parsons, S. A. (2007). Struvite crystallisation and recovery using a stainless steel structure as a seed material. *Water Research*, 41(11), 2449–2456. <https://doi.org/10.1016/j.watres.2007.03.002>
- Le Corre, K. S., Valsami-Jones, E., Hobbs, P., & Parsons, S. A. (2009). Phosphorus recovery from wastewater by struvite crystallization: A review. *Critical Reviews in Environmental Science and Technology*, 39(6), 433–477. <https://doi.org/10.1080/10643380701640573>
- Le Corre, Kristell S, Valsami-Jones, E., Hobbs, P., & Parsons, S. A. (2005). Impact of calcium on



- struvite crystal size, shape and purity, 283, 514–522. <https://doi.org/10.1016/j.jcrysgro.2005.06.012>
- Lee, J. E., Rahman, M. M., & Ra, C. S. (2009). Dose effects of Mg and PO<sub>4</sub> sources on the composting of swine manure. *Journal of Hazardous Materials*, 169(1–3), 801–807. <https://doi.org/10.1016/j.jhazmat.2009.04.026>
- Lee, S. H., Yoo, B. H., Kim, S. K., Lim, S. J., Kim, J. Y., & Kim, T. H. (2013). Enhancement of struvite purity by re-dissolution of calcium ions in synthetic wastewaters. *Journal of Hazardous Materials*, 261, 29–37. <https://doi.org/10.1016/j.jhazmat.2013.06.072>
- Levenspiel, O. (1986). *Ingeniería de las reacciones químicas*. (REVERTÉ, Ed.) (Departamen. Oregon).
- Li, B., Boiarkina, I., Young, B., Yu, W., & Singhal, N. (2018). Prediction of Future Phosphate Rock : A Demand Based Model. *Journal of Environmental Informatics*, 31(1), 41–53. <https://doi.org/10.3808/jei.201700364>
- Li, Bing, Boiarkina, I., Young, B., & Yu, W. (2016). Quantification and mitigation of the negative impact of calcium on struvite purity. *Advanced Powder Technology*, 27(6), 2354–2362. <https://doi.org/10.1016/j.appt.2016.10.003>
- Li, Bing, Boiarkina, I., Yu, W., Ming, H., Munir, T., Qian, G., & Young, B. R. (2019). Phosphorous recovery through struvite crystallization : Challenges for future design. *Science of the Total Environment*, 648, 1244–1256. <https://doi.org/10.1016/j.scitotenv.2018.07.166>
- Li, Bing, Ming, H., Boiarkina, I., Yu, W., Fei, Y., Qian, G., & Young, B. R. (2019). Phosphorus recovery through struvite crystallisation : Recent developments in the understanding of operational factors. *Journal of Environmental Management*, 248(May), 109254. <https://doi.org/10.1016/j.jenvman.2019.07.025>
- Liu, Xiaoning; Hu, Zhengyi; Zhu, Chunyou; Wen, Guoqi; Meng, X. (2013). Influence of process parameters on phosphorus recovery by struvite formation from urine. *Water Science & Technology*, 68(11), 2434–2440. <https://doi.org/10.2166/wst.2013.514>
- Liu, J. (2018). *Chemical equilibrium modeling of phosphorus removal and recovery processes for advanced wastewater treatment*. Colorado State University.
- Liu, X., Wen, G., Hu, Z., & Wang, J. (2018). Coupling effects of pH and Mg / P ratio on P recovery from anaerobic digester supernatant by struvite formation. *Journal of Cleaner Production*, 198, 633–641. <https://doi.org/10.1016/j.jclepro.2018.07.073>
- Liu, Y., & Qu, H. (2017). Interplay of digester supernatant composition and operating pH on impacting the struvite particulate properties. *Journal of Environmental Chemical Engineering*, 5(4), 3949–3955. <https://doi.org/10.1016/j.jece.2017.07.065>
- Liu, Z., Zhao, Q., Lee, D., & Yang, N. (2008). Enhancing phosphorus recovery by a new internal recycle seeding MAP reactor, 99, 6488–6493. <https://doi.org/10.1016/j.biortech.2007.11.039>
- López, J. C. (2017). *Recuperação de nitrogênio e fosforo na forma de estruvita, a partir de lodo gerado em processo biológico de tratamento de esgoto*. Universidade de São Pablo.
- Lu, Q., He, Z. L., & Stoffella, P. J. (2012). Land application of biosolids in the USA: A review. *Applied and Environmental Soil Science*, 2012(October 2014). <https://doi.org/10.1155/2012/201462>
- Maaß, O., Grundmann, P., & Von Bock Und Polach, C. (2014). Added-value from innovative value chains by establishing nutrient cycles via struvite. *Resources, Conservation and Recycling*, 87, 126–136. <https://doi.org/10.1016/j.resconrec.2014.03.012>

- MADS. (2019). *Estrategia Nacional de Economía Circular*. Gobierno de Colombia. Bogotá: Ministerio de Ambiente y Desarrollo Sostenible; Ministerio de Comercio, Industria y Turismo. Retrieved from [http://www.andi.com.co/Uploads/Estrategia Nacional de Economía Circular-2019 Final.pdf\\_637176135049017259.pdf](http://www.andi.com.co/Uploads/Estrategia Nacional de Economía Circular-2019 Final.pdf_637176135049017259.pdf)
- Mangin, D., & Klein, J. . (2004). Fluid dynamic concepts for a phosphate precipitation reactor design. In E. Valsami-Jones (Ed.), *Phosphorus in Environmental Technology: Principles and Applications* (Ilustrada, pp. 358–401). IWA Publishing.
- Marti, N., Bouzas, A., Seco, A., & Ferrer, J. (2008). Struvite precipitation assessment in anaerobic digestion processes. *Chemical Engineering Journal*, *141*, 67–74. <https://doi.org/10.1016/j.cej.2007.10.023>
- Marti, N., Ferrer, J., Seco, A., & Bouzas, A. (2008). Optimisation of sludge line management to enhance phosphorus recovery in WWTP. *Water Research*, *42*(18), 4609–4618. <https://doi.org/10.1016/j.watres.2008.08.012>
- Martínez, A. A. (2017). Tendencias en el tratamiento integral de aguas residuales. In *Congreso internacional ambiental Manizales*. Manizales.
- Mehta, C. M., & Batstone, D. J. (2013). Nucleation and growth kinetics of struvite crystallization. *Water Research*, *47*(8), 2890–2900. <https://doi.org/10.1016/j.watres.2013.03.007>
- Mehta, C. M., Khunjar, W. O., Nguyen, V., Tait, S., & Damien, J. (2015). Technologies to Recover Nutrients from Waste Streams : A Critical Review. *Environmental Science and Technology*, *45*(May 2014), 385–427. <https://doi.org/10.1080/10643389.2013.866621>
- Meijer, S. C. F., Van Der Spoel, H., Susanti, S., Heijnen, J. J., & Van Loosdrecht, M. C. M. (2002). Error diagnostics and data reconciliation for activated sludge modelling using mass balances. *Water Science and Technology*, *45*(6), 145–156. <https://doi.org/10.2166/wst.2002.0102>
- Metcalf, & Eddy. (1995). *Ingeniería de aguas residuales*. (M. GRAW-HILL, Ed.). Madrid.
- Michen, B., & Graule, T. (2010). Isoelectric points of viruses. *Journal of Applied Microbiology*, *109*(2), 388–397. <https://doi.org/10.1111/j.1365-2672.2010.04663.x>
- Mihelcic, J. R., Fry, L. M., & Shaw, R. (2011). Global potential of phosphorus recovery from human urine and feces. *Chemosphere*, *84*(6), 832–839. <https://doi.org/10.1016/j.chemosphere.2011.02.046>
- Minambiente. Resolución 631 De 2015, RESOLUCIÓN Diario Oficial No. 49.486 de 18 de abril de 2015 § (2015).
- Ministerio de ambiente Uruguay. (1998). *Estándares de vertido, comparación de los límites fijados por la legislación vigente en el ambito del Area Metropolitana de Buenos Aires, Provincias de Buenos Aires y Santa Fe y en la República Oriental del Uruguay*. (M. de ambiente Uruguay, Ed.). gub.uy. Retrieved from [https://www.dinama.gub.uy/oan/documentos/uploads/2016/12/Estandares\\_de\\_vertido\\_Carsen.pdf](https://www.dinama.gub.uy/oan/documentos/uploads/2016/12/Estandares_de_vertido_Carsen.pdf)
- Ministerio del Ambiente - MINAM. 003-2010-MINAM (2010). Perú. Retrieved from <https://sinia.minam.gob.pe/normas/limites-maximos-permisibles-lmp-efluentes-plantas-tratamiento-aguas>
- Ministerio secretaria general de la presidencia-MSGP. Decreto 90, 90 § (2001). Chile. Retrieved from <https://www.bcn.cl/leychile/navegar?idNorma=182637>
- Missen, R., Mims, C., & Saville, B. (1999). *Introduction to chemical reaction engineering and kinetic*. University of Toronto. Toronto: John Wiley and Sons, Inc.

<https://doi.org/10.1002/9783527823376.ch1>

- Molinos-Senante, M., Sala-Garrido, R., & Hernández-Sancho, F. (2010). Estudio de viabilidad del proceso de recuperación del fósforo contenido en las aguas residuales: una aproximación económica. *Rect@*, *11*(1).
- Mollah, M., Sánchez, C., Barría, K., Ferrán, D., & Vallester, E. (2018). Estudio del comportamiento hidrodinámico de un filtro biológico de flujo ascendente, utilizando mazorcas de maíz como material de soporte. *Revista de Iniciación Científica*, *4*(1), 50–54. <https://doi.org/10.33412/rev-ric.v4.1.1867>
- Möller, K., & Müller, T. (2012). Effects of anaerobic digestion on digestate nutrient availability and crop growth: A review. *Engineering in Life Sciences*, *12*(3), 242–257. <https://doi.org/10.1002/elsc.201100085>
- Montgomery, D. (2004). Diseño y análisis de experimentos. *Limusa Wiley*. Mexico.
- Morales, N., Boehler, M. A., Buettner, S., Liebi, C., & Siegrist, H. (2013). Recovery of N and P from Urine by Struvite Precipitation Followed by Combined Stripping with Digester Sludge Liquid at Full Scale, 1262–1278. <https://doi.org/10.3390/w5031262>
- Moulessehou, A., Gallart-Mateu, D., Harrache, D., Djaroud, S., de la Guardia, M., & Kameche, M. (2017). Conductimetric study of struvite crystallization in water as a function of pH. *Journal of Crystal Growth*, *471*, 42–52. <https://doi.org/10.1016/j.jcrysro.2017.05.011>
- Mousavi, S. E. (2017). *Modeling struvite precipitation in a batch reactor using a population balance model in a 3-D computational fluid dynamic ( CFD ) framework*. Concordia University. Retrieved from [https://spectrum.library.concordia.ca/982370/1/Mousavi\\_MASc\\_S2017.pdf](https://spectrum.library.concordia.ca/982370/1/Mousavi_MASc_S2017.pdf)
- Moussa, S. Ben, Tlili, M. M., Batis, N., & Amor, M. Ben. (2011). Influence of temperature on struvite precipitation by CO<sub>2</sub>-degassing method, *260*(3), 255–260. <https://doi.org/10.1002/crat.201000571>
- Muhmood, A., Lu, J., Dong, R., & Wu, S. (2019). Formation of struvite from agricultural wastewaters and its reuse on farmlands: Status and hindrances to closing the nutrient loop. *Journal of Environmental Management*, *230*(May 2018), 1–13. <https://doi.org/10.1016/j.jenvman.2018.09.030>
- Munch, E. V, & Barr, K. (2001). Controlled Struvite Crystallisation for Removing Phosphorus From Anaerobic Digestion Sidestreams. *Water Research*, *35*(1), 151–159. Retrieved from <papers2://publication/uuid/5F580838-F82C-4EBD-8592-CA322F4EAE40>
- Muys, M., Phukan, R., Brader, G., Samad, A., Moretti, M., Haiden, B., ... Spiller, M. (2021). A systematic comparison of commercially produced struvite: Quantities, qualities and soil-maize phosphorus availability. *Science of the Total Environment*, *756*, 143726. <https://doi.org/10.1016/j.scitotenv.2020.143726>
- Naranjo, D. (2009). *DEVELOPMENT OF A WATER TREATMENT COMPACT SYSTEM*. Universidad de Antioquia.
- Neczaj, E., & Grosser, A. (2018). Circular Economy in Wastewater Treatment Plant—Challenges and Barriers. *Proceedings*, *2*(11), 614. <https://doi.org/10.3390/proceedings2110614>
- Nedelciu, C. E., Ragnarsdottir, K. V, Schlyter, P., & Stjernquist, I. (2020). Global phosphorus supply chain dynamics: Assessing regional impact to 2050. *Global Food Security*, *26*(100426), 10. <https://doi.org/https://doi.org/10.1016/j.gfs.2020.100426>
- Nelson, N. O. (2000). *Phosphorus Removal from Anaerobic Swine Lagoon Effluent as Struvite and Its Use as a Slow-Release Fertilizer*. North Carolina State University.

- Ohlinger, K. N., Young, T. M., & Schroeder, E. D. (1998). Predicting struvite formation in digestion. *Water Research*, *32*(12), 3607–3614. [https://doi.org/10.1016/S0043-1354\(98\)00123-7](https://doi.org/10.1016/S0043-1354(98)00123-7)
- Palacio, J. A., Toro, F. M., Flores, M. T., Gómez, E. A., & Molina, F. J. (2016). *Estudio de la problemática ambiental del embalse Porce II para la gestión integral y adecuada del recurso hídrico*. Medellín.
- Pastor, L., Mangin, D., Barat, R., & Seco, A. (2008). A pilot-scale study of struvite precipitation in a stirred tank reactor: Conditions influencing the process. *Bioresource Technology*, *99*(14), 6285–6291. <https://doi.org/10.1016/j.biortech.2007.12.003>
- Pastor, L., Mangin, D., Ferrer, J., & Seco, A. (2010). Struvite formation from the supernatants of an anaerobic digestion pilot plant. *Bioresource Technology*, *101*(1), 118–125. <https://doi.org/10.1016/j.biortech.2009.08.002>
- Pastor, Laura. (2006). *Investigations on the Recovery of Phosphorus from Wastewater by Crystallization*. <https://doi.org/10.1177/004057368303900411>
- Pastor, Laura. (2008). *Estudio de la precipitación y recuperación del fósforo presente en las aguas residuales en forma de estruvita*. Universidad politecnica de Valencia. Retrieved from <papers2://publication/uuid/6B827EFD-E5BB-4CC5-8E14-69F7E86896A1>
- Pathak, A., Dastidar, M. G., & Sreekrishnan, T. R. (2009). Bioleaching of heavy metals from sewage sludge by indigenous iron-oxidizing microorganisms using ammonium ferrous sulfate and ferrous sulfate as energy sources: A comparative study. *Journal of Hazardous Materials*, *171*(1–3), 273–278. <https://doi.org/10.1016/j.jhazmat.2009.05.139>
- Patiño, P., Cruz, C., Torres, P., & Laín, S. (2012). Hydrodynamic evaluation of a hydraulic clarifier through hydraulic behaviour indicators and simplified flow models. *Ingeniería e Investigación*, *32*(1), 77–82.
- Pérez, A., & Torres, P. (2008). Evaluación del comportamiento hidrodinámico como herramienta para optimización de reactores anaerobios de crecimiento en medio fijo. *Revista Facultad de Ingeniería*, (45), 27–40.
- Ping, Q., Li, Y., Wu, X., Yang, L., & Wang, L. (2016). Characterization of morphology and component of struvite pellets crystallized from sludge dewatering liquor: Effects of total suspended solid and phosphate concentrations. *Journal of Hazardous Materials*, *310*, 261–269. <https://doi.org/10.1016/j.jhazmat.2016.02.047>
- Prywer, J., Torzewska, A., & Płociński, T. (2012). Unique surface and internal structure of struvite crystals formed by *Proteus mirabilis*. *Urological Research*, *40*(6), 699–707. <https://doi.org/10.1007/s00240-012-0501-3>
- Puig, S., van Loosdrecht, M. C. M., Colprim, J., & Meijer, S. C. F. (2008). Data evaluation of full-scale wastewater treatment plants by mass balance. *Water Research*, *42*(18), 4645–4655. <https://doi.org/10.1016/j.watres.2008.08.009>
- Puig, S., van Loosdrecht, M. C. M., Flameling, A. G., Colprim, J., & Meijer, S. C. F. (2010). The effect of primary sedimentation on full-scale WWTP nutrient removal performance. *Water Research*, *44*(11), 3375–3384. <https://doi.org/10.1016/j.watres.2010.03.024>
- Qiu, G., & Ting, Y.-P. (2014). Direct phosphorus recovery from municipal wastewater via osmotic membrane bioreactor (OMBR) for wastewater treatment. *Bioresource Technology*, *170*, 221–229. <https://doi.org/10.1016/j.biortech.2014.07.103>
- Rahaman, M. ., Ellis, N., & Mavinic, D. . (2008). Effects of various process parameters on struvite precipitation kinetics and subsequent determination of rate constants. *Water Science &*

- Technology*, (February). <https://doi.org/10.2166/wst.2008.022>
- Rahaman, M. S., & Mavinic, D. S. (2009). Recovering nutrients from wastewater treatment plants through struvite crystallization: CFD modelling of the hydrodynamics of UBC MAP fluidized-bed crystallizer. *Water Science and Technology*, 59(10), 1887–1892. <https://doi.org/10.2166/wst.2009.214>
- Rahaman, M. S., Mavinic, D. S., Bhuiyan, M. I. H., & Koch, F. A. (2006). Exploring the Determination of Struvite Solubility Product from Analytical Results. *Environmental Technology*, 27, 951–961. <https://doi.org/10.1080/09593332708618707>
- Rahman, M., Liu, Y., Kwag, J., & Ra, C. (2011). Recovery of struvite from animal wastewater and its nutrient leaching loss in soil. *Journal of Hazardous Materials*, 186(2–3), 2026–2030. <https://doi.org/10.1016/j.jhazmat.2010.12.103>
- Rahman, M. M., Salleh, M. A. M., Rashid, U., Ahsan, A., Hossain, M. M., & Ra, C. S. (2013). Production of slow release crystal fertilizer from wastewaters through struvite crystallization - A review. *Arabian Journal of Chemistry*, 7(1), 139–155. <https://doi.org/10.1016/j.arabjc.2013.10.007>
- Ramos Contreras, C., Ramos Contreras, I., Jaramillo, C. N., & Molina Pérez, F. (2015). Validación e implementación de una metodología para la determinación de carbono orgánico total en suelos y sedimentos según ISO 14235:1998, 11(21), 9–17.
- Rao, K. C. k., Otoo, M., Drechsel, P., & Hanjra, M. A. (2017). Resource recovery and reuse as an incentive for a more viable sanitation service chain. *Water Alternatives*, 10(2), 493–512.
- Rasban, W. (2016). Image J. National institutes of Health. Retrieved from <http://imagej.nih.gov/ij>
- Regy, S., Mangin, D., Klein, J. P., & Lieto, J. (2002). *Phosphate recovery by struvite precipitation in a stirred reactor. Lagep (laboratoire d'automatique et de genie des procedes)/CEEP (Centre Europe' en d'Etude des Polyphosphates)* (Vol. 02). Retrieved from <http://www.nhm.ac.uk/research-curation/departments/mineralogy/researchgroups/phosphaterecovery/LagepReportS>. PDF 1–65.
- Republica de Ecuador. Libro VI, Norma de calidad ambiental y de descarga de efluentes: recurso agua. Anexo 1 (2008). Ecuador: Presidencia de la República de Ecuador. Retrieved from [www.cip.org.ec](http://www.cip.org.ec)
- Reza, A., Shim, S., Kim, S., Ahmed, N., Won, S., & Ra, C. (2019). Nutrient leaching loss of pre-treated struvite and its application in Sudan grass cultivation as an eco-friendly and sustainable fertilizer source. *Sustainability (Switzerland)*, 11(15), 1–14. <https://doi.org/10.3390/su11154204>
- Rodrigues, S. (2014). *Precipitação de estruvita: Recuperação de nitrogênio e fósforo utilizando fontes alternativas de reagentes*. Universidade Federal de Minas Gerais.
- Rojas, Angela. (2009). *Caracteización Y Análisis De Las Corrientes De La Línea De Agua Y De Fango De Una Planta Piloto De Guas Residuales De Grupo De Investigación Calagua*.
- Rojas, Armando, & García, A. (2010). Análisis de la curva de distribución del tiempo de residencia en un sistema de lixiviación. *Tecnología Química*, 61–68.
- Romero-Güiza, M. S., Mata-Alvarez, J., Chimenos-Rivera, J. M., & Astals-Garcia, S. (2016). Nutrient recovery technologies for anaerobic digestion systems: An overview. *Revista ION*, 29(1), 7–26. <https://doi.org/10.18273/revion.v29n1-2016001>
- Ronteltap, M., Maurer, M., Hausherr, R., & Gujer, W. (2010). Struvite precipitation from urine - Influencing factors on particle size. *Water Research*, 44(6), 2038–2046.

- <https://doi.org/10.1016/j.watres.2009.12.015>
- Ryu, H., & Lee, S. (2016). Struvite recovery from swine wastewater and its assessment as a fertilizer, *21*(1), 29–35.
- Sánchez, J., & Gallo, S. (2009). Evaluation of the hydraulic behaviour of an aerobic reactor and an anaerobic reactor in a small domestic wastewater treatment plant. *Avances En Recursos Hidráulicos*, *20*, 65–80.
- Shaddel, S., Grini, T., Andreassen, J. P., Østerhus, S. W., & Ucar, S. (2020). Crystallization kinetics and growth of struvite crystals by seawater versus magnesium chloride as magnesium source: towards enhancing sustainability and economics of struvite crystallization. *Chemosphere*, *256*, 2020. <https://doi.org/10.1016/j.chemosphere.2020.126968>
- Shaddel, S., Ucar, S., Andreassen, J., & Østerhus, S. W. (2019). Engineering of struvite crystals by regulating supersaturation-Correlation with phosphorus recovery , crystal morphology and process efficiency. *Journal of Environmental Chemical Engineering*, *7*(1), 102918. <https://doi.org/10.1016/j.jece.2019.102918>
- Sharpley, A. N. (1995). Soil phosphorus dynamics: agronomic and environmental impacts. *Ecological Engineering*, *5*(2–3), 261–279. [https://doi.org/10.1016/0925-8574\(95\)00027-5](https://doi.org/10.1016/0925-8574(95)00027-5)
- Shih, K., & Yan, H. (2016). Chapter 26 - The Crystallization of Struvite and Its Analog K-Struvite From Waste Streams for Nutrient Recycling. In M. N. . Prasad & K. Shih (Eds.), *Environmental Materials and Waste* (pp. 665–686). Elsevier Inc. <https://doi.org/10.1016/B978-0-12-803837-6.00026-3>
- Shim, S., Won, S., Reza, A., Kim, S., & Ahmed, N. (2020). Design and Optimization of Fluidized Bed Reactor Operating Conditions for Struvite Recovery Process from Swine Wastewater. *Processes*, *8*(422), 1–17. <https://doi.org/doi:10.3390/pr8040422>
- Shu, L., Schneider, P., Jegatheesan, V., & Johnson, J. (2006). An economic evaluation of phosphorus recovery as struvite from digester supernatant. *Bioresource Technology*, *97*(17), 2211–2216. <https://doi.org/10.1016/j.biortech.2005.11.005>
- Siciliano, A., Limonti, C., Curcio, G. M., & Molinari, R. (2020). Advances in struvite precipitation technologies for nutrients removal and recovery from aqueous waste and wastewater. *Sustainability (Switzerland)*, *12*(18). <https://doi.org/10.3390/su12187538>
- Snoeyink, V., & Jenkins, D. (1980). *Water chemistry*. New York: John Wiley and Sons.
- Stamou, A. I. (2008). Improving the hydraulic efficiency of water process tanks using CFD models. *Chemical Engineering and Processing: Process Intensification*, *47*(8), 1179–1189. <https://doi.org/10.1016/j.cep.2007.02.033>
- Stratful, I., Scrimshaw, M. D., & Lester, J. N. (2001). Conditions influencing the precipitation of magnesium ammonium phosphate. *Water Research*, *35*(17), 4191–4199. [https://doi.org/10.1016/S0043-1354\(01\)00143-9](https://doi.org/10.1016/S0043-1354(01)00143-9)
- Suleiman, Y., Ibrahim, H., Anyakora, N. V, Mohammed, F., Abubakar, A., Aderemi, B. O., & Okonkwo, P. C. (2013). DESIGN AND FABRICATION OF FLUIDIZED-BED REACTOR. *International Journal Of Engineering And Computer Science*, *2*(5), 1595–1605.
- Szymanska, M., Ewa, S., Was, A., Sosulski, T., van Pruissen, G. W. P., & L. Cornelissen, R. (2019). Struvite — An Innovative Fertilizer from Anaerobic Digestate Produced in a Bio-Refinery. *Energies*, *12*(296), 1–9. <https://doi.org/10.3390/en12020296>
- Talboys, P. J., Heppell, J., Roose, T., Healey, J. R., Jones, D. L., & Withers, P. J. A. (2016). Struvite : a slow-release fertiliser for sustainable phosphorus management? *Plant Soil*, 109–123.

- <https://doi.org/10.1007/s11104-015-2747-3>
- Tang, P., & Ma, H. (2016). Effects of Solution pH and Seed Material on MAP Crystallization, *4*(6), 171–177. <https://doi.org/10.11648/j.ijepp.20160406.13>
- Tansel, B., Griffin, L., & Monje, O. (2018). Struvite formation and decomposition characteristics for ammonia and phosphorus recovery : A review of magnesium-ammonia- phosphate interactions. *Chemosphere*, *194*, 504–514. <https://doi.org/10.1016/j.chemosphere.2017.12.004>
- Tarragó, E., Puig, S., Rusalleda, M., Balaguer, M. D., & Colprim, J. (2016). Controlling struvite particles' size using the up-flow velocity. *Chemical Engineering Journal*, *302*, 819–827. <https://doi.org/10.1016/j.ccej.2016.06.036>
- Tarragó, Elena. (2017). *Assessment of struvite and K-struvite recovery from digested manure*. Universitat de Girona.
- Tchobanoglous, G., Stensel, H.D., Tsuchihashi, R., Burton, F., Abu-Orf, M., Bowden, G., Pfrang, W. (2015). *Tratamento de efluentes e recuperação de recursos*. (AMGH Editora Ltda, Ed.) (Metcalf &). Porto Alegre.
- The International Centre for Diffraction Data (ICDD). (2001). PDF-2. Newtown Square, USA. Retrieved from [www.icdd.com](http://www.icdd.com)
- Theregowda, R. B., González-Mejía, A. M., Ma, X., & Garland, J. (2019). Nutrient Recovery from Municipal Wastewater for Sustainable Food Production Systems: An Alternative to Traditional Fertilizers. *Environmental Engineering Science*, *36*(7), 833–842. <https://doi.org/10.1089/ees.2019.0053>
- Trenkel. (2010). *Slow and Controlled-Release and stabilized Fertilizers*. IFA (Vol. 53). Paris: International fertilizer industry asociation-IFA. Retrieved from [https://www.fertilizer.org/images/Library\\_Downloads/2010\\_Trenkel\\_slow release book.pdf](https://www.fertilizer.org/images/Library_Downloads/2010_Trenkel_slow%20release%20book.pdf)
- Ulfa, R., Machdar, I., Yunardi, Y., Rinaldi, W., & Jauharlina, J. (2020). Residence time distribution study in laboratory scale struvite crystallization reactor with online conductivity measurement. *IOP Conference Series: Materials Science and Engineering*, *845*(1). <https://doi.org/10.1088/1757-899X/845/1/012003>
- United States Environmental Protection Agency (EPA). (1996). METHOD 3052:MICROWAVE ASSISTED ACID DIGESTION OF SILICEOUS AND ORGANICALLY BASED MATRICES, *26*(4), 551–556. Retrieved from <https://www.epa.gov/sites/production/files/2015-12/documents/3052.pdf>
- Uysal, A., & Kuru, B. (2013). EXAMINATION OF NUTRIENT REMOVAL FROM ANAEROBIC EFFLUENT OF THE DAIRY PROCESSING INDUSTRY BY STRUVITE PRECIPITATION USING THE RESPONSE SURFACE METHODOLOGY, *22*(5), 1380–1387.
- Uysal, A., Yilmazel, Y. D., & Demirer, G. N. (2010). The determination of fertilizer quality of the formed struvite from effluent of a sewage sludge anaerobic digester. *Journal of Hazardous Materials*, *181*(1–3), 248–254. <https://doi.org/10.1016/j.jhazmat.2010.05.004>
- Valsami-Jones, E. (2005). *Phosphorus in Environmental Technology Principles and Applications*. London: IWA Publishing. <https://doi.org/10.2166/9781780402758>
- Valve, H., Ekholm, P., & Luostarinen, S. (2020). The circular nutrient economy : needs and potentials of nutrient recycling. In *Handbook of the Circular Economy*. Edward Elgar Publishing Ltd.
- Vasconcelos, C. (2013). *Estudio De La Cristalización Y Recuperación De Hidroxiapatita En Un Reactor De Tanque Agitado*. Universitat Politècnica de Catalunya.

- Veverka, V., & Madron, F. (1997). Chapter 3 Mass (single-component) balance. In *Material and Energy Balancing in the Process Industries* (Vol. 7, pp. 25–58). Computer Aided Chemical Engineering. [https://doi.org/10.1016/S1570-7946\(97\)80003-X](https://doi.org/10.1016/S1570-7946(97)80003-X)
- Von Sperling, M. (2007). Activated Sludge and Aerobic Biofilm Reactors. In *Biological Wastewater Treatment in Warm Climate Regions* (Vol. 5, p. 313). London, New York: IWA Publishing. <https://doi.org/10.2166/9781780402123>
- Wang, D., Li, X., Ding, Y., Zeng, T., & Zeng, G. (2009). Nitrogen and phosphorus recovery from wastewater and the supernate of dewatered sludge. *Recent Patents on Food, Nutrition & Agriculture, 1*(NOVEMBER), 236–242. <https://doi.org/10.2174/2212798410901030236>
- Wang, J., Ye, X., Zhang, Z., Ye, Z., & Chen, S. (2017). ScienceDirect Selection of cost-effective magnesium sources for fluidized struvite crystallization. *Journal of Environmental Sciences, 70*, 144–153. <https://doi.org/10.1016/j.jes.2017.11.029>
- Warmadewanthi, & Fitri Rajabi Bachtiar, Y. (2019). Study of struvite crystallization from fertilizer industry wastewater by using fluidized bed reactor. *MATEC Web of Conferences, 276*, 06006. <https://doi.org/10.1051/mateconf/201927606006>
- Webb, K. M., & Ho, G. E. (1992). SOLUBILITY AND ITS APPLICATION TO A PIGGERY EFFLUENT PROBLEM. *Water Science and Technology, 26*(9), 2229–2232. <https://doi.org/https://doi.org/10.2166/wst.1992.0703>
- Wilfert, P., Dugulan, A. I., Goubitz, K., Korving, L., Witkamp, G. J., & Van Loosdrecht, M. C. M. (2018). Vivianite as the main phosphate mineral in digested sewage sludge and its role for phosphate recovery. *Water Research* (Vol. 144). Elsevier Ltd. <https://doi.org/10.1016/j.watres.2018.07.020>
- Wolf, D., & Resnick, W. (1963). RESIDENCE TIME DISTRIBUTION IN REAL SYSTEMS. *Ind. Eng. Chem. Fundamen, 2*(4), 287–293. <https://doi.org/https://doi.org/10.1021/i160008a008>
- World Bank. (2019). *From-Waste-to-Resource-in-Latin-America-and-the-Caribbean*. Retrieved from <https://www.worldbank.org/en/topic/water/publication/wastewater-initiative>
- WSP- Water and sanitation Program. (2013). Latin America and Caribbean: Economics of Sanitation Initiative. Retrieved from <https://www.wsp.org/content/latin-america-and-caribbean-economics-sanitation-initiative#:~:text=In Latin America%2C 117 million,20%25 of wastewater is treated.&text=These ratios place Nicaragua among,lowest access in the region.>
- Wu, Q., & Bishop, P. L. (2004). Enhancing struvite crystallization from anaerobic supernatant. *Journal of Environmental Engineering and Science, 3*(1), 21–29. <https://doi.org/10.1139/S03-050>
- Wu, Y., Luo, J., Zhang, Q., Aleem, M., Fang, F., Xue, Z., & Cao, J. (2019). Potentials and challenges of phosphorus recovery as vivianite from wastewater: A review. *Chemosphere, 226*, 246–258. <https://doi.org/10.1016/j.chemosphere.2019.03.138>
- Yan, H., & Shih, K. (2016a). Effects of calcium and ferric ions on struvite precipitation: A new assessment based on quantitative X-ray diffraction analysis. *Water Research, 95*, 310–318. <https://doi.org/10.1016/j.watres.2016.03.032>
- Yan, H., & Shih, K. (2016b). Effects of calcium and ferric ions on struvite precipitation: A new assessment based on quantitative X-ray diffraction analysis. *Water Research, 95*, 310–318. <https://doi.org/10.1016/j.watres.2016.03.032>
- Yates, J. G., & Lettieri, P. (2016). *Fluidized-Bed Reactors : Processes and Operating Conditions*. London: Springer International Publishing. <https://doi.org/10.1007/978-3-319-39593-7>



- Ye, X., Ye, Z., Lou, Y., Pan, S., Wang, X., Kuang, M., & Chen, S. (2016). A comprehensive understanding of saturation index and up flow velocity in a pilot-scale fluidized bed reactor for struvite recovery from swine wastewater. *Powder Technology*, 295, 16–26. <https://doi.org/10.1016/j.powtec.2016.03.022>
- Ye, Z., Shen, Y., Ye, X., Zhang, Z., Chen, S., & Shi, J. (2014). Phosphorus recovery from wastewater by struvite crystallization: Property of aggregates. *Journal of Environmental Sciences (China)*, 26(5), 991–1000. [https://doi.org/10.1016/S1001-0742\(13\)60536-7](https://doi.org/10.1016/S1001-0742(13)60536-7)
- Yetilmezsoy, K., Ilhan, F., Kocak, E., & Akbin, H. M. (2017). Feasibility of struvite recovery process for fertilizer industry: A study of financial and economic analysis. *Journal of Cleaner Production*, 152, 88–102. <https://doi.org/10.1016/j.jclepro.2017.03.106>
- Yu, R., Geng, J., Ren, H., Wang, Y., & Xu, K. (2013). Struvite pyrolysate recycling combined with dry pyrolysis for ammonium removal from wastewater. *Bioresource Technology*, 132, 154–159. <https://doi.org/10.1016/j.biortech.2013.01.015>
- Yuan, P., & Kim, Y. (2017). Increasing phosphorus recovery from dewatering centrate in microbial electrolysis cells. *Biotechnology for Biofuels*, 10(1), 1–8. <https://doi.org/10.1186/s13068-017-0754-8>
- Yulistyorini, A. (2016). *Phosphorus Recovery from Wastewater through Enhanced Micro-algal Uptake*. University of Leeds.
- Zhang, D. M., Chen, Y. X., Jilani, G., Wu, W. X., Liu, W. L., & Han, Z. Y. (2012). Optimization of struvite crystallization protocol for pretreating the swine wastewater and its impact on subsequent anaerobic biodegradation of pollutants. *Bioresource Technology*, 116, 386–395. <https://doi.org/10.1016/j.biortech.2012.03.107>
- Zhang, T., Ding, L., & Ren, H. (2009). Pretreatment of ammonium removal from landfill leachate by chemical precipitation. *Journal of Hazardous Materials*, 166(2–3), 911–915. <https://doi.org/10.1016/j.jhazmat.2008.11.101>
- Zhang, T., Jiang, R., & Deng, Y. (2017). Phosphorus Recovery by Struvite Crystallization from Livestock Wastewater and Reuse as Fertilizer: A Review. In *Physico-Chemical Wastewater Treatment and Resource Recovery*. <https://doi.org/10.5772/65692>

# ANNEXES

## Annex 1. General Materials and Methods

### Analytical methods

This section presents the main analytical techniques used in the research project. The analyses were developed mainly in the laboratory of the Environmental Management and Modelling GAIA research group (Medellin-Colombia). Analyses of chapter 6 were developed in the Interdisciplinary Group for Molecular Studies (GIEM) (Medellin-Colombia). The analytical methods of chapter 3 and 4 were developed in the Institute of agri-food Research and Technology (IRTA, Spain) and the laboratories of the Institute for Public Health and Environmental Engineering (iPHEE), School of Civil Engineering, University of Leeds (UK). All the analyses were performed following Standard Methods (APHA, 2017).

In the University of Leeds (UK),  $\text{NH}_4^+\text{-N}$ , TKN-N, TP,  $\text{P-PO}_4^{3-}$  and COD concentrations in the solution were determined using a predesigned methodology of HACH. These were test LCK 302 and 305 (ammonium), APC350 and APC350o (phosphate and orthophosphate), APC238 (Total Kjeldahl Nitrogen) and LCK514 (COD). After sample preparation, the cuvettes were put in an automatic HACH sample reader (AP3900 MULTI, Laboratory Robot). The other analysis techniques are presented below.

### *Liquid Phase Analysis Techniques*

#### ❖ *Orthophosphate concentration ( $\text{PO}_4^{3-}\text{-P}$ ):*

The samples were previously filtered with 0.45- $\mu\text{m}$  filter paper and then analysed by the ascorbic acid colourimetric method (4500-P E) proposed by the Standard Methods (APHA et al., 2017).

In an acid medium, ammonium molybdate and antimony potassium tartrate react with orthophosphate to form a phosphomolybdic acid. This complex is reduced by ascorbic acid to form a deep blue compound whose absorbance is measured at a wavelength of 880 nm. The equipment used was a Spectroquant Pharo 300 spectrophotometer (see Figure 44A), at a wavelength of 880 nm and the calibration curve was performed in the range 0-1 mg / L of phosphorus.

In the IRTA laboratory orthophosphate concentration was determined by ionic chromatography with Chemical Suppression of Eluent Conductivity (4110B) according to Standard Methods (APHA et al., 2017).

Ion chromatography is a process that allows the separation of ions and polar molecules based on the charge properties of the molecules. Anion exchange chromatography retains anions using positively charged functional groups, such as a quaternary ammonium cation. The equipment used was a Metrohm 861 Advanced Compact IC equipped with a Metrosep A Supp 5-250 column and an 853 CO<sub>2</sub> suppressor.

❖ **Total phosphorus concentration (TP):**

The determination of the total phosphorus concentration requires the prior conversion of all the phosphorus present to orthophosphate. The conversion was made by dissolving the solids in the sample with nitric acid, thus converting all the precipitated phosphorus into soluble phosphorus. Once in the orthophosphate form, its concentration is measured according to the method outlined in the previous section (colourimetric method).

❖ **Total Kjeldahl Nitrogen (TKN) and ammoniacal nitrogen (NH<sub>4</sub><sup>+</sup>-N)**

The technique used to establish the concentration of TKN and ammonium is based on the Kjeldahl method (4500-NH<sub>3</sub> B, C) proposed by the Standard Methods (APHA et al., 2017).

In the presence of H<sub>2</sub>SO<sub>4</sub>, potassium sulphate (K<sub>2</sub>SO<sub>4</sub>), and cupric sulphate (CuSO<sub>4</sub>) catalyst, amino nitrogen of many organic materials is converted to ammonium. Free ammonia also is converted to ammonium. After addition of a base, the ammonia is distilled (Buchi B-324; Figure 44B) from an alkaline medium and absorbed in boric acid. The ammonia is determined by titration (848 Titrino plus Metrohm) with a standard mineral acid (H<sub>2</sub>SO<sub>4</sub>). In the determination of ammoniacal nitrogen, the process begins with the distillation.

❖ **Metal concentration**

The samples were previously filtered with 0.45-µm filter paper and then were analysed by flame atomic absorption spectrometry (3111B-D) proposed by the Standard Methods to determine the Ca, Mg, K, Al, Pb, Cr, Cd, Cu, Ni and Zn concentrations (APHA et al., 2017).

In flame atomic absorption spectrometry; a sample is aspirated into a flame and atomised. A light beam is directed through the flame, into a monochromator, and onto a detector that measures the amount of light absorbed by the atomised element in the flame. The equipment used was a spectrophotometer, ThermoScientific iCE 300 SERIES (see Figure 44C) and the calibration curve was performed in the range 0.1-4 mg / L and was different for each metal evaluated.

In the IRTA and University of Leeds laboratory Ca<sup>2+</sup>, Mg<sup>2+</sup> and K<sup>+</sup> concentrations were determined by ionic chromatography according to the Standard Test Method for Determination of Dissolved Alkali and Alkaline Earth Cations and Ammonium in Water and Wastewater by Ion Chromatography (ASTM D6919 – 09).

Cation exchange chromatography retains positively charged cations because the stationary phase shows a negatively charged functional group, such as phosphoric acid. The equipment used in IRTA was Metrohm 790 personal IC equipped with a Metrohm Metrosep C4 150/4.0 column; meanwhile, the equipment used in the University of Leeds was Metrohm 850 professional IC equipped with a Metrosep C4 100/4.0 column.

❖ **Alkalinity**

The samples were analysed by Titration Method (2320 B) according to the Standard Methods (APHA et al., 2017). Hydroxyl ions present in a sample because of dissociation or hydrolysis of solutes react with additions of standard acid. Alkalinity thus depends on the end-point pH used. H<sub>2</sub>SO<sub>4</sub> (0.02 N)

was used for the titration, and 4.3 was the End-point pH used due to the high alkalinity of the samples (>500 mgCaCO<sub>3</sub>/L). The equipment used was titration 848 Titrino plus Metrohm.

❖ *Solids*

Total solids (TS), Total dissolved solids (TDS), Total suspended solids (TSS), Volatile solids (VS) and Settleable solids (SS<sub>Set</sub>) concentrations were determined according to Standard Methods (2540-B, C, D, E, F).

Sample aliquots of 50 mL were dried at 103 to 105 °C to drive off the water in the sample. The residue obtained was cooled, weighed, and dried again at 550° C to drive off volatile solids in the sample. The total, fixed, and volatile solids are determined by comparing the mass of the sample before and after each drying step. For TSS determination, samples were previously filtered with 0.45-µm filter paper.



Figure 44. Spectrophotometer (P); Bushi Detilator (N determination) and spectrophotometer (metals concentration).

***Solid-phase analysis techniques***

At the end of each experiment (including the batch and reactors tests), the precipitates were filtered and dried at room temperature for 24 hours. Later they were characterised in terms of N, P, metals, Total organic carbon (TOC) and humidity. The sludges and biosolids also were characterised according to the procedures presented below.

❖ *Total phosphorus concentration (TP):*

The method consisted of the conversion of the forms of phosphorus present into orthophosphate, employing the ignition method of Andersen (1976). The quantification was made with the colorimetric method of ascorbic acid, as in the determination of orthophosphates and TP in water.

❖ *Total Kjeldahl Nitrogen (TKN) and ammoniacal nitrogen (NH<sub>4</sub><sup>+</sup>-N)*

The procedure used for the solid phase was the same as that described for the liquid phase.

❖ *Metal concentration*

The metals determination was developed by microwave-assisted acid digestion (closed reflux) methodology, according to EPA 3052 (1996), quantified by flame atomic absorption spectrometry (FLAA) (3111B-D) in the same way as the water quantification (APHA et al., 2017).

This methodology uses a representative sample of 0.5 g, which is digested for 15 min with 9 mL of concentrated nitric acid and 3 mL of hydrofluoric acid, using heating in a microwave oven. A temperature of 180 ± 5 °C is reached in approximately 5.5 minutes and is kept there for 9.5 minutes

for a complete reaction. After reaching cooling, the content is transferred to a falcon tube and centrifuged, so that the solid particles are decanted, and thus the sample can be quantified.

❖ **Total organic carbon (TOC)**

The samples were analysed by sulphochromic oxidation method under the ISO 14235 standard (ISO, 1998), as a tool to evaluate the organic matter content in the product obtained.

The organic carbon present in the sample was oxidised in a mixture of a solution of potassium dichromate (in excess) and sulfuric acid at a temperature of  $135\text{ }^{\circ}\text{C} \pm 2\text{ }^{\circ}\text{C}$ . The dichromate ions, which are orange in solution, were reduced to  $\text{Cr}^{3+}$  ions, and the solution turns green. The intensity of this green colour was measured spectrophotometrically. This methodology was validated by the laboratory of the GAIA research group (Ramos et al., 2015).

❖ **Humidity**

The moisture content in the sludges and biosolids was determined with the same methodology of TS. The samples were dried at 103 to 105 °C for 12 hours, minimum, then cooled to balance the temperature in an individual desiccator containing fresh desiccant and, lastly, weighted.

Moreover, the decomposition of struvite has been reported to be dependent on temperature, rate of heating, and pH (for wet decomposition). Struvite heated at elevated temperatures ( $>100^{\circ}\text{C}$ ) in the presence of small amounts of water for 24 h, releases ammonia from the solid phase, and can be partially transformed into newberyite, and bobierrite (Athanasius P. Bayuseno & Schmahl, 2019).

According to the thermogravimetric analysis (TGA) developed by Bhuiyan et al.,(2008) mass loss begins at a temperature around  $55^{\circ}\text{C}$  and is essentially complete when temperature is above  $250^{\circ}\text{C}$ . In addition, they found that boiling struvite with water in excess resulted in the loss of five water molecules from the struvite structure, which is then transformed into the monohydrate, dittmarite.

Struvite can also decompose at lower temperatures with slow heating rates. At a heating rate of  $1^{\circ}\text{C}/\text{min}$ , the decomposition occurred in three steps ( $39.5$ ,  $57.8$ ,  $82.6^{\circ}\text{C}$ ) with loss of ammonia occurring before the loss of crystal water. At a heating rate of  $2^{\circ}\text{C}/\text{min}$ , decomposition occurred at  $85^{\circ}\text{C}$  with simultaneous loss of ammonia and water molecules (Frost et al., 2004). According to Tansel et al. (2018), struvite decomposition occurs as shown in Figure 45.

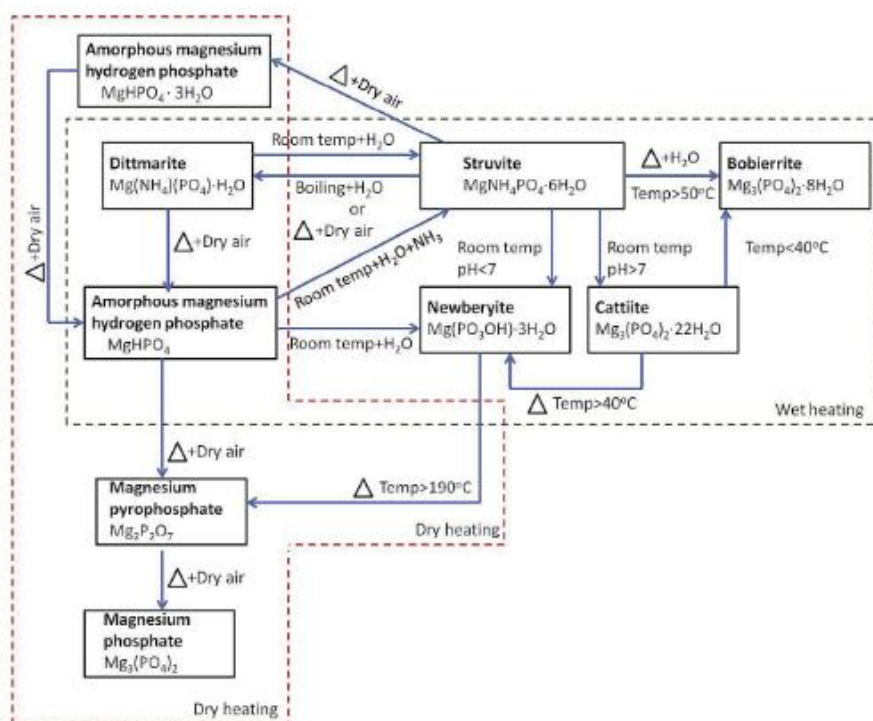


Figure 45. Transformation of struvite under wet and dry heating conditions (Tansel et al., 2018).

Although many contradicting experimental results of the effect of temperature on the struvite decomposition have been reported in the literature (Athanasius P. Bayuseno & Schmahl, 2019), most of the studies have found a significant effect of temperature on struvite decomposition at temperatures of 55°C and above. Therefore, to determine the moisture present in the struvite, the samples were dried in an oven at 50 °C for 24 h. The test was conducted in duplicate. The humidity estimates were made from the mass variations of the struvite samples before and after the drying process.

### *Characterisation of the precipitates*

#### ❖ *X-ray diffraction (XRD)*

X-rays are electromagnetic radiation of the same nature as light but with a much shorter wavelength. The unit of measurement in the x-r region is the angstrom (Å), equal to  $10^{-10}$  m and the x-rays used in diffraction have wavelengths in the range 0.5-2.5 Å while the wavelength of visible light is on the order of 6000 Å. The most widespread use of x-ray powder diffraction is for the identification of crystalline compounds by their diffraction pattern.

The solids collected in each of the assays were analysed to determine the crystalline compound in question. Once air-dried and powder-crushed, the solids samples were taken to the X-ray spectroscopy unit of Catalysts and Adsorbents Group from Universidad de Antioquia (Medellín, Colombia) (solids from chapters 3,5 and 6), Universidad Autónoma de Barcelona (Cerdanyola, Spain) (solids from chapter 4.1) and University of Leeds (UK) (solids from chapter 4.2), where they were analysed.

At Universidad de Antioquia and Universidad Autónoma de Barcelona, struvite samples were examined by X-ray diffraction (XRD) on an XPert PANalytical Empyrean Series II diffractometer with a PIXcel 3D and 1D detector 2012 model, using Cu K-alpha radiation. The XRD patterns were recorded in the scanning range of 2-theta from 10°–60°. A small angular step of 2-theta = 0.0220° and a fixed counting time of 90 s was used (see Figure 46). At the University of Leeds, the equipment used was the Bruker D2 phaser. Data were collected and processed using High Score Plus 3.0 software. Identification of the phase peaks was accomplished by comparing the observed XRD patterns to the standard struvite compiled by the Joint Committee on Powder Diffraction and Standards (ICDD,2001).



Figure 46. XRD Equipment used at the Universidad Autónoma de Barcelona

### ❖ *Scanning electron microscopy (SEM)*

SEM is an electron microscope that uses a focused beam of electrons to react with the sample and produce a topological image with the sample's relative composition. The signals that derive from electron-sample interactions reveal information about the sample, including external morphology (texture), chemical composition, and crystalline structure and orientation of materials making up the sample. EDX spectroscopy is involved in the detection of the elemental composition of a substance by using a scanning electron microscope. EDX can detect elements that possess an atomic number higher than boron. These elements can be detected at a concentration of less than 0.1% (Abd Mutalib et al.,2017).

To perform sample preparation, the samples were fixed on a graphite tape, thinly coated in gold (Au) (DENTON VACUUM Desk IV equipment and E5000 Sputter Coater-Polaroid Equipment Limited) and analysed in a high vacuum scanning electron microscope to obtain high-resolution images (SEM, JEOL JSM 6490 LV and ZEISS EVO®MA10) and to evaluate the morphology and topography of the samples. The elemental analysis of these samples was conducted with an X-ray Microscope-EDX (INCA PentaFETx3 Oxford Instruments) (Figure 47).

The analyses were developed in the centre of Advanced Microscopy, University Research Headquarters (SIU), Universidad de Antioquia and in the microscopy service from Universidad Autónoma de Barcelona (<https://sct.uab.cat/microscopia/node/158>).



Figure 47. Scanning electron microscope (SEM).

#### ❖ *Determination of particle size*

The morphology and particle size of the precipitate obtained in each test were determined using an inverted microscope BOECO BIB100 at 4, 10, 20 and 40 X objectives with a digital camera B-CAM 16 megapixel 1 / 3.33" Panasonic CMOS sensor (Figure 48). The viewing software used was Boeckel B-View x64 version compatible with Windows XP / Vista / 7/8/10. After calibrating the image scale, the sizes of at least 60 particles were measured for each test using the Image J software.



Figure 48. Inverted microscope

### Main calculations

#### ❖ *Saturation index (SI) - MINTEQ SOFTWARE*

The occurrence of struvite precipitation depends on the supersaturation of the solution. Supersaturation is regarded as the driving force of crystallisation. 'Supersaturation' is applicable to a solution when the concentration of the solute is more than its equilibrium concentration (Ghosh et al., 2019). Often, supersaturation is expressed in terms of the supersaturation ratio (SSR) or saturation index (SI), as shown in Equation 18 and Equation 19.

$$SSR = \frac{IAP}{K_{sp}} \quad \text{Equation 18}$$

$$SI = \log_{10} SSR \quad \text{Equation 19}$$

where  $K_{sp}$  is the thermodynamic solubility product of struvite and IAP represents the ion activity product of magnesium, ammonium and phosphate. Extensive studies, involving the calculation of the solubility product ( $K_{sp}$ ) value for struvite, have been conducted by several researchers. These values of  $K_{sp}$  range from  $4.37 \times 10^{-14}$  to  $3.89 \times 10^{-10}$  ( $pK_{sp}$  from 9.41 to 13.36; Rahaman et al. 2006), however,



the most commonly used value is  $10^{-13.26}$  at 25 °C (Ohlinger et al., 1998). The IAP can be calculated with Equation 20:

$$\text{IAP} = \{\text{Mg}^{2+}\}\{\text{NH}_4^+\}\{\text{PO}_4^{3-}\} = \gamma_{\text{Mg}^{2+}} \cdot \gamma_{\text{NH}_4^+} \cdot \gamma_{\text{PO}_4^{3-}} \cdot [\text{Mg}^{2+}][\text{NH}_4^+][\text{PO}_4^{3-}] \quad \text{Equation 20}$$

where [i] shows the molar concentration and  $\gamma_i$  represents the activity coefficient of species i. The thermodynamic equilibria and constants considered to determine the speciation can be found in the literature (Galbraith & Schneider, 2014). The value of  $\gamma_i$  depends on the ionic strength and valency of the corresponding elements and is given by Equation 21. The ionic strength is defined by Equation 22 (X. Ye et al., 2016).

$$-\log \gamma_i = AZ_i \left( \left[ \frac{\sqrt{I}}{1 + \sqrt{I}} \right] - 0.31 \right) \quad \text{Equation 21}$$

$$I = 0.5 \sum [i] Z_i^2 \quad \text{Equation 22}$$

where  $Z_i$  is the valency of species i, A is Debye–Hückel constant with the value of 0.509 at 25 °C.

If  $SI > 0$ , it means oversaturation for that product; if  $SI < 0$ , under saturation; and if  $SI = 0$ , apparent equilibrium concerning the solid.

The chemical speciation and activity-based supersaturation were determined by free thermodynamic calculation program Visual MINTEQ 3.1. Using the composition of raw centrate as input, the model's output was used to estimate what minerals could be formed.

Visual MINTEQ is a chemical equilibrium computer program that has an extensive thermodynamic database that allows for the calculation of speciation, solubility, and equilibrium of solid and dissolved phases of minerals in an aqueous solution (Gustafsson, 2013). Visual MINTEQ is a Windows version of MINTEQA2 ver 4.0, which was released by the USEPA in 1999.

Visual Minteq software included a large updated database, which could be modified by the user to use specific data needed. The main screen of the program featured the input data for pH, temperature, ionic strength, and component's concentration as well as the desired units for concentration, which needs be introduced by the user (Figure 49). In the results report the user can see the species distribution, saturation indices, in which a list of the possible compounds that could be formed as a function of the saturation index (SI) is shown and equilibrated mass distribution, in which the total concentration of each component is shown, classified into dissolved, adsorbed and precipitated phases (Tarragó, 2017).

In this research, the visual Minteq V 3.1 program was used mainly for the calculation of the saturation indices (SI) of all possible precipitates in the system within different ranges of pH, temperature and phosphate concentrations.



Figure 49. Visual Minteq's input interface.

### ❖ *Phosphorous precipitation and recovery*

Two types of phosphorus efficiencies were calculated according to Pastor et al. (2008): precipitation efficiency (PP) and recovery efficiency (PR).

**Precipitation efficiency-PP (%)**: PP is calculated as the percentage of the soluble phosphorus (SP) entering the reactor that precipitates, according to Equation 23.

$$PP(\%) = \frac{(PO_4^{3-} - P)_{INF} - (PO_4^{3-} - P)_{EFF}}{(PO_4^{3-} - P)_{INF}} * 100 \quad \text{Equation 23}$$

**Recovery efficiency-PR (%)**: PR considers both precipitation and crystal growth efficiency. It is obtained as the percentage of the total phosphorus (TP) entering the reactor that is not lost with the effluent (Equation 24).

$$PR(\%) = \frac{(TP)_{INF} - (TP)_{EFF}}{(TP)_{INF}} * 100 \quad \text{Equation 24}$$

Where the  $(PO_4^{3-} - P)$  and  $(TP)$  are the concentrations of soluble phosphorus and total phosphorus and the sub-scripts "INF" and "EFF" represent influent and effluent, respectively.

The difference between precipitation efficiency and recovery efficiency corresponds to the fine crystals lost in the effluent of the reactor. In the section  $\square$  ammonia nitrogen in the effluent was measured in the sample with and without filtering, the difference between the N removal percentages calculated from both samples was also interpreted as the loss of fines by the reactor effluent.

❖ *Struvite purity and PMAP*

The moles of volatilised nitrogen as  $\text{NH}_3$  were calculated according to Equation 25 proposed by Capdevielle et al.(2013).

$$(\text{NH}_3 - \text{N})_{\text{volatilised}} = (\text{NH}_4 - \text{N})_{\text{initial in liquid}} - (\text{NH}_4 - \text{N})_{\text{final in liquid}} - (\text{NH}_4 - \text{N})_{\text{final in solid}} \quad \text{Equation 25}$$

Where  $(\text{NH}_4\text{-N})$  is the molar mass of ammonia (mol). The initial and final molar mass in the liquid was calculated with the  $\text{NH}_4\text{-N}$  concentration (mol/L) and the volume of the solution, meanwhile, the final molar mass in the solid was determined with the  $\text{NH}_4\text{-N}$  concentration in the solid (Kg/g) and the mass of the precipitate (g).

Assuming all N that did not volatilise has precipitated as struvite, the precipitated moles of N will give the moles of phosphorus precipitated as struvite (*nMAP*), based on the N: P = 1 molar ratio of the struvite. Therefore, the precipitated moles of struvite (*nMAP*) were calculated according to Equation 26.

$$\mathbf{n\ MAP} = (\text{NH}_4 - \text{N})_{\text{initial in liquid}} - (\text{NH}_4 - \text{N})_{\text{final in liquid}} - (\text{NH}_3 - \text{N})_{\text{volatilized}} \quad \text{Equation 26}$$

The percentage of phosphate as struvite ( $\%P_{\text{MAP}}$ ) was calculated relating the precipitated moles of struvite (*nMAP*) with the initial moles of  $\text{PO}_4^{3-}\text{-P}$  according to Equation 27.

$$\%P_{\text{MAP}} = \frac{\mathbf{n\ MAP}}{(\text{PO}_4 - \text{P})_{\text{initial}}} \times 100 \quad \text{Equation 27}$$

In some cases in which the precipitated moles of N ( $n_N$ ) were not available, it was assumed that the precipitated moles of magnesium ( $n_{\text{Mg}}$ ) were equal to the moles of struvite as suggested by Pastor (2008).

The purity of the struvite was initially verified with the DRX and SEM-EDX tests and in some cases the determination of metals in the precipitates, however, a percentage of purity was also calculated from the moles of N precipitated and the mass of collected precipitate as suggested by Ye et al. (2016), according to the Equation 28.

$$\mathbf{Purity(\%)} = \frac{\mathbf{n\ MAP \cdot M_{struvite}}}{\mathbf{m_{product}}} \times 100 \quad \text{Equation 28}$$

where  $M_{\text{struvite}}$  is the molar mass of struvite (245 g /mol), and  $m_{\text{product}}$  is the mass of the product (g).

## Annex 2. Reactors design

The effectiveness of the struvite recovery process depends on the reactor type as well as on the recovery efficiency and the quality of the recovered product (X. Ye et al., 2016). Among the reactors, the most commonly used are *continuous stirred-tank reactor (CSTR)* and *fluidised bed reactors (FBRs)*. The CSTR is simple in design and widely used in the industries, but high mixing intensity often produces fine and impure struvite crystals (Desmidt et al., 2014). FBR can produce struvite crystals with desirable qualities, but due to the fluidisation of particles that needs a high upward flow velocity, fine particles can be lost to the effluent and therefore the P recovery efficiency could be reduced (Fattah, 2012; Shim et al., 2020).

In this project, these two types of reactors were designed, and later they were compared in terms of quality and quantity of the struvite obtained. This section describes the main features of the two designs.

### Preliminary tests on a laboratory scale

Before designing the reactors, preliminary tests were conducted to evaluate the synthesis of struvite under different molar ratios, verify the behaviour of the pH with the addition of NaOH and test the behaviour of an existing CSTR reactor under different concentrations of phosphorus and solids.

#### ❖ *Struvite synthesis in jar tester*

Throughout the precipitation of struvite, proton (H<sup>+</sup>) is released (see Equation 29), thus lowering the pH level of the precipitating solution.



Hence it is possible to relate the reaction rates and their kinetic orders by measuring the change in pH of the solution. In other words, the rate of struvite crystallisation can be calculated by measuring the pH change (Bayuseno et al. 2020).

Therefore, in this project, different tests were conducted on a laboratory scale varying the molar ratios of the struvite constituent ions (Mg<sup>2+</sup>, NH<sub>4</sub><sup>+</sup> and PO<sub>4</sub><sup>3-</sup>) and the rate of reduction of the pH was observed. At the end of each test, the samples were filtered to save and later analyse the struvite formed. These tests were conducted to know under what conditions struvite precipitates, in addition to knowing the behaviour of the pH to automate the reactors.

#### ❖ *Description of the experiments*

The experimental design consisted of evaluating three Mg: P: N molar ratios: 1: 1: 1, 0.9: 1: 2.4 and 1:1:59. The first one corresponds to the theoretical relation for struvite formation, the second is the optimal molar ratio recommended by Pastor (2006), and the third is the actual molar ratio of the sludge dewatering centrate adjusting the moles of Mg to the P moles. In the first two molar ratios evaluated, the concentration of the constituent ions was varied by multiplying their concentrations x7 and x3 (this to increase the amount of struvite formed and to be able to appreciate the precipitate).

The experiment was conducted in a jar tester; the stirring speed was kept fixed at 100 RPM. Two solutions of 250 ml were prepared in distillate water to obtain a final volume of 500 mL for each test. The first solution was prepared using  $\text{MgSO}_4 \cdot 7\text{H}_2\text{O}$  (Sigma–Aldrich > 99%), and the second one by mixing  $\text{NaH}_2\text{PO}_4 \cdot 2\text{H}_2\text{O}$  (Sigma–Aldrich > 99%) and  $\text{NH}_4\text{Cl}$  (Sigma–Aldrich > 99%). The pH in each solution was adjusted at nine by the addition of sodium hydroxide ( $\text{NaOH}$  0.5M). The solution for the test 1:1:1 x7 was prepared to obtain a final concentration of  $7.0 \text{ mmol} \cdot \text{L}^{-1}$  for each constituent ion ( $168 \text{ mg Mg} \cdot \text{L}^{-1}$ ,  $217 \text{ mg P} \cdot \text{L}^{-1}$ ,  $98 \text{ mg N} \cdot \text{L}^{-1}$ ), meanwhile the P and Mg concentration in the test 1:1:59 was  $1 \text{ mmol} \cdot \text{L}^{-1}$  that correspond to  $31 \text{ mg P} \cdot \text{L}^{-1}$  and  $24 \text{ mg Mg} \cdot \text{L}^{-1}$ . The two stock solutions were mixed and allowed to react during 1 h at  $25^\circ\text{C}$ . The description of the experiment is presented in Figure 50A.

To evaluate the variation in pH with the addition of  $\text{NaOH}$ , continuous experiment was conducted under the Mg: P: N molar ratio 0.9: 1: 2.4 in 900 mL, during 2 hours at  $25^\circ\text{C}$ , using peristaltic pumps for the addition of the solutions (Figure 50B).

The pH behaviour in all tests was followed during the reaction, and its evolution with time was then measured (every 3 minutes). Water conductivity and temperature were measured with a conductivity meter (WTW cond 3110), pH was verified with a pH meter (IQ Scientific Instrument). Finally, the precipitates obtained were characterised by X-ray diffraction (XRD Diffractometer D5005), scanning electron microscopy (SEM) and thermogravimetric analysis (TGA Q500).

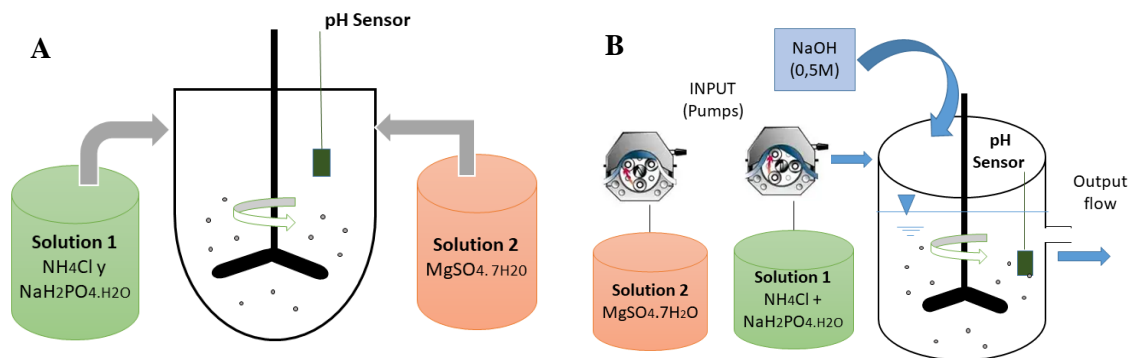


Figure 50. Batch (A) and continuous (B) experiments for struvite synthesis.

### ❖ Results and discussion

The minimum pH reduction occurred in the experiment with the real characteristics of the centrate (molar ratio 1:1:59 and  $32 \text{ mg P} / \text{L}$ ), obtaining a reduction of only 0.12 pH units in 94 minutes, which indicated that the struvite precipitation was minimal ( Figure 51).

Nevertheless, in the tests in which the molar ratio was multiplied by 3, that corresponds to  $3 \text{ mmol L}^{-1}$  for the first test ( $24 \text{ mg Mg}^{2+} \cdot \text{L}^{-1}$ ,  $93 \text{ mg P-PO}_4^{3-} \cdot \text{L}^{-1}$ ,  $14 \text{ mg N -NH}_4^+ \cdot \text{L}^{-1}$ ) and  $2.7 \text{ mmol Mg}^{2+} / \text{L}$ ,  $3 \text{ mmol PO}_4^{3-} / \text{L}$  and  $7.2 \text{ mmol NH}_4^+ / \text{L}$  ( $65.6 \text{ mg Mg}^{2+} \cdot \text{L}^{-1}$ ,  $93 \text{ mg P-PO}_4^{3-} \cdot \text{L}^{-1}$  y  $100,8 \text{ mg N -NH}_4^+ \cdot \text{L}^{-1}$ ) for the second test, the pH was reduced to 0.66 units and 0.88 units in one hour respectively. In addition, the pH behaviour was influenced by the molar ratio and the concentration of the solutions. When the concentration was multiplied by 7, regardless of the molar ratio, the pH drops sharply in the first 10 min and then remains relatively stable, which may be due to the high supersaturation of the solution. However, when the concentration was multiplied by 3 was observed a progressive and

slower pH reduction than in the higher concentrations (x7), which could favour growth over the nucleation (Figure 51) and the molar relationship suggested by Pastor (2006) presented a greater reduction in pH than in the equimolar relation.

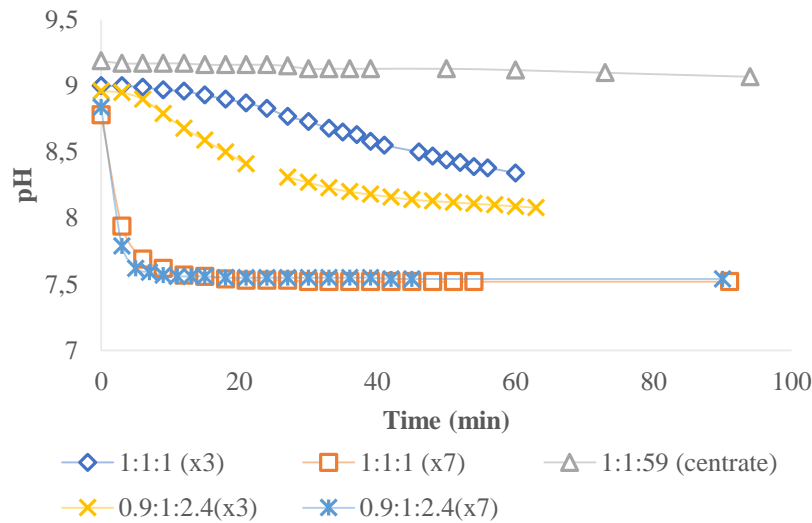


Figure 51. Behavior of pH in Batch experiments

In continuous experiments, it was observed that it is possible to maintain the pH relatively constant by adding NaOH in small pulses. The variation of pH in the experiment was between 8.74 and 9.21, so an on-off controller could be an economical and useful strategy to control the pH in the reactors to be designed (Figure 52).

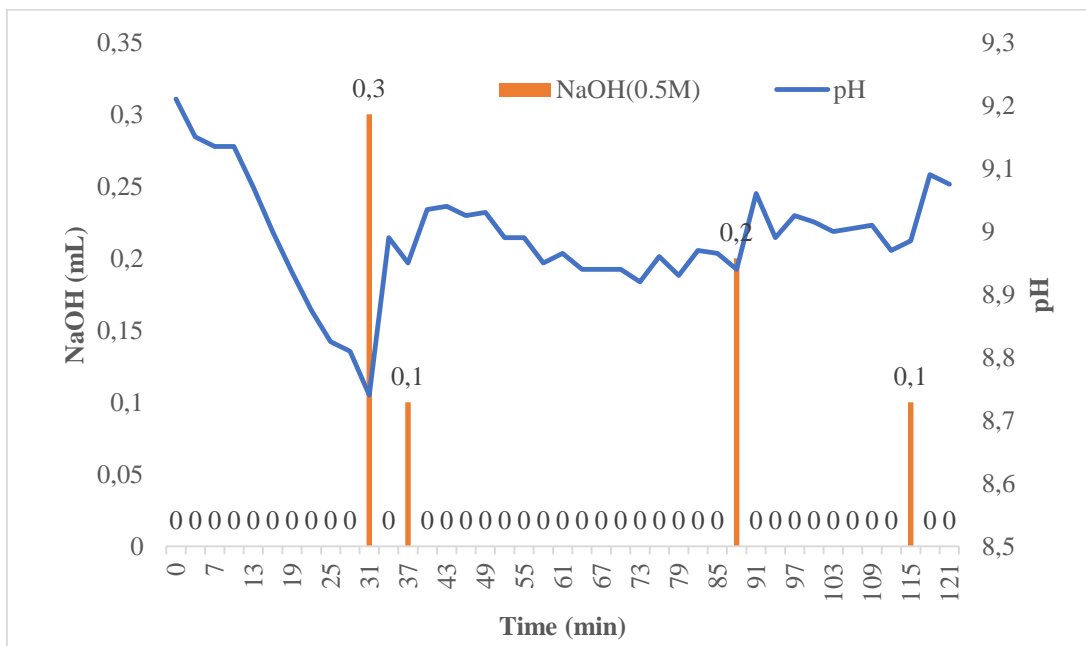


Figure 52. The behaviour of pH in continuo experiment (Mg:P: N -0.9:1:2.4)

Figure 53 shows that the powdered XRD pattern of reference (Sigma–Aldrich) and synthesised struvite matched very well and, the orthorhombic pattern observed in the scanning electron

micrograph (SEM) for both samples is consistent with the morphology reported for this compound. Therefore, the synthesis method used in this study is suitable to produce struvite.

In addition, Figure 54 shows the TGA curves for reference (patron) and synthesised struvite. These data indicate that mass loss begins at a temperature around 100°C and is essentially complete when the temperature reached above 250°C (at this point, 51% of the original mass loss occurred; Acelas, Flórez, & López, 2015). This mass loss corresponds to the following decomposition reaction for struvite, Equation 30:



According to TGA results in the first loss of mass was 46.5% on average for the four precipitates evaluated and 44.89% for the reference (patron); meanwhile, the second was 8.78% and 9.24% % for the reference and synthesised struvite, respectively. These results agree with the theoretical mass loss for the formula ( $\text{NH}_4\text{MgPO}_4 \cdot 6\text{H}_2\text{O}$ ) which is 51.42% which is made up of mass loss of water as 44.08% and ammonia as 7.34%. It is possible to observe the same behaviour for all samples, which confirms the identity of the synthesised struvite (Figure 54).

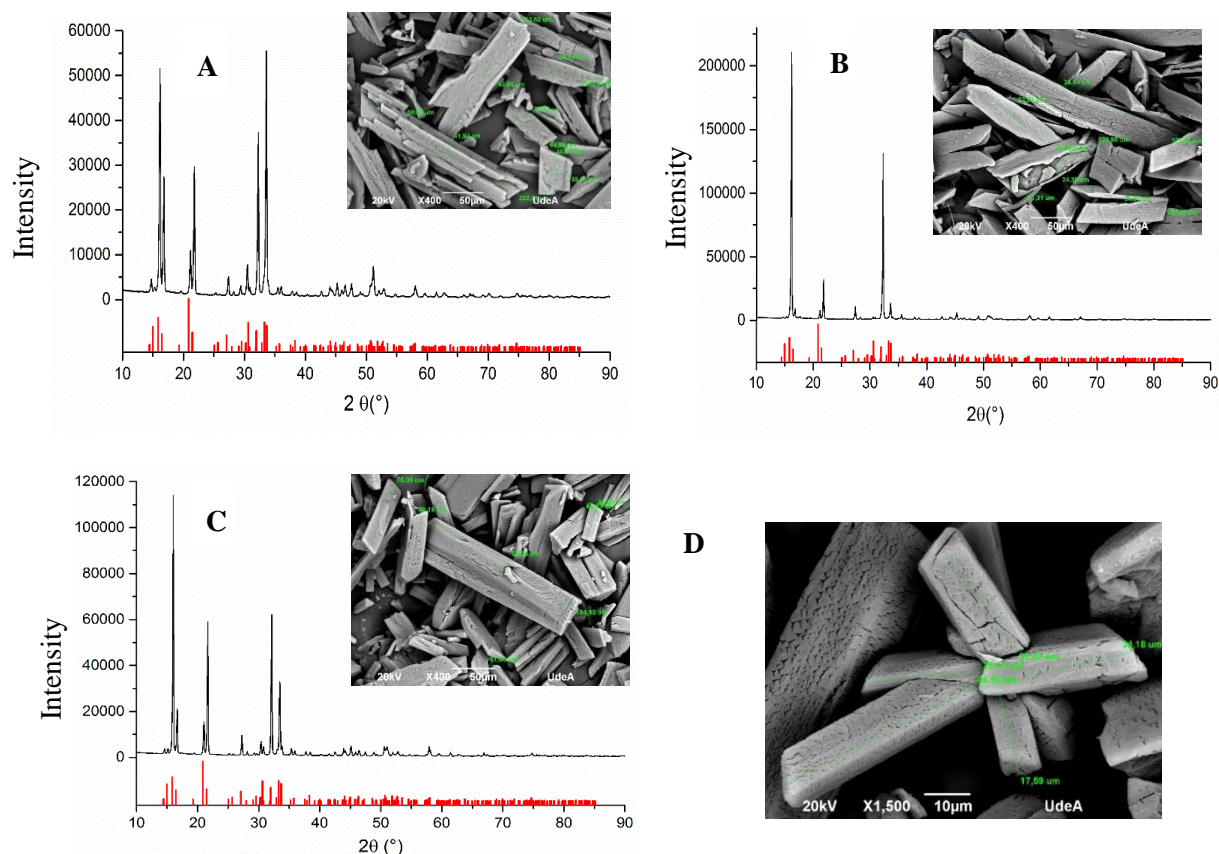


Figure 53. XRD and SEM analysis. A. Test 1:1:1x7; B. Test 0.9:1:2.4 x7; C. Test 0.9:1:2.4x3; D. SEM Test 0.9:1:2.4 continuous.

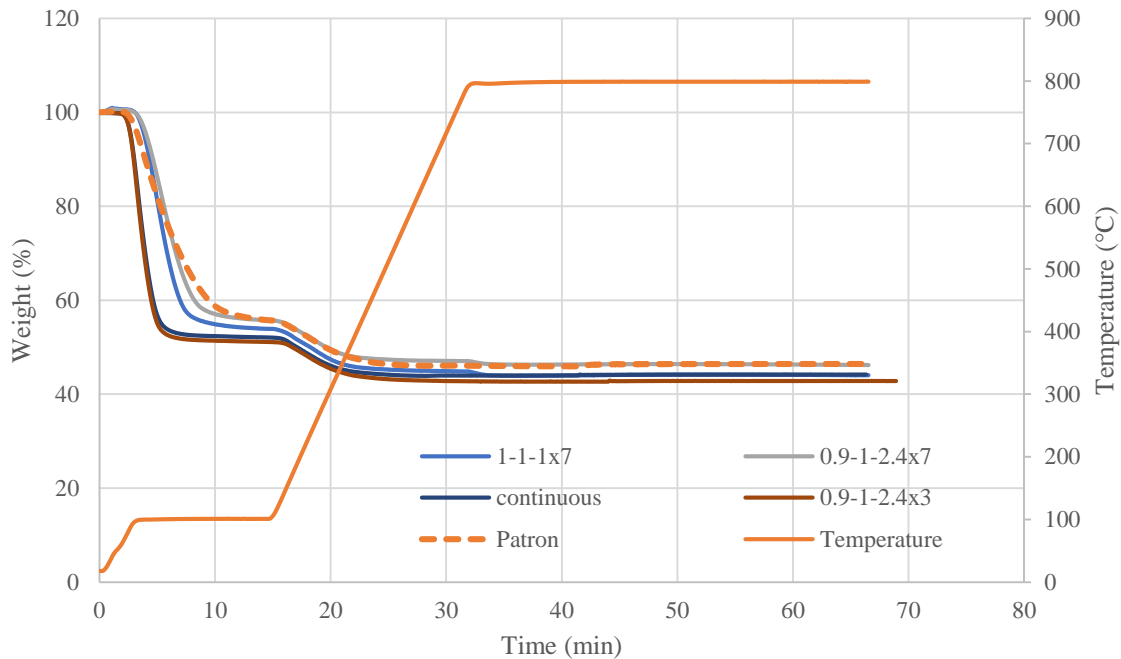


Figure 54. Thermogravimetric analysis (TGA).

❖ *Tests in a continuous stirred tank reactor (CSTR)*

According to Pastor (2006), the stirred tank reactor is a simple and flexible technology, easy to implement in a WWTP and capable of absorbing fluctuations in operating conditions, achieving precipitation efficiencies of 78 to 95% and recovery efficiencies of 46 to 86%. Therefore, in these preliminary tests, we wanted to evaluate the efficiency of a CSTR reactor designed by Regy et al. (2002) and evaluated by different investigations, including Pastor et al. (2008) and Cerrillo et al. (2014). The pilot plant consisted of two peristaltic pumps for the addition of Mg and the real centrate from La Llagosta WWTP (Barcelona), as well as an automatic pH controller (Figure 55). More information on the used reactor can be found in Cerrillo (2012).



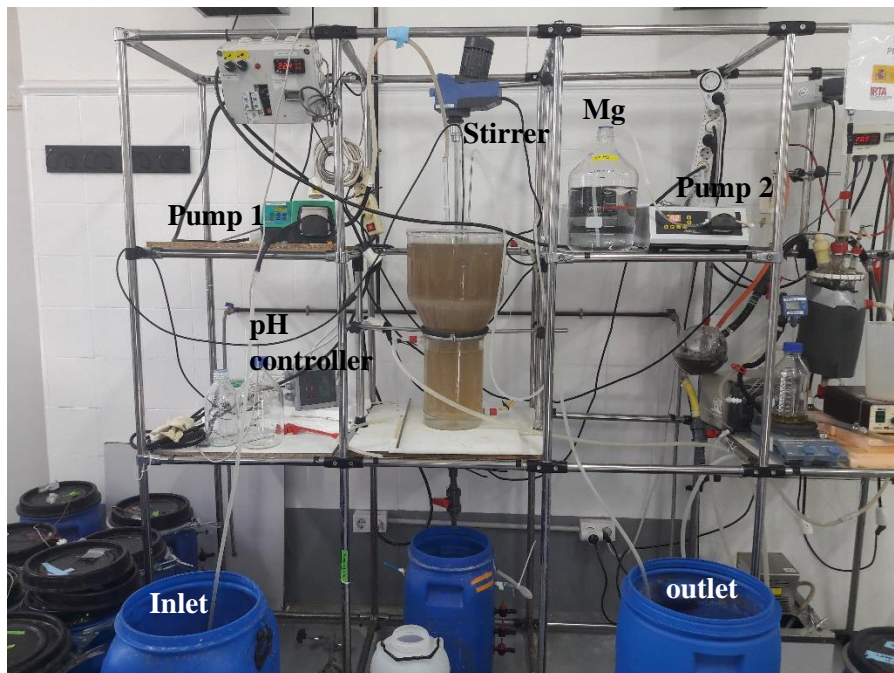


Figure 55. Experimental setup with a 20 L CSTR reactor at the IRTA research institute.

#### ❖ *Description of the experiments*

The experimental design consisted of evaluating two concentrations of phosphorus (60 and 120 mgP.L<sup>-1</sup>) and TSS (90 and 800 mg TSS.L<sup>-1</sup>) on the CSTR reactor (20L) under a constant stirred speed of 280 RPM at 30 hours. The TSS concentration was adjusted using the digested sludge from the La Llagosta WWTP and the P concentration using NaH<sub>2</sub>PO<sub>4</sub>·2H<sub>2</sub>O as a reagent. The Mg: Ca molar relation remained constant at 2 to reduce Ca precipitation. The input flow was of 1.68 L.h<sup>-1</sup>, and the HRT was 11.9 h. The concentration of PO<sub>4</sub><sup>3-</sup>-P, NH<sub>4</sub>-N and K<sup>+</sup>, Ca<sup>+</sup> and Mg<sup>2+</sup> were measured in the reactor affluent and effluent. The N: P molar ratio was on average 17, and the initial NH<sub>4</sub> concentration ranged between 480 and 894 mg NH<sub>4</sub>-N. L<sup>-1</sup>, which correspond to typical concentrations of sludge dewatering centrates.

The phosphorus as struvite (PMAP) was calculated according to the relationship between the removed moles of Mg and P, considering that all the removed Mg precipitated as struvite. The P that precipitated with Ca and K was calculated as the ratio between the removed moles of Ca and K and the removed moles of P, respectively (P-Ca, P-K). A loss of fines (FL) was also calculated through the difference between the removal of ammoniacal N (%) before and after filtering the effluent samples (0.45 µm filters).

#### ❖ *Results and discussion of preliminary and exploratory tests*

According to the results, the N removal increased with the initial P concentration, mainly due to the greater formation of struvite (on average, 21% N removal at 120 mg P/L). The removal of P and Mg was similar in all tests and higher than 85 and 88% respectively, however, a lower removal of Ca and higher PMAP was observed in the tests that presented a higher concentration of TSS (on average 22 % Ca removal and 63% PMAP). K removal was minimal in all tests (< 8%), possibly due to the high concentration of ammonium N that favours the formation of struvite over K-struvite (Table 27 and Figure 56). The loss of fines (FL) was lower in the tests that presented the highest concentration of

solids; this can be because the suspended solids provide an embryo for the first stage of crystal formation and therefore improve the precipitation of struvite (Le Corre et al., 2005). However, TSS carries impurities such as organic matter, pathogens, and heavy metals that could affect the quality of struvite. With the XRD analysis, it was found that the recovered product was struvite, however with the EDX analysis impurities were observed in the precipitates of the tests under the highest concentration of solids, especially Cu, Zn, Fe and Ca (Figure 57 and Figure 59).

Although there is no significant interference of the solids in the struvite precipitation and these showed positive results by reducing the amount of Ca precipitated and increasing the PMAP, the solids can affect the struvite quality for its use as fertiliser. No significant effect of the two P concentrations was observed on struvite formation. In some tests, a strong affinity of struvite to the glass walls of the reactor was observed, this has been reported by other authors as fouling and can influence the final recovery of the precipitate (Pastor, 2008).

With this preliminary test, it was demonstrated that it is possible to recover struvite from the real sludge dewatering concentrates using a stirred reactor and under different levels of P and TSS. However, it is necessary to develop a complete experimental design, with a greater number of replications to verify the results obtained.

Table 27. Tests conditions and principal results.

Test	Initial condition		Mg, Ca, K with P (%)			NH <sub>4</sub> -N removal (%)		FL (%)
	P(mg/L)	TSS(mg/L)	PMAP (%)	P-Ca (%)	P-K (%)	filtered	unfiltered	
1	60	90	53	46	5	19	13	6
2	60	800	66	26	6	16	15	1
3	120	90	52	49	2	30	22	8
4	120	800	62	22	3	21	20	1

- FL represent the loss of fines

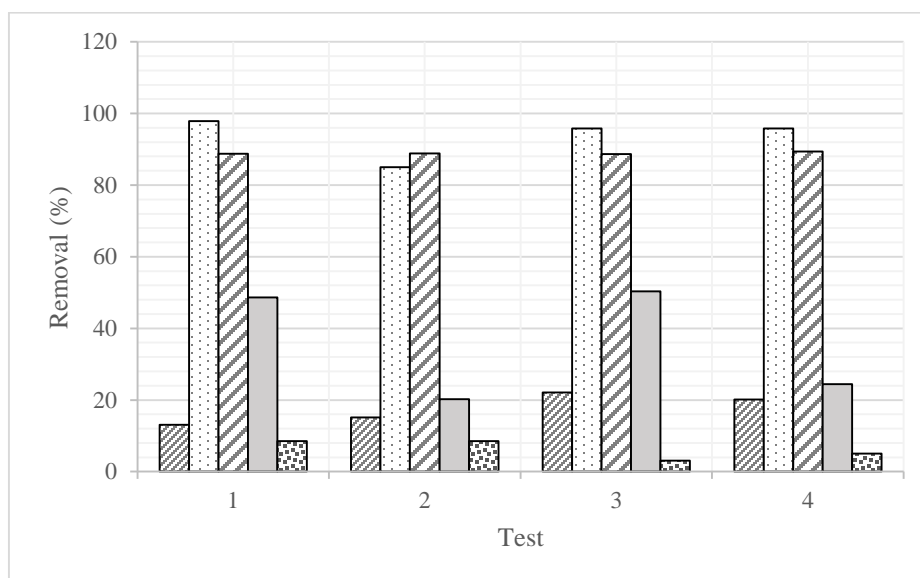

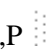



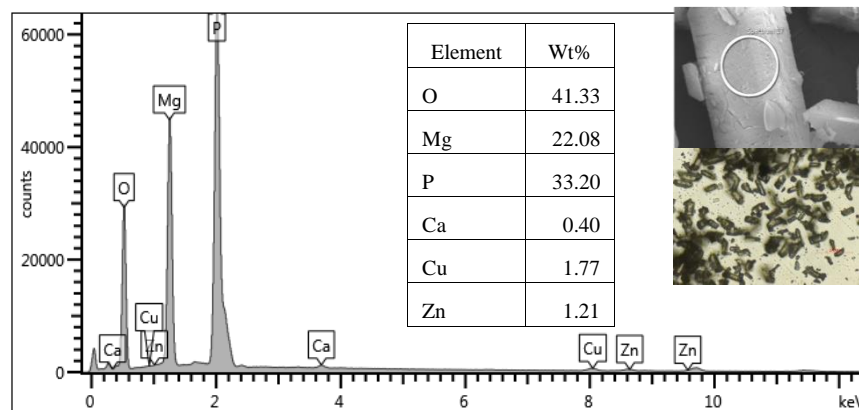
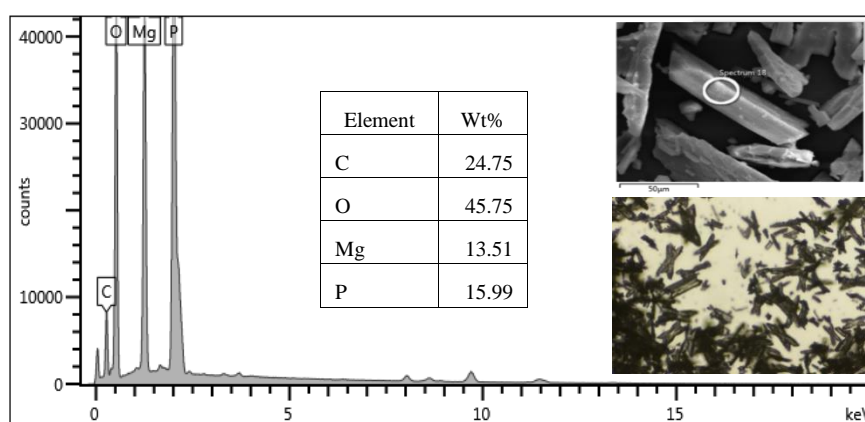
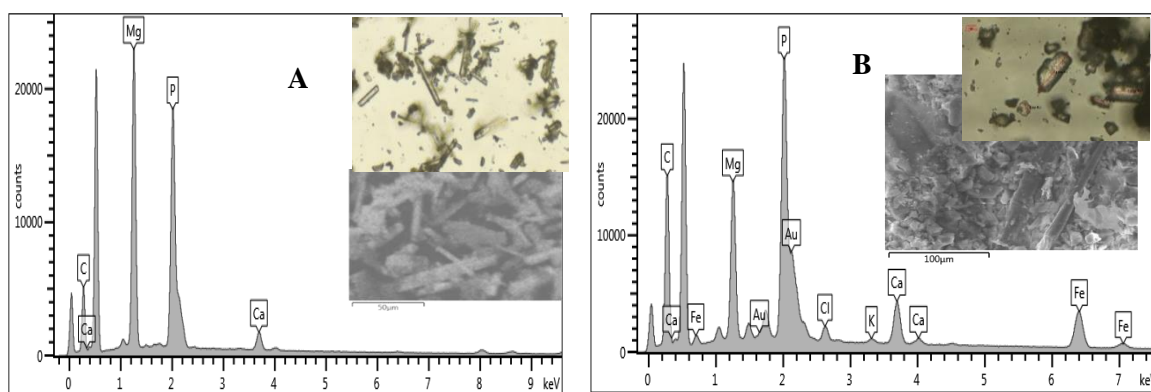


Figure 56. N, P, Mg and Ca removal (%). N , P , Mg , Ca , K 

Figure 57.EDX Test 2 (60 mg  $\text{PO}_4^{3-}$ -P.L $^{-1}$  and 800 mg TSS -L $^{-1}$ ) 6<sup>TH</sup> FEBRUARYFigure 58.EDX Test 3 (120 mg  $\text{PO}_4^{3-}$ -P.L $^{-1}$  and 90 mg TSS -L $^{-1}$ )21th FebruaryFigure 59.EDX Tests 1 (A) and 4 (B) (60, 120 mg  $\text{PO}_4^{3-}$ -P.L $^{-1}$  – 90 and 800 TSS -L $^{-1}$ , respectively)

### Complete stirred tank Reactor (CSTR) design.

The CSTR reactor is one of the most used reactors for crystallisation at an industrial level because it is simple, flexible, and it is capable of absorbing fluctuations in different operating conditions. The acrylic CSTR reactor of this research had a working volume of 5L and was designed according to Regy et al. (2002), with separate reaction and sedimentation zones (Figure 60). This reactor was

operated in continuous mode to the liquid phase (centrate), which enters in the mixing zone and flows out at the top of the settler.

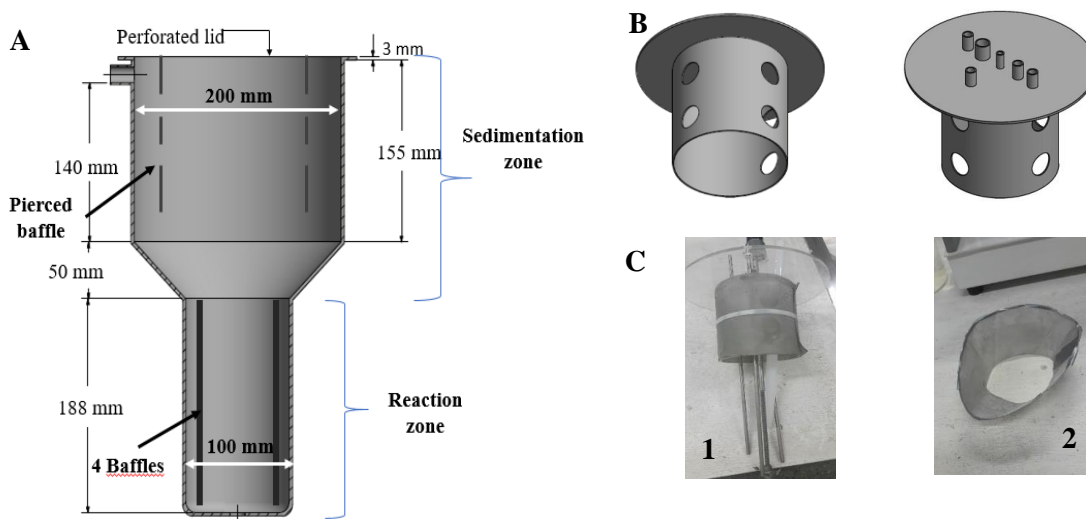


Figure 60. CSTR Design. A- Reactor dimensions. B- Lid and top baffle details. C- Stainless steel meshes used in the top baffle (C-1) and the conical (C2) part of the settler.

The sedimentation zone aims to minimise the loss of fine crystals that can be drawn out of the reactor with its effluent. The settling zone is located above the reaction zone and is cone-shaped with an angle of  $45^\circ$  between the two zones. This part is equipped with a pierced baffle to guide the flow. The reactor lid is attached to the upper baffle and the stirrer. It has holes where the pH and temperature probes and the stainless-steel tubes are placed for centrate and reagent dosing (Figure 60B). Due to the high affinity of struvite for stainless steel (Doyle et al., 2002), the reactor was also equipped with two stainless steel meshes dimensioned to fit in the upper reactor baffle (C1) and conical section (C2), both in the sedimentation zone. Both meshes were made of woven wire stainless steel 0.212 mm hole, 0.152 mm wire (mesh 70-AISI 304) to act as a seed material to grow struvite and maximise its recovery (Le Corre et al. 2007).

The reaction zone was designed according to the recommendation presented by Mangin & Klein (2004). The reaction zone was equipped with four baffles to prevent the formation of vortex effects during mixing. The number of baffles (4) in the reaction zone was different from the number of impeller blades (2) to reduce the risk of entering in resonance (Valsami-Jones, 2005). The width of the baffles was 10 mm ( $dr/10$ ); the diameter of the impeller was 55 mm ( $0.5-0.6 dr$ ). The space between the baffles and the tank wall was 3 mm ( $dr/30$ ), it is necessary to prevent the accumulation of solid particles on the baffles.

According to Mangin & Klein, (2004), a correct flow circulation is obtained when the liquid height is approximately equal to the tank diameter ( $H_L = dr$ ), and when the propeller is positioned at  $h = (1/3) H_L$  from the bottom of the tank. Therefore, the propeller was positioned at 60 mm from the bottom of the reactor, and it was considered that the zone of good mixing occurred mainly in the first 100 mm of the reaction zone (bottom-up).

The way to enter the reagents and the type of flow in the reactor were two variables that were considered during the design. In double jet precipitation, the two reactants are fed in simultaneously,

through two distinct tubes. Two main configurations of the tubes are then possible. The reactants can be fed close together (Figure 61A), or far apart from each other (Figure 61b). In the first case, the two fresh and concentrated feed solutions are directly mixed. High local supersaturation may then occur, leading to elevated rates of nucleation and small mean crystal size. Inversely, if the two feed points are far away from each other, the two plumes of fresh feed are mixed with the bulk without directly exchanging mass between each other. In this way, a large dilution of both reactants occurs. Supersaturation levels much lower than in the first case are obtained, leading to a larger mean crystal size (Mangin & Klein, 2004). Therefore, the stainless-steel tubes used to enter the concentrate, the Mg and the NaOH were positioned as far away as possible.

The type of stirrer can also influence the particle size obtained and the quality of the mixture. Impellers can be divided into two main categories, depending on the flow they generate inside the vessel: radial flow impellers and axial flow impellers. Axial flow impellers are essentially propellers. They are always installed so that the outflow is directed towards the bottom of the vessel Figure 61. Propellers generate high circulating flow rates. The shear rate is low, even near the impeller, and rather homogeneously distributed in the entire vessel. The profiled propeller of type TT from Mixel™ was recommended by Mangin & Klein, (2004) and was used by Pastor (2008), however in this research was used a more simply axial flow impeller that is shown in Figure 61c. This type of impeller makes it possible to reduce the shear force and improve the mixing in the reactor.

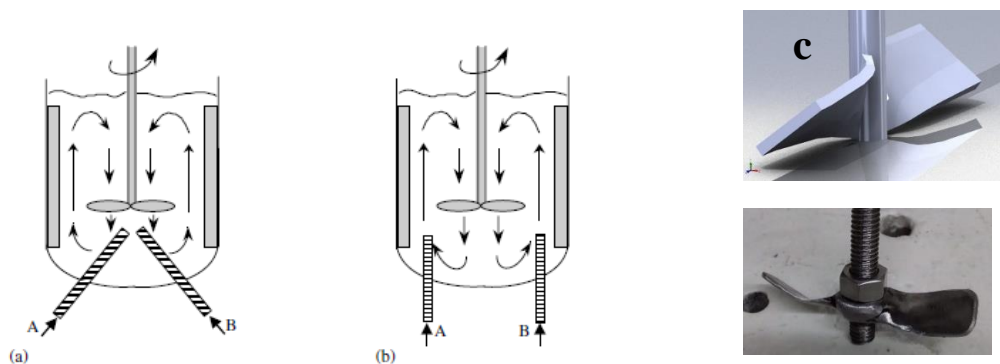


Figure 61. Axial flow and ways to enter reagents into a solution(a, b). C- Impeller used in this research

The instrumental reactor control system was developed as a research project by the bioengineering student Cristian C. Acevedo. The system has temperature and pH sensors, a stirring system with variable speed (180 to 365 RPM) and an LCD for displaying the values in real-time.

The system is controlled by an Atmega 2560 microcontroller arranged on a commercial Arduino Mega board. An On / Off control routine was programmed to activate a peristaltic pump connected to a NaOH (1M) solution. The pump was switched ON when the pH dropped below a set point (in tests it was 9) and switched OFF when the solution was above the set point. The system also had a DC motor to which was applied a pulse-width modulation (PWM), enabling varying the stirring speed of the system (Figure 62). Temperature and pH sensors were developed by the company DFRobot ([https://wiki.dfrobot.com/Analog\\_pH\\_Meter\\_Pro\\_SKU\\_SEN0169](https://wiki.dfrobot.com/Analog_pH_Meter_Pro_SKU_SEN0169)). The main advantage of this type of control system was its low cost.

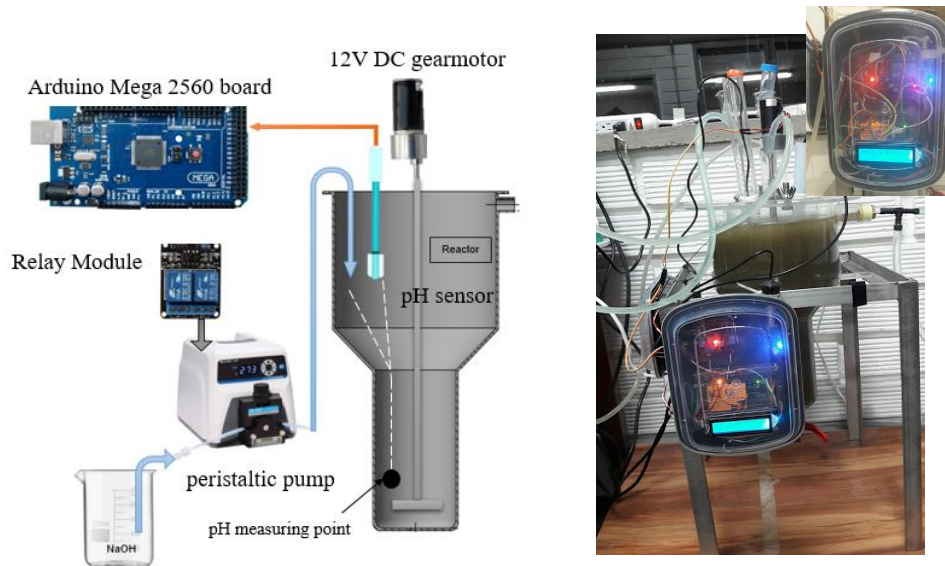


Figure 62. Control system in CSTR reactor

The struvite crystallisation system was composed for the reactor present in Figure 60, an axial impeller (Figure 61), four stainless steel injection tubes connected to an air pump and three peristaltic pumps for dosing the sludge dewatering centrate (9 mL/min),  $MgCl_2 \cdot 6H_2O$  (2.3 mL/min), and 1M NaOH (1.1 mL/min) to maintain the pH at the desired value using an on-off control system (Figure 62). The flow enters the lower part of the reactor (reaction zone) through the stainless-steel tubes, and the effluent leaves the upper part of the settling zone through an overflow. This reactor was operated in continuous mode to the liquid phase and batch mode for struvite collection. The main characteristics of the pilot plant are presented in Figure 63.

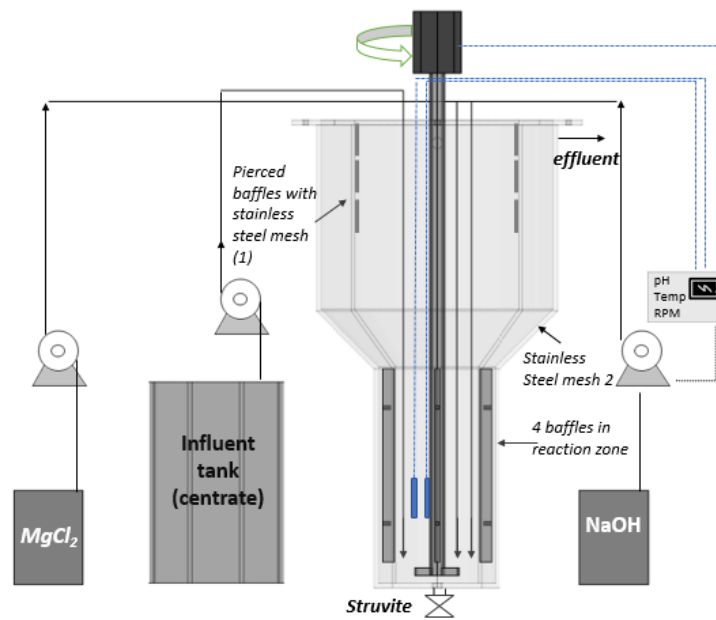


Figure 63. Schematic of the crystallisation pilot plant (CSTR reactor)

## Fluidised bed reactor (FBR) design

A fluidised bed reactor (FBR) consists of a vertical cylinder, filled with solid particles which are brought to fluidised state by the reactant solutions fed at the bottom of the cylinder. All the crystallisation processes can, a priori, occur along the column, with the ideal case being the growth of crystals only on the fluidised particles. FBRs can be operated with or without effluent recycling.

At a low flow rate, the particles are packed and immobile. An increase of the flow rate increases the pressure drop across the bed. This pressure drop is due to the frictional forces between the fluid and the particles. The increase of the pressure drop will continue until the frictional drag on the particles equals their apparent weight (actual weight minus buoyancy). At that stage, the particles can rearrange to offer less resistance to the fluid flow. If the flow rate is increased further, the individual particles are separated from one another and become freely supported in the fluid. The bed is said to be fluidised (Mangin and Klein, 2004).

The design of an FBR and the choice of the operating conditions depend on several criteria, including the minimum fluidising velocity, i.e. the minimum superficial velocity of flow at which fluidisation takes place and the terminal settling velocity of the particles, i.e. the maximum superficial velocity of flow at which entrainment of particles takes place. The main operating parameters considered in the design were: the inlet flow rate ( $Q_i$ ), the mass of solid particles ( $m_s$ ), the particle size ( $d_p$ ), the solid density ( $\rho_s$ ) and the fluid density ( $\rho_f$ ). Generally, the FBR is operated by controlling the flow rate, with all the other parameters being fixed. The range of inflow-rates, to generate correct fluidisation, is then quite narrow.

For the design, a bibliographic review of the FBR reactors used on a laboratory scale and at an industrial level for different processes and especially for the crystallisation of struvite was conducted. FBR reactors are divided into several zones of ascending diameter to allow the separation of particles of different sizes. In this case, it was decided to divide the reactor into two zones. The reactor of 6.5 L (useful volume) was made in acrylic, with a bottom (volume 2.5 L, diameter 80mm), and top (volume 2.8 L, diameter 140 mm) zone. The parts of the reactor were joined with conically shaped structures ( 1.2 L ) at an angle of  $45^\circ$  in order to reduce the crystal loss at each junction (Guadie et al., 2014). The principal reactor dimensions are presented in Figure 64.

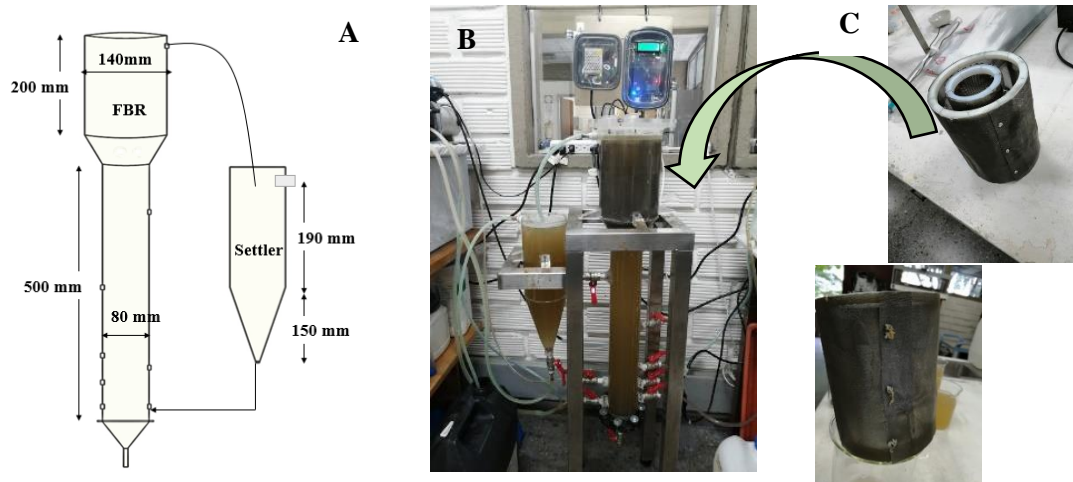


Figure 64. FBR Design. A-FBR dimensions, B- Picture FBR, C-Detail of the stainless steel meshes.

Since the bottom diameter is smaller than the upper one, as the liquid flows upwards, its flow velocity decreases and leads to the segregation of the crystals formed. The reactor was also equipped with two concentric stainless steel meshes dimensioned to fit in the top part to use them as a substrate to grow struvite (Le Corre et al., 2007) and reduce the loss of fines through the effluent (Figure 64-C).

The superficial velocity of flow ( $U$ ) is simply the velocity the fluid would have through the column in the absence of particles. It is linked to the total inlet fluid flow rate ( $Q$ ) and the fluidiser cross-sectional area ( $A_s$ ) by:

$$U = \frac{Q}{A_s} \quad \text{Equation 31}$$

The minimum fluidisation velocity can be calculated using different equations, including the equation of Ergun (1952), Abrahamsen and Geldart (1973), Thonglimp (1981), Carman (1937), among others (Yates & Lettieri, 2016). In this research, the Ergun equation was used, which for relatively small particles ( $<100\mu\text{m}$ ), Reynolds number ( $Re$ ) is low and can be expressed as (Missen et al., 1999; Suleiman et al., 2013):

$$u_{mf} = \frac{g (\rho_p - \rho_f) \cdot d'_p{}^2}{150 \cdot (1 - \epsilon_{mf}) / \epsilon_{mf}^3} \quad \text{Equation 32}$$

Where:

$\rho_p$  and  $\rho_f$  are the particle and fluid density, respectively.

$d'_p$  is the effective particle diameter, and for cylindrical solid particle, it depends on particle diameter ( $d_p$ ) and the height of the cylinder ( $h_c$ ).  $d'_p = \frac{3 \cdot d_p}{(2 + d_p/h_c)}$

$\epsilon_{mf}$  is the sphericity at the incipient fluidisation point. It depends on sphericity factor ( $\phi$ ) and for spherical particles is around 0.4.

$\phi = \frac{A_{sphere}}{A_{particle}}$ ;  $A_{sphere}$  is the surface area of a sphere having the same volume as the particle, while  $A_{particle}$  is the particle surface area.

To calculate  $U_{mf}$ , the average particle size obtained in preliminary tests was measured (mean  $35\mu\text{m}$  wide and  $92\mu\text{m}$  high), a particle density of  $1695.12\text{ Kg}\cdot\text{m}^{-3}$  and the density and viscosity of water at  $25^\circ\text{C}$  was used.  $U_{mf}$  was also calculated with Abrahamsen and Geldart (1973), Thonglimp (1981) equations (Alvarez Cuenca & Anthony, 1995) and was compared with the result obtained with the Ergun equation.

The fluid flow rate through a fluidised bed is limited firstly by  $U_{mf}$  and secondly by entrainment of solids by the liquid. This upper limit to superficial fluid velocity,  $U_{max}$ , is approximated by the terminal settling velocity of the particles, which, for a spherical particle, can be estimated by:

If  $Re_p < 1$  (laminar regime):



$$U_{max} = \frac{g \cdot dp^2 (\rho_s - \rho_f)}{18 \cdot \mu} \quad \text{Equation 33}$$

Where  $Re_p$  is the particle Reynolds number:

$$Re_p = \frac{\rho_f \cdot U_{max} \cdot dp}{\mu} \quad \text{Equation 34}$$

if  $1 < Re_p < 1000$  (intermediary regime) or if  $1000 < Re_p < 4 \times 10^5$  (turbulent regime)  $U_{max}$  can be calculated according to the equations Equation 35 and Equation 36, respectively (Mangin & Klein, 2004):

Equation 35

$$U_{max}^{1.4} = \frac{0.072 g d_p^{1.6} (\rho_S - \rho_F)}{\rho_F^{0.4} \mu^{0.6}}$$

Equation 36

$$U_{max}^2 = \frac{3 g d_p (\rho_S - \rho_F)}{\rho_F}$$

The  $U_{max}$  was calculated first, and the condition on  $Re_p$  was verified posterior, to allow validation of the calculated  $U_{max}$ .  $U_{max}$  was multiplied by a correction factor ( $n$ ) that depends on the sphericity (0.8) and the  $Re_p$  (Alvarez Cuenca & Anthony, 1995).

To obtain proper fluidisation, the superficial velocity of flow ( $U$ ), must be considerably greater than the minimum fluidisation velocity,  $umf$ . However, to avoid excessive entrainment,  $U$  should be less than the terminal velocity,  $U_{max}$ . Thus, the ratio  $U_{max}/umf$  was a guide to the selection of the value of  $U$ . In practice, values of  $U$  are 30 to 50 times the value of  $umf$  (Missen et al., 1999). Additional information on the calculations and equations used for the design of the FBR reactor can be found at Alvarez Cuenca and Anthony (1995); Mangin and Klein (2004); Missen et al. (1999); Suleiman et al. (2013) and Yates and Lettieri (2016). The principal design parameters are presented in Table 28.

Table 28. Principal operational conditions and design parameters.

Flow Velocity (U)	Minimum fluidisation velocity (Umf)	Terminal settling velocity (Umax)
Influent flow Qi (mL/min)	17.0	d'p (um) 44.49
Recirculation flow Qr (mL/min)	114.0	Rep 0.08
Qr/Qi	6.7	Umax spheres (m/h) 4.75
Flow velocity Principal section(m/h)	1.6	Umax real (m/h) 10.06
Flow velocity Top clarify (m/h)	0.5	Umf Ergun(m/h) 0.06
		Umf Abrahamsen(m/h) 0.05
		U/Umf 26.53
		U>Umf; U<Umax OK

In the FBR reactor, while large crystals are accumulated at the bottom, finer particles flow out from the reactor and are recycled back with the effluent through the external settler of 2.2 L, using a peristaltic pump at a rate of 114mL/min. Influent and reagents solutions were supplied to the FBR at

the bottom ports, using peristaltic pumps at a rate of 13 mL/min for centrate and 2.3 mL/min for  $MgCl_2 \cdot 6H_2O$ . A pH probe was introduced in the top part to control and maintain the pH constant during the crystallisation process, using the same control system of the CSTR tests. The NaOH (1M) application rate was 5 mL/min (dosage applies only at pH below 9). The main characteristics of the pilot plant are presented in Figure 65.

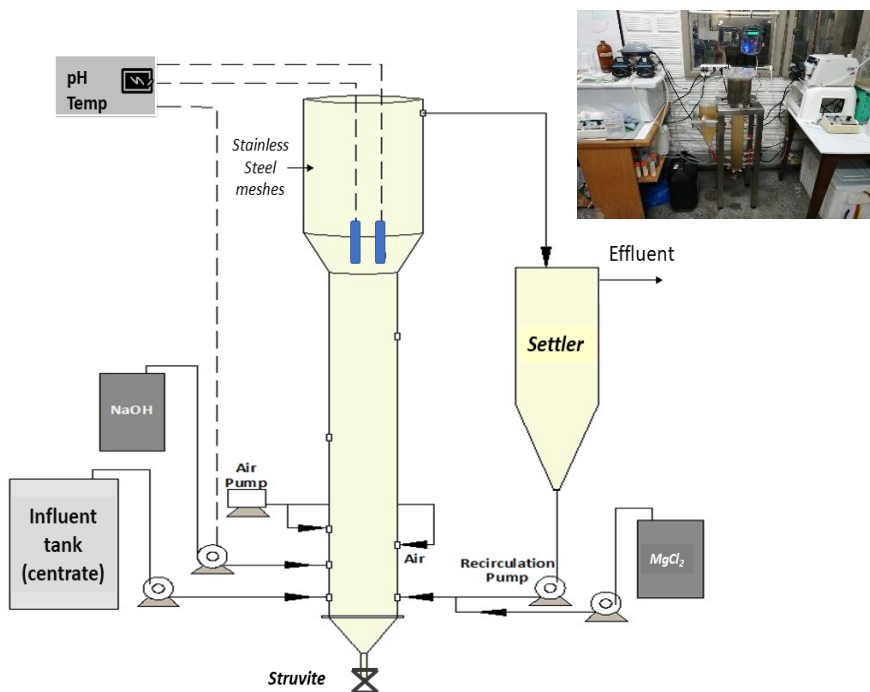


Figure 65. Schematic of the crystallisation pilot plant (FBR reactor)

## **Annex 3. Residence time distribution in CSTR and FBR reactors in ideal situation, undisturbed by the crystallisation process.**

Residence time distribution (RTD) analysis is a useful tool to explain the hydrodynamic behaviour of a reactor. In this study, RTD was applied in two laboratory-scale struvite crystallisation reactors (CSTR and FBR) to estimate the degree of non-ideality and its effect on the reactor's performance. An impulse-response tracer (NaCl saturated solution) approach and a conductivity meter to detect the NaCl at the effluent of the reactor were applied. The trend curve method and the Wolf-Resnick model was applied to perform the hydrodynamic analysis. The main findings from this study showed that both reactors have a non-ideal flow pattern with a predominance of thorough mixing (>70%), the presence of short circuits in both reactors was also identified. It is suggested to apply the FBR reactor to solutions with a high level of saturation because it has a higher percentage of thorough mixing that could favour crystal growth.

### **Introduction**

The measurement and analysis of residence time distribution (RTD) is an important tool in the study of continuous flow systems. A study of available experimental data shows that the usual assumptions of perfect mixing or plug flow do not correspond to the situation existing in real flow systems (Wolf & Resnick, 1963). RTD knowledge is fundamental for reactor design since it allows knowing system kinetics for planning design options to maintain desired flow patterns and compare the influence of different configurations and modifications in reactors (Stamou, 2008).

The ideal reactors are divided into two main types –the perfect mixing reactor and plug flow reactor. The non-ideal reactors are these systems, which differ significantly from the two ideal cases. In most cases, non-ideal flow is undesirable and could be avoided with appropriate design of the systems. However, even with appropriate design, the non-ideal flow can be maintained, then it should be recorded appropriately in mathematical models (Kostov et al., 2011).

Tools such as hydraulic performance indicators and simplified flow models based on tracer studies have led to a reactor's hydrodynamic evaluation from field data. According to the dosage method, tracer studies may be instantaneous addition type (using a concentration  $C_0$  at the reactor inlet for a concise period) or continuous addition (continuously injecting a  $C_0$  concentration of tracer at a constant rate) (Patiño et al., 2012). Normally a tracer is added to the inlet stream, and the concentration of the tracer in the outlet stream is measured as a function of time.

The design of wastewater treatment systems has focused primarily on the biochemical process, leaving hydrodynamic aspects in the background such as flow characteristics, mixing regime, residence times, reactor geometry, etc., which influence the performance of the processes conducted during the treatment (Pérez & Torres, 2008). The design of crystallisers is also mainly focused on chemical processes, and the use of tracers for RTD in reactors for struvite crystallisation has been little studied.

Most of the studies of hydrodynamics in struvite precipitation systems have been conducted in batch type systems or fluidised bed reactors mainly using computational fluid dynamics (CFD) (Mousavi, 2017; Rahaman & Mavinic, 2009); however, this modelling can be complex and require long

simulation times. Among the few studies developed using tracers is that of Ulfa et al. (2020) that developed an RTD analysis to explain the hydrodynamic behaviour of a continuous stirred tank reactor for struvite crystallisation. They found that impeller location and impeller speed have a significant effect on actual HRT and effective volume of the reactor.

The hydrodynamic conditions in a precipitation reactor can affect the size and quantity of the produced particles strongly (Valsami-Jones, 2005) since they play an important role in preventing local supersaturation (Ali, 2005). For this reason, in this work, the flow of a CSTR and an FBR reactor was characterised by the residence times distribution (RTD) model, whose purpose is to describe how mass transport occurs inside a reactor that works continuously (Levenspiel, 1986). The objective of this research was to determine their main characteristics as a flow pattern, dead zones and hydraulic short circuits by using salt as a tracer. To evaluate the hydraulic behaviour of the reactors, the trend curve analysis and the Wolf-Resnick model were applied (CEPIS, 2004; Levenspiel, 1986; Wolf & Resnick, 1963).

## Methodology

### ❖ *Tracer study*

Tests using 99.5 % sodium chloride (NaCl) as a tracer were performed to determine the hydraulics of the CSTR and FBR reactors. The procedure involved adding an instant dose of 3 and 3.5 g of NaCl to the CSTR and FBR reactors, respectively. The tests complied with the minimum ratio of three times the theoretical HRT (28.3 and 27.3 hours for CSTR and FBR reactors respectively). Tap water was constantly fed into the flow. Samples were taken during and after tracer injection in the effluent of each reactor. The conductivity was measured in each sample using the WTW Cond 3110 conductivity meter.

Conductivity data were expressed in terms of tracer concentration (mg/l NaCl) by interpolating previously prepared concentration on a calibration curve (conductivity *cf* NaCl; Figure 67). The calibration curve was made by preparing 10 known concentrations of NaCl in tap water (between 0 and 1000 mg/L) as is shown in Figure 66 and Figure 67. NaCl was chosen as a tracer because it can be easily analysed.

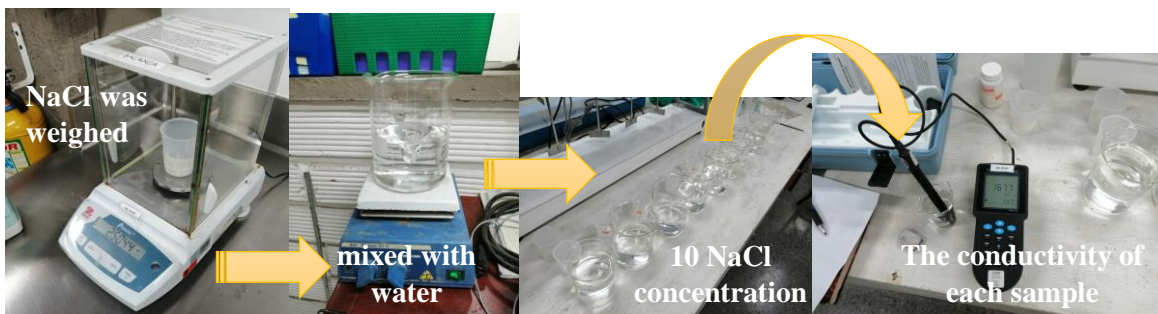


Figure 66. Methodology to perform the calibration curve

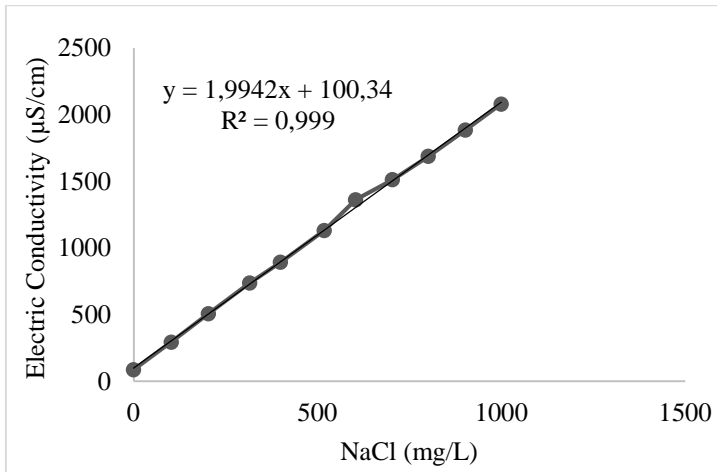


Figure 67. Calibration curve: NaCl vs Electric conductivity.

Tracer concentration data in the effluent were analysed using the trend curve method and the model proposed by David Wolf and William Resnick (1963), both recommended by CEPIS to study the hydraulics of the reactors (Cánepa de Vargas, 2004).

#### ❖ *Wolf and Resnick model*

The residence time distribution for real single-stage continuous flow systems can be represented by an F-function (percentage of tracer leaving the system over time  $t$ ) of the form of Equation 37, where  $t$  is the hydraulic residence time,  $t_0$  is the theoretical residence time,  $\eta$  is the measure of mixing efficiency and  $\varepsilon$  is a measure of the phase change in the system (Wolf & Resnick, 1963).

$$F(t) = 1 - e^{-\eta \frac{(t-\varepsilon)}{t_0}}; \quad F(t) \geq 0 \quad \text{Equation 37}$$

According to Cánepa de Vargas (2004), the Equation 37 can be rewritten as a function of the dead zones ( $m$ ), the plug flow ( $P$ ) and the theoretical hydraulic retention time ( $t_0$ ) as is shown in the Equation 38

$$F(t) = 1 - e^{-\frac{1}{(1-P)(1-m)} \left[ \frac{t}{t_0} - P(1-m) \right]} \quad \text{Equation 38}$$

Reordering terms and taking the natural logarithm of both terms:

$$\ln[1 - F(t)] = -\frac{1}{(1-P) * (1-m)} * \left( \frac{t}{t_0} \right) + \frac{P}{(1-P)} \quad \text{Equation 39}$$

Which corresponds to the equation of a straight line, whose slope is  $b$  and the intercept is  $a$

$$\ln[1 - F(t)] = a + b * \left( \frac{t}{t_0} \right) \quad \text{Equation 40}$$

Furthermore,  $F(t)$  can be calculated with the NaCl concentrations using Equation 41 (Cánepa de Vargas, 2004):

$$F(t) = \frac{\sum_{i=0}^{n=tf} (C_i - C_o) i * 100}{\sum C_i - C_o} \quad \text{Equation 41}$$

Where  $C_o$  is the initial concentration of the tracer substance (mg /L) and  $C_i$  is the concentration in an instant  $t_i$ .

The data of  $\ln(1-F(t))$  and  $t/t_o$  were graphed and fitted to a straight line (Equation 40) using the Statgraphics program, as is shown in Figure 68.

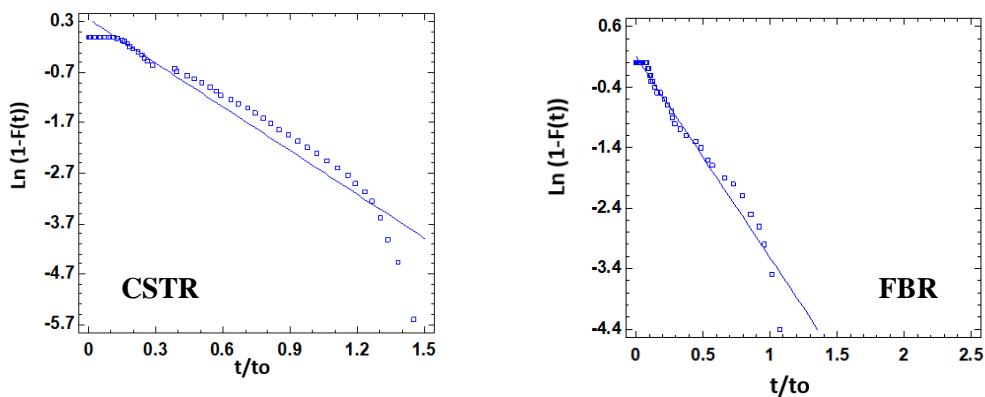


Figure 68. Amount of tracer remaining in each reactor-Curve  $\ln(1-F(t))$  and linear fit

With the slope ( $b$ ) and the intercept ( $a$ ) of the straight line, the plug flow ( $P$ ) and dead zones ( $m$ ) percentages were calculated (Equation 39 and Equation 40). The percentage of mixed-flow ( $M$ ) was calculated as:

$$M = 100 - P$$

#### ❖ *Trend curve method*

The qualitative analysis is performed by interpreting the main parameters of the tracer distribution curve in the reactor effluent. Where:

- $t_i$ : initial time from when the tracer is applied until it appears in the effluent.
- $t_{10}$ : time corresponding to the passage of 10% of the total amount of the tracer
- $t_p$ : modal time, corresponding to the presentation of the maximum concentration.
- $t_m$ : median time, corresponding to the passage of 50% of the amount of tracer.
- $t_o$ : mean retention time or theoretical retention time =  $V / Q$ .
- $t_{90}$ : time corresponding to the passage of 90% of the total amount of the tracer.
- $t_f$ : time that passes until the entire tracer passes through the reactor.
- $C_o$ : initial concentration.
- $C_p$ : maximum concentration at the outlet.
- $t_c$ : Time the concentration is greater than  $C_p / 2$ .
- $t_b$ : Time the concentration is greater than  $C_p / 10$

With the analysis of these parameters and relationships between them, the presence of hydraulic short circuits, dead zones, and the predominance of plug or mixed flow could be evaluated using the procedure described by Cánepa de Vargas (2004) and Naranjo (2009).

## **RTD Results and discussion in ideal situation**

The tracer curve in the effluent of the crystallisation systems is shown in Figure 69 and Figure 70. In CSTR reactor the tracer appears in the effluent at 48 min (110 mg/L) meanwhile in the FBR occurs first at 4 min (1.09 mg/L) then slightly increase and at 46 min appears a higher concentration (74.4 mg/L). This difference could be explained by the up-flow velocity in the FBR (1.6 m/h in principal section) that is higher than the up-flow velocity in the CSTR (0.09m/h in reaction zone) and possibly the presence of hydraulic short circuits in the FBR reactor.

Since the tracer appears in the effluent, the NaCl concentration in both reactors progressively increases as is characteristic of real reactors that present a combination of plug flow and complete mixing. In CSTR reactor there is not only the peak of maximum concentration at 101 min (482 ppm), but also at 561 and 610 min with a concentration of 193 and 175 ppm of tracer, respectively, that theoretically gives an idea of the presence of dead zones. Another small peak is also observed after these times. This phenomenon can be explained by the presence of areas within the system that retain the tracer and then gradually release it (Armando Rojas & García, 2010).

A long decreasing "tail" can be observed in the trend curve of both reactors after reaching the maximum concentration ( $C_p$ ) but with a slow trend and little symmetry in the curve (less Gaussian and more exponential), which suggests previously that the behaviour of reactors tends to be more like a mixed flow (Sánchez & Gallo, 2009). The "tail" can also indicate that the tracer remains in the reactor longer than theoretical retention time due to hydraulic phenomena such as eddies and internal recirculation (Armando Rojas & García, 2010).

According to Hirsch (1969) cited by Mollah et al. 2018 and Pérez and Torres 2008, the plug flow fraction is considered up to the first inflexion point of the curve where the concavity changes ( $t=48$  min and 46 min for CSTR and FBR, respectively). Between the previous point and the inflexion point in the descending branch of the curve, which corresponds to 164 min and 150 min (CSTR an FBR, respectively), the flow is considered dual (piston and mixed) and from this time the predominant flow is mixed (between 2.7 - 28 hours and 2.5-25h hours for CSTR an FBR, respectively). Table 29 details a series of qualitative relationships that allowed us to analyse the behaviour of the trend curve.

According to the trend curve method, both reactors have a predominance of mixed flow and presence of hydraulic short circuits. The relation  $t_m/t_o$  also indicated the possible presence of dead zones in the CSTR reactor.

Annex 3. Residence time distribution in CSTR and FBR reactors in ideal situation, undisturbed by the crystallisation process.

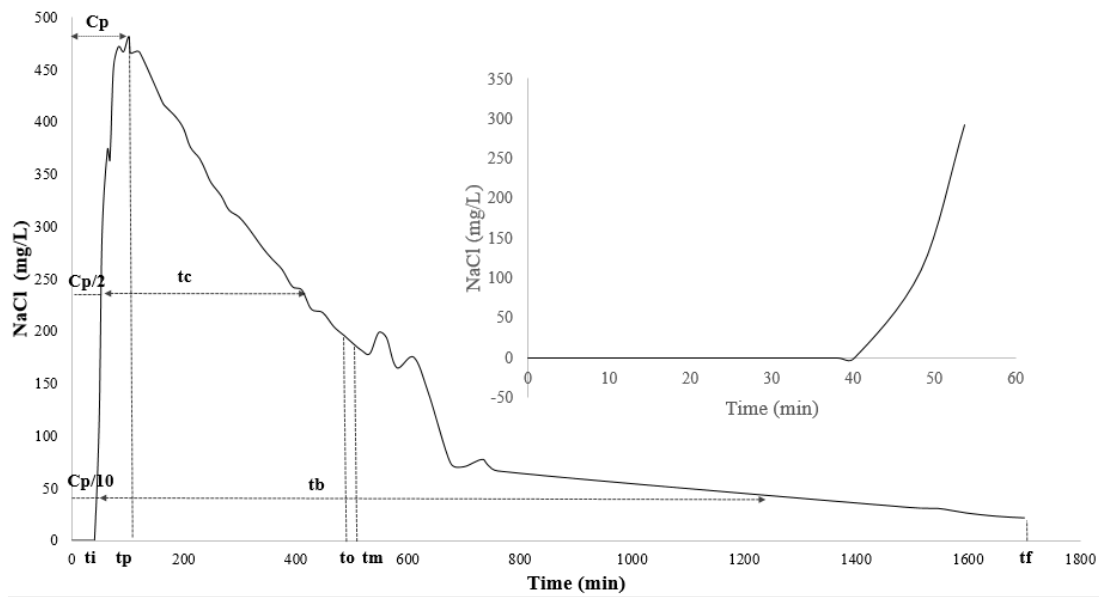


Figure 69. Tracer distribution curve in the CSTR reactor effluent.

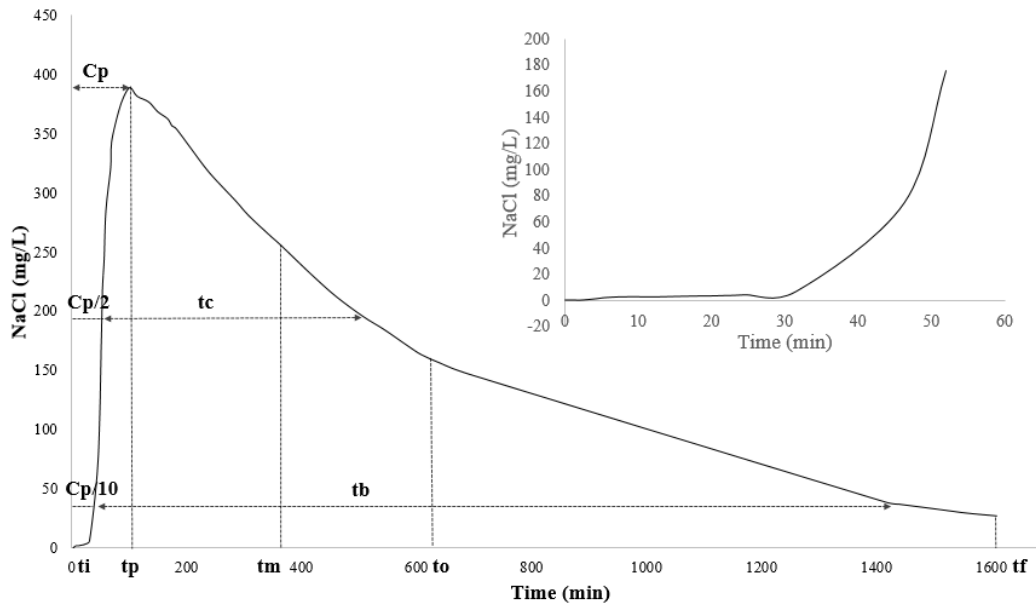


Figure 70. Tracer distribution curve in the FBR reactor effluent.

Table 29. Results obtained by applying the tracer trend curve method (time in minutes).

Parameter	CSTR	FBR	Relation	CSTR	FBR	Description*
to	503.25	635.04**	-	-	-	Theoretical retention time
tp	101.17	102.00	tp/to	0.201	0.161	tp/to=1 plug flow; tp/to=0 mixed flow; If tp/to=1 and ti/to>0.5 plug flow



Annex 3. Residence time distribution in CSTR and FBR reactors in ideal situation, undisturbed by the crystallisation process.

						ti/to=0(complete mixed flow); ti/to=1(plug flow); ti/to=0 mixed flow; <0.3 short circuits
ti	48.33	4.33	ti/to	0.096	0.007	
tc	350.62	459.26	tc/to	0.697	0.723	tc/to=0.7 mixed-flow
tb	1100.80	1380.42	tb/to	2.187	2.174	tb/to=2.3 mixed flow
tm	519.52	364.15	tm/to	1.032	0.573	tm/to<1 short circuit; tm/to>1 undesired tracer, trial error accumulation or dead zones
e	2.88	2.21	-	-	-	e=0 plug flow; e>2.3 mixed flow

\*Adapted from Cánepa de Vargas (2004); Patiño et al. (2012) and Pérez and Torres (2008)

\*\* Theoretical retention time calculated as the relation between total volume ( FBR+settler) and the influent flow rate.

The quantitative hydraulic characterisation was obtained by fitting the data to the Wolf-Resnick model as was showed in the methodology section. The main results are presented in Table 30.

According to the results, the hydraulic behaviour of the reactors is similar, both show a predominance of thorough mixing (>74%) and a high percentage of dead zones (>53%). The results can be explained because both systems have a high volume of sedimentation to reduce the loss of fines. In the sedimentation zone, the mixture is little, therefore, the percentage of dead zones increases. In addition, CSTR reactor was designed to produce a complete mixing in the reaction zone and although the FBR reactor had an elongated geometry that can improve plug flow, the high recirculation rate favoured complete mixing (Levenspiel, 1986). According to Valsami-Jones (2005), the CSTR acts as a perfectly mixed reactor (mixing zone) followed by a plug flow (sedimentation zone).

As is shown in Figure 71 the data predicted by the Wolf-Resnick model fitted very well to the real data ( $R^2 > 93\%$ ), which verifies the veracity of the results found. In addition, the results found by the two methods are congruent.

Table 30. Results of applying Wolf-Resnick model.

Characteristic	Reactor	
	CSTR	FBR
Model	$\ln(1-F(t)) = 0.3573 - 2.8982(t/t_o)$	$\ln(1-F(t)) = 0.1118 - 3.3302(t/t_o)$
R-Squared	93.35	96.96
R-Squared (adjusted for d.f.)	93.22	96.88
Plug flow fraction (%) (P)	26	10
Complete mix fraction (%) (M)	74	90
Dead area (%) (m)	53	67

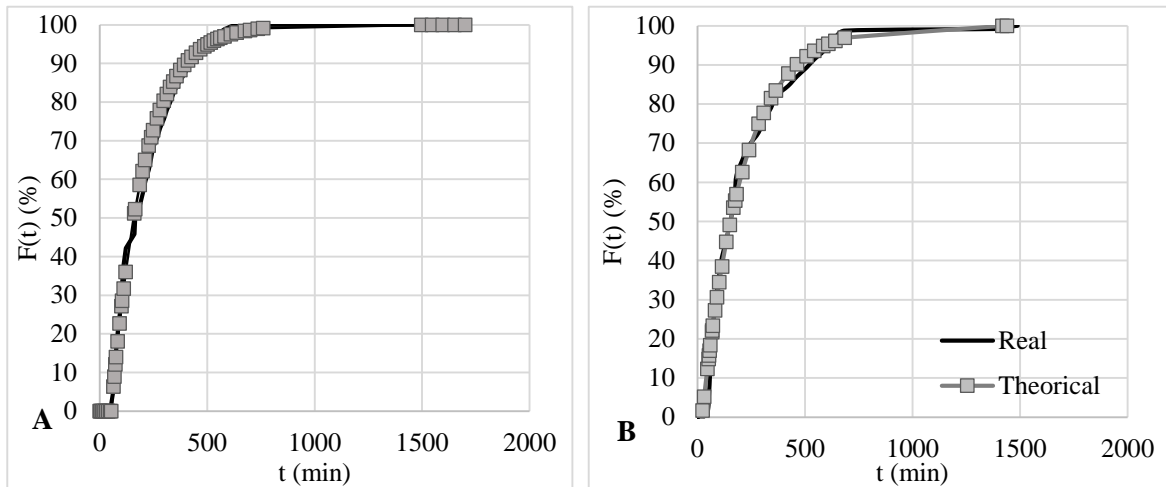


Figure 71. Model Fit-Observed (real) and Predicted Values(theoretical). A- CSTR Reactor and B- FBR Reactor.

In the literature, there are a great variety of reactors that have shown good results for the formation of struvite, however at a high level of supersaturation, as in the case of the sludge dewatering centrate, it is more recommended to use a reactor with a predominance of a complete mixture to reduce the levels of supersaturation and favour the formation of larger crystals. Therefore, both reactors have favourable hydraulics for their application in the struvite formation of sludge dewatering centrate, however, due to its higher percentage of complete mixing (90%), it is likely that the FBR reactor favours more the crystal growth.

## Conclusions

- Using the trend curve method, it was possible to determine that both reactors present a predominance of mixed flow and the presence of short circuits.
- The Wolf-Resnick model confirmed the predominance of mixed flow in both reactors (> 70%) and detected the presence of dead zones (> 54%) that may be mainly due to the sedimentation zone of both systems.
- A mixing flow can support the struvite formation process under high supersaturation conditions by reducing supersaturation levels and increasing crystal size.

## Annex 4. Supplementary information to chapter 5

Table 31. Test in CSTR reactor. In Aeration and seed material (SM) factors -1 and 1 represent without and with aeration and SM, respectively. In P concentration factor (C), -1,0 and 1 represent 30, 70 and 120 mg P-PO<sub>4</sub><sup>3-</sup>.L<sup>-1</sup>.

Test (T)	C	Aeration	SM
1	1	-1	-1
2	1	1	-1
3	-1	1	-1
4	0	1	-1
5	-1	-1	-1
6	0	-1	-1
7	1	1	-1
8	0	-1	1
9	-1	-1	1
10	1	1	1
11	1	-1	1
12	-1	1	1

Test (T)	C	Aeration	SM
13	0	1	1
14	-1	-1	-1
15	1	-1	1
16	0	1	-1
17	0	-1	1
18	-1	-1	1
19	1	1	1
20	0	1	1
21	-1	1	-1
22	0	-1	-1
23	1	-1	-1
24	-1	1	1

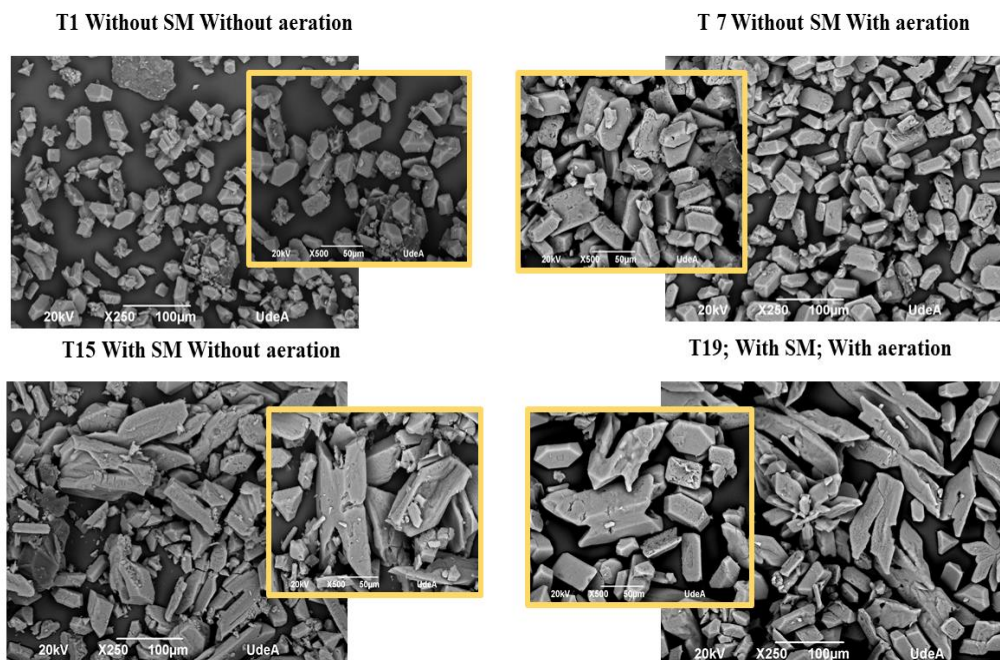


Figure 72. SEM in CSTR reactor at 2.4 SI and different conditions of SM and aeration.

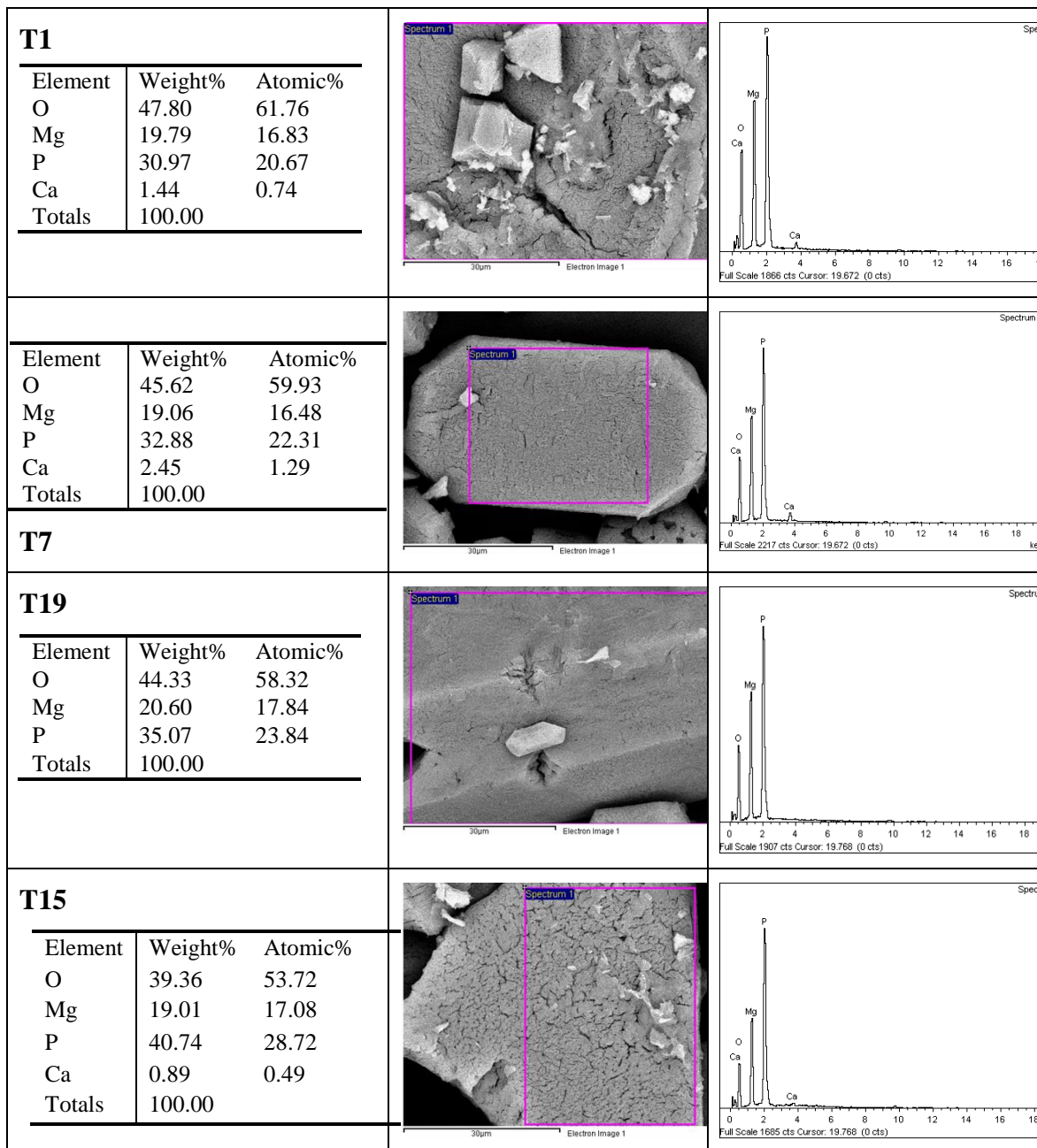


Figure 73. EDX from CSTR reactor precipitates.

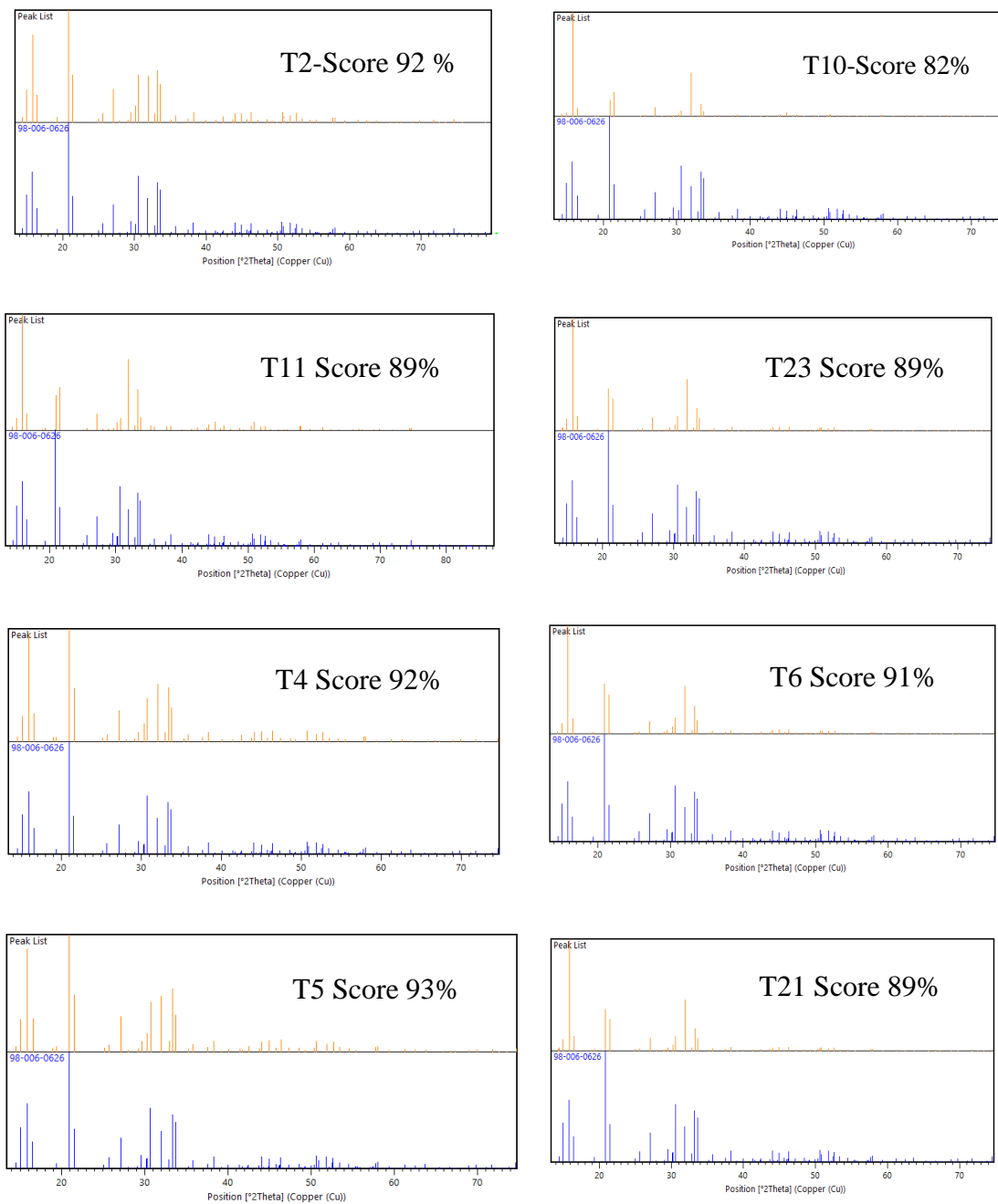

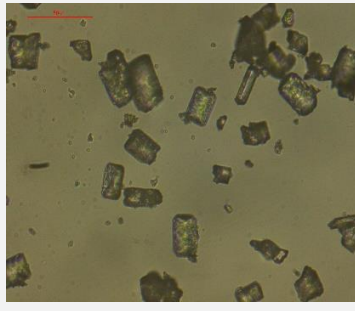
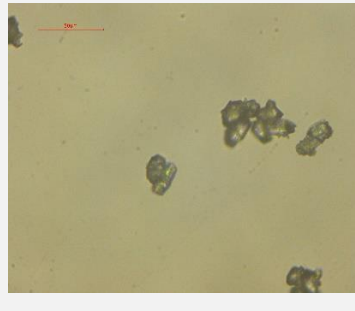
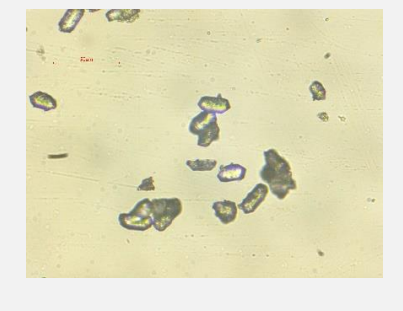

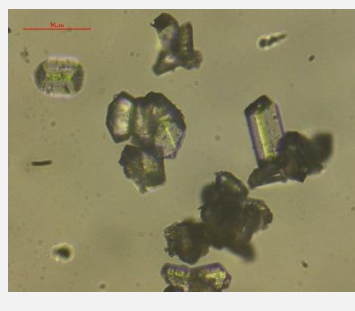
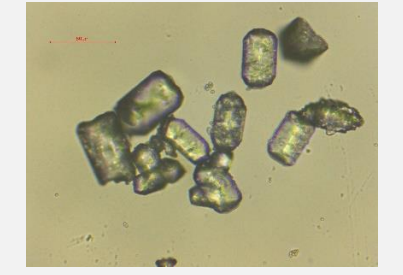
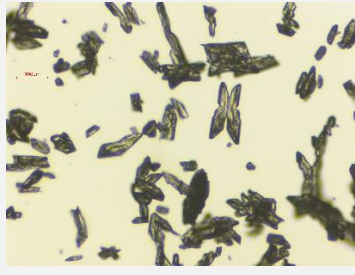
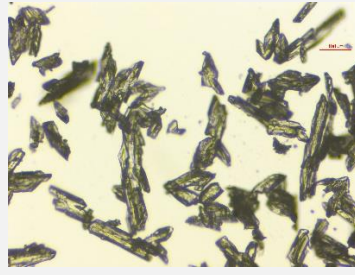
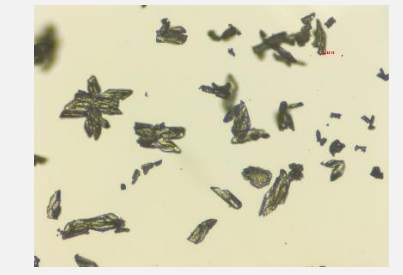
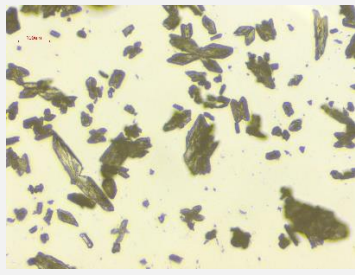
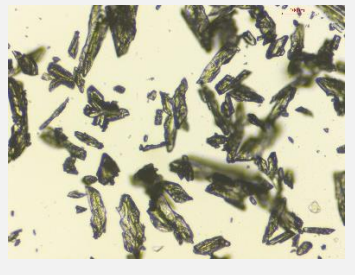


Figure 74. XRD of precipitates from CSTR test. Score represent the similarity (%) between the peak list of the pattern (struvite) and each sample (High score software). Blue lines are the peak list of struvite pattern.

Table 32. Microscope images of precipitates obtained in CSTR reactor

<b>T1 (40x)</b>	<b>T2(40x)</b>	<b>T3(40X)</b>
		
<b>T4 (40x)</b>	<b>T5 (40x)</b>	<b>T6 (40x)</b>
		
<b>T7(40X)</b>	<b>T8(10X)</b>	<b>T9(10X)</b>
		
<b>T10</b>	<b>T11</b>	<b>T12(10X)</b>
		

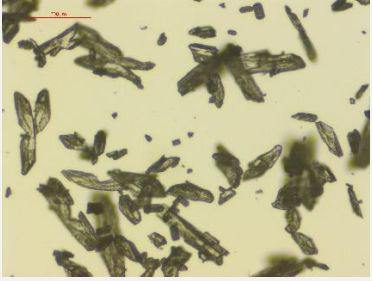

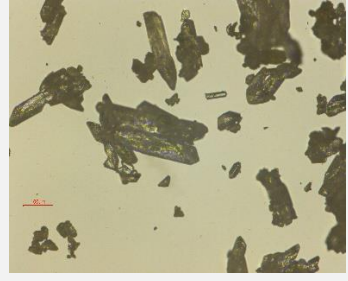
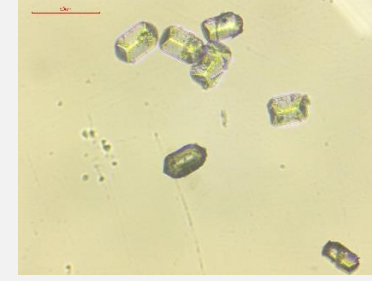
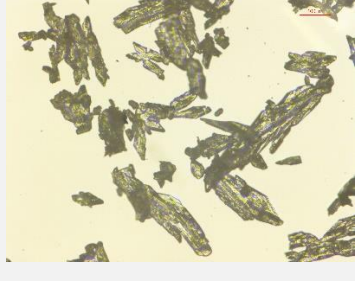
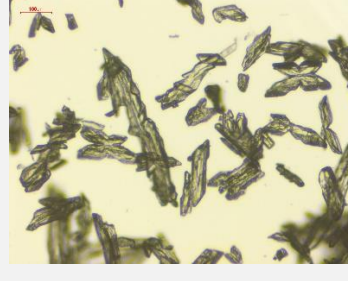
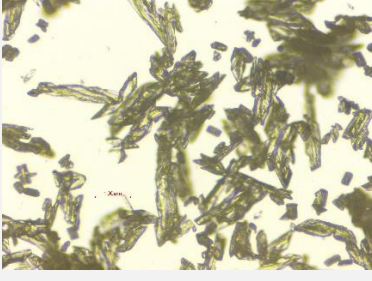
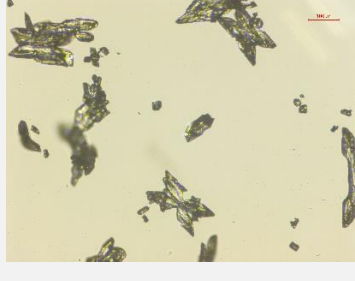



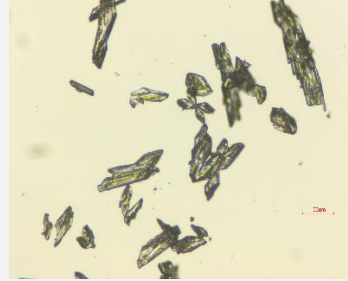
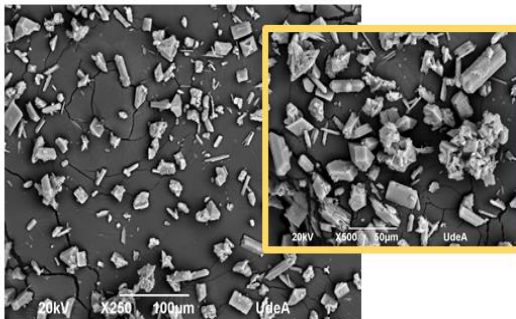
<b>T13 (10X)</b>	<b>T14 (40X)</b>	<b>T15 (10X)</b>
		
<b>T16 (40X)</b>	<b>T17(10X)</b>	<b>T18(10X)</b>
		
<b>T19 (10X)</b>	<b>T20(10X)</b>	<b>T21</b>
		
<b>T22(10X)</b>	<b>T23(40X)</b>	<b>T24(10X)</b>
		

Table 33. Tests in FBR reactor. In Aeration and seed material (SM) factors -1 and 1 represent without and with aeration and SM, respectively. In P concentration factor (C), -1, 0 and 1 represent 30, 70 and 120 mg P-PO<sub>4</sub><sup>3-</sup>·L<sup>-1</sup>.

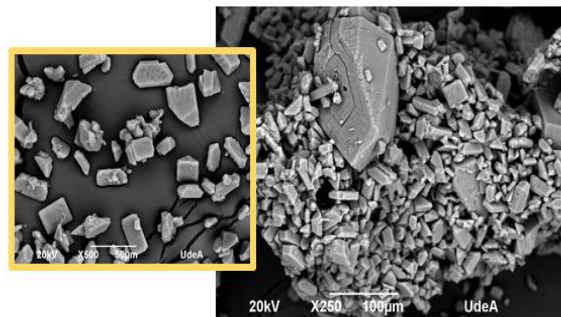
Test	C	Aeration	SM
1	0	-1	-1
2	-1	1	-1
3	1	-1	1
4	-1	-1	-1
5	0	-1	1
6	-1	1	1
7	1	1	1
8	-1	-1	-1
9	1	1	1
10	-1	1	-1
11	-1	-1	1
12	1	-1	-1

Test	C	Aeration	SM
13	1	1	-1
14	0	1	1
15	0	1	-1
16	0	-1	-1
17	1	1	-1
18	-1	1	1
19	0	1	-1
20	0	-1	1
21	1	-1	1
22	0	1	1
23	-1	-1	1
24	1	-1	-1

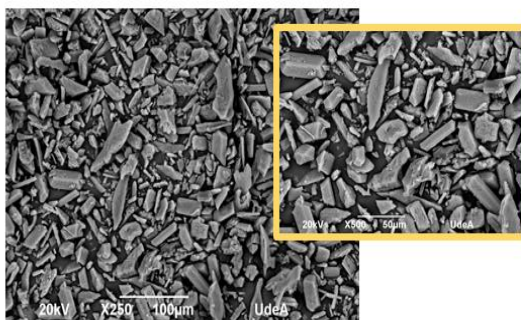
**T12 Without SM Without aeration**



**T 17 Without SM With aeration**



**T3 With SM Without aeration**



**T9; With SM; With aeration**

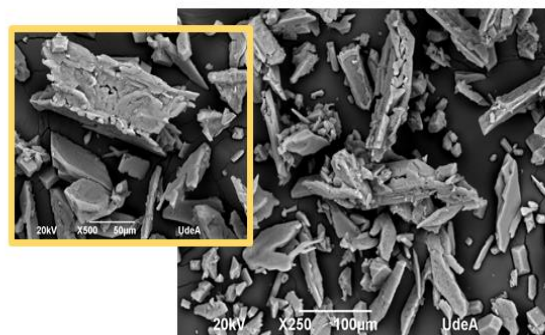


Figure 75. SEM in FBR reactor at 2.4 SI and different conditions of SM and aeration.



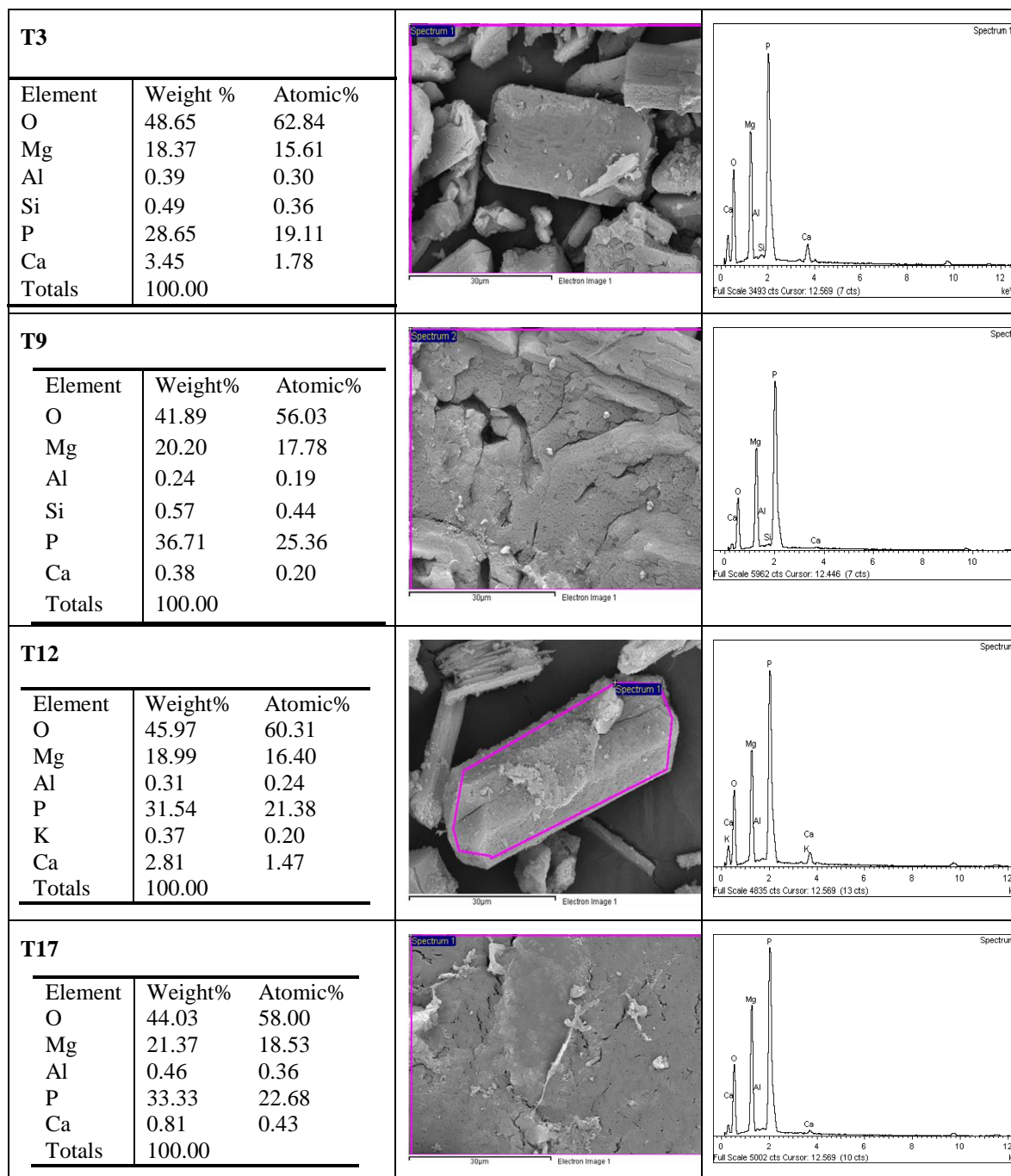


Figure 76. EDX from FBR reactor precipitates

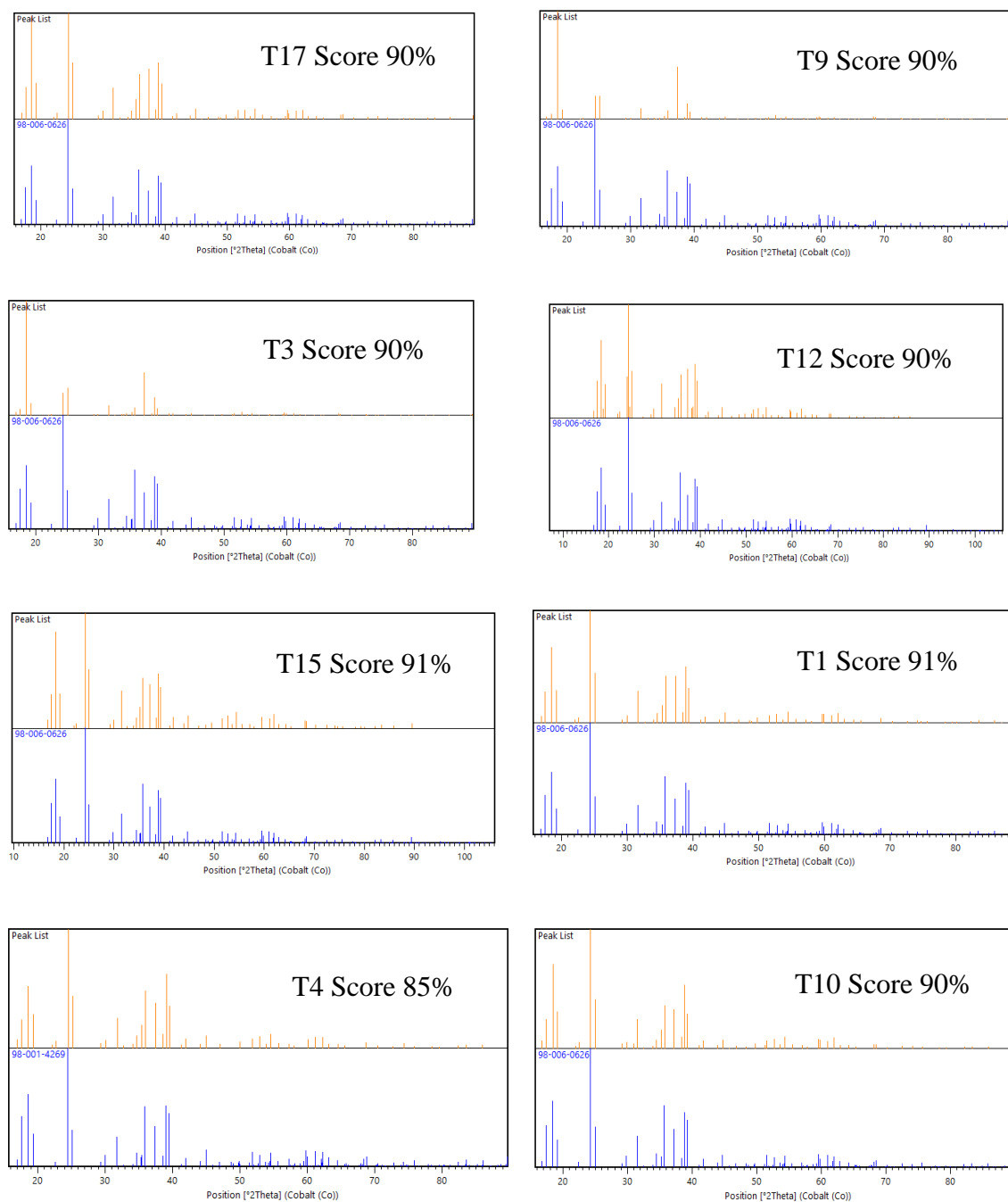

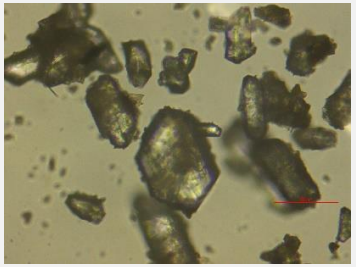
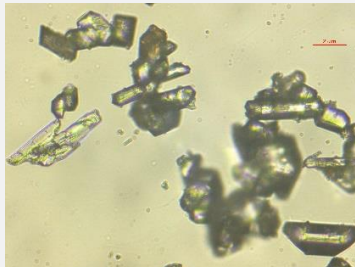
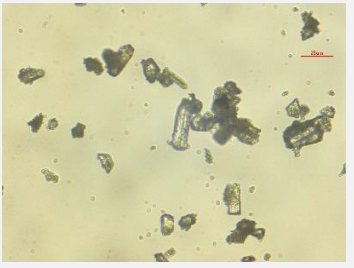
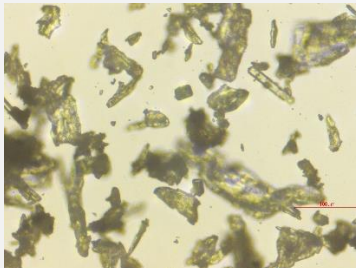
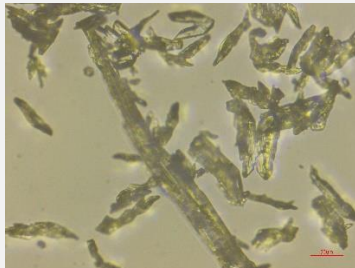
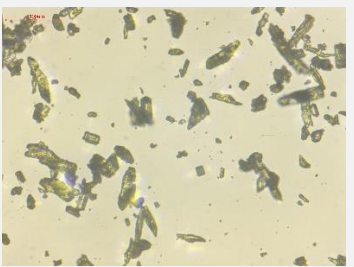

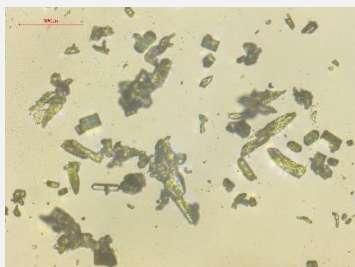

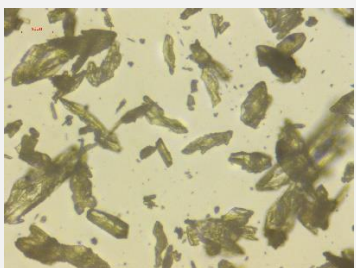

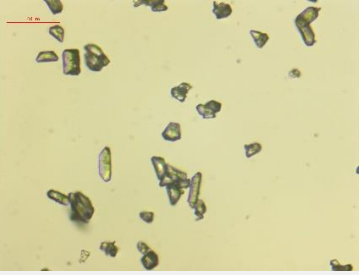

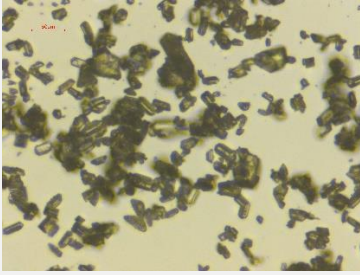
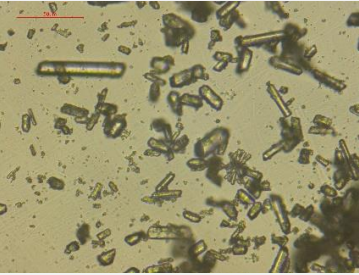
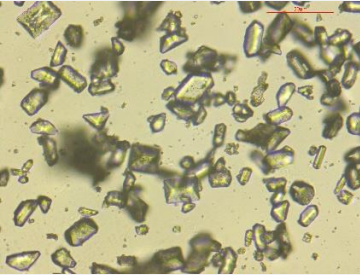
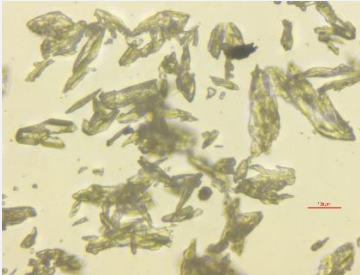
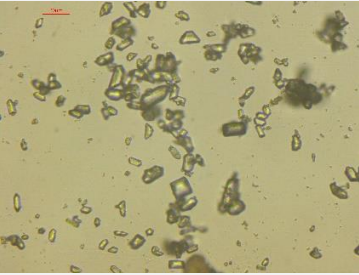

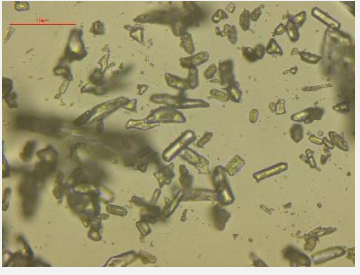
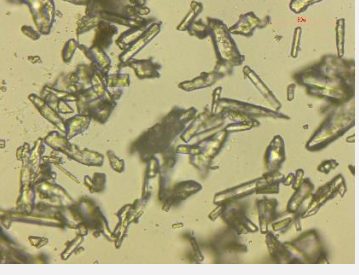
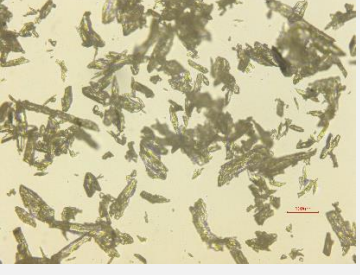


Figure 77. XRD of precipitates from FBR test. Score represent the similarity (%) between the peak list of the pattern (struvite) and each sample (High score software). Blue lines are the peak list of struvite pattern

Table 34. Microscope images of precipitates obtained in FBR reactor

<b>T1 (40X)</b>	<b>T2 (40X)</b>	<b>T3 (40X)</b>
		
<b>T4 (40X)</b>	<b>T5(20X)</b>	<b>T6(20X)</b>
		
<b>T7 (20X)</b>	<b>T8 (40X)</b>	<b>T9(20X)</b>
		
<b>T10 (40X)</b>	<b>T11(20X)</b>	<b>T12(40X)</b>
		

<b>T13 (40X)</b> 	<b>T14 (40X)</b> 	<b>T15(20X)</b> 
<b>T16 (40X)</b> 	<b>T17 (40X)</b> 	<b>T18(20X)</b> 
<b>T19 (40X)</b> 	<b>T20 (40X)</b> 	<b>T21(40X)</b> 
<b>T22(40X)</b> 	<b>T23(10X)</b> 	<b>T24 (40X)</b> 